NASA Contractor Report 174888

Dilution Jet Configurations in a Reverse Flow Combustor

James Zizelman

Case Western Reserve University
Cleveland, Ohio

April 1985

Prepared for

NATIONAL AERONAUTICS AND SPACE ADMINISTRATION
Lewis Research Center
Under Grant NSG-3206

DILUTION JET CONFIGURATIONS IN A REVERSE FLOW COMBUSTOR

Abstract

by

JAMES ZIZELMAN

Results of measurements of both temperature and velocity fields within a reverse flow combustor are presented. Flow within the combustor is acted upon by perpendicularly injected cooling jets introduced at three different locations along the inner and outer walls of the combustor. The oddity of such combustor configurations is best exemplified by recognizing that flows within them accelerate both transversely and longitudinally.

Each experiment is typified by a group of parameters: density ratio, momentum ratio, spacing ratio, and confinement parameter. Two more quantities, Froude number and Mach number, although calculated were found not to be important in these experiments. Measurements of both temperature and velocity are presented in terms of normalized profiles at azimuthal positions through the turn section of the combustion chamber. A rake of probes that spans the combustor laterally allows for the

presentation of some three dimensional plots giving some indication of the lateral spreading. In addition, jet trajectories defined by minimum temperature and maximum velocity give a qualitative indication of the location of the jet within the cross flow. Results of a model from a previous temperature study are presented in some of the plots of data from this work.

During injection from all three injection locations (inner wall prior to the turn, outer wall prior to the turn, and outer wall into the turn) a migration of the injected fluid toward the inner wall is observed both from temperature and velocity fields.

Penetration into the cross flow is shown to be affected as follows: increasing injection jet momentum increases penetration, increasing the ratio of the jet density to the cross flow density increases penetration, and increasing spacing between jets in multiple jet injection increases penetration.

Lateral spreading seemed to be greater during higher momentum injection and during injection from the outer wall.

The above conclusions appear consistent with

the flow field that sets up in the combustor. The flow is observed as inertially dominated and characteristically irrotational as a pressure gradient develops to support fluid turning.

TABLE OF CONTENTS

	Page
ABSTRACT	i
LIST OF SYMBOLS	vii
CHAPTER I - INTRODUCTION	1
CHAPTER II - PREVIOUS RELATED STUDIES	8
2.1. The Free Jet	8
2.2. Jet Injection into a Non-Accelerating Medium	12
2.3. Two Dimensional and Multiple Jets	22
2.4. Reverse Flow Combustor Experiments	25
CHAPTER III - THE REVERSE FLOW COMBUSTOR: APPARATUS, EXPERIMENTAL PROCEDURES, AND ERROR	26
3.1. Apparatus	26
3.2. Experimental Procedures	37
3.3. Experimental Preliminaries	39
3.4. Presentation of Expected Error	50
CHAPTER IV - CONCLUSIONS FROM THE PREVIOUS REVERSE FLOW COMBUSTOR STUDY	53
CHAPTER V - SINGLE JET INJECTION DATA AND CONCLUSIONS	55
5.1. No Injection	55
5.2. Low Momentum Injection--Outer Wall--Prior to Bend	58
5.3. High Momentum Injection--Outer Wall--Prior to Bend	60
5.4. Low Momentum Injection--Inner Wall--Prior to Bend	62
5.5. High Momentum Injection--Inner Wall--Prior to Bend	64

		Page
5.6.	Low Momentum Injection--Outer Wall--Into the Bend	65
5.7.	High Momentum Injection--Outer Wall--Into the Bend	68
5.8.	Conclusions from Normalized Radial Profiles	69
5.9.	Lateral Distributions	72
5.10.	Additional Conclusions from Lateral Plots	76
CHAPTER VI -	MULTIPLE JET INJECTION AND CONCLUSIONS	78
6.1.	High Momentum Injection--Outer Wall--Prior to Bend	79
6.2.	High Momentum Injection--Inner Wall--Prior to Bend	85
6.3	High Momentum Injection--Outer Wall--Into the Bend	89
6.4.	Conclusions from Normalized Radial Profiles	92
6.5.	Lateral Profiles	94
CHAPTER VII -	GENERAL CONCLUSIONS AND RECOMMENDATIONS	97
CHAPTER VIII -	DATA PLOTS	99
APPENDIX 1 -	SAMPLE CALCULATIONS	162
APPENDIX 2 -	SPECIFICATION SHEETS	164
APPENDIX 3 -	START-UP, SHUT-DOWN, AND EXPERIMENTAL PROCEDURES	170
APPENDIX 4 -	COMBUSTOR OPERATIONS SOFTWARE	176
APPENDIX 5 -	ERROR ANALYSIS	193
REFERENCES		203

LIST OF SYMBOLS

A	Area
b	Jet radius
b_o	Initial jet radius
C_D	Coefficient of drag
Dr	Density ratio, ρ_{jo}/ρ
E_1	Entrainment coefficient
E_2	Entrainment coefficient
h_w	Differential pressure in mm water
H_o	Combustor height at entrance
H_1	Combustor height at exit
J	Momentum Ratio, $\frac{\rho_{jo} V_{jo}^2}{\rho V^2}$
l	Perimeter of turbulent jet
P_s	Static pressure
P_T	Total pressure
ΔP	Total pressure - static pressure
q	Volumetric flux
q_j	Jet volumetric flux
q_{jo}	Initial jet volumetric flux
R	Gas constant for air
R_i	Radius of inner wall prior to bend
R_o	Radius of outer wall prior to bend
s	Longitudinal jet coordinate

Sr	$\frac{\text{Spacing ratio, length between jet centers}}{2b_o}$
T	Cross flow temperature
T_{jo}	Initial jet temperature
T_l or T_L	Local temperature
V	Cross flow velocity
V_e	Entrainment velocity
V_{jo}	Initial jet velocity
V_{jx}	X-direction jet velocity
V_{jy}	Y-direction jet velocity
V_l or V_L	Local velocity
x, X	x-axis
y, Y	y-axis
z, Z	z-axis

GREEK

τ	Normalized temperature, $\frac{T_l - T}{T_{jo} - T}$
γ	Normalized velocity, $\frac{V_l}{V} - 1$
θ	Angle of jet centerline from initial cross flow streamlines
ξ	Longitudinal jet coordinate

CHAPTER I

INTRODUCTION

In recent years, many studies have been made that deal directly with the concept of jet injection. Both theoretical and experimental work has been done. Much of this work deals with one of the following configurations: (1) jet injection into a non-moving environment, (2) perpendicular jet injection into a medium with constant velocity, and (3)multiple jet and two-dimensional jet injection into a medium with constant velocity.

Work of the above description can be viewed in most of the references in the bibliography. It must be remembered, however, that these studies are not addressing the problem of turbulent jet injection into an accelerating medium. The studies involving a moving cross flow are set up to provide a constant area for the flow, and hence a constant velocity. In most dilution jet applications in jet engine combustors, this type of investigation is entirely adequate because the chamber involved is really nothing more than a straight-through annulus resulting in cross flow velocities that remain nearly the same from inlet to exit. However, in the geometry of the reverse flow combustor, the cross

flow negotiates a 180° turn while experiencing a decrease in cross sectional area. This geometric complexity gives rise to experimental studies such as this one associated with determining both velocity and temperature fields throughout the combustor. From this information, immediate qualitatve conclusions are available as well as more detailed information describing the flow conditions for use as experimental input to a semi-empirical model. As can be seen, then, this investigation has some peculiarities resulting from the unique combustor design. By the nature of the geometry, the flow must accelerate both longitudinally and transversely as it negotiates the 180° turn.

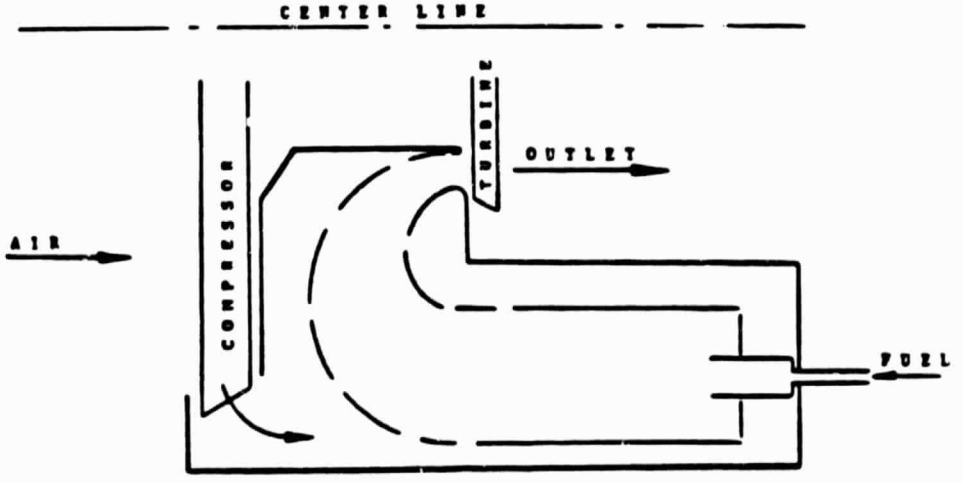

Figure 1: Simplified Combustor Geometry[18]

When one examines the combustor more closely, it becomes evident that one can identify two apparent modes of acceleration. The first to be identified is the transverse acceleration that must exist perpendicular to the flow direction due to the fact that the flow negotiates the turn. The second identifiable acceleration is that due to the cross sectional area decrease as one approaches the exit. This acceleration is in the direction of the flow. By rotating the schematic in figure 1 about the centerline, one can see that this combustor is acutally an annulus turned inside of itself. This gives rise to more acceleration in the direction of the flow because the inner annulus (the exit) is of smaller radius, and therefore carves out less area. The following figures depict the two modes of acceleration:

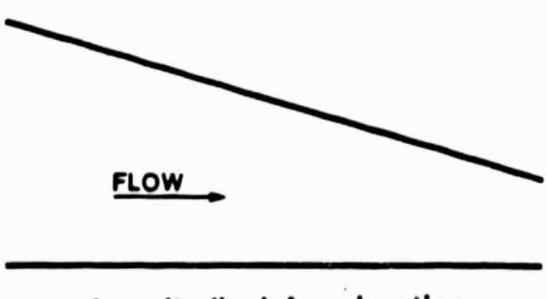

Longitudinal Acceleration

Figure 2: Longitudinal Acceleration

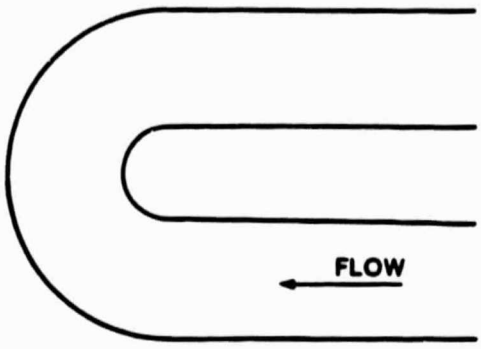

Transverse Acceleration

Figure 3: Transverse Acceleration

Due to this unique combustor design, little theoretical, semi-empirical, or purely empirical information is available that describes flow conditions within the combustor. Lipshitz[18], in a recent study using a model reverse flow combustor, generated a large quantity of empirical information regarding temperature fields throughout the turn section of the combustor. However, an attempted model to predict jet trajectories in single jet injection showed poor agreement with trajectories inferred from the temperature profiles apparently due to the lack of informaiton regarding the cross flow velocity field. In the case of Lipshitz's experiment, a thermal jet trajectory location was defined as the minimum temperature observed between

the inner and outer walls of the combustor at a given angular position in the turn section. Individual trajectcry locations could then be connected with a smooth line.

To more fully examine the complexities of this combustor with its various cooling jet injection configurations, an experiment was designed to gather both temperature and velocity data from the end of the primary zone (at the entrance to the turn section) to the outlet of the combustor (at the turbine blades). Both radial (from inner wall to outer wall) and azimuthal (angularly through the turn) sampling points were set up so that both the velocity and temperature fields could be well represented.

In an actual turbine-engine situation, it is advantageous to know what effect changes in dilution jet injection would have on temperature and velocity fields at the outlet of the combustor. Since the outlet is the location of the turbine blades, knowing detailed information here gives one the ability to operate the engine at a higher, more efficient temperature with considerably less uncertainty as to when mechanical failure of the blades will occur. Of course, the preferred

temperature profile at the blades is best exemplified by figure 4.

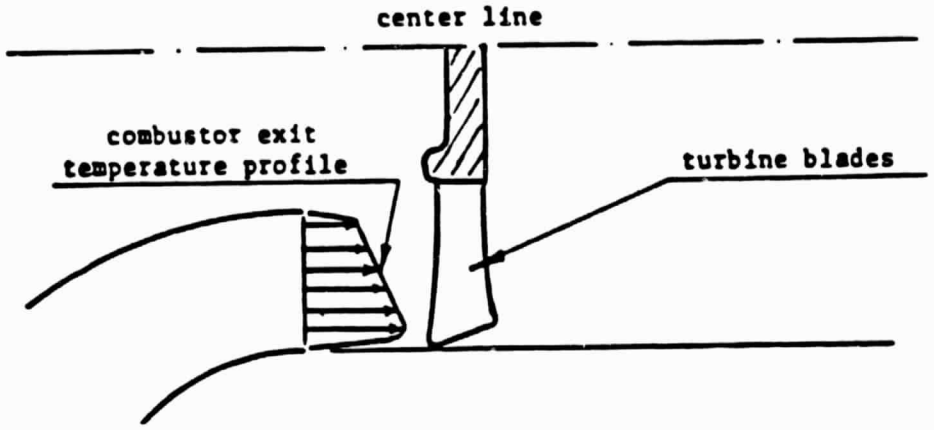

Figure 4: Preferred temperature profile (turbine)[18]

Figure 4 shows a temperature profile that increases in going from the root to the tip of the blade. The reasoning here is based upon centrifugal loading. At the root, the blade structure must exert enough inward force to support nearly the entire length of the blade thereby causing this location to experience the maximum stress. Now, choose a position near the tip of the blade. Here, the only centrifugal loading is that caused by that small portion between your chosen position and the blade tip. It follows that the stress in the blade at the tip approaches zero. As one begins to operate a jet engine near its allowable maximum, the limit is usually set by the mechanical capability of the

turbine blades, so the lower the temperature at the maximum stress location, the longer the blade can maintain mechanical integrity.

Additionally, a known velocity profile at the exit would allow a more detailed calculation of convective heat transfer coefficients of the turbine blades, resulting in a more thorough understanding of the heat transfer taking place, again providing the opportunity to operate the engine at a more efficient temperature.

It can be seen, then, that if enough information is gathered, it will be possible to tailor both velocity and temperature profiles at the outlet by merely changing the dilution jet initial conditions. It is this tailoring that makes this work so important.

CHAPTER II

PREVIOUS RELATED STUDIES

Since this research concerns itself with a specific geometric design, there is relatively little information regarding temperature and velocity profiles and trajectories. In fact, one previous study by Lipshitz[18] is all that is known to exist. However, some studies have been made that relate in a generic way because the basic concept of jet injection is investigated. As stated earlier, these studies include: (1) free turbulent jet injected into a non-moving medium, (2) turbulent jet injected perpendicularly into a non-accelerating medium, and (3) multiple jets and two-dimensional jets injected into a non-accelerating medium. Since these specific types of studies will not aid a great deal in the understanding of this one, they will be reviewed here fairly quickly. In a later chapter, a presentation of the temperatue study conclusions by Lipshitz[18] will be conducted.

2.1. The Free Jet

As is suggested in any work on the fluid

mechanics of jets, turbulent profiles are generally considered to be self-similar, that is, the velocity profiles remain similar with respect to the space variable. Discussions on similarity solutions for the free jet can be viewed in works by Abramovich[1] and Albertson[2]. Using the idea of the similarity solution, it becomes evident that in the fully developed region of a free jet, the jet boundary layer grows linearly as a function of distance from the origin, i.e.,

$$b \propto s \qquad \text{(II.1)}$$

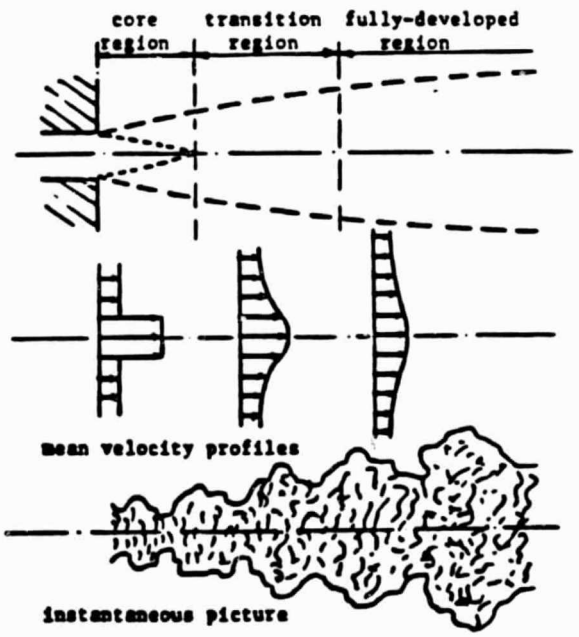

Figure 5: A turbulent free jet[18]

In addition, the similarity solution allows one to recognize that the centerline velocity of the jet decays as the inverse of the distance travelled from the origin:

$$V_j \propto \frac{1}{s} \qquad \text{(II.2)}$$

Investigating further, one can see from Albertson[2] and Ricou and Spalding[25] that the gross volume flux for a single turbulent free jet was found to be given by:

$$\frac{q_j}{q_{jo}} = \frac{0.16 * s}{b_o} \qquad \text{(II.3)}$$

Something that goes hand in hand with the idea of gross volume flux is the notion of entrainment. Qualitatively, it is a measure of how much fluid experiences motion in the direction of an injected jet. Rouse, Yih, and Humphreys[26] in an early work investigated injection where the jet and the ambient fluids were of different densities. Their modification to the gross volume flux equation (II.3) manifests itself in a density correction factor as follows:

$$\frac{q_j}{q_{jo}} = \frac{0.16 * s}{b_o} \left[\frac{\rho_a}{\rho_j} \right]^{1/2} \qquad \text{(II.4)}$$

In the above analyses, the consideration is given to the free turbulent jet pictured in figure 5 above. In such a turbulent jet, the velocity profile at the origin is nearly uniform. From the origin outward, there are three distinct regions of the jet: (1) the potential core, (2) the transition region, and (3) the fully developed region. The center of the potential core region is referred to as the core. At this location, the fluid has the same properties as the fluid issuing from the nozzle of the jet. Still in the potential core region, but moving laterally from the centerline, a free shear layer must be encountered. In this area, the fluid smoothly returns to the ambient conditions. This potential core region has been seen to exist about four to five nozzle diameters downstream of the jet. It is this type of information that becomes useful in the analysis of the data of this investigation as a guide to give some rough idea about what to expect.

The second region is the transition region, immediately followed by the fully developed region. It is typical for the transition region to dissipate

ten nozzle diameters downstream of the injection location. Of course, these estimated distances depend largely on the initial conditions of the jet as it issues from the nozzle. After transition has occurred in the second region, the jet remains turbulent.

2.2 Jet Injection into a Non-Accelerating Medium

In studies involving a single jet introduced into a non-accelerating cross flow, it is typical for a round jet to be issued perpendicularly into the oncoming flow with what is considered a uniform velocity profile. Also, it is generally considered typical for the cross flow duct to be of constant cross sectional area to eliminate acceleration. As the jet moves outward from the nozzle, a complex deflection begins to occur. Figure 6 below illustrates this typical injection configuration.

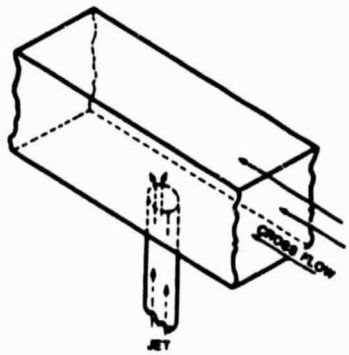

Figure 6: Injection configuration for a non-accelerating cross flow.

In an attempt to qualitatively describe how the "jet bending" is taking place, a number of different mechanisms have been identified and can be considered. First, as the jet issues from the nozzle, it can be viewed as a slug of fluid, even a rigid cylinder, that has associated with it a coefficient of drag, C_D.[1] As the dynamic pressure of the cross flow begins to exert force on the "cylinder" of fluid, it begins to experience a drag in the direction of velocity of the cross flow. Immediately, of course, a "bending over" of the jet begins to appear. As quickly as this occurs, the drag force vector forms two components: one tangentially along the deformed jet and one normal to it.

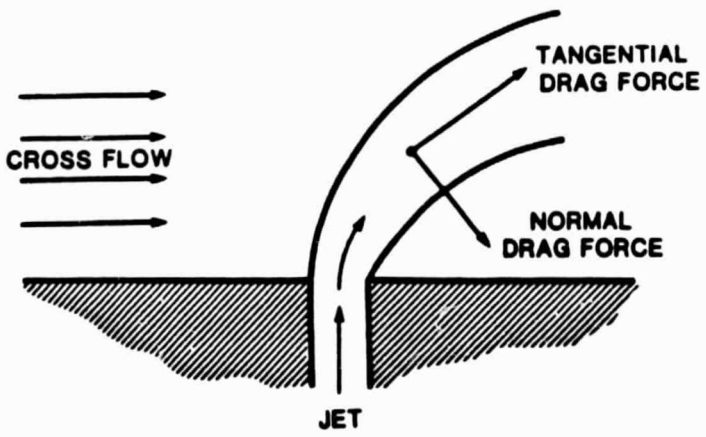

Figure 7: Jet bending due to the drag mechanism.

Another mechanism which is attributed to the complex bending of a jet injected perpendicularly into a cross flow is jet entrainment. As the jet penetrates outward into the cross flow, it pulls along with it particles of fluid belonging to the cross flow, due to the frictional force apparent there. As these cross flow particles are entrained, so, too, is the momentum associated with them. Since the momentum vector of the cross flow is perpendicular to that of the issuing jet, it follows that this becomes a mechanism responsible for the direction change of the jet. This momentum transfer, in other words, causes the jet to acquire a velocity component in the direction of the cross flow.

The third mechanism is related to the first and second in that it considers the jet to be a cylindrical slug of fluid, and gives some physical meaning to entrainment. In this mechanism, though, one looks more in-depth at what occurs fluid dynamically as fluid passes over a cylinder. Most obviously, there is a high pressure area where the cross flow impinges upon the issuing jet. Secondly, a low pressure wake forms downstream of the cylinder as the flow detaches. The cross flow, then, will

begin to flow in the direction of the favorable pressure gradient, or into the low pressure region behind the jet. This action sets up a pair of vortices, causing the jet to become kidney-like in shape as seen in the figure below.

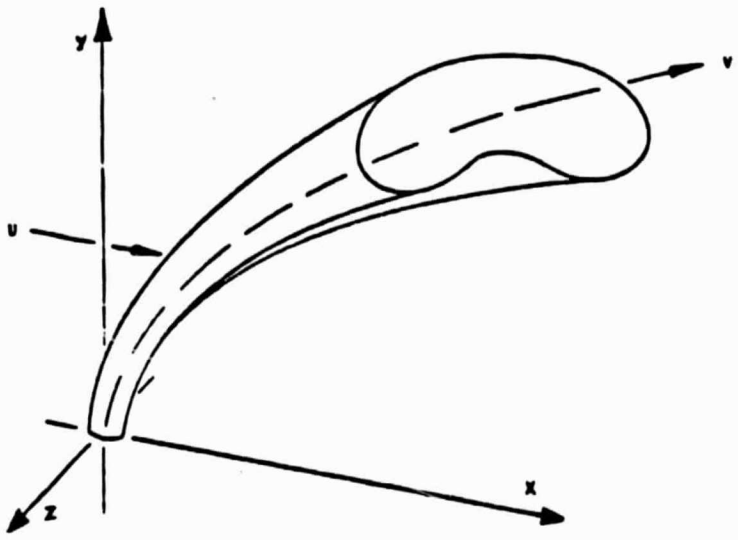

Figure 8: Vortex pair formation in a jet.

This induced vortex action is held partially responsible for the entrainment that occurs in cross flow injection situations. Platten and Keffer[23] show that the increased spreading rate associated with this injection configuration is attributable to this vortex pair formation as well.

Just as the free jet was disassembled into its three basic regions, the single jet in a cross flow

can be similarly viewed. This type of jet also has three principal regions, the first of which is referred to as the potential core and is based mainly on the jet to cross flow momentum ratio but is also somewhat dependant on the jet Reynolds number based on initial jet diameter[24].

The next region identifiable is downstream of the potential core and is fully turbulent. Vorticity produced by the cross flow negotiating around the cylindrical jet gives rise to the formation of the vortex pair within the jet, giving it a kidney shape while average jet velocities begin to diminish toward the ambient value rather quickly. After a relatively short distance, the jet trajectory becomes nearly parallel to that of the cross flow. This zone is commonly referred to as the "zone of maximum deflection,"[24] or the "curvilinear zone."[17]

In the third zone, the "far field zone,"[16] the two vortices are literally overrun by the cross flow and subsequently swept downstream at velocities nearly that of the cross flow, although such conditions are reached asymptotically. Additionally, the amount of circulation appears to decrease as one moves downstream. This zone is

known to exist up to 1000 nozzle diameters downstream. Again, these statements serve as crude approximations of the reverse flow combustor because they do not consider acceleration of the cross flow, but a general idea of what to expect is presented.

The most successful modelling of a jet in a cross flow includes some consideration for jet entrainment. In this brief discussion on related works, some of those are presented now. Fan[10] developed an interesting model for the jet entrainment. For this fluid mechanism, he suggested an entrainment coefficient, E. Using this coefficient, the development was taken further, and an entrainment velocity was defined as follows:

$$V_e = E(\mathrm{abs}(V_j - V)) = E((V_{jx} - V)^2 + V_{jy}^2)^{1/2} \qquad \text{(II.5)}$$

In a turbulent jet, as mentioned above, mass flux within the turbulent region increases by entraining the surrounding fluid as progression downstream occurs. In accordance with Kamotani and Greber[14], and using the coordinates of figure 8, the rate of increase of mass flux is given by:

$$\frac{dq}{d\xi} = \rho \cdot 1 \cdot V_e \qquad \text{(II.6)}$$

where ρ is the density of the cross flow, 1 is the perimeter of the turbulent region, and V_e is the entrainment velocity, or the velocity with which the turbulent front is advancing into the cross flow at a particular ξ.

Equation II.5 shows E being used as a correlation coefficient for the entrainment velocity that uses the vector difference between local jet and local cross flow velocities. The value of E was found to fall in the range of 0.4 to 0.5 for V_j/V ratios ranging from five to 20. This correlation, however, is intended for a uniform area cross flow, and begins to break down under acceleration.

Hoult et al[13] show an asymptotic solution for jet trajectories compared to experimental values at various velocity ratios. From this investigation, yet another description of entrainment velocity was developed. In this correlation, the description of entrainment is dependant upon the difference between local jet velocity and the parallel and normal components of the cross flow velocity. It contains two entrainment coefficients.

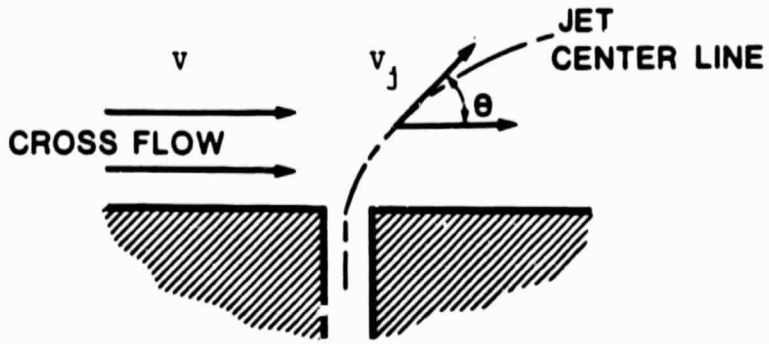

Figure 9: Diagram for Hoult's entrainment equation.

The correlation developed is as follows:

$$V_e = F_1(V_j - V\cos(\theta)) + E_2(V\sin(\theta) \qquad (II.7)$$

The values for E_1 and E_2 are given as 0.11 and 0.6 respectively for a velocity ratio ranging from one to ten.

In a similar development, Kamotani and Greber[14] constructed a mathematical relation depicting entrainment velocity which is also dependant on cross flow velocities both tangential and normal to the jet trajectory. In this development, however, the value of jet velocity used was taken as the maximum value of fluid speed in a given normal plane instead of the average jet velocity as had been in earlier investigations. Their relation is written:

$$V_e = E_1(V_{jmax} - V\cos(\theta)) + E_2V\sin(\theta) \qquad (II.8)$$

where Θ is defined in figure 9. The values of E_1 and E_2 were seen to vary with changing jet to cross flow momentum ratio, J. For instance, with J = 15.3, E_1 and E_2 were found to be 0.07 and 0.32 respectivley. As J was increased to 59.6, E_1 and E_2 were found to be 0.067 and 0.182 respectivley. Incidentally, Kamotani and Greber[14] showed that for a single jet, a decrease in the channel height did not have a considerable affect on the trajectory of the jet unless the opposing wall was brought so near that the jet impinged on its surface. They also show that increasing momentum ratio caused increased penetration of the trajectory into the cross flow.

In addition to the above statements concerning perpendicular jet injection, numerous other studies have been done using a wide array of experimental techniques and theoretical approaches. As an overview, some of these will be stated here. Chien and Schetz[7] actually took the time to solve the three-dimensional Navier-Stokes equations and energy equation written in terms of vorticity, velocity, and temperature. Specifically, they solved the single jet perpendicular injection into a cross

flow problem. Comparisons with a laminar cross flow experiment did show good agreement. However, when modifications were made to more closely model a turbulent buoyant jet, less promising results were seen. Analysis showed that trajectory information was quantitatively acceptable, but the three-dimensional informaiotn was only qualitativley acceptable. Inaccuracies were blamed on the simple turbulence model. Campbell and Schetz[6] also produced a three-dimensional analysis for the jet in a cross flow. Their scheme for predicting trajectories included buoyancy forces and entrainment terms in the momentum equation perpendicular to the trajectory. Finally, one of the only investigations performed on a non-uniform cross flow was done by Sucec and Bowley[28]. This investigatcn was not detailed combining drag and entrainment concepts into a single force. This approach uses the Abramovich idea that the jet can be treated as a cylinder in a cross flow.

As can be seen, then, little work pertains directly to flow within the reverse flow combustor by the nature of its odd geometry. However, the work described here does allow one to make some intelligent judgements as to what might be expected.

2.3. Two-Dimensional Jets and Multiple Jets

In a jet engine combustion chamber, it is typical for jets to be injected in rows that normally run perpendicular to the length of the combustor. In this work, the study of multiple jet injection is conducted. Therefore, it becomes important to scan quickly some related jet investigations to get a notion of what to expect.

As spacing between a multiple number of jets in a row decreases, the behavior of the row becomes increasingly similar to that of a two-dimensional slot jet. Albertson[2] showed both theoretically and experimentally, that in the case of a free slot jet, the velocity is a function of the reciprocal of the square root of the distance from the jet:

$$V_j \propto \frac{1}{s^{1/2}} \qquad \text{(II.9)}$$

Also, spreading of the jet is a function of the square root of the distance from the jet injection point:

$$b \propto s^{1/2}. \qquad \text{(II.10)}$$

This behavior is quite different from that of a single round jet described above. Lastly, Albertson[2] gives an expression for volume flux as:

$$\frac{q_j}{q_{jo}} = 0.62 \left[\frac{s}{b_o} \right]^{1/2} \qquad \text{(II.11)}$$

In searching for literature on rows of single jets, it was found that all of the work was experimental in nature. Empirical correlations generally accompanied the experimental results. This type of work is inevitably useful only for similar flow configurations, since the governing correlations do not normally include a provision for different cross flow geometry and injection geometry.

One of the most important results from the multiple jet investigations is the concept of vortex interaction between adjacent jets. Vortex interaction causes a downward movement of the jet trajectory. However, in the limit where the spacing between adjacent jets becomes very small, the vortex formation is limited, hence the downwash is less. Experiment shows the deteriorating trajectory is followed by a higher trajectory as the spacing

continues to decrease. In the following diagram,

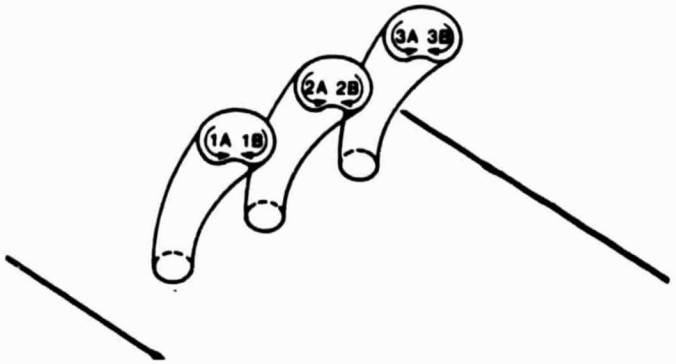

Figure 10: Schematic of vortex interaction

each kidney shape represents a single jet. Each shape contains two arrows indicating the vortex pair associated with each jet. Upon examination of the effects on jet two above, one can see that vortex 1B has a downward effect on jet 2. Vortex 1A, however, has an upward effect, but since the distance from vortex 1A to jet 2 is larger than the distance from vortex 1B to jet 2, the resultant effect is a downward tendency. The effect of the vortices associated with jet 3 on jet 2 are identical to those of jet 1 on jet 2. It must be noted, however, in the limit as one decreases the spacing between the jets, the vortex formation is hindered and the effect described above becomes minimal. During injection into a confined cross flow, as one

decreases the spacing ratio and approaches the geometry of a two-dimensional slot jet, a second mechanism that has a downward effect on the jet trajectory is defined. As the injected flow becomes increasingly two-dimensional, the cross flow must pass over the top of the jet and not between individual jets . The resultant effect is a supressed trajectory to allow the cross flow sufficient area.

2.4. Reverse Flow Combustor Experiments

One previous study on jet injection in a reverse flow combustor is avaiable. After the presentation of descriptions of the physical facility, experimental procedures, and relevant parameters, conclusions from this study will be summarized. In addition, in the presentation of data from this work, trajectories from the model developed in the previous work will be shown and compared to experimental trajectories.

CHAPTER III

THE REVERSE FLOW COMBUSTOR: THE APPARATUS, EXPERIMENTAL PROCEDURES, AND ERROR

3.1. Apparatus

For this experimental project, data was taken from a 90° subsection model of a reverse flow combustor. This model combustor was designed and built exclusively for the purpose of performing dilution jet injection experiments. Dimensions of the combustor are similar to full-size rigs in operation. Figure 11 shows a schematic of the experimental rig fully dimensioned. From this schematic, the aspect ratio of the apparatus , defined as:

$$AR = \frac{\text{Mean Combustor Arclength}}{\text{Combustor Channel Height}}$$

is calculated to be 7.125 for the primary zone (that section downstream of the fuel injection but upstream of the turn) and 7.00 at the exit. With such aspect ratios, it is expected that at the centerline of the combustor, no secondary flows with significance will exist. The primary zone of the device is constructed from Inconnel-750X super

alloy, allowing wall temperatures of up to 1200°F (650°C) without significant warpage. The turn section is constructed from split 90° stainless steel elbows. Figure 12 shows a photographic view of the entire set-up including supporting apparatus required for device operation and data acquisition.

The fuel used in this model combustor is natural gas. As is typical in using natural gas for fuel, air is used as the oxidizing agent in the combustion process. In addition, air is used as the primary cooling agent as well as the dilution jet cooling agent. Consequently, all of these air requirements are taken from the same source, a centrifugal blower that develops one psig while delivering two lbs. of air per second. The natural gas is supplied at 0.4 psig.

The injection points of the combustor exist in four distinct rows, three on the outer wall and one on the inner wall. The spacing between the dilution jet ports is different for each row. Each row is placed perpendicular to the length of the combustor on rays extending from the combustor centerline. Each row contains 21 ports each with an initial nozzle diameter of 7.11 mm.

The combustion process occurs 432 mm upstream

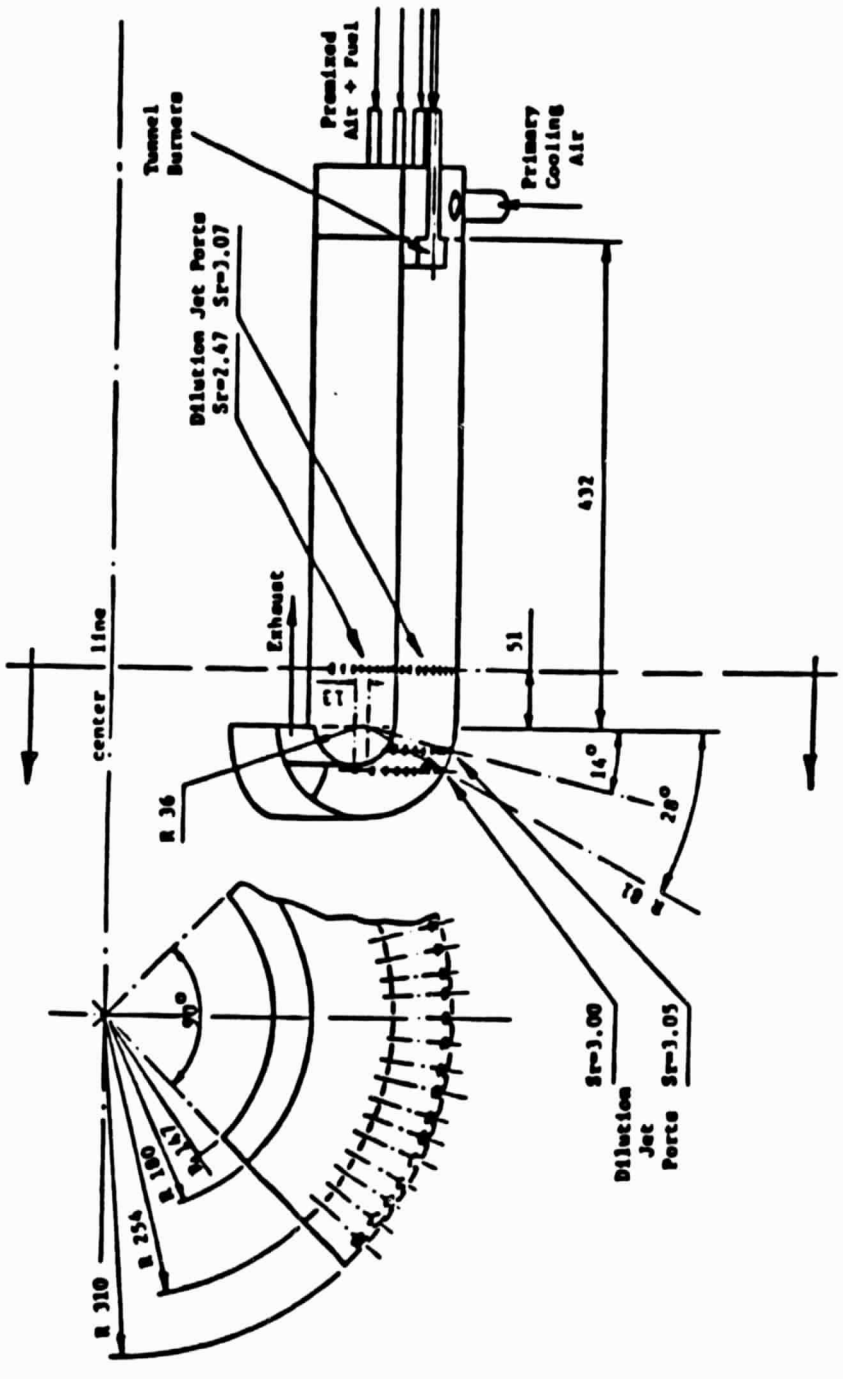

Figure 11: Principal Combustor Dimensions (mm)

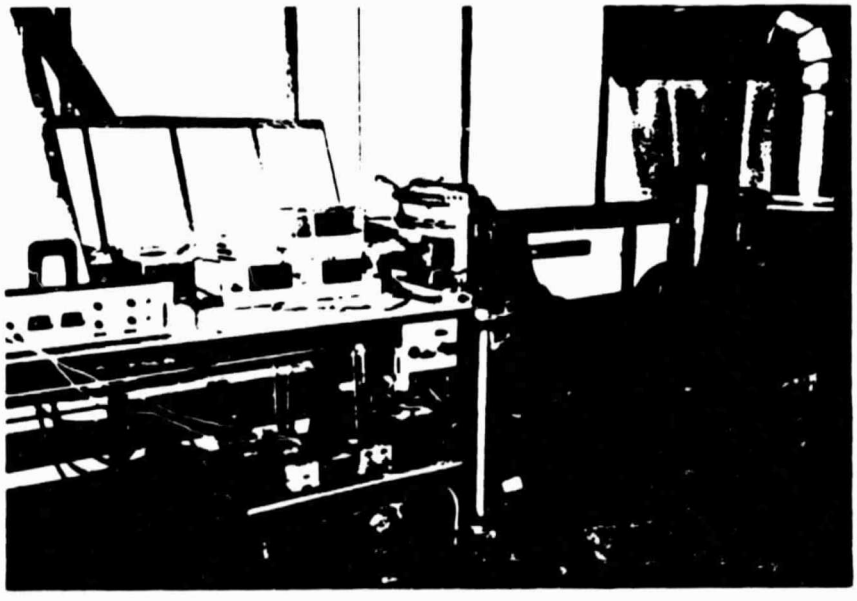

Figure 12: Photographic view of experimental apparatus

of the 180° bend in the combustor. At this point, nine burners are situated that deliver a mixture of natural gas and air that is slightly fuel rich. The mixing of air and natural gas for the premixied flame occurs outside the combustor. Although each natural gas burner has an adjustment to vary the quantity of fuel delivered, no such convenience exists for the combustion air delivery. It is assumed that an equal amount of air is delivered to each burner from the manifold-like apparatus that is attached to the end of the combustion air delivery pipe. Within the combustion chamber, the primary cooling air is delivered from a series of small holes that encircle each burner. It is thought that the hot combustion gas mixes with the primary cooling air as it moves down stream. Once again, there is no indication whether or not each primary cooling air delivery station is experiencing the same mass flux from the cooling air manifold. It may be seen later that this lack of information may result in a skewed temperature or velocity profile in the combustor before the turn and without injection.

As was stated earlier, all of these requirements are met by using a centrifugal blower.

This centrifugal blower delivers air to four pipes in a network. Each pipe is equipped with an orifice meter to determine its flow rate. The natural gas delivery is monitored in the same manner. Using an ASME[3] standard on orifice meters, calibration curves previously determined were verified. The pressure taps used in the orifice meters most closely approximate the corner tap type. The orifice plates used are sharp edged. The following table shows pipe and orifice sizes used for the experiment:

	Pipe(in.)	Orifice(in.)
Combustion Air	4.297	1.400
Cooling Air	4.297	2.418
Dilution Jet Air	4.297	0.904
Natural Gas	2.255	0.502

The procedure used to verify the calibration curves uses empirical information. Required information for this particular experiment includes inlet pressure before the orifice plate, specific weight of the flowing gas, orifice to pipe ratio, and a correlation coefficient taken from ASME[3]. Each of the orifice meters were calibrated in this way, and each matched within 0.5% the calibration

equations found in the previous experiment. Additionally, the following calibration equations represent the resulting curves:

$$\text{Combustion Air (Kg/s)} = 0.0030(h_{w,comb})^{1/2}$$

$$\text{Cooling Air (Kg/s)} = 0.0094(h_{w,cool})^{1/2}$$

$$\text{Dilution Air (Kg/s)} = 0.0012(h_{w,dil})^{1/2}$$

$$\text{Natural Gas (Kg/s)} = 0.0003(h_{w,natgas})^{1/2}$$

In the above equations, the values of h_w are the manometer readings and must be given in mm of water differential.

In a logical progression, the next topic to be discussed is the data gathering capability of the system. As shown in figure 13 below, a rake of probes is attached to a rotating and traversing mechanism.

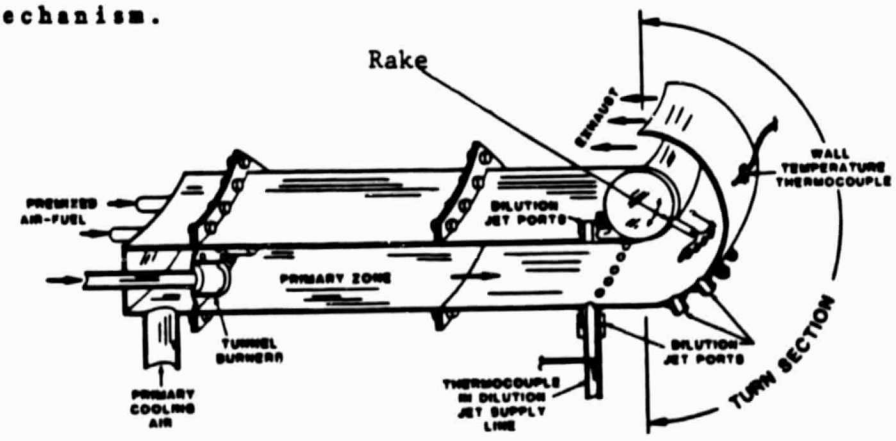

Figure 13[20]: Cutaway sketch of the combustor

Using figure 13 as a guide, a radial movement within the combustor is from wall to wall as shown by the arrow placed beside the five-probe rake. Azimuthal movement is an angular displacement through the turn as shown by the curved arrow.

The rake of probes consists of 10 distinct probes at five locations (spaced at 3.57 initial jet radii apart). As can be seen in figure 14, the probes are located 0.50 inches (12.7 mm) apart giving a total rake width of 2.00 inches (50.8 mm). At each location exists a pitot-static tube, 0.167 inches (4.24 mm) in diameter for the measurement of total and static pressure from which velocity can be calculated. Tack-welded to each pitot-static tube is a chromel-alumel thermocouple measuring 0.01 inches (0.254 mm) in diameter for temperature measurement of the flow.

Total and static pressure values from each tube are routed to five individual pressure transducers. The transducer used is Setra Systems High Accuracy model 239 for pressure ranging from 0 to 0.2 psid. An excitation voltage of 24 volts is required to operate each device. The output of the transducer ranges from zero to five volts and is directly proportional to the input delta pressure.

Appendix 2 gives full details of the device by presenting a factory specification sheet.

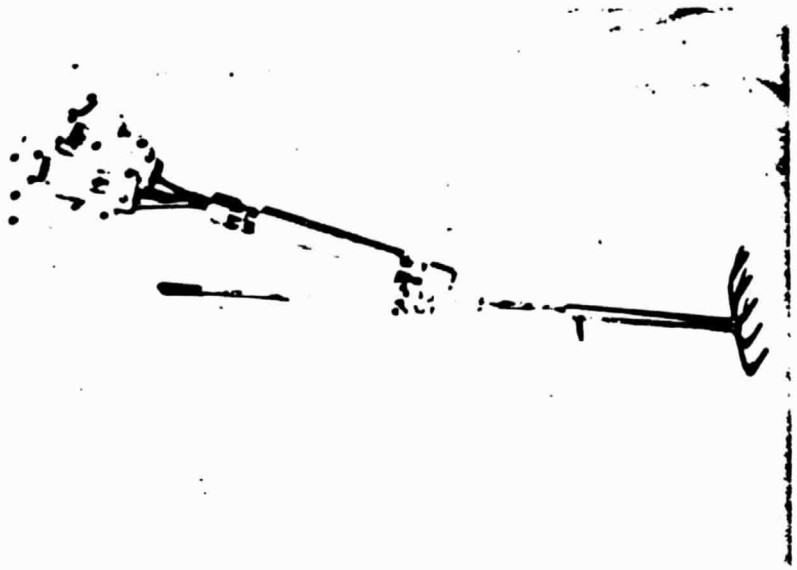

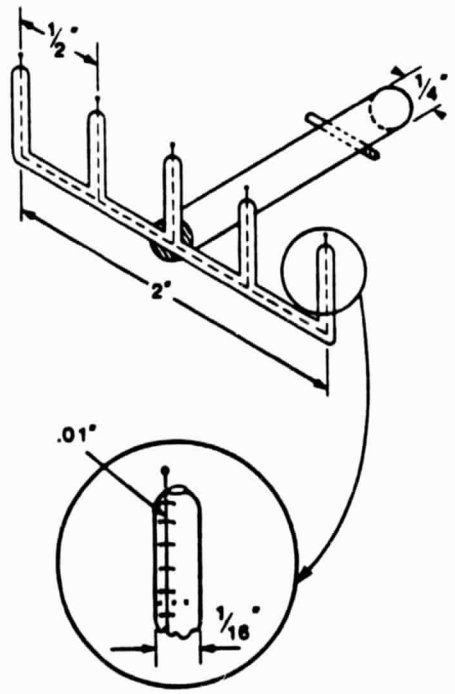

Figure 14: Pitot-Static/Thermocouple Rake

Each thermocouple is routed to a switching box and ultimately to a model 400A Doric Trendicator digital temperature measuring device. The Doric Trendicator is equipped with an analog linearizing circuit. This circuit reads the LED display of the device and outputs a voltage in millivolts identical to the number on the display.

All five transducer outputs and the five analog temperature signals are then routed to an IBM personal computer, model XT. Since the signals are analog, it is first necessary to process them through an analog to digital conversion system. The system used in this case is the Labmaster model manufactured by Tecmar, Inc. This particular board allows 12 bit accuracy. In addition, it is possible to channel the input signal through a programmable gain so that it remains as near full scale as possible for the most accurate conversions. The software used to take and process the data as it is converted or typed at the keyboard was written entirely by this author. Additionally, programming to output information as plots or in formatted form was written by this author.

The system also has some supporting apparatus that should be mentioned here. A major component

that was designed and built is a safety mechanism. Its basic purpose is to halt the flow of natural gas by closing an in-line electric gas valve when flame blow-out is detected. The schematic below describes the apparatus:

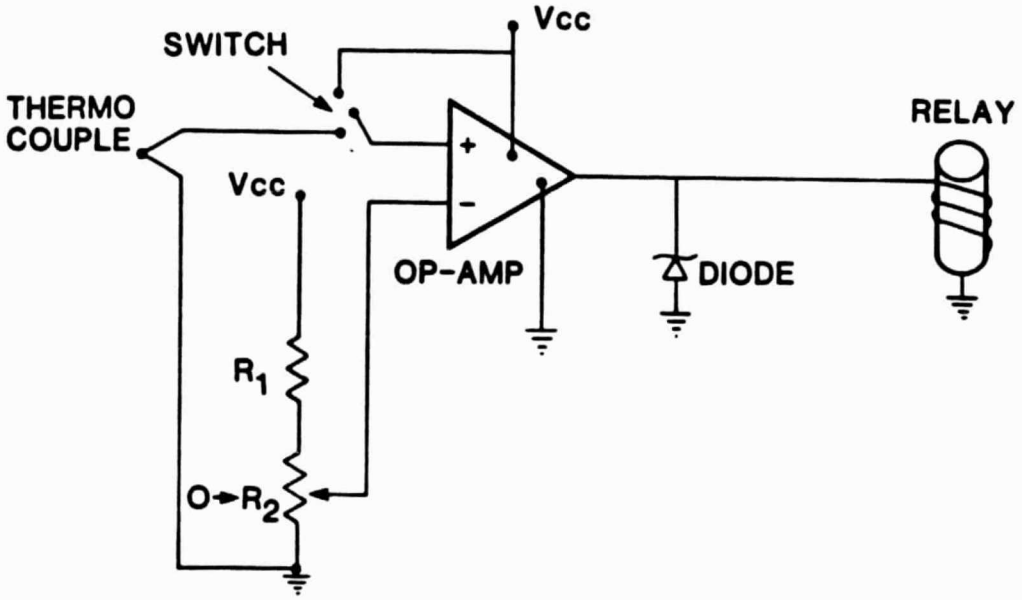

Figure 15: Safety control mechanism schematic.

Through the use of an operational amplifier, a comparator circuit was constructed. One input to the op-amp is the voltage generated across the junction of a thermocouple. The other input is an adjustable voltage for comparison. When the thermocouple voltage falls below that set by the adjustable one, the op-amp shuts down. This, in turn, cuts current to the relay that controls the

power to the natural gas valve thereby closing it.

Three DC power supplies are used in this experiment, as well. One is used to supply power to the safety control mechanism. The other two are mounted in the transducer panel supplying the required excitation voltage for them.

3.2. Experimental Procedures

When one wants to run an experiment using the model reverse flow combustor, one simply operates through a computer and a series of computer programs. This series of programs can be viewed in Appendix 4. Found in Appendix 3 is a detailed version of the experimental procedure including crucial start-up and shut-down procedures. The first general purpose of these programs is to create a means by which to acquire and store pressure and temperature data and calculate velocities. Secondly, proper storage gives the ability to later retrieve this information and print it so that each experiment can be properly and easily identified.

With the IBM XT at the experimental site, at the outset of each run, one must input relevant information via the keyboard. This information typically characterizes the experiment in progress.

Specifically, the following must be identified:

1. Filename
2. The row in which jets appear, if any
3. The number of dilution jets, if any
4. The number of unused jets between operating jets
5. Choice of azimuthal data taking increment.
6. Combustor pressure
7. Barometric pressure
8. Combustion air flow rate
9. Primary cooling air flow rate
10. Dilution jet air flow rate
11. Natural gas flow rate
12. Cooling jet temperature
13. Cross flow temperature
14. Six wall temperatures

The software saves these values for future reference. Additionally, the software performs all the necessary conversions to metric units as well as placing the manometer readings into the corresponding calibration equations. After displaying each calculated value, a provision is made for adjustments to the subsequent operating conditions. If any are required, all calculations are re-performed. Lastly, the software then sets up the data acquisition procedure. Automatically, five delta-pressures are taken from the five pitot-static tubes while temperature data is taken one thermocouple at a time. After the set is taken, velocity is calculated and appears immediately on

the CRT, and the whole group is sent to the storage file.

Since the azimuthal spacing increment through the combustor is chosen at the time of experiment, there is not a fixed number of data point locations. As an example, however, if one chooses 20° as the azimuthal increment (this was by far the most commonly used increment in this investigation), a total number of 76 rake locations results. With five probes on the rake, this generates 380 data points. In the chapter on presentation of data, these locations are identfied in detail. In addition, data point averaging and standard deviation calculations will be discussed.

In the above discussion, radial rake movement was defined. Figure 16 points out that this radial movement is not really radial with respect to the center of curvature of the inner wall or the outer wall of the combustor. This is a result of the probes extending into the flow 13 mm.

3.3. Experimental Preliminaries

As with any scientific investigation, there are a group of important quantities that tend to characterize the experiment. In this case, of

course, pressure and temperature measurements are taken so that detailed temperature and velocity fields can be examined within the combustor.

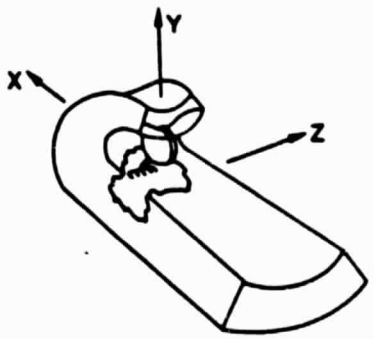

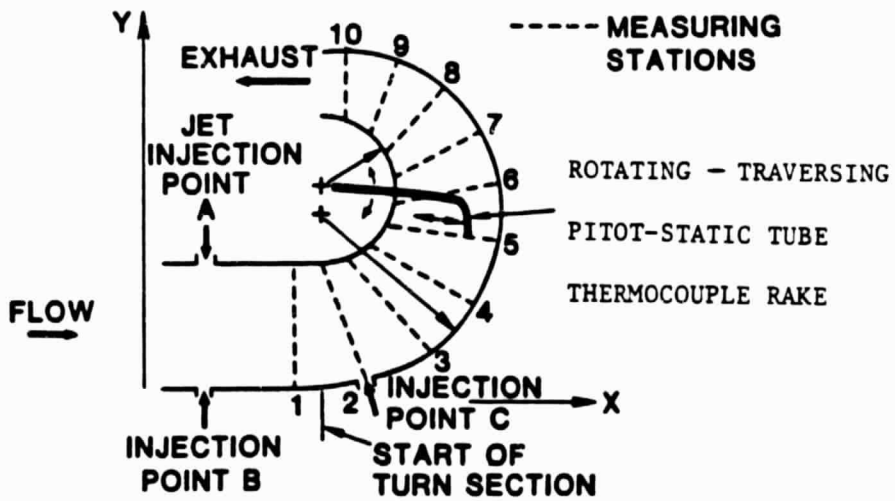

Figure 16: Combustor Coordinates and Measuring Stations[20]

However, in addition, there are governing quantities that provide uniqueness for each given procedure. The first of these quantities is the density ratio,

Dr, defined as:

$$Dr = \frac{\rho_{jo}}{\rho}$$

and is usually referred to as the ratio of the density of the injection fluid to that of the cross flow. In this investigation, this non-dimensional parameter typically is about 2.15 or 2.75. These two distinct values of Dr arise from using two distinct cross flow temperatures. Specifically, about 710°F (650 K) and 1020°F (820 K) are the common cross flow temperatures. The dilution jet injection occurs at room temperature, generally somewhere near 70°F(300 K). From this information, densities of both gasses are calculable through the ideal gas equation.

For each density ratio, experiments can also be characterized by momentum ratio, J, defined as:

$$J = \frac{\rho_{jo} V_{jo}^2}{\rho V^2}$$

This quantity is typically referred to as the ratio of the momentum associated with the jet initially to that of the cross flow. It typically ranges from zero (no injection) to about 11.7. The

cross flow velocity for this rig ranges from eight to 12 m/s while jet injecton velocities are normally between 12 and 22 m/s.

Thirdly, a characterizing parameter, injection jet spacing ratio, Sr, is defined as follows:

$$Sr = \frac{\text{Distance between jet centerlines}}{2b_o}$$

This variable in the operation of the combustor allows one to examine the effect of bringing individual jets closer and closer together. In addition to this variable, there is a variable concerning injection jet location. Injection can occur from the inner wall (the wall with the smaller radius of curvature in the turn section) prior to the bend or from the outer wall prior to the bend or in the bend.

With these characterizing parameters, the analysis of the acquired data is more sensibly accomplished since detailed information is available as to how the dilution jets compare with the cross flow.

With the acquisition of temperature, total pressure, and static pressure at five probe locations, local velocity is calculated as follows:

$$V_1 = \left[\frac{2(P_T - P_s)}{\rho_1} \right]^{1/2}$$

This relation for velocity is found from the Bernoulli equation. Of course, this assumes that the measured flow is incompressible and suffers from no frictional losses. In this investigation, Ma is typically 0.02 for the cross flow and 0.05 for the jet. With this information, it can be said that the compressibility effect on the accuracy of the velocity measuring device is negligible for this purpose. Also, since the Ma is much less than one, it can be said that there is never a significant deviation between impact and static temperatures.

One can now effectively characterize an experiment in the reverse flow combustor and have confidence in the quantities being measured.

Presentation of the data from this experiment is done in a variety of plots. Information plotted on them are generally normalized temperature and velocity profiles. The normalization for temperature is derived from the pattern factor Pf, a parameter used to examine temperature non-uniformity within combustion chambers. The pattern factor is defined as:

$$Pf = \frac{(T_{max} - T_{ave})}{(T_{ave} - T_{jo})}$$

The normalized temperature relation used here is defined as:

$$\tau = \frac{(T_1 - T)}{(T_{jo} - T)}$$

The normalization of velocity is as follows:

$$\gamma = \frac{V_1}{V} - 1$$

This normalization gives the deviation from the cross flow velocity anywhere in the combustor. Cross flow conditions are the temperature and velocity one finds at the first azimuthal measuring station, midway between the outer and inner walls. Figure 16 shows that the first azimuthal measuring location is the one immediately before the turn section.

For purposes of plotting simplicity, the combustor sketch shown in figure 16 was unwrapped, such that the inner wall became a straight line, and the outer wall became a mathematical curve moving closer to the inner wall depicting the area decrease that occurs in moving through the combustor. Shown in

figure 17 is a set of radial normalized temperature profiles characteristic of this combustor at the lower Dr with no dilution jet injection taken from the center probe of the rake. The numbers along the bottom curve (the outer wall) are the azimuthal abscissae locations corresponding to those in figure 16. Looking closely at the first azimuthal test location, one can identify nine tests points that move radially from the inner wall to the outer wall. The one nearest the inner wall is radial position 95, the next one toward the outer wall is 85 and so on until one arrives at that point closest to the outer wall which is labeled 15. As one moves azimuthally through the combustor, one can see that the number of radial positions decreases. At the exit, for instance, only five radial positions exist: position 95 at the inner wall through position 55 at the outer wall. The area decrease can be seen by noticing that the outer wall has moved significantly closer to the inner wall. More specifically, there are nine equally spaced (1.56 initial jet radii) radial positions at azimuthal stations one through five. Azimuthal station six has eight radial positions, azimuthal station seven has seven, azimuthal station eight has six, and

azimuthal stations nine and ten have five radial positions.

At the top of the plot is a set of information that characterizes the particular plot. In this case, we see Dr = 2.23 identifying the cross flow temperature, and a zero J due to the fact that there is no injection, and an Sr labeled "no injection" to avoid confusion.

Upon examining the profiles themselves, one can see that at each azimuthal station, the profile can move to the right or the left of the abscissa (lines drawn out by the probe tips during radial movement). Moving to the right indicates a temperature that is greater than the cross flow temperature. Moving to the left of the abscissa indicates that the local temperature has fallen below that of the cross flow (and τ has become positive). In the case of jet injection, it is not uncommon to observe profiles to the extreme left of their respective abscissae.

Examining figure 18, once observes a set of normalized velocity profiles for the same flow conditions as those for the temperature profile in figure 17. The plot is identical except for the magnitude of unity for the normalized quantity. In this plot, movement to the right of the abscissa

indicates a velocity that is greater than the cross flow velocity. Conversely, movement to the left of the baseline indicates a velocity magnitude less than that at the cross flow location.

Figures 19 and 20 make use of the five-probe rake. These plots are referred to as lateral representations of the flow conditions. Both figures 19 and 20 indicate normalized temperature profiles, but these can be made for velocity as well. In the case of figure 19, represented is the lateral span of the rake at one particular azimuthal location and one particular radial position. In figure 20, a three-dimensional view is constructed by using all the radial positions at a given azimuthal station. As can be seen on these plots, all the characterizing information is present including data locations.

Each "+" sign shown on the plots is a data point. Each data point, as discussed earlier, is constructed from various temperature and pressure information. In this experiment, every temperature and pressure measurement is actually an average of 25 samples. The analog to digital conversion software is set up so that 25 samples are taken, the average calculated and stored and the standard

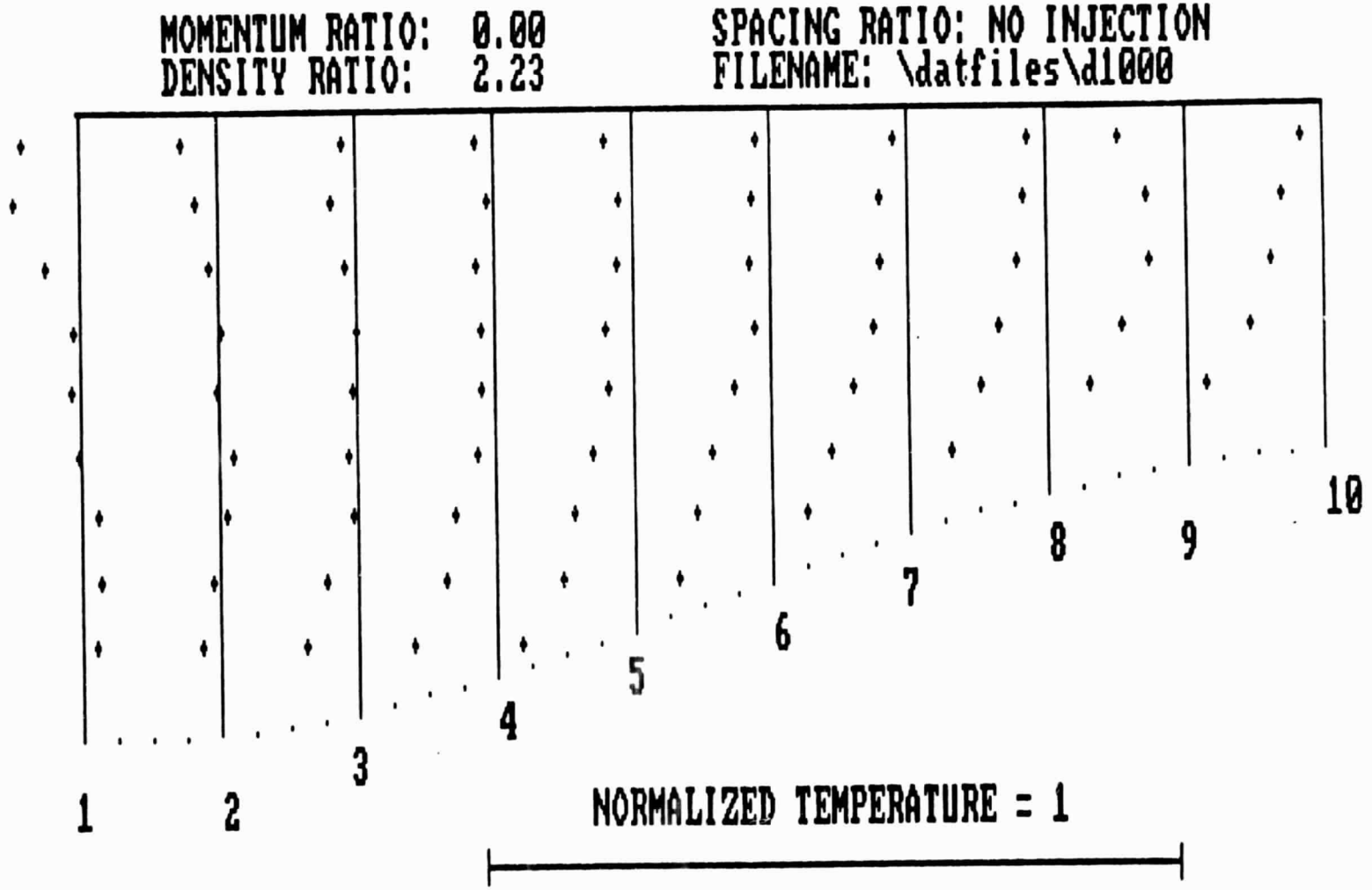

Figure 17: τ, No Injection.

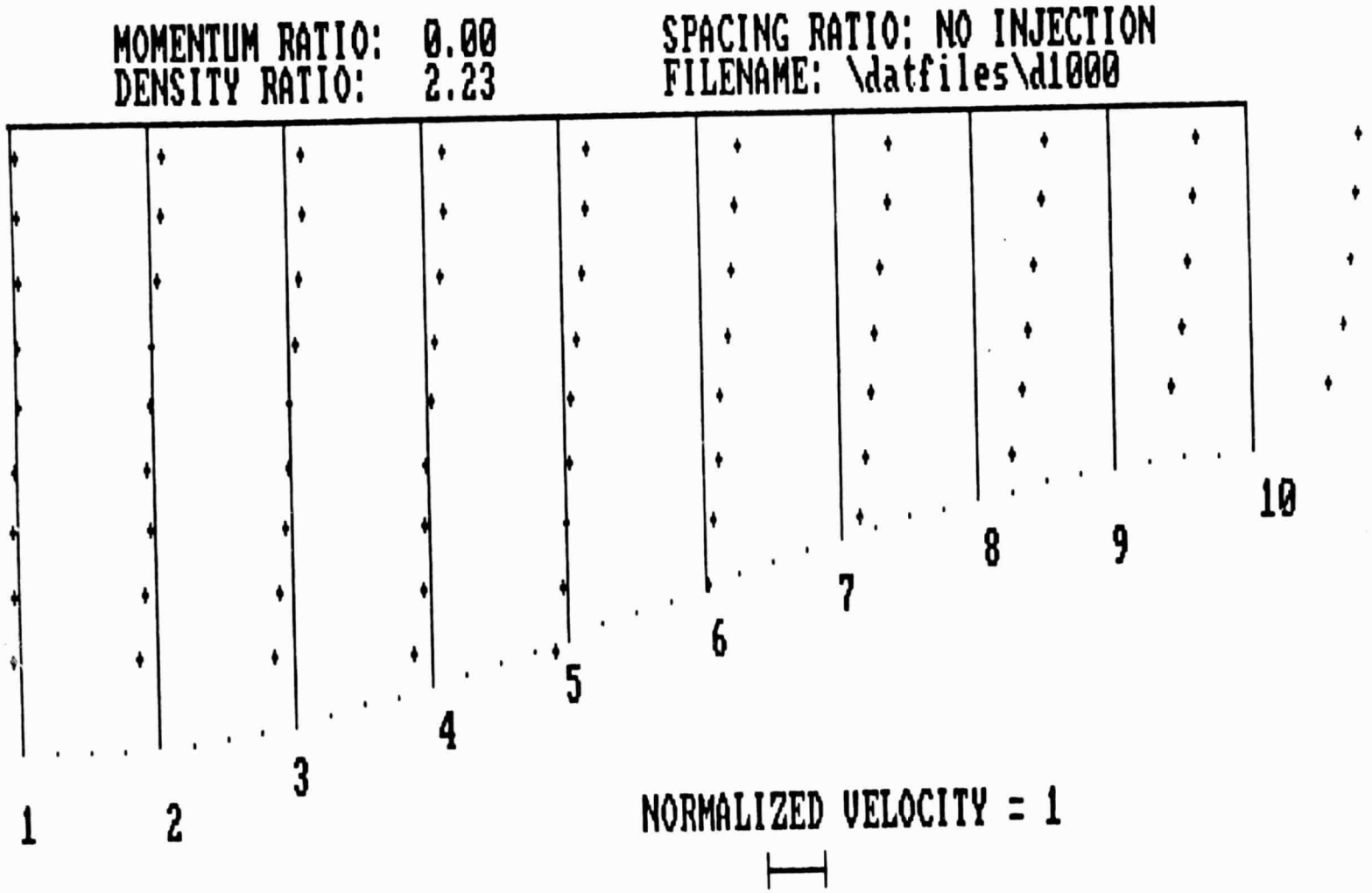

Figure 18: γ, No Injection.

deviation calculated and presented. This method of data acquisition allows the experimentor to obtain a reasonable average from fluctuating conditions. In addition, the calculation of standard deviation is helpful in the error analysis. Also, a growing standard deviation indicates some problem with the data gathering apparatus and allows one to search out the problem before it propagates through all the data.

3.4. Presentation of Expected Error

Using a conservative error analysis clearly documented in detail in Appendix 5, the following errors are expected. The values listed are percentages of the indicated quantity.

Temperature, $T \pm 1.2\%$

Pitot-static pressure, $P_T - P_s \pm 4.2\%$

Velocity, $V \pm 2.7\%$

Normalized temperature, $\tau \pm 6.5\%$

Normalized velocity, $\gamma \pm 6.6\%$

Momentum ratio, $J \pm 18\%$

Density ratio, $Dr \pm 6.4\%$

On the data plots, the error in τ corresponds to ± 3 data point widths. The error in γ corresponds to ± 0.25 data point widths.

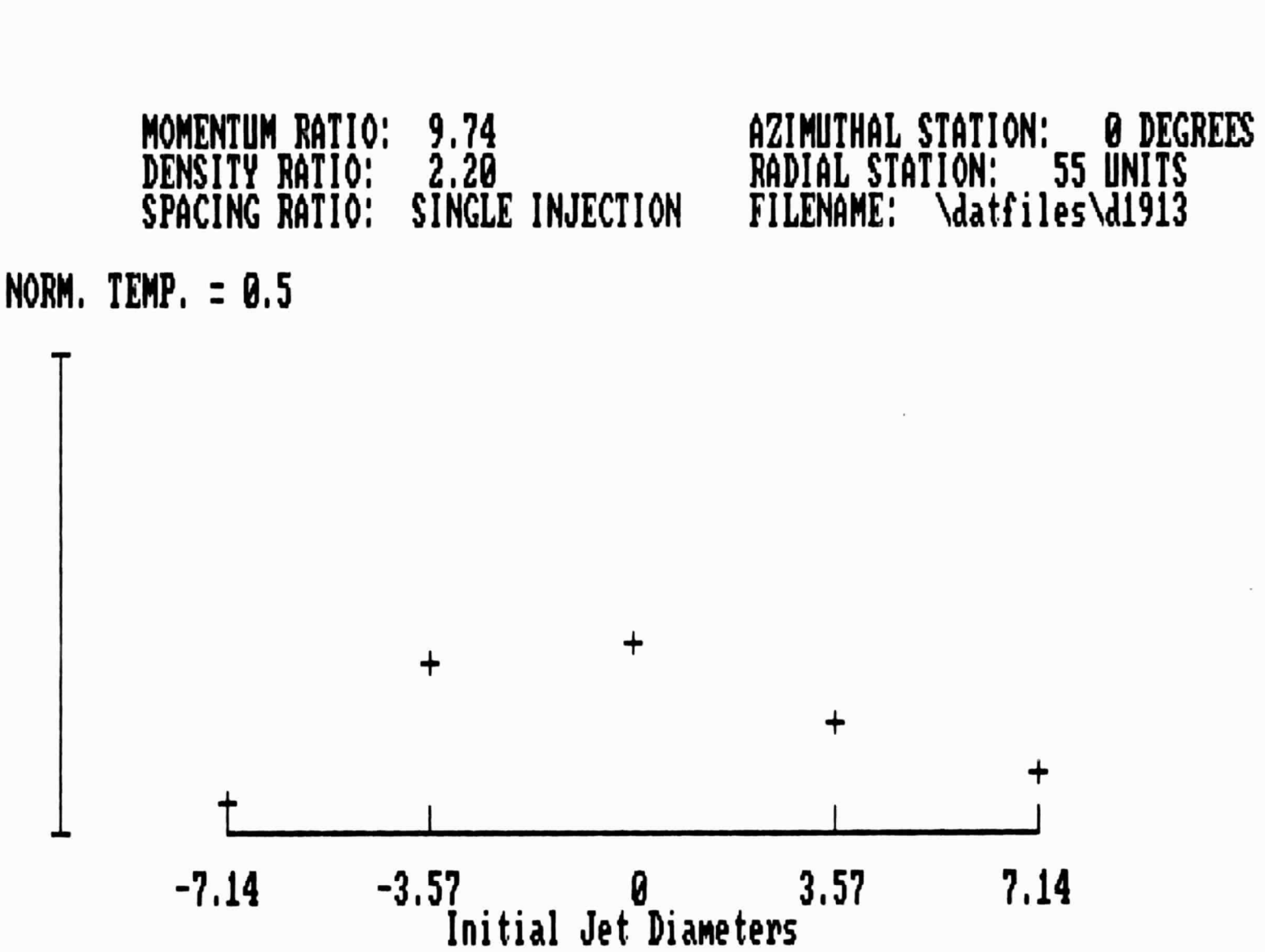

Figure 19: Representative Lateral Plot of τ, Outer Wall Prior to Bend, 0^{o}.

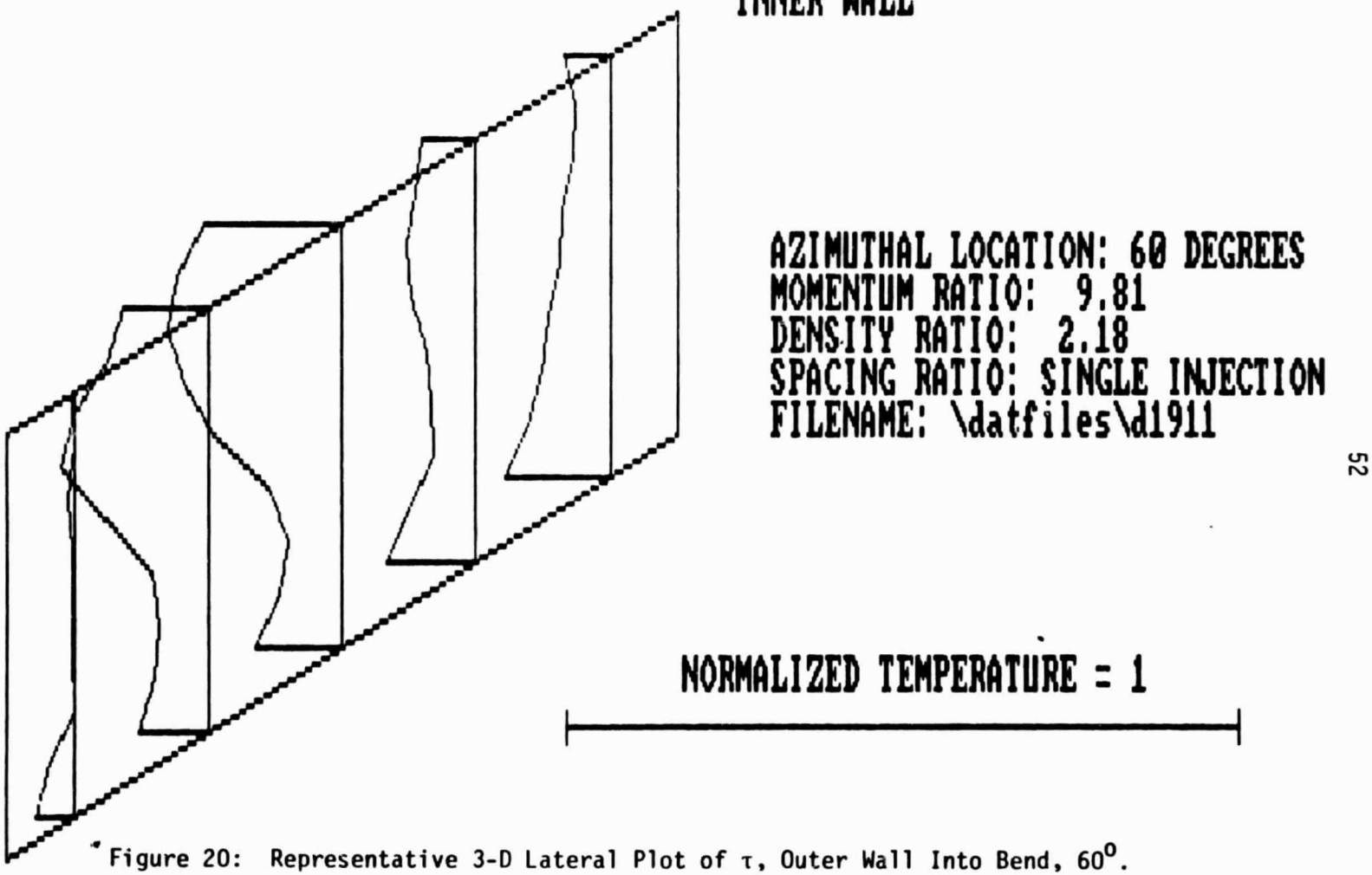

Figure 20: Representative 3-D Lateral Plot of τ, Outer Wall Into Bend, 60^{o}.

CHAPTER IV

CONCLUSIONS FROM PREVIOUS REVERSE FLOW COMBUSTOR STUDY

Prior to presenting data and conclusions from this investigation, a summary of the conclusions found from the previous temperature study[18] is given below. As a presentation of the model formulated in the previous work, calculated dilution jet trajectories are shown along with the experimental trajectories of this work where possible in the next chapter.

The summary is as follows:

1. Increasing density ratio gives rise to a deeper penetration of the jet into the cross flow.
2. Increasing momentum ratio gives rise to a deeper penetration into the cross flow.
3. Inward drifting phenomenon identified due to the nature of the flow accelerating along the inner wall.
4. Longitudinal acceleration suppresses single jet thermal spreading rate.
5. Confinement effect, measured by the ratio of channel height to initial jet diameter, suppresses trajectory as spacing ratio

decreases.

6. Smoothing of radial temperature gradients occurs far before the exit.
7. Tightly spaced row of jets injected from the inner wall attaches to that wall, shielding it from the outer hot stream. Injection from the outer wall penetrates deeply into the cross flow and does not attach to the outer wall.
8. Very low momentum flow injected from the outer wall tends to stay there through the turn.
9. Apparently, proper injection can result in a desired temperature profile.

CHAPTER V

SINGLE JET INJECTION DATA AND CONCLUSIONS

In this chapter, a representative group of single jet injection configurations will be examined in detail by looking closely at radial and lateral plots. To obtain a representative group, one must look at injection from the inner wall before the bend (14.67 initial jet radii upstream, point A in figure 16), injection from the outer wall before the bend (14.28 initial jet radii upstream, point B in figure 16), and injection from the outer wall into the bend (5.53 initial jet radii into the bend, point C in figure 16).

Enough information must be examined so that trends associated with changing momentum and density ratios become evident. In this section, spacing ratio is not important.

Below, find observations from individual tests with conclusions drawn from all of them at the close of the chapter.

5.1 No Injection

To properly analyze the effects of dilution jet

injection on flow conditions in the combustor, one must first examine the results associated with no injection. In figure 17, one can see that temperatures seem to be skewed near the inner wall just prior to the bend. Calculating the pattern factor for this position, one finds that the value never exceeds 0.07. Comparing this value to the typical value of 0.2 found in the exit patterns of operational combustors[18], it can be said the the oncoming cross flow has a relatively flat profile.

With movement downstream, one sees a decrease in normalized temperature, indicating that temperatures are falling below that of the defined cross flow. This decrease in temperature is attributable to heat losses through the combustor walls.

Examining the normalized velocity profiles presented in figure 18, the immediately obvious feature is that the radial profile at the first azimuthal station is quite uniform. As one moves downstream, an increase in velocity is detected from inner wall to outer wall. In addition, an increase in velocity at the inner wall with respect to the outer wall is observed. This phenomenon is attributable to the fact that the inertially

dominated flow attempts to negotiate the turn like an irrotational one. For this to occur, a greater acceleration at the inner wall with respect to the outer wall is necessary. It is also thought, that due to this greater acceleration, a drifting inward of mass is expected to satisfy conservation of mass. Lastly, pressure must increase from inner to outer wall to support the turning fluid.

Generally, to identify a temperature trajectory of cool injected fluid, one connects the minimum temperature at one azimuthal position to the minimum at the next. However, in doing this, one must be careful to consider the profiles with no injection to avoid choosing an inappropriate maximum τ. In identifying velocity trajectories, one connects the maximum velocities. In this case, one must clearly consider the increasingly skewed profiles that appear through the turn section. Typically, during injection, one sees a velocity decrease downstream of the wake created by the "cylinder" of fluid that obstructs the flow. As one moves from the injection wall, a jump in velocity is detected indicating probe movement out of the wake and into a region where velocities become greater than those expected with no injection.

5.2. Low Momentum Injection--Outer Wall--Prior to Bend

Examining figure 21, one can see that at azimuthal station one, all values of τ are affected except the two nearest the inner wall. These positions are showing a temperature decrease, and hence, a τ increase. Radial position 65 shows the maximum τ, thereby qualifying for the trajectory location.

At azimuthal station two, a significant temperature decrease occurs at radial positions 45 through 95 with a maximum τ occurring at 75. This shows movement closer to the inner wall.

At azimuthal station three, significant temperature deterioration occurs at positions 65 through 95 with maximum deviation occurring at position 85. Azimuthal location four shows lower temperatures at the inner wall with maximum τ occuring agian at position 85, showing the thermal trajectory quite close to the inner wall.

Azimuthal stations from this point to the exit show temperature decreases at the inner wall region, but no maxima can be identified. It can be said qualitatively that the injection jet does migrate toward the inner wall even at these locations, but

due to mixing in the radial direction, a trajectory is no longer meaningful.

Figure 22 shows the normalized velocity plot for this case. As indicated earlier, at the injection point, the jet acts as a flow obstruction to the cross flow, causing a low pressure, low velocity wake downstream. As one exits from the wake, one expects to experience a jump in velocity followed by some velocity distribution within the spreading jet. At the first azimuthal measuring station, one observes a significant decrease in velocity at radial positions 15 through 45. The jump is observed at position 55 with the maximum occurring at position 75.

At azimuthal station two, the jump is observed again, with maximum γ occuring at position 75. This choice for the trajetory location is a little less obvious. Position 75 also shows the maximum positive deviation from that for the no injection situation.

After azimuthal position two, some increased velocities can be detected but trajectories are no longer definable. In comparison to the temperature profiles, these show a much less drastic change due to injection. Trajectories are definable for a

lesser distance downstream as well. When one considers a free jet as a very crude approximation, one sees a deterioration in velocity proportional to the inverse of the distance from the virtual origin, giving velocities at the start of the turn section already much less than that of the cross flow. With this in mind, these velocity deviations seem reasonable.

5.3. High Momentum Injection--Outer Wall--Prior to Bend

Examining the temperature profiles for high momentum injection from the outer wall (J = 9.74), one observes that all the radial positions of the first azimuthal station are showing a temperature decrease. The maximum τ occurs at radial position 65, qualifying this as the trajectory position.

Radial position 85 shows the maximum temperature decrease at the second azimuthal station, while the brunt of the cooling seems to be at radial positions 45 through 95, near the inner wall. The indication here, again, is that the thermal trajectory is moving toward the inner wall.

At azimuthal station three, radial positions 65 through 95 indicate cooling due to injection. In

this radial set however, the maximum τ occurs at the radial position nearest the wall (95). This is somewhat suspect, but when comparing this profile to that for no injection, one can see that the temperature deviation is also greatest at this position. This verifies that with the higher momentum ratio, injection from the outer wall does in fact migrate to the inner wall. Downstream of azimuthal position three, one observes that cooling is more evident at the inner wall, but due to mixing, trajectory locations are no longer apparent.

Figure 24 gives the normalized velocity profiles for this injection configuration. Examining the first azimuthal location, the same wake phenomenon is evident. Wake flow conditions occur until a jump in velocity is detected at radial positon 65. From 65 to 95, flow velocities are higher than expected for the no injection configuration. Maximum γ occurs at position 75, the trajectory location.

Azimuthal position two exhibits a small jump in velocity near the inner wall at position 85. Already at this position, a maximum is not really detectable, nor is a maximum positive deviation from the no injection profile. The velocity trajectory,

then, is near the inner wall at this point, but is not technically definable.

Azimuthal stations three, four, and continuing downstream have smoothed so that no velocity deviation is detectable.

5.4. Low Momentum Injection--Inner Wall--Prior to Bend

Examining the temperature plots shown in figure 25 for inner wall injection at J = 5.80, one sees at azimuthal station one, a large temperature decrease in all radial locations but the one nearest the outer wall. Maximum τ occurs at radial position 65, labeling that position as the trajectory location.

Azimuthal station two exhibits a similar variance from the no injection profile with the greatest temperature deviation occurring at radial position 75, near the inner wall. This indicates that after a penetration into the cross flow, the jet begins to migrate back toward the inner wall.

Continuing with this thought, as one examines azimuthal positions three and four, one finds that maximum τ occurs at radial position 85 in both cases. This shows a continued movement of the thermal trajectory back toward the inner wall with movement downstream.

Further downstream, a definite cool region exists at the inner wall for quite a long distance. In fact, more cooling at the inner wall with respect to the outer wall is evident even at the exit. Apparently, mixing at the inner region is less than that at the outer wall.

Examining the plot of γ shown in figure 26, one should be aware of the profile for no injection. Upon observance of azimuthal station one, the expected wake is evident from the inner wall out to radial position 55. Recall that for injection from the outer wall, the wake region was located from the outer wall toward the center. The expected velocity jump does occur at radial station 45. This station also serves as the trajectory location since it is also the local maximum γ.

Azimuthal station two indicates a similar profile as above. Once again, the wake effect is evident at the inner wall from radial positions 55 to 95. At position 45, one sees a peak velocity and one that qualifies for the trajectory location.

After this point, smoothing of the velocity profiles causes difficulty in identifying trajectory locations. A quick observation here is that in the inner wall injection configuration, velocity

trajectories tend to deviate more from the temperature trajectories than in the outer wall injection case. Also, the velocity trajectory does not migrate as perceptably toward the inner wall as the temperature trajectory.

5.5. High Momentum Injection--Inner Wall--Prior to Bend

Figure 27 indicates at azimuthal position one a significant temperature deterioration near the inner wall. In this case, the maximum τ occurs at radial position 55, the first trajectory location. In this higher momentum case, all of the temperatures along the station have been lowered, giving rise to the idea of greater penetration due to greater momentum ratio.

Temperature profiles at azimuthal station two show a similar behavior but not quite as skewed as station one. Here again, all temperatures seem to be affected, but not to the same degree as in station one. The trajectory location is at radial position 55.

Azimuthal station three begins to flatten somewhat, but a maximum is still observable at radial position 65. Even azimuthal station four shows a maximum, also at position 65. After this

position, considerable cooling is seen throughout the combustor, although cooling at the inner wall is much more pronounced. This set of profiles shows that even at this elevated momentum ratio, a migration toward the inner wall is evident after a deep penetration into the cross flow.

Radial velocity plots shown in figure 28 for this injection configuration show behavior consistent with the temperature plots. Upon close examination of the initial azimuthal station, the lower wake velocity is observed at radial positions 55 through 95. At location 45 a jump in velocity occurs with γ peaking at position 35. Position 35 is marked as the velocity trajectory position.

At azimuthal station two, the expected velocity jump is seen near position 45 with the peak in γ occurring at radial position 35, clearly marking it as the trajectory location.

Downstream of azimuthal station three, the profiles begin to flatten out and take the form of those seen with no injection: a positive velocity gradient sets up from outer to inner wall.

5.6. Low Momentum Injection--Outer Wall-Into the Bend

This injection configuration differs from all

those presented earlier in that it delivers dilution cooling air from the outer wall 5.63 initial jet radii downstream of the start of the turn section.

Upon examining figure 29, the most obvious change is that the first two azimuthal measuring locations are nearly unaffected by the upstream injection.

Dramatically at station three, there exists a highly skewed profile with maximum τ occurring at radial position 35. Radial positions 55 through 95 show almost no temperature change whatsoever. This shows that penetration here is limited in comparison to the upstream injection locations. Obviously, maximum τ and the trajectory location are at radial position 35.

Azimuthal location four shows significant temperature reduction at radial position 55, the recognized trajectory position. Note here that temperatures at both walls remain near those observed with no injection. Little spreading of the jet has occurred by this azimuthal location.

Azimuthal position five, however, begins to show significant cooling along the inner wall, while the outer wall remains at its previous temperature. This serves as yet another confirmation of the

migration toward the inner wall, even with a relatively weak initial penetration. At this location, one can observe maximum τ and consequently the trajectory location at radial position 75.

Surprisingly, at azimuthal station six, a trajectory location can visually be located at radial position 75. In addition, significant cooling can be observed from radial positions 35 through 95. After this azimuthal location, cooling along the inner wall is clearly more prominent, but trajectory locations are no longer identifiable.

Figure 30 displays the normaized velocity profiles for this low momentum injection from the outer wall into the bend. First, no effect is noticed at the first two azimuthal locations. At location three, one sees the typical velocity decrease at radial position 15 due to a flow disturbance at the injection point. At radial position 25, a marked jump in velocity to above what is expected in the no injection configuration is observed. Although no maximum γ is seen, it is likely that the velocity trajectory location is near the inner wall.

Azimuthal position four and those further

downstream show no evidence of velocity trajectories, with the profiles resuming the typically irrotaional one of the no injection plot.

5.7. High Momentum Injection--Outer Wall--Into the Bend

The temperature profiles shown in figure 31 present results for J = 9.81. Just as in the case of low momentum injection into the turn section, no detecable change occurs at the first two azimuthal stations while the third sees a major temperature decrease. Positions 65 through 95 appear unaffected at station three, with skewing beginning at station 55 and the maximum τ occurring at position 35. Note that this trajectory, as well as all the others, is marked on its associated baseline.

Azimuthal station four shows marked skewing as well, with its maximum τ occurring at radial position 75, showing a definite migration of the high momentum injection toward the inner wall.

Azimuthal locations five and six show an increase in τ as one moves toward the inner wall. In both cases, maximums occur at the radial position nearest the inner wall (95) or at most, one position away from the inner wall (85). Again, this is strong evidence suggesting migration toward the

inner wall.

Figure 32 shows the normalized radial velocity profiles for high momentum injection into the bend. As is true with all the velocity profiles, variations are somewhat subtle. At azimuthal station three, the jump in velocity and maximum γ occur at radial position 25. This, then, is the location of the trajectory.

Examining azimuthal station four, one sees a marked increase in velocity near inner the wall with the jump occurring at position 75. The local maximum is observed at position 85, giving it the velocity trajectory identification. Further downstream, some velocity increase is detectable near the inner wall, but not significant enough to choose trajectory positions.

5.8. Conclusion From Normalized Radial Profiles

To this point, various representative flow configurations for single jet injection have been discussed in detail. In each subsection of this chapter, normalized radial temperature and velocity profiles were the basis of these discussions. Thermal and velocity trajectories were defined where possible. At this point, it is necessary to look at

all the profiles, and make conclusions concerning the general bahavior. In summary, the following conclusions are evident from these profiles:

1. Without injection, temperature profiles show a pattern factor within reasonable limits set up by operational combustors. Generally, a low temperature region exists along the outer wall of the combustor due to heat transfer through the walls. Velocity profiles show a fairly uniform condition at the inlet to the turn section. As the inertially dominated flow attempts to negotiate the turn like an irrotational one, particles at the inner wall must accelerate with respect to those at the outer wall. This gives rise to an increase in velocity at the inner wall with respect to the outer wall. In addtion, an area decrease through the turn section causes an increase in velocity. As the acceleration occurs along the inner wall, conservation of mass calls for a movement of fluid toward this region. Also, pressure increases as one moves from inner wall to outer wall in the turn section.

2. The injection of cooling air at the inner wall before the bend, the outer wall before the bend, and the outer wall into the bend all cause significant

changes in temperature and velocity downstream of their respective injection locations.

3. The greater the momentum ratio, the deeper the penetration into the cross flow according to both temperature and velocity profiles.

4. The greater the density ratio, the deeper the penetraton into the cross flow.

5. Migration of the injection jet toward the inner wall occurs during injection from all locations. This indicates that the centrifugal effect of a heavier fluid naturally moving toward the outer wall of a turning channel is overcome by the pressure and migration effects discussed in (1).

6. Both thermal and velocity trajectories allow one to make the same statements concerning jet movement in the cross flow, although they rarely coincide. for all azimuthal stations.

7. Although still qualitatively consistent, velocity and temperature trajectories show a greater deviation from each other during injection from the inner wall. The velocity profiles typically show a deeper penetration and a slower return to the inner wall than the temperature trajectories. This is due to the recirculation zone that is set up downstream of the injection location. During injection from

the inner wall the trajectory moves back through the radial positons associated with the wake region, but further downstream.

8. During injection from the inner wall, cooling and increased velocities are more apparent along the inner wall even at the exit giving rise to the conclusion that a jet injected from this wall experiences less mixing due to its position.

9. Velocity and temperature profiles at azimuthal stations nearest the exit for outer wall injection prior to the turn and in the turn are quite similar for similar injection conditions.

10. Lipshitz[18] developed a model to predict the centerline of an injected jet from conservation equations and empirical relations. Three velocity and three temperature plots from those discussed above have computed model trajectories marked on them for comparison. Agreement is poor for all cases except velocity trajectory from the inner wall. In this case, though, too few velocity trajectory locations are identifiable for a conclusive comparison.

5.9. Lateral Distributions

Also plotted for various azimuthal locations in

the combustor are lateral plots that make use of the five-probe rake. With these plots, one can view laterally across the combustor at given radial and azimuthal positions. In addition, one can view laterally all of the radial positions at a given azimuthal station resulting in a three-dimensional plot of combustor conditions. Ten of these plots, each for one of the ten azimuthal stations, gives a three dimensional plot of combustor conditions for the entire turn section.

Plots of this type were generated for various azimuthal positions downsteam of injection to investigate jet spreading behavior.

Upon examining the three-dimensional plots for no injection (figures 33 through 36) plotted at 60° increments from the start of the turn section to the exit, one observes that there is a non-uniformity laterally across the rake width. From prior to the turn continuing completely through the combustor to the exit one sees that this three-dimensionality takes the same form: an increase in τ when going from -7.14 initial jet radii to 7.14 initial jet radii across the combustor centerline. Each plotted line represents a probe location. Probe one is at the far left and is -7.14 initial jet radii from the

combustor centerline. Probe five is at the far right and 7.14 initial jet radii from the combustor centerline. Probes two, three, and four fall logically between these two.

As indicated in the radial velocity plots, combustor velocity is fairly insensitive to single jet injection more than two or three azimuthal stations (40° to 60°) downstream of the injection point. Therefore, only thermal plots will be used for investigating lateral spreading.

When examining the plots for low momentum injection from the outer wall (figures 37 through 40), the most obvious change occurs in figure 37 (first azimuthal station). Probes two and three show a significant temperature decrease, while the others remain relatively unaffected. This results in a three-dimensional look to the plot, and indicates that jet spreading is still quite limited at this point.

At 60°, the plot shows the flow returning to the condition seen in the no injection plot, where decrease in temperature is detected in going from probe one to five. However, upon careful examination, one can see a definite increase in temperature when going from probe four to five,

giving evidence that lateral spreading is not complete. The plots for 120° and 180° show that the temperature distribution has returned to one similar to that for no injection, indicating that spreading across the rake width is complete.

The set of plots for outer wall injection at a high momentum ratio (figures 41 through 44) shows similar behavior to the low momentum configuration. At the high momentum ratio, though, lateral spreading seems complete at an azimuthal value of 60°. This is faster than the low momentum configuration.

Three-dimensional lateral plots for injection from the inner wall at a low momentum ratio (figures 45 through 48) and at a high momentum ratio (figures 49 through 52) show similar behavior. In both of these cases, lateral spreading does not seem complete at 60° . By 120°, however, profiles look no different than those for no injection, indicating that lateral spreading has surpassed the width of the rake.

Finally, from the plots above, individual radial positions can be identified and plotted. Two plots with low momentum injection from the outer wall and two with high momentum injection from the

inner wall are presented (figures 53 through 56). In figures 53 and 54 one can see that the center probe temperature regains temperature in moving from 0° to 100° azimuthally. In this case, the outer probes do not detect a significant change in temperature. Figures 55 and 56 show similar plots for high momentum injection from the inner wall. In this case, the center probe temperature also shows a rebounding toward the cross flow value. The outermost probes indicate a more significant decrease in temperature this time, giving evidence of wider spreading.

5.10. Additional Conclusions From Lateral Plots

11. Lateral spreading rate increases with increasing momentum ratio. This is in agreement with the experiment by Kamotani and Greber[14].

12. Lateral spreading rate is greater for outer wall injection than for inner wall injection. This observation confirms conclusion eight above, indicating that mixing is greater at the outer wall region than the inner wall region.

In the following chapter, multiple jet injecton will be considered. There, lateral plots will become important again in the determination of two-

dimensional behavior of a closely spaced row of jets and how this affects trajectory.

CHAPTER VI

MULTIPLE JET INJECTION DATA AND CONCLUSIONS

All of the introductory information that pertains to single jet injection such as definitions for τ and γ as well as numerical values for pattern factors apply here as well. Once again, as the flow irrotationally negotiates the turn section, acceleration of fluid particles along the inner wall with respect to the outer wall occurs. From mass conservation, a migration of fluid inward is evident. Additionally, an increase in pressure is experienced when going from inner wall to outer wall to support the turning fluid.

As was true for single jet injection, experiments were carried out at momentum ratios from about 3.7 to about 11.7. Density ratios ranged from about 2.15 to about 2.75. With multiple jets, though, two more parameters become a part of the investigation: spacing ratio and confinement ratio. Spacing ratio, Sr, defined above, varied from 2.67 to 9.21. Each injection configuration was tested in three spacing ratios: the smallest, followed by double that, followed by triple that. Values for spacing ratio differ from outer wall to inner wall

since injection ports are positioned on rays extending from the combustor centerline.

Confinement ratio, defined as:

$$\text{Confinement Ratio} = H_o/b_o$$

is 16.77 for injection prior to the bend and 16.95 for injection into the bend.

Data acquisition procedures, plotting procedures, and trajectory identification procedures are identical to those used in single jet injection.

Upon examing the data and conclusions from single jet injection, one can see the effects of changing momentum ratio and density ratio. Therfore, it is unnecessary to present data that displays the effects of changing these parameters. Instead, injection location and spacing ratio will be the variables here. On each plot, though, two trajectories are marked. One is that for the row of jets, and the other is for the single jet for comparison.

6.1. High Momentum Injection--Outer Wall--Prior to Bend

This section contains information on three different spacing ratios for this flow

configuration. First examining the normalized temperature profile with the widest spacing ratio shown in figure 57 one discovers as spacing ratio of 9.21. The profiles are inevitably similar to those of a single jet. The trajectory location (maximum τ is at radial positions 55, 75, and 85 for azimuthal location one, two, and three respectively. Comparing these locations to those found in single injection, one finds that the obvious difference is a shorter penetration, and a continued "lower" trajectory. Even though some suppression of trajectory is detected, a cooling region along the inner wall is evident even as far downstream as the exit.

The velocity profiles for this configuration (figure 58) are also quite similar to the high momentum single injection profiles. In this case, the velocity jump at azimuthal position one occurs at radial position 55. The maximum γ occurs at radial position 65. Looking closely at azimuthal positions two and three, one can see that the radial positions closest to the inner wall actually show no change in velocity. However, at position two, radial location 75 is seen as having the greatest positive deviation from the no injection velocity.

At position three, radial location 75 is indicated as having the largest positive displacement from the no injection velocity. Although these positions do not stand out as definite local maximums, they are likely trajectory locations by comparison to profiles with no injection. Further downstream, one can no longer identify with any certainty any trajectory location, but a noticeable velocity increase along the inner wall is evident. From the velocity trajectory estimates in the previous chapter, one can see an apparent ''lower'' penetration amounting to at least one radial position.

Remaining at high momentum injection from the outer wall, the spacing ratio is decreased to 6.14 by adding four jets for a total of 11. The question to ask now is how does this affect the flow within the combustor.

Looking at the temperature profile diagram shown in figure 59, a marked increase in τ is detected about midway between combustor walls at azimuthal station one. At radial position 55, τ peaks, giving the thermal trajectory location. Similarly, position 75 at azimuthal station two qualifies as the second trajectory location.

Azimuthal position three becomes a little more difficult to analyze since the maximum local τ actually occurs at the endpoint (position 95). By comparison with the no-injection configuration, it can be seen that the trajectory really cannot be pinpointed. However, positions 75 through 95 indicate the most temperature deviation. It is likely, then, that the trajectory falls somewhere between these two radial positions.

At azimuthal measuring station four, a peak is again detectable as a trajectory location at radial station 85. Marked cooling is detected downstream across the combustor with the inner wall region affected the most. In comparison with single jet temperature profiles, this spacing ratio does not produce noticeably different results from the larger Sr. The initial thermal trajectory location shows some suppression. This mild suppression seems to be carried downstream as well.

The velocity profile (figure 60) at azimuthal station one displays the typical jump in velocity at radial point 55. Position 65 is near the peak γ and deviates the greatest from the no injection configuration, giving indicaiton as the trajectory location.

At both azimuthal stations two and three, velocity trajectory locations are difficult to detect. However, upon careful examination, it appears that trajectories lie somewhere between radial positions 65 and 95 due to increased velocity in this region. The initial trajectory location shows evidence of some suppression by appearing one radial position lower than in the single jet case. Velocity trajectory locations downstream of the initial one cannot be identified clearly enough, so a statement concerning suppression in this region cannot be made.

Once again, keeping with high momentum injection from the outer wall, the number of jets is increased to 21, producing a spacing ratio of 3.07. This is the smallest value for this parameter for jets injected from the outer wall before the bend. Examining the normalized profiles for this case (figures 61 and 62), trajectory suppression is immediately evident.

The radial temperature profiles show a peak τ at radial position 25 for the first azimuthal station. The second azimuthal abscissa shows an obvious peak at radial position 45. Radial position 55 is the maximum τ for azimuthal station three.

These three trajectory locations marked on figure 61 show a significant suppression in comparison with the single jet case. By the third azimuthal station in the single jet case, the trajectory was identified as existing along the inner wall. For 21 jets, though, the trajectory is located only at the midpoint between the two walls.

Upon examining the velocity profiles, one does not find such a dramatic change in trajectory location. At azimuthal position one, the velocity jump occurs at radial location 35. Velocities 55 through 95 appear fairly uniform. In contrast, with no injection, velocity increases in going from 55 to 95. The point with the largest deviation from from the no injection profile is position 65, identifying this as the location of the trajectory.

At azimuthal baseline two, one observes the velocity jump at radial position 55. Points 65 through 95 display an increase over the no injection case, with no particular γ exhibiting a maximum. It is concluded that the velocity trajectory must fall somewhere between radial points 65 and 95, with the exact location unidentifiable.

Azimuthal station three is similar to two in behavior with the trajectory locaiton falling

between radial positions 75 and 95. As one moves downstream, an increase in velocity is observable at all radial locations. This behavior gives some evidence of suppression, but nowhere near the magnitude of suppression displayed in the thermal profiles. In addition, with this large number of injection jets (21), the increased mass flux is indicated by the noticeably higher velocity as far downstream as the exit.

6.2. High Momentum Injection--Inner Wall--Prior to Bend

Due to a probe problem, only pressures were obtainable from the rake for multiple jet injection from the inner wall. So that some statement could be made concerning the relative behavior of multiple jets from the inner wall, temperature data was taken from Lipshitz[18]. This temperature data was then used to calculate a local density which, in turn, was used in the calculation of local velocity. Due to probe geometry differences between the previous temperature study and this study, it becomes evident that probe tip location for each case differs by two to three millimeters. It is estimated, that as a maximum, this could result in a local temperature error of 100°F near the injection point. This

results in an additional error in local velocity of about 5%, according to the procedure used in estimating error in Appendix 5. The error in γ then increases to about 19%. However, this still results in a error band on the normalized velocity profiles slightly less than the width of one data point. Therefore, qualitative trends depicted by these profiles remain believable.

Following the same procedure as earlier, using a high momentum ratio (9.68) and the low density ratio (2.18), each of the three possible spacing ratios are investigated. The injection of seven jets results in a spacing ratio of 7.41, a relatively large value. Normalized temperature profiles seen in figure 63 show that at azimuthal position one, the maximum τ occurs at radial position 75, indicating a shallow penetration.

Azimuthal position two shows a maximum at the same radial position. Strikingly, from azimuthal abscissa three and continuing downstream, the maximum τ occurs at position 95, against the inner wall. It appears as if the thermal jet trajectory, then, is directed along the inner wall as well. In comparison with the single jet thermal trajectory for a similar momentum ratio, considerable

suppression of trajectory is evident, even at this wide spacing ratio.

The velocity profiles, again in this case, do not show such a dramatic suppression (see figure 64). The velocity jump at azimuthal baseline one occurs at radial position 65, with the maximum deviation from the no injection velocity occurring at position 45.

Azimuthal station two shows similar behavior with maximum γ occurring at radial position 55. Station three also has a trajectory location at position 55. Downstream of position four, increased velocities across the combustor are detectable.

In comparing these velocity profiles to temperature profiles for the same set of flow conditions, one sees that they predict a much deeper penetration than their thermal counterparts. However, in comparing them to the velocity profiles for single jet injection, one sees that a suppressed behavior is evident.

Decreasing the spacing ratio to 4.94 by increasing the number of dilution jets to 11, one would expect further suppression in accordance with what occurred during injection from the outer wall. Examining the first azimuthal station of the

temperature profiles (figure 65), one observes a maximum τ at radial position 75. Position two shows the maximum τ at radial position 85, identifying both of these positions as trajectory locations.

Position three and those downstream show the maximum τ falling against the inner wall, showing a suppressive behavior in comparison with the single jet. However, this thermal trajectory suppression is apparently no greater than the wider spacing ratio configuration.

The velocity profiles shown in figure 66 depict trajectories appearing at radial position 55 for the first three azimuthal baselines. This, again, shows suppression in comparison with the single jet, but no appreciable difference from the 7.41 spacing ratio. Also, as above, the velocity trajectories indicate a deeper penetration into the cross flow.

By using 21 cooling jets, a spacing ratio of 2.47 is achieved. Upon examining the temperature profiles in figure 67, one finds the most striking change in profiles thus far. At all azimuthal baselines, without exception, the maximum τ occurs at radial position 95, indicating quite a significant suppression of thermal trajectory. Single injection of the same momentum ratio normally

produces a trajectory somewhere near the midpoint of the combustor.

Examining the velocity profiles given in figure 68 for this flow configuration, dramatic suppressive behavior is again detected. At the initial azimuthal station, velocity is seen to peak at radial position 55. Azimuthal position two shows maximum velocity occurring at position 65. Position three indicated radial location 75 while positons four and five both show radial position 85 as the location for maximum γ. As can be seen by the indicated trajectory for the single jet, these profiles, too, show supression so great that velocity trajectory as well moves very near the inner wall.

6.3. High Momentum Injection--Outer Wall--Into the Bend

Again following similar procedures as above, the first configuration to be discussed is the one with the widest spacing ratio. Upon examining the temperature profile diagram in figure 69, it is easily seen that injection occurs just upstream of the third azimuthal station. A huge temperature decrease is detected at this station, with τ peaking at radial position 35.

Azimuthal station four gives the peak τ at radial position 75, indicating the trajectory is moving toward the inner wall. Azimuthal station four, then, depicts radial position 75 as its trajectory location as well, while station five indicates position 85. In comparison with the single jet injection configuration, there is no perceivable difference in penetraion into the cross flow as is obvious during injection prior to the turn section.

The velocity profiles in figure 70 are just as difficult to interpret as those were for single jet injection. Although not clear, radial position 25 is the likely location for the velocity trajectory at azimuthal position three. Even less clear, azimuthal positon four indicates a likely trajectory position as 75, the position with the maximum deviation from the no injection configuration. In agreement with the thermal trajectories, these do not indicate any suppressive behavior.

Adding four jets to the earlier seven, one achieves an Sr = 6.00. At the injection locations prior to the bend, a decrease in spacing ratio generally led to a suppression of the jet trajectory in the cross flow. Upon examining the normalized

temperature profiles in figure 71, one sees the skewed temperatures at azimuthal station three. Incidentally, both temperature and velocity appear unchanged upstream of injection throughout the course of multiple jet injection into the bend.

Azimuthal station three shows radial position 35 serving as the trajectory location by exhibiting the maximum τ. Position four also shows quite a skewed profile with its maximum τ appearing at radial position 65. Both azimuhtal positions five and six show trajectory locations at radial position 75. With this trajectory, suppresive behavior is becoming evident.

The velocity profiles (figure 72), as in the past, show nowhere near the dramatic change seen in the temperature profile. At azimuthal station three, the maximum local γ occurs at radial position 25. The next azimuthal station shows a clear trajectory location at radial position 75. Downstream of this location, it becomes impossible to define a trajectory. With the trajectory located as it is, however, a slight supression of approximately one radial position is observed. Although some suppression is evident, migration of the jet toward the inner wall remains intact.

The final spacing ratio at this injection location is 3.00. It is achieved by injecting 21 jets. In figure 73, one sees the first thermal trajectory location at azimuthal station three is found at radial positon 25. Azimuthal station four shows the maximum τ at radial position 45. Downstream of this location, a trajectory is no longer definable. Although cooling exists across the combustor, one sees easily a marked increase in cooling at the outer wall. The trajectory pointed out by this set of data shows a definite suppression toward the outer wall.

The velocity profile seen in figure 74 is similar to those observed above. Azimuthal station three shows the velocity trajectory at radial position 25. Radial position 65 is identified at azimuthal positon four as the trajectory location by exhibiting the maximum γ. Downstream of this azimuthal station, the trajectory is no longer meaningful. However, with the trajectory shown, it is easy to conclude the some suppression toward the outer wall takes place. This suppression does not stop the migration toward the inner wall.

6.4. Conclusions From Normalized Radial Profiles

To this point, a representative group of tests examining the effects of spacing ratio have been closely examined. Each test was looked at individually. At this time, it is important to make some general statements concerning these tests:

1. As was expected from Lipshitz[18], trajectories determined from velocities generally show a greater penetration into the cross flow than those determined from temperature. This seems to be a result of the recirculation zone set up downstream of the injection location by the issuing dense jet.
2. This deviation increases as spacing ratio decreases since the low pressure recirculation zone becomes more pronounced as the jet becomes increasingly two-dimensional.
3. Injection from the inner wall shows penetration into the cross flow, followed by a migration back toward the inner wall. As spacing ratio decreases, this penetration becomes suppressed. At minimum spacing ratio, the maximum τ occurs at inner wall without exception.
4. For injection from the outer wall, one can identify migration toward the inner wall as well. Again, as in the single jet configurations, this is attributed to the drifting and pressure gradient

effects overcoming the centrifugal effects. As Sr decreases, there is a noticeable suppression toward the outer wall, but migration toward the inner wall remains evident.

5. This suppression is attributed to two phenomena: As spacing ratio decreases, it becomes increasingly difficult for the cross flow to pass between individual jets. Instead of penetrating through the denser fluid, it passes over it, suppressing its trajectory. Also, as spacing ratio decreases, a significant low pressure recirculation zone sets up downstream, since according to experiment, the cross flow tends pass over the injected fluid. This low pressure causes the injected jet to collapse against the wall from which it was injected. In the case of the inner wall, this low pressure adds to an already low pressure region resulting in significant suppression. In the case of the outer wall, this low pressure fights a high pressure region, resulting in some suppression, but a continued migration toward the inner wall as the turn is negotiated.

6.5. Lateral Profiles

To examine the notion of two-dimensionality downstream of the injection point, three-dimensional

lateral plots were produced, making use of the width of the rake. As in the single jet case, since velocity two or more azimuthal stations downstream of the injection point seems somewhat unaffected, these plots make use of temperature distributions only.

Injection from the outer wall at the higher momentum ratio and wide spacing ratio is represented in figures 75 through 78. At the initial azimuthal station (0°), once observes the three-dimensionality of temperature at that point. Since the set of injection jets do not continuously span the combustor width, cross flow has the ability to flow inbetween them, thereby causing little or no suppression, as observed experimentally.

Examining the lateral plots further downstream (60°, 120°, and 180°), a degree of three dimensionality remains, even at the exit. This shows that the spacing is in fact wide enough to allow the cross flow to penetrate between them.

As one examines the tight spacing ratio (J = 3.08) for high momentum injection from the outer wall (figures 79 through 82), one observes immediately at 0° that the flow is nearly two-dimensional. By 60°, the flow is clearly two-

dimensional. The two figures showing downstream locations again show little or no change laterally from probe one to five.

From these lateral plots, the suppression of jet trajectory can again be attributed to the low pressure recirculation zone that forms downstream of the injection location. This region is more pronounced during injection with small spacing ratios because, as shown here, because the the row of jets causes the cross flow to pass over the top.

Kamotani and Greber[14] show a suppression in trajectory with decreasing spacing ratio until spacing ratio falls below about two or three. At this point, the issuing jet acts nearly like a slot jet and the trajectory shows less suppression. In this experiment, spacing ratio evidently cannot be decreased to the point where suppression begins to deteriorate.

CHAPTER VII

GENERAL CONCLUSIONS AND RECOMMENDATIONS

This is the second work using a reverse flow combustor that investigates the perpendicular injection of a cooling jet into a hot cross flow that is accelerating both longitudinally and transversely.

This work shows that there is, in fact, good agreement between trends associated with thermal and velocity trajectories. Both trajectories indicate a migration toward the inner wall independent of injection location, density ratio, momentum ratio, and spacing ratio.

The semi-empirical model developed by Lipshitz[18] for a single jet shows similar agreement as it did in his experiment. It is in need of better entrainment information along with knowledge of the pressure field throughout the combustor. Considering the vortex structure that sets up during perpendicular injection, a model which uses this as its dominant effect is under development.

With the experimental data available from this study, from the previous temperature study, and the

expected empirical information on entrainment, all of the necessary components are available to carry out a careful investigation to produce a semi-empirical model for a single jet as well as a row of jets.

From these experiments, then, it can be seen that injection from the outer wall allows cooling at the inner wall due to the migration effect. This is practically useful since injection from the outer wall is more easily carried out. Since migration toward the inner wall is evident, cooler temperatures and higher velocities can be developed there. If cooling of the outer wall is desired, the leakage of cooling air from the outer wall injection ports at low momentum ratios will result in a cool region along that wall.

Compact reverse flow combustors are a viable alternative. Flow conditions within them are predictable, and desirable modifications can be made through dilution jet injection.

CHAPTER IX

DATA PLOTS

The following pages contain all of the data plots described and referred to above.

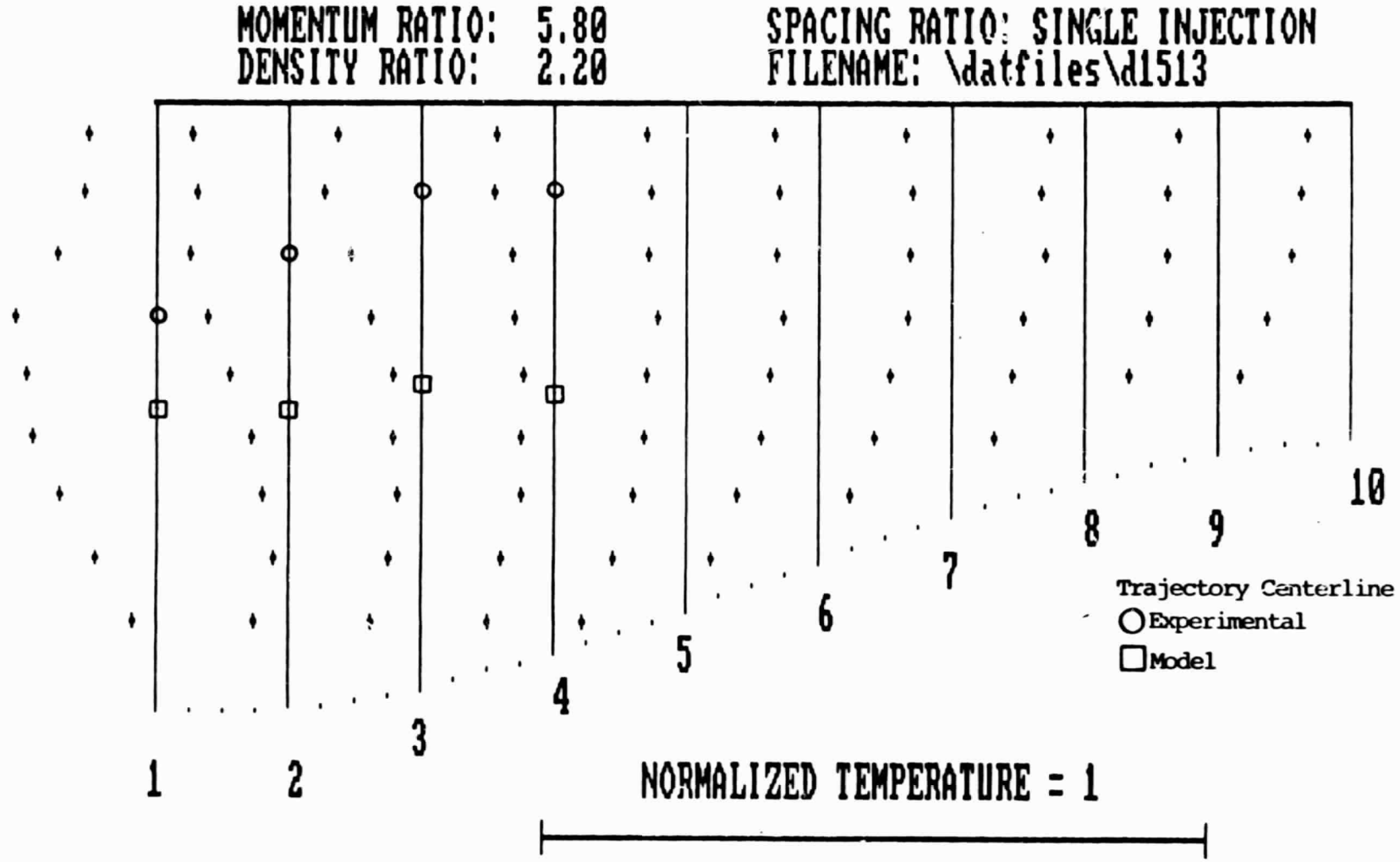

Figure 21: τ, Low J, Outer Wall Prior to Bend.

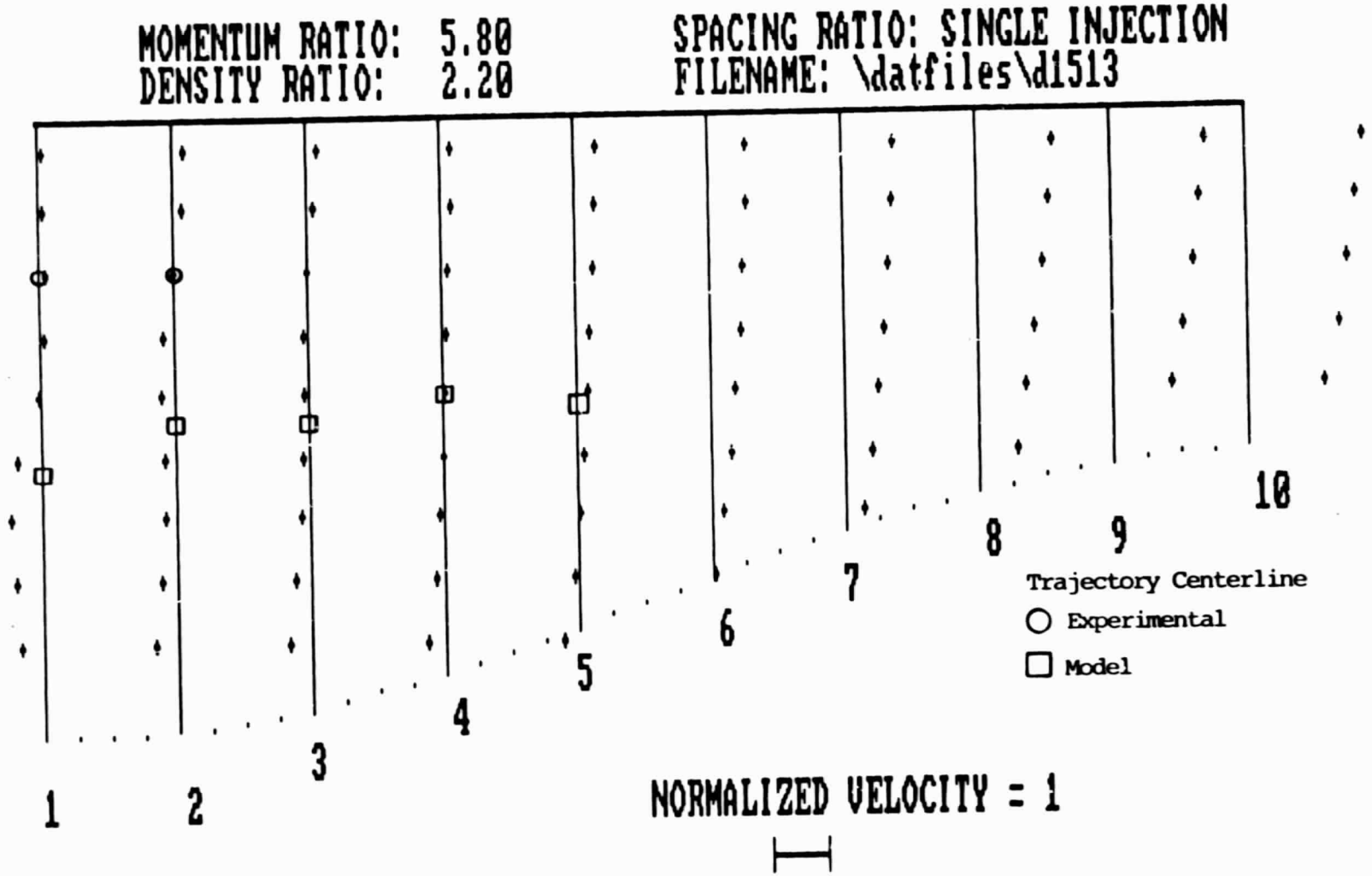

Figure 22: γ, Low J, Outer Wall Prior to Bend.

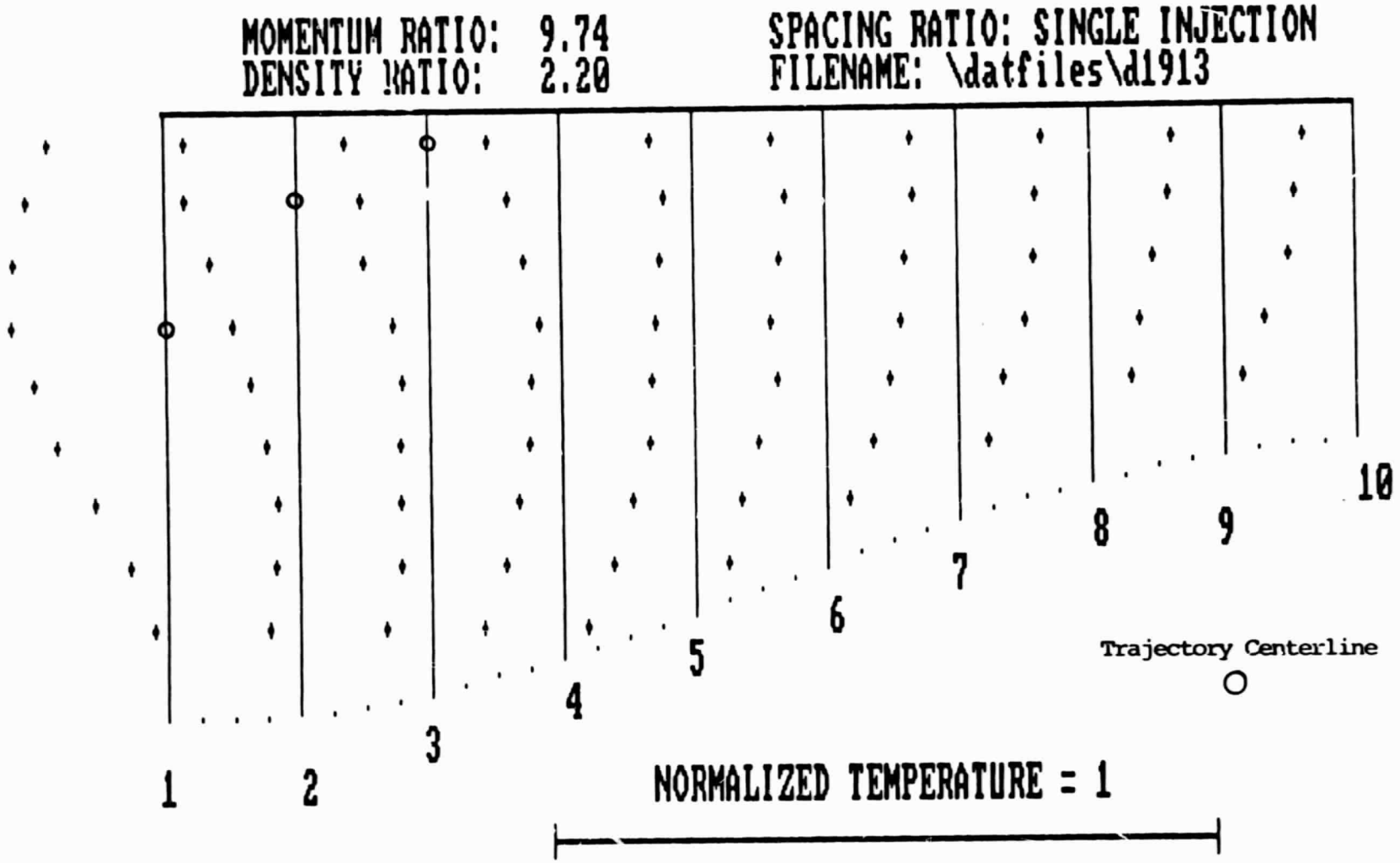

Figure 23: τ, High J, Outer Wall Prior to Bend.

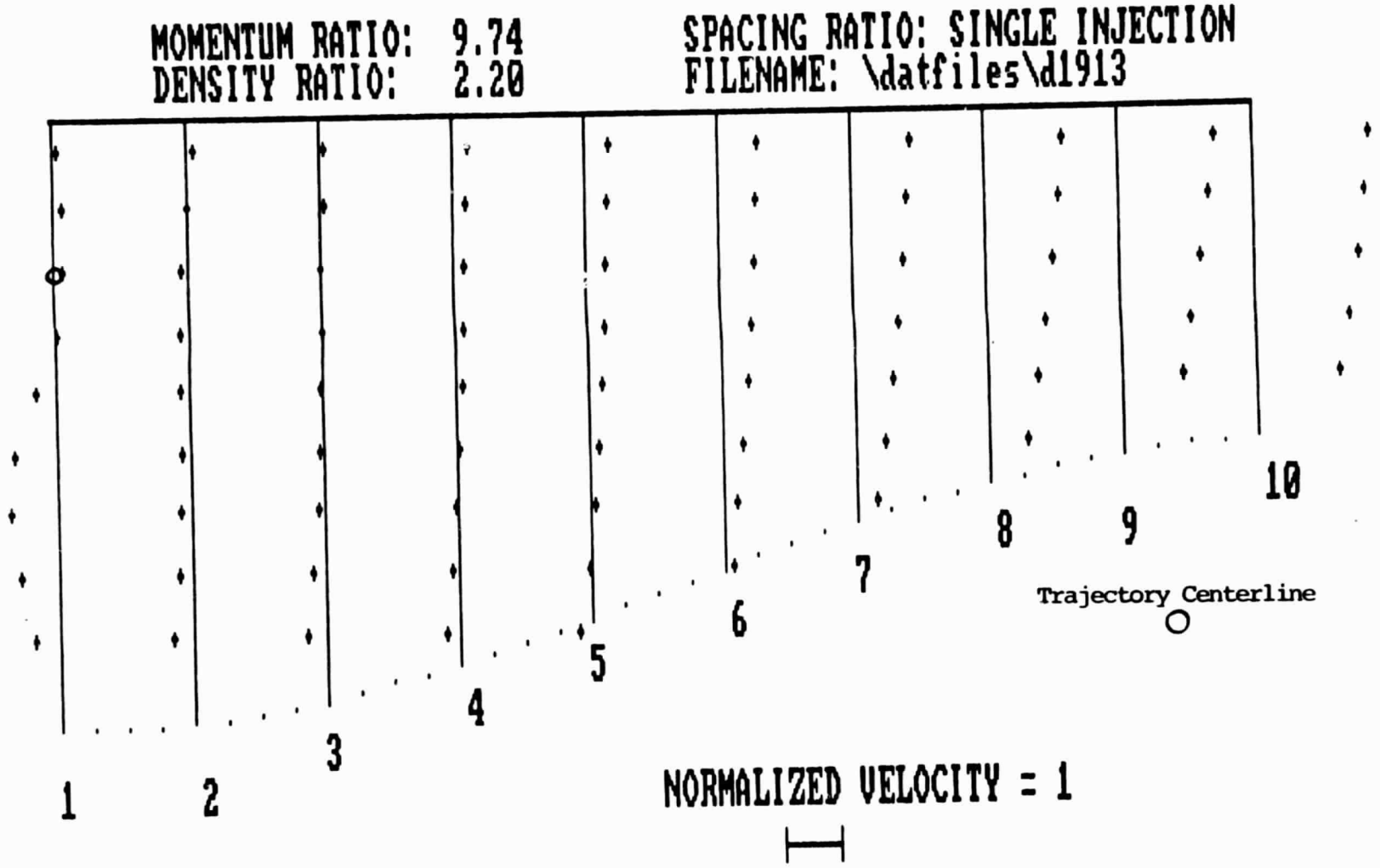

Figure 24: γ, High J, Outer Wall Prior to Bend.

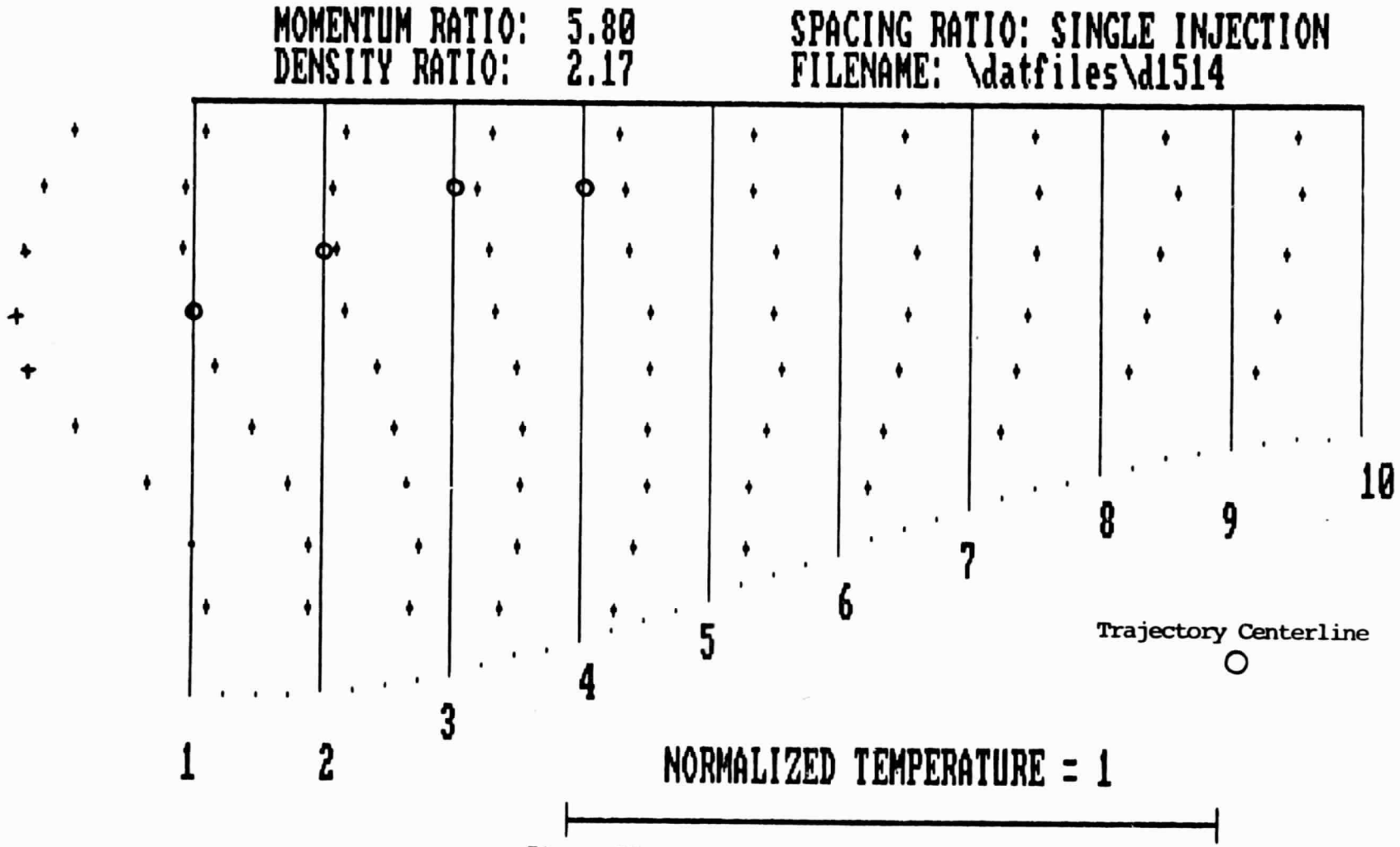

Figure 25: τ, Low J, Inner Wall.

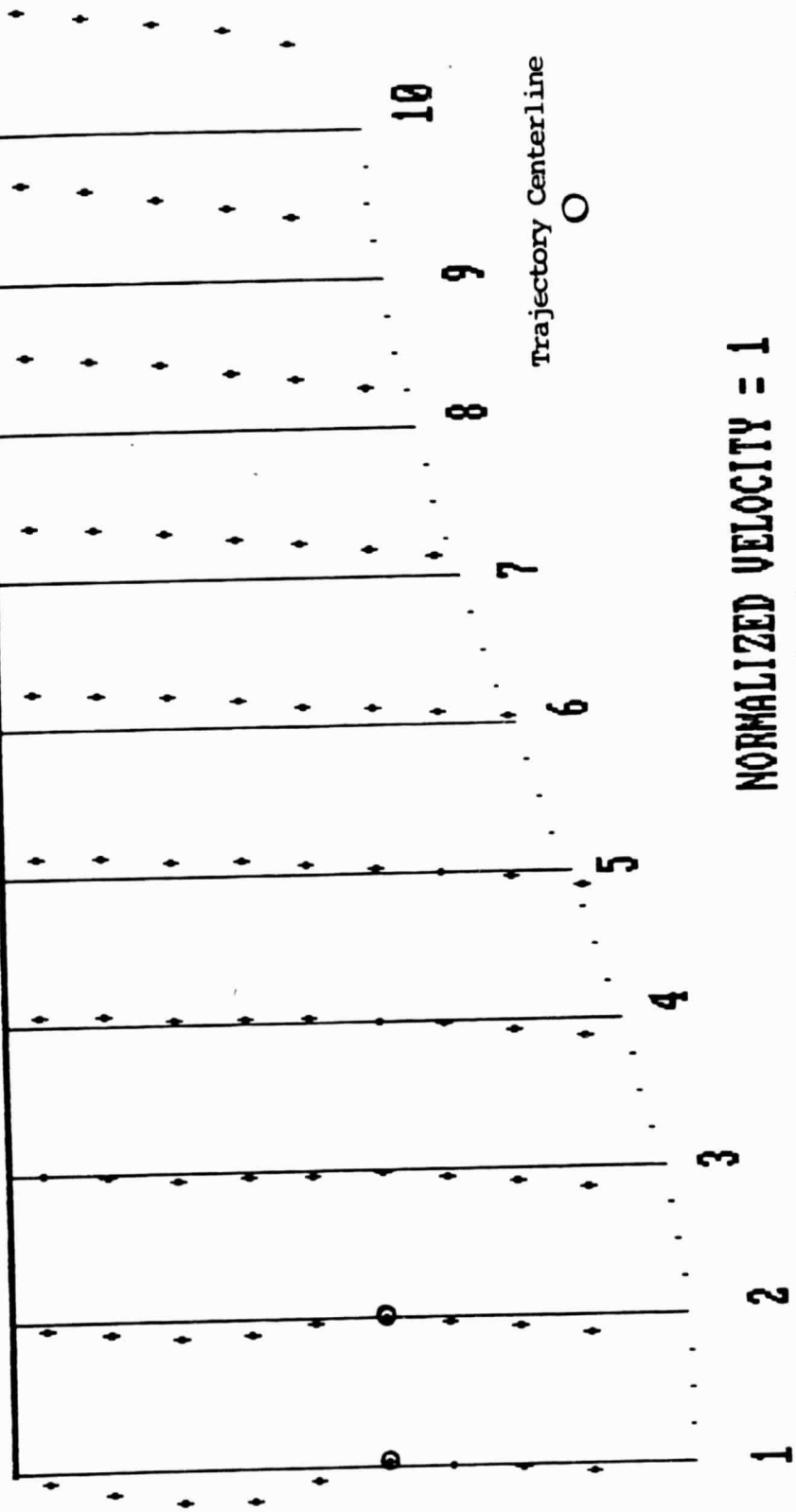

Figure 26: Y, Low J, Inner Wall.

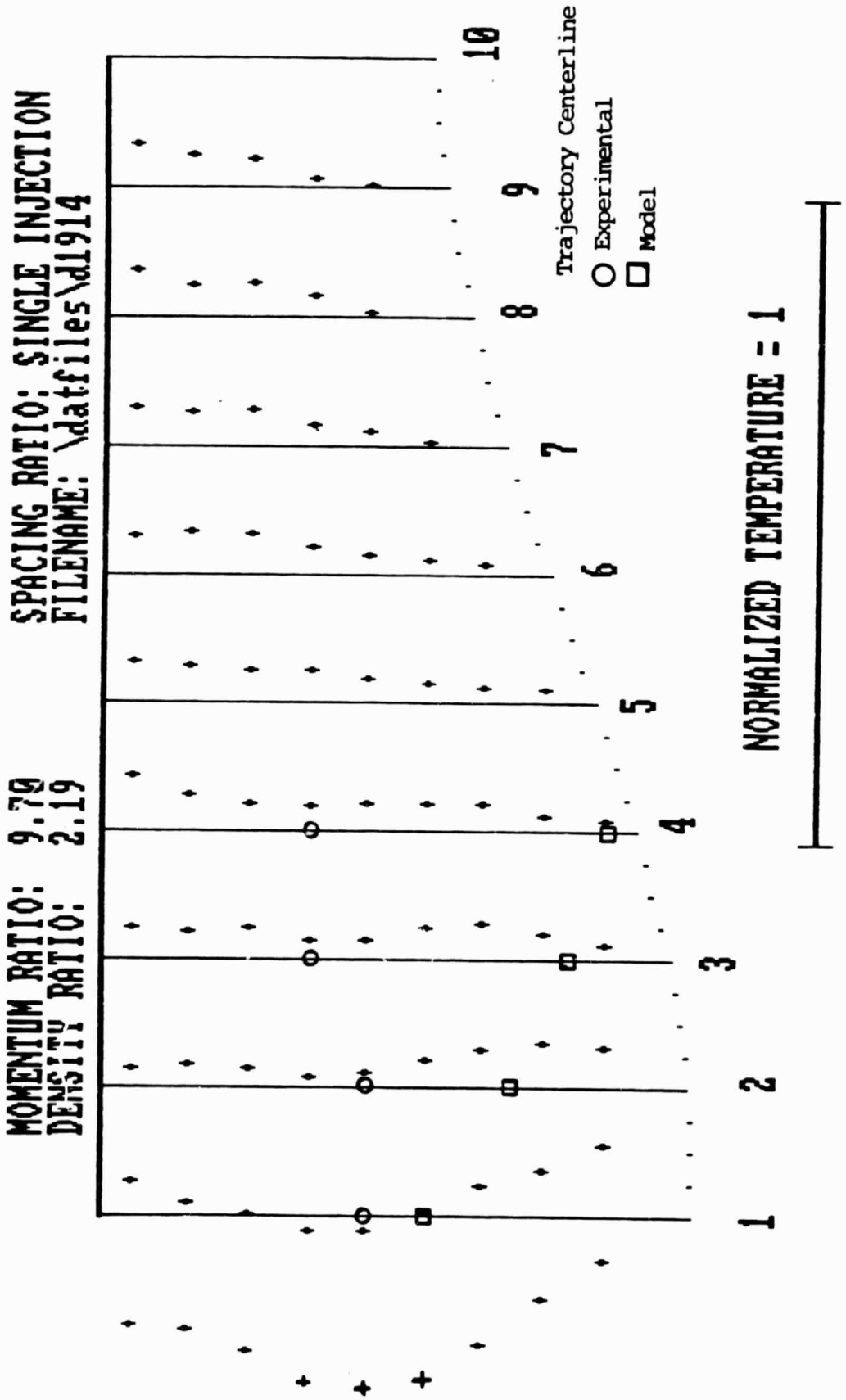

Figure 27: τ, High J, Inner Wall.

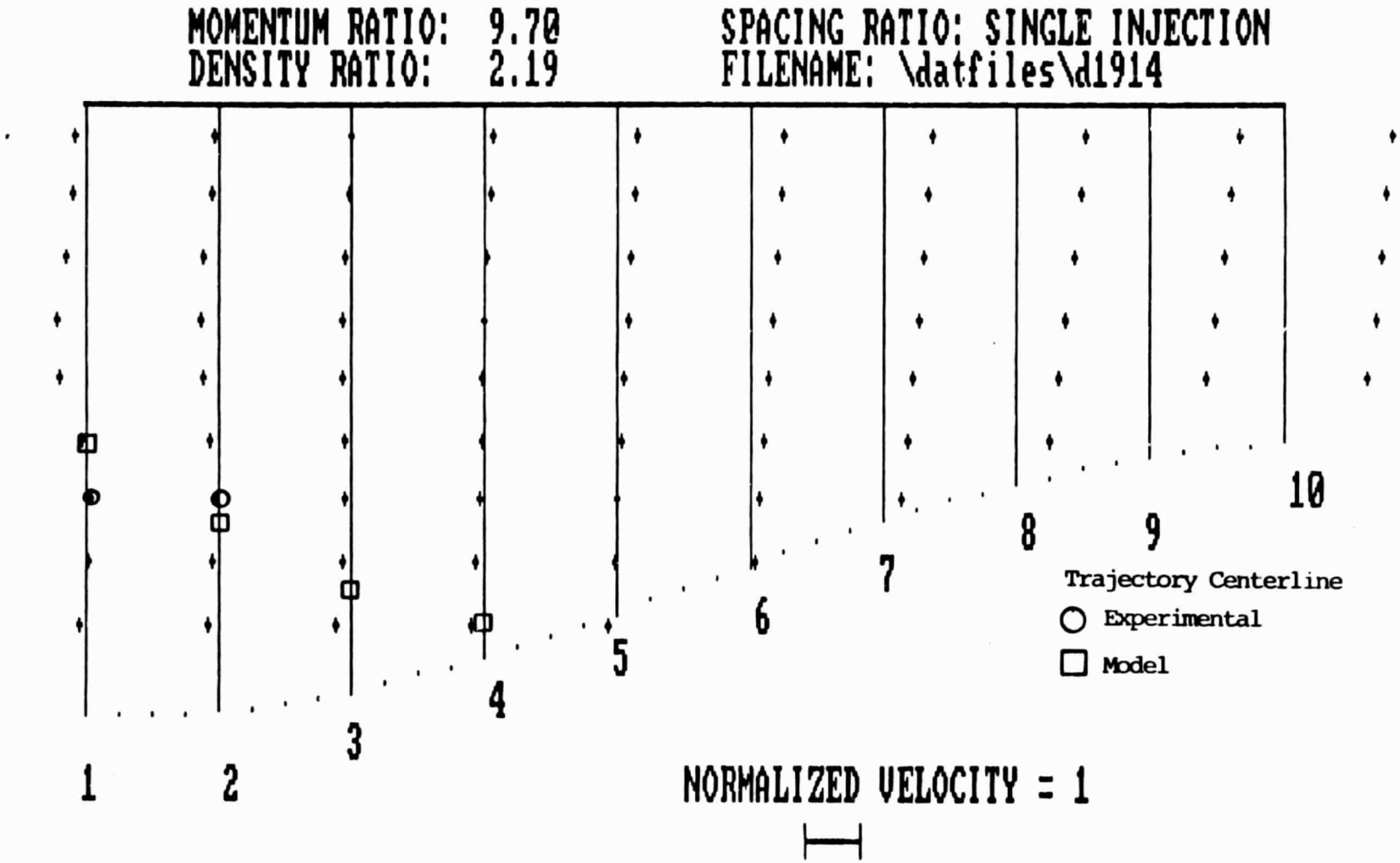

Figure 28: γ, High J, Inner Wall.

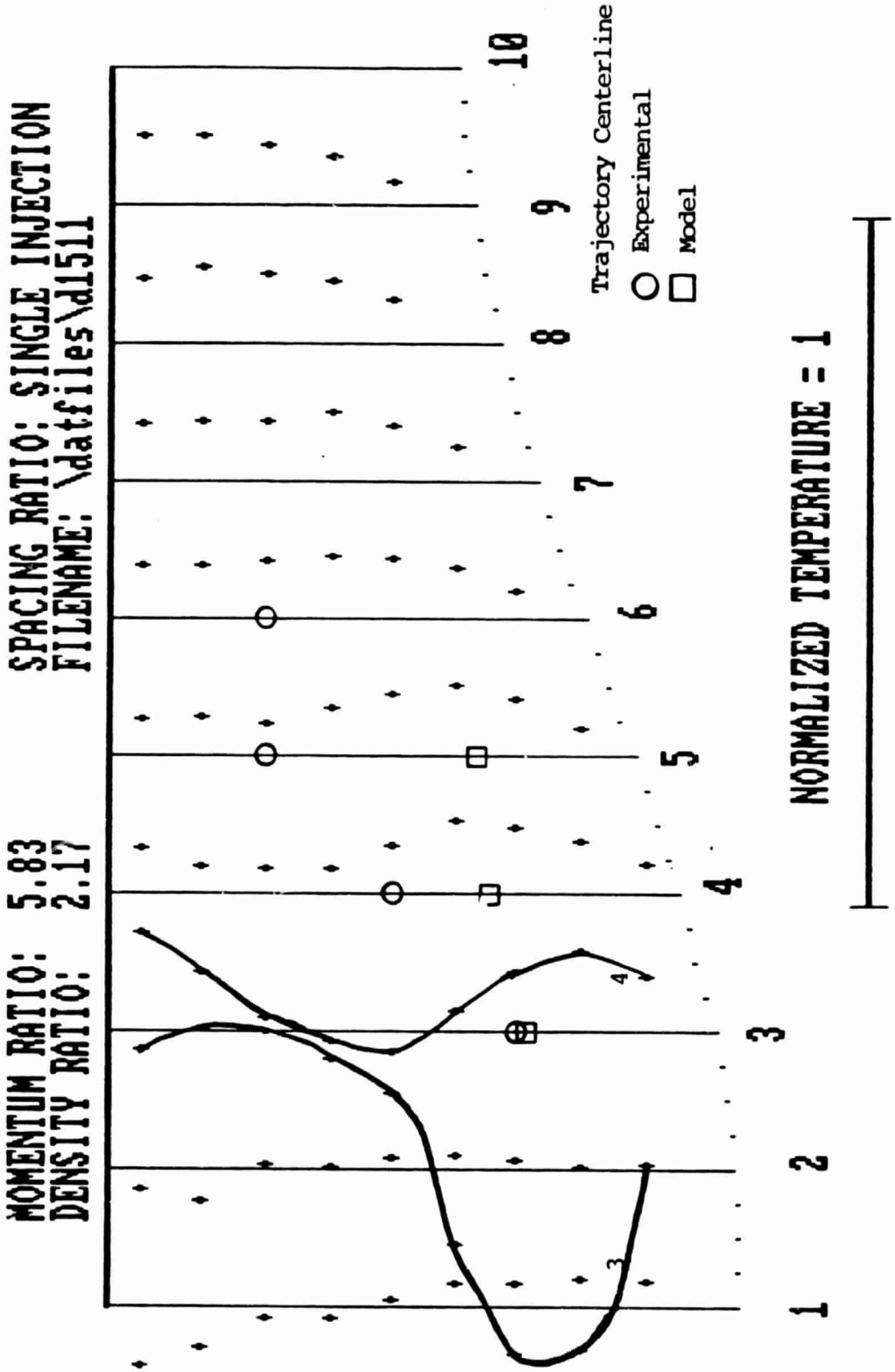

Figure 29: τ, Low J, Outer Wall Into Bend.

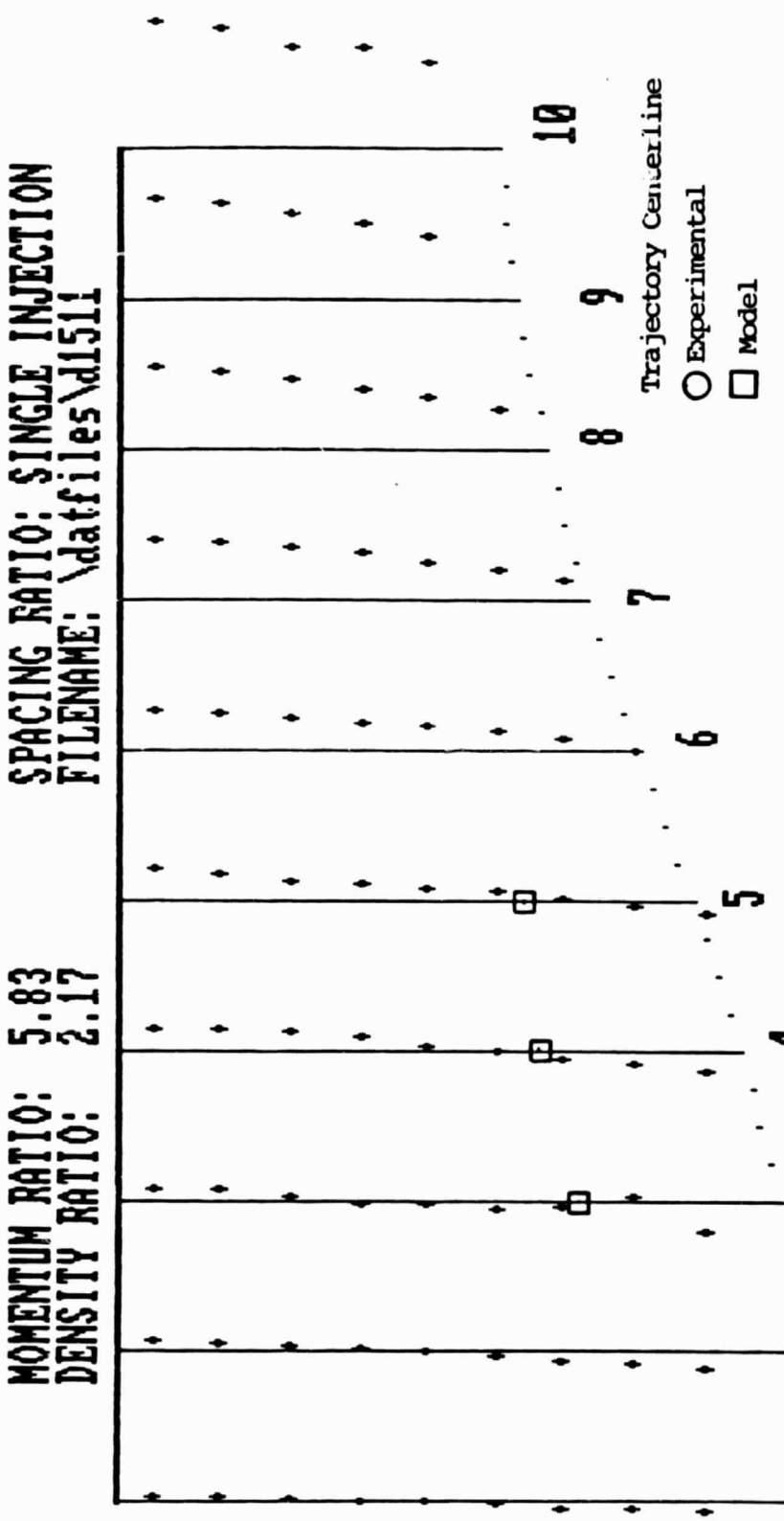

Figure 30: Y, Low J, Outer Wall Into Bend.

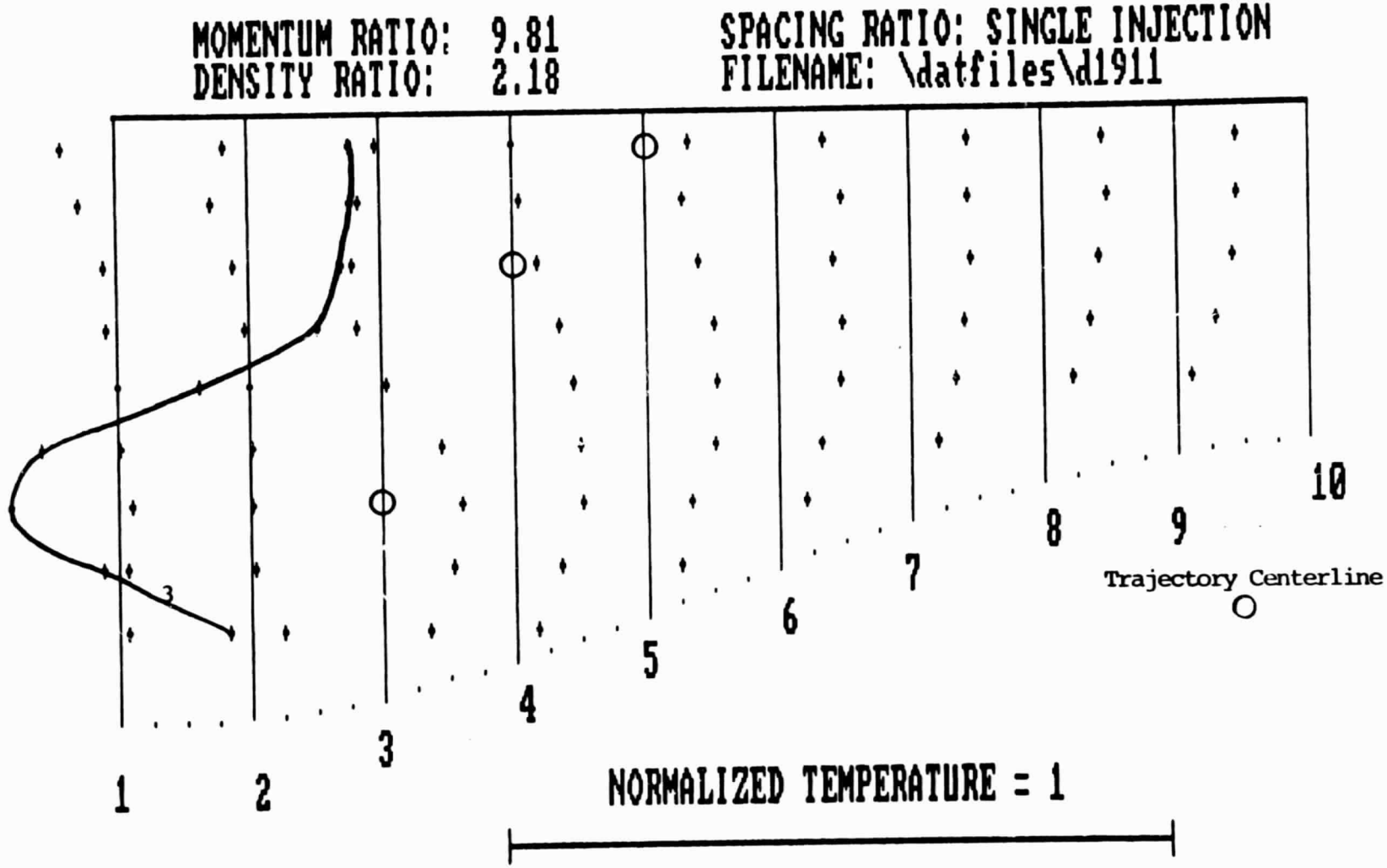

Figure 31: τ, High J, Outer Wall Into Bend.

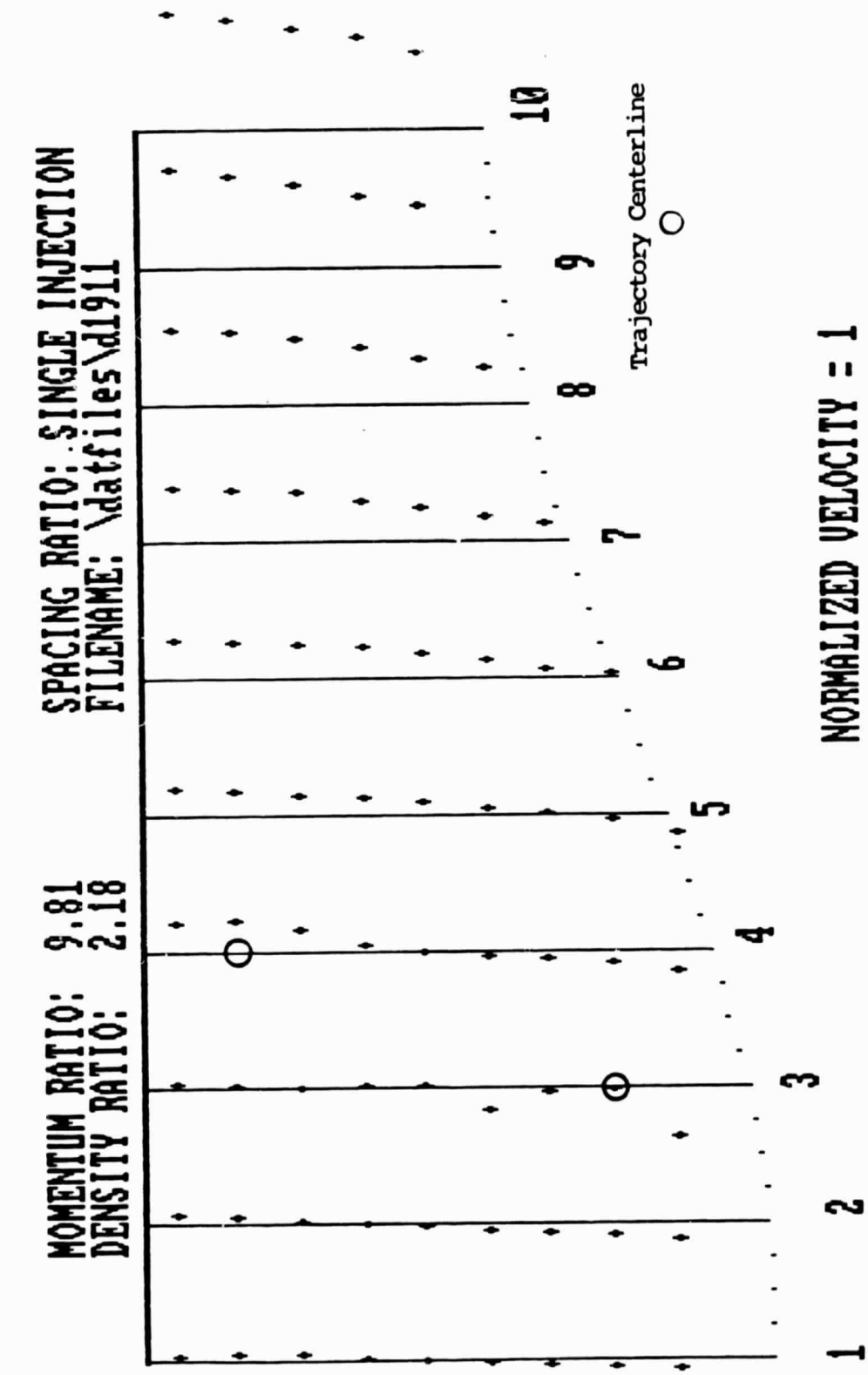

Figure 32: γ, High J_n Outer Wall Into Bend.

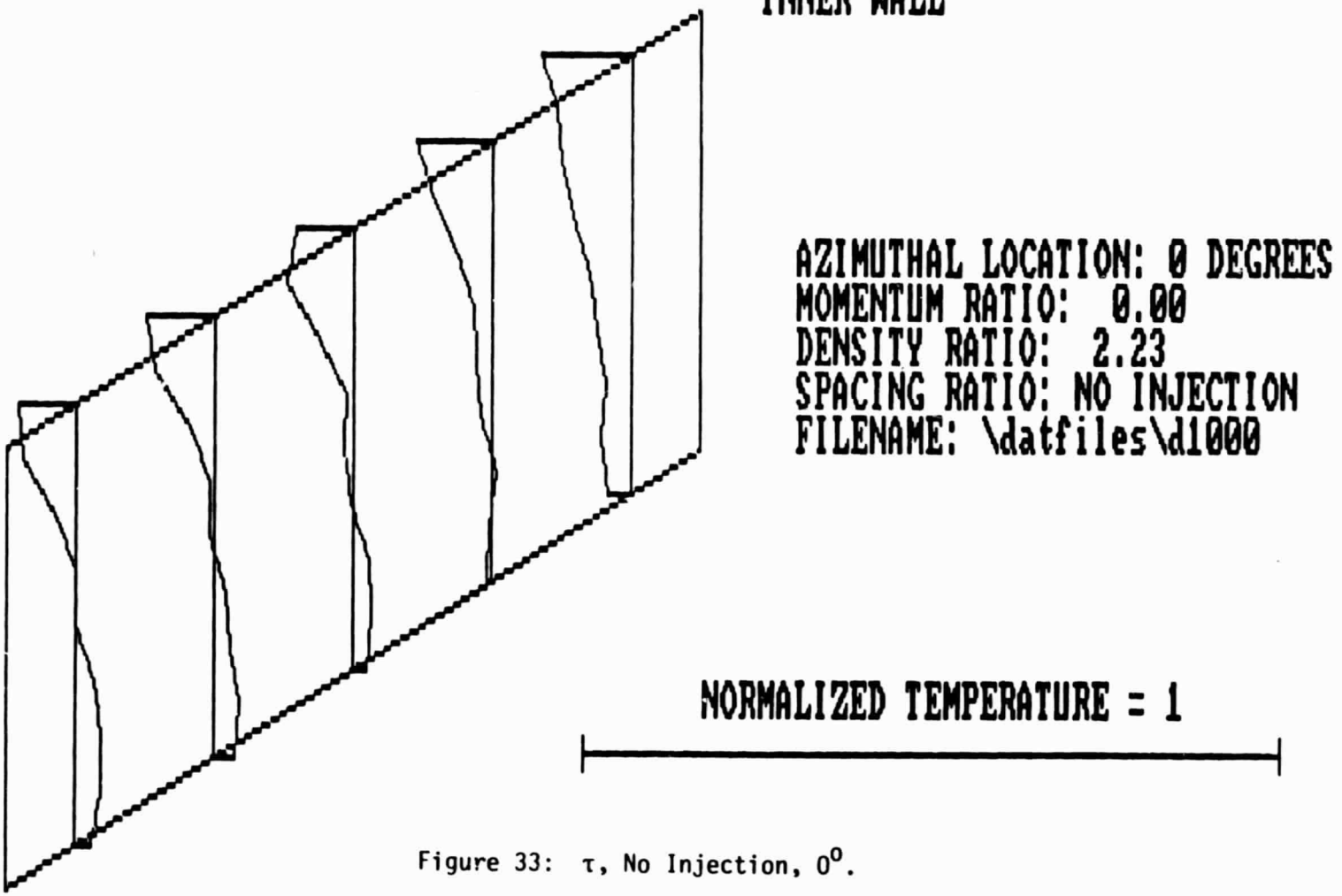

Figure 33: τ, No Injection, 0^{o}.

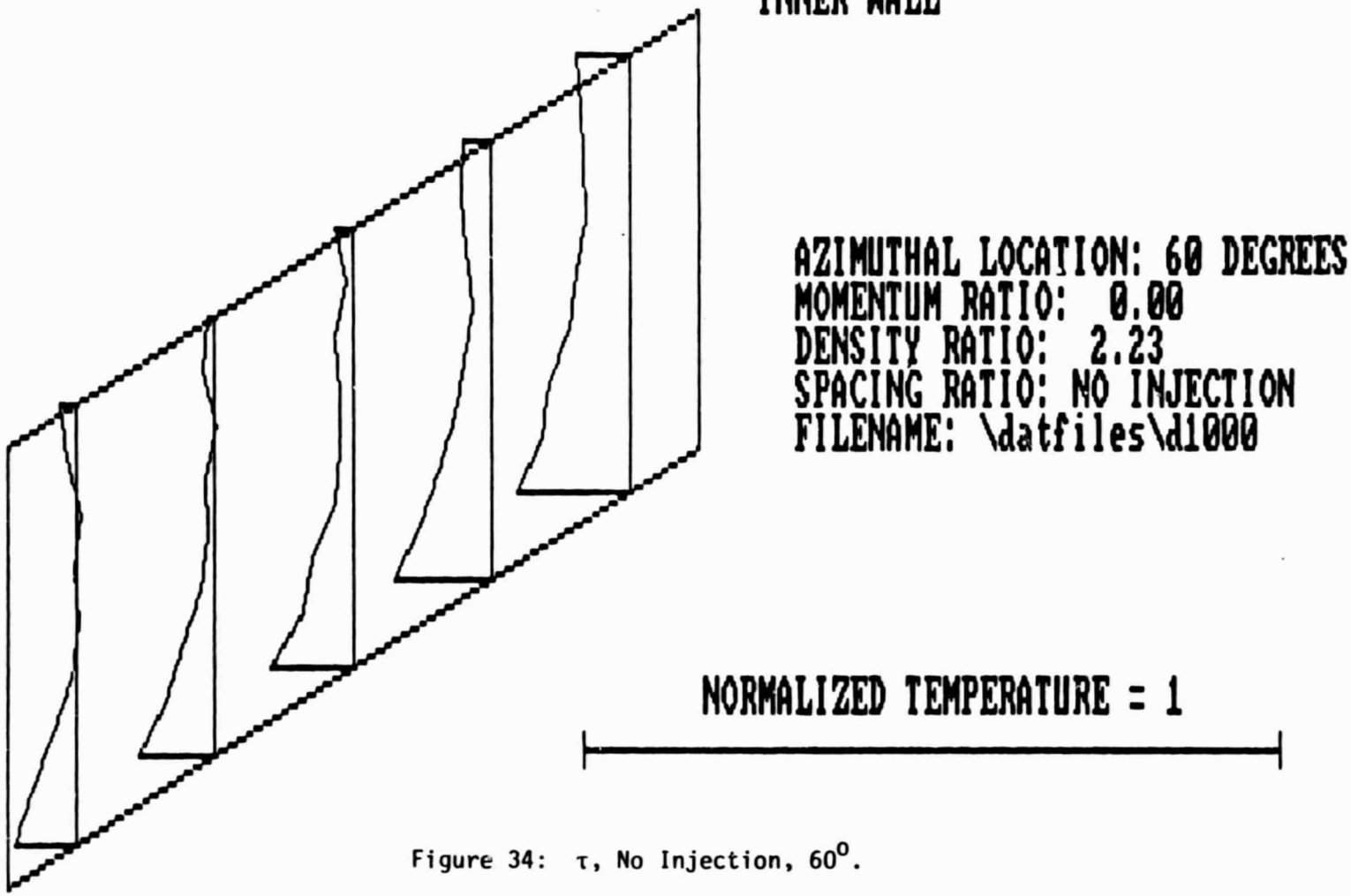

Figure 34: τ, No Injection, 60^{o}.

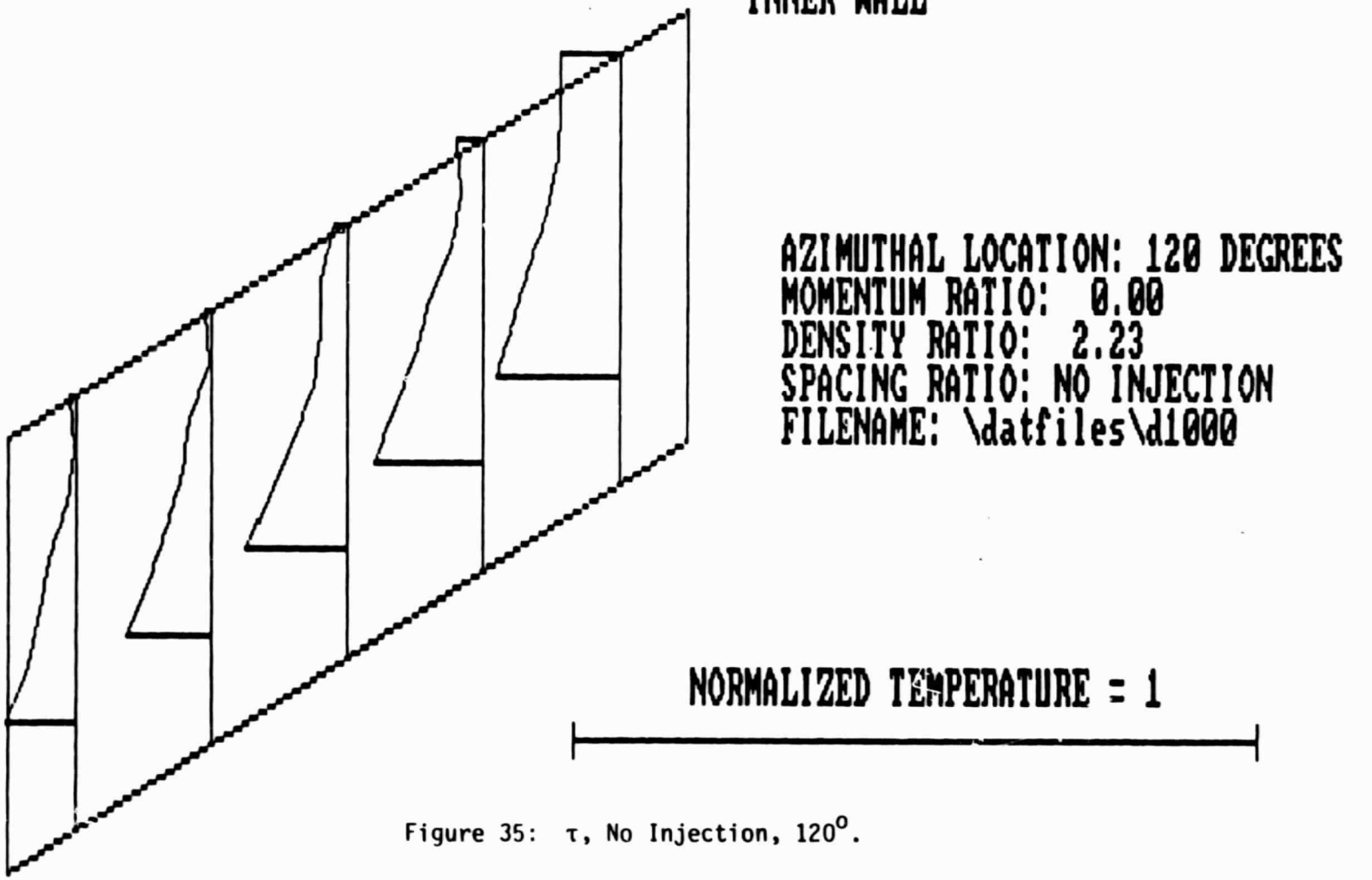

Figure 35: τ, No Injection, 120^{o}.

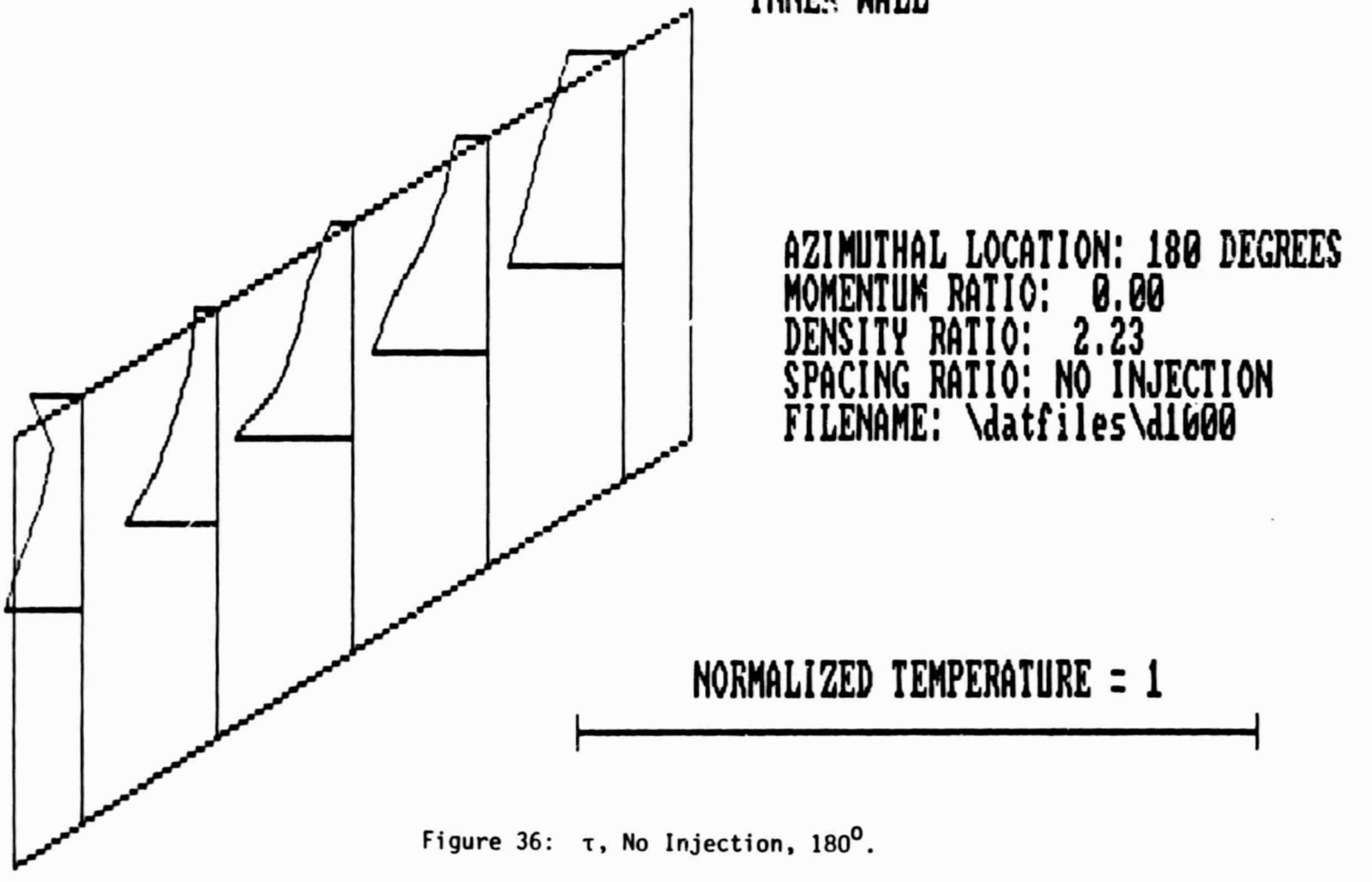

Figure 36: τ, No Injection, 180^{o}.

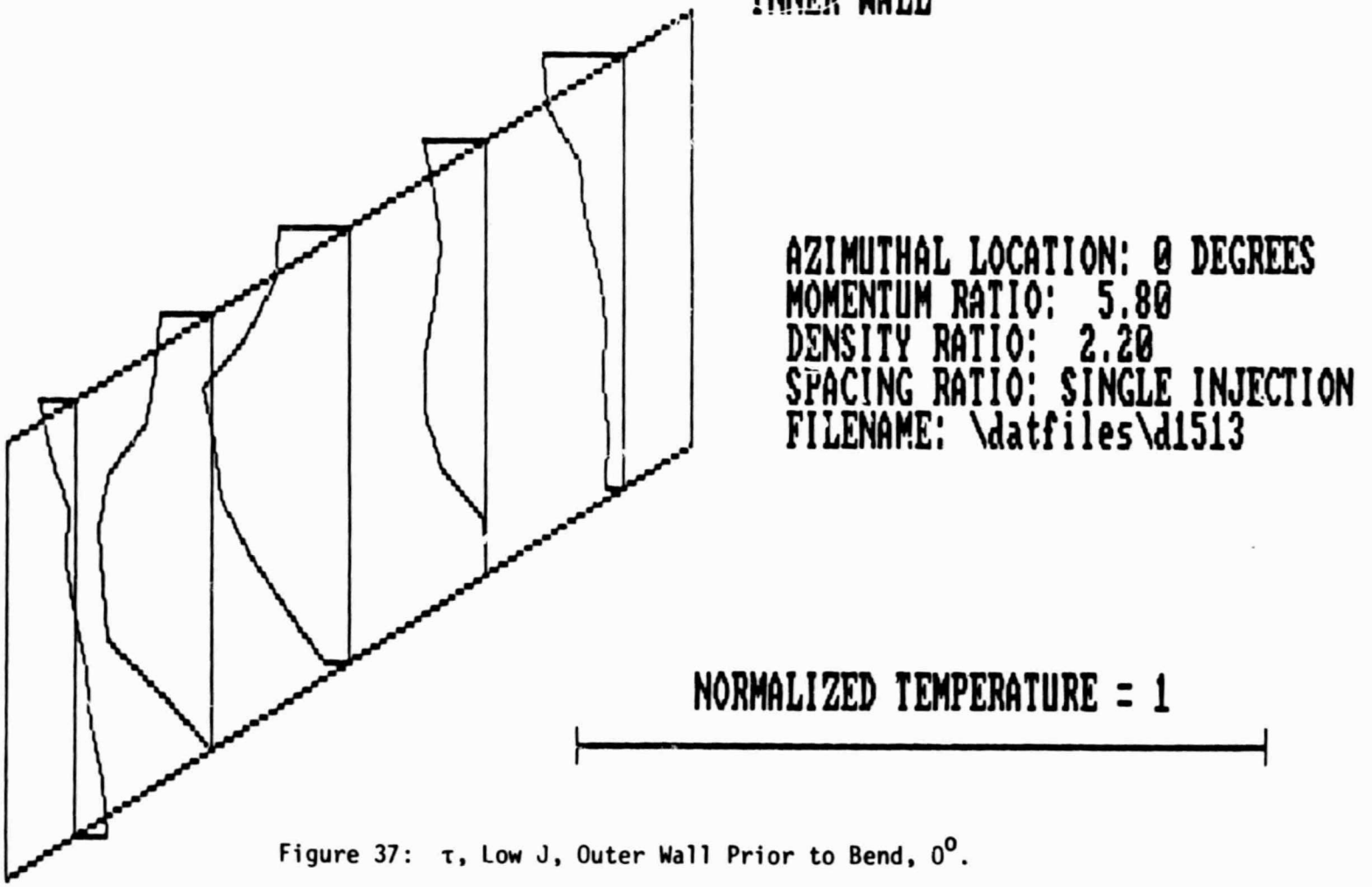

Figure 37: τ, Low J, Outer Wall Prior to Bend, 0^{o}.

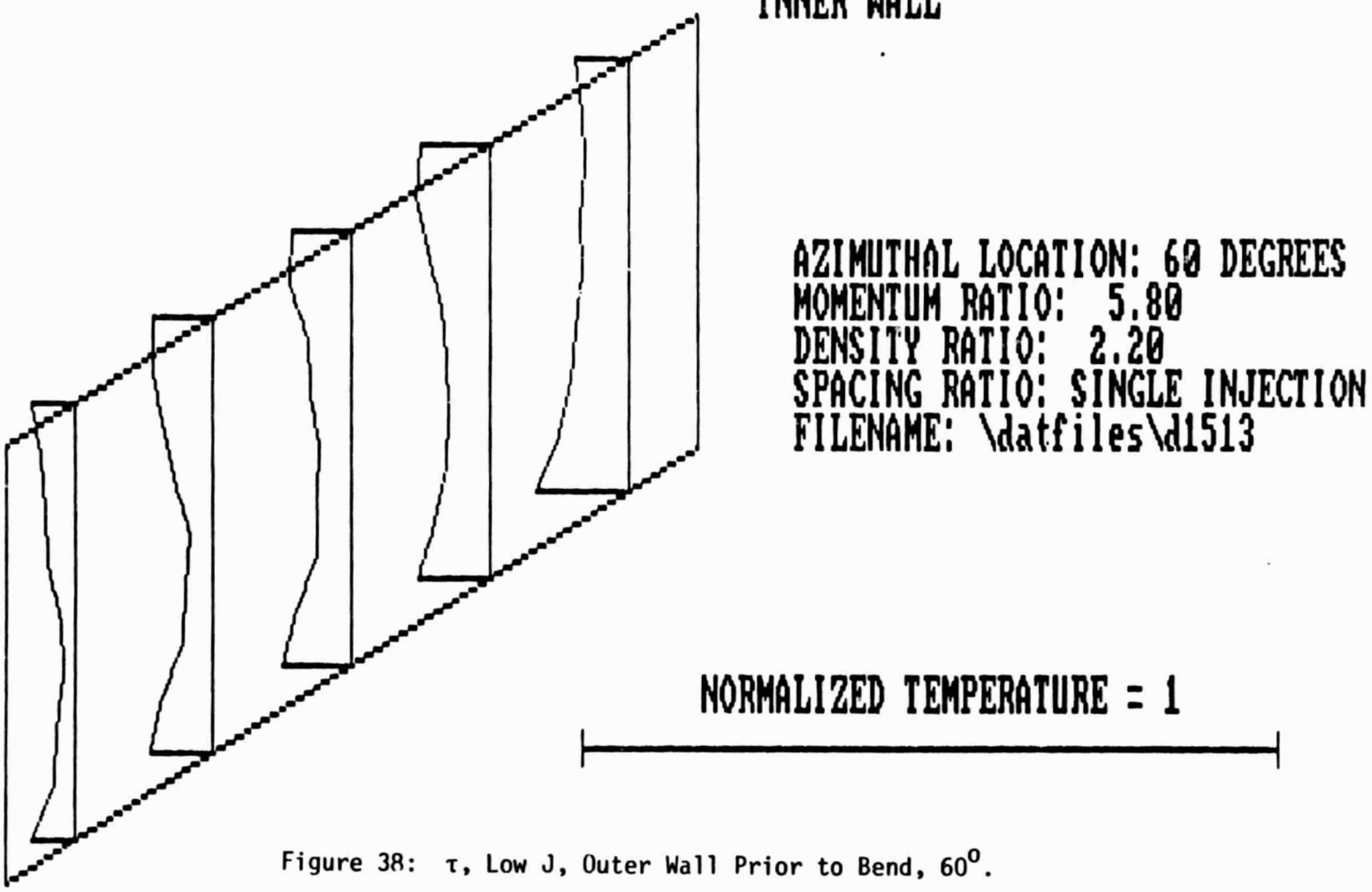

Figure 38: τ, Low J, Outer Wall Prior to Bend, 60^{o}.

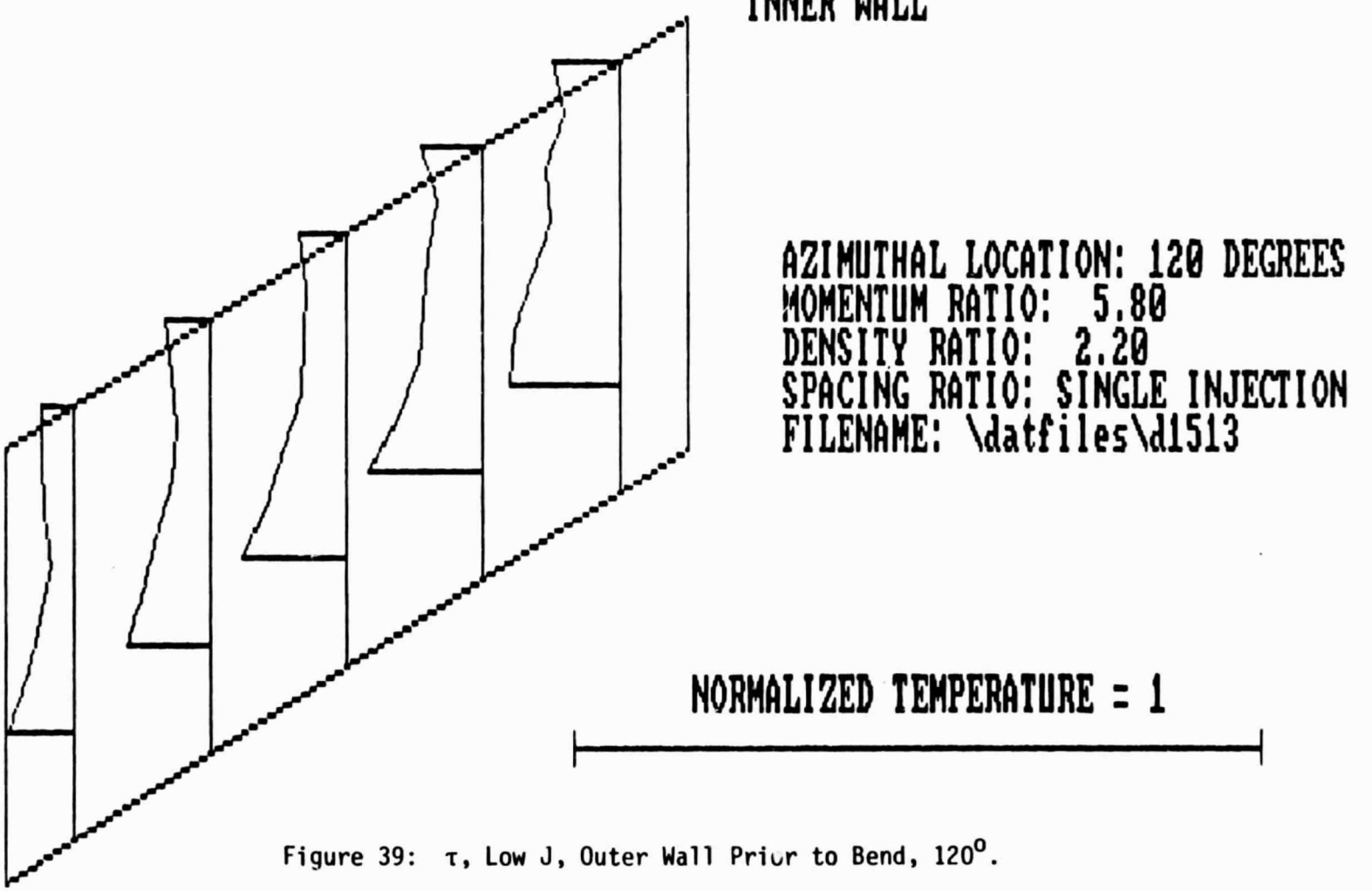

Figure 39: τ, Low J, Outer Wall Prior to Bend, 120^{o}.

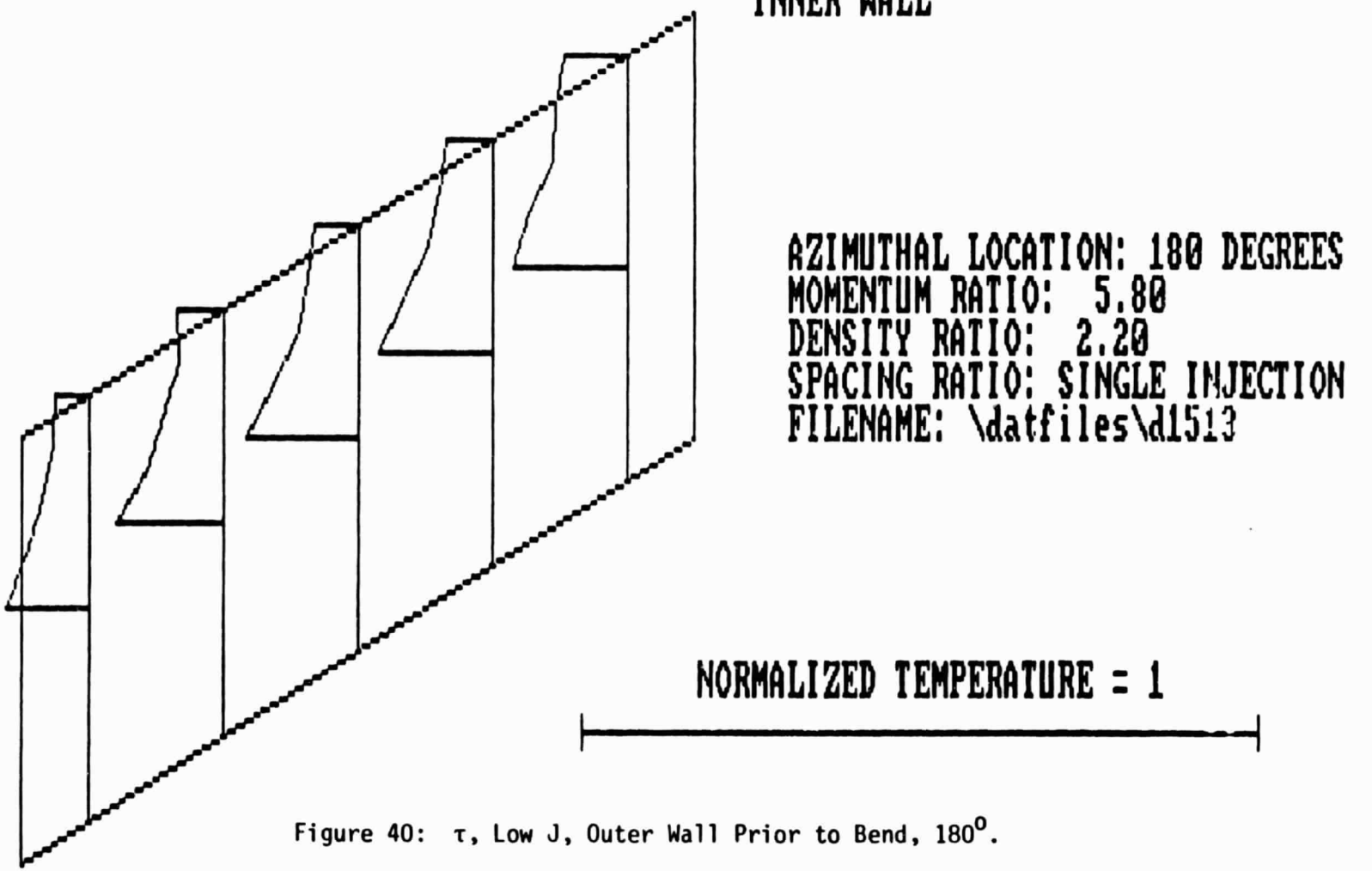

Figure 40: τ, Low J, Outer Wall Prior to Bend, 180^{o}.

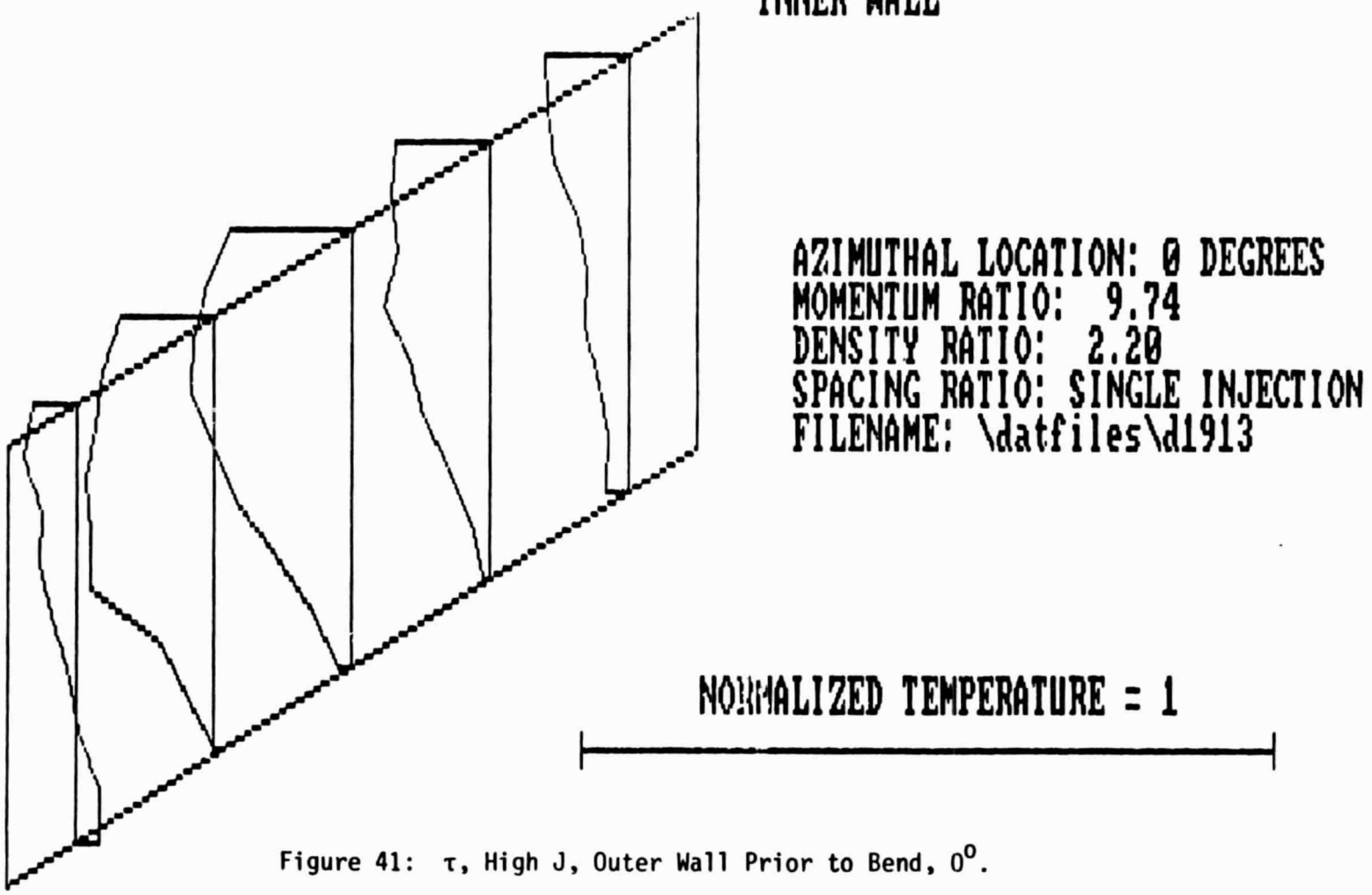

Figure 41: τ, High J, Outer Wall Prior to Bend, 0^{o}.

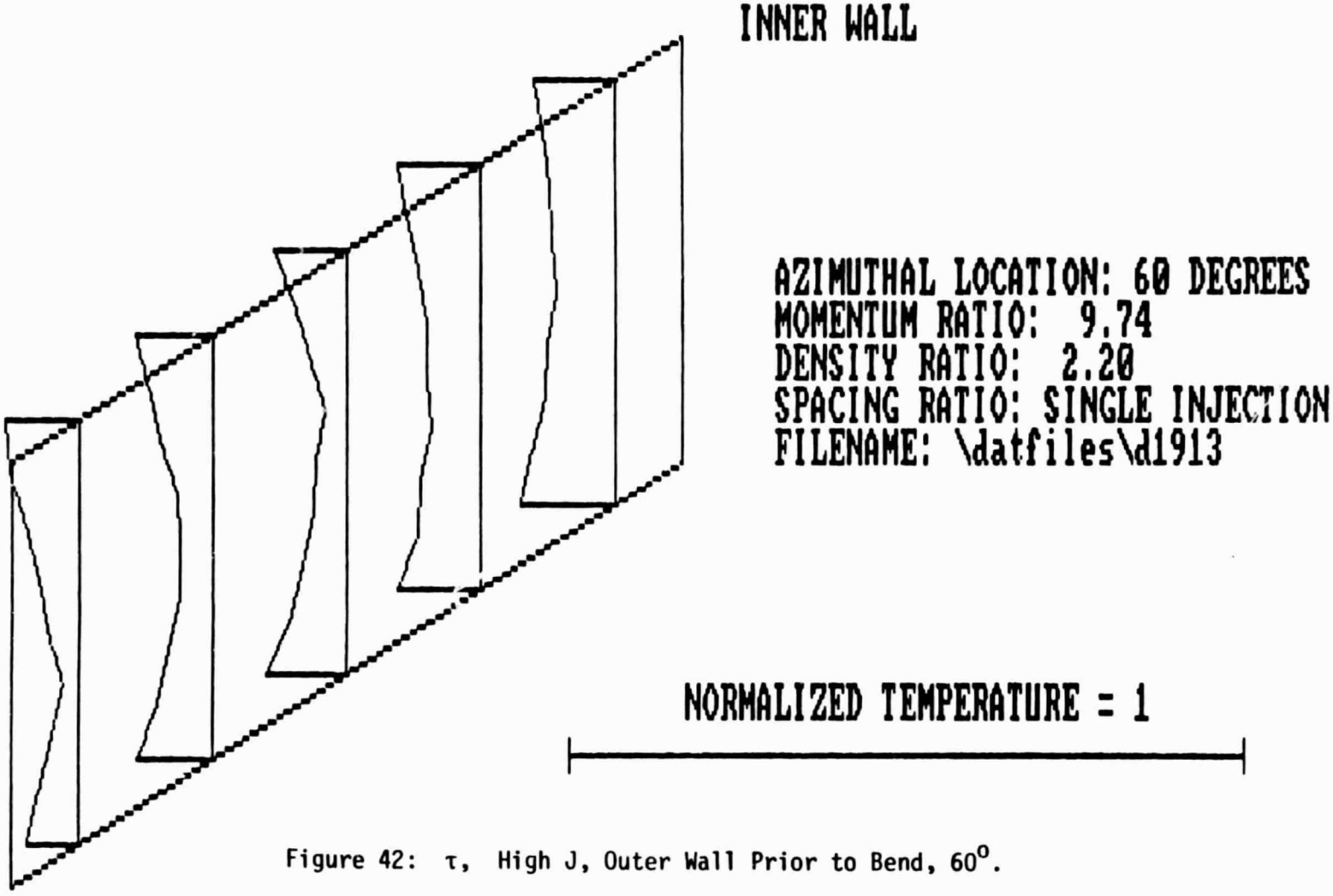

Figure 42: τ, High J, Outer Wall Prior to Bend, 60^{o}.

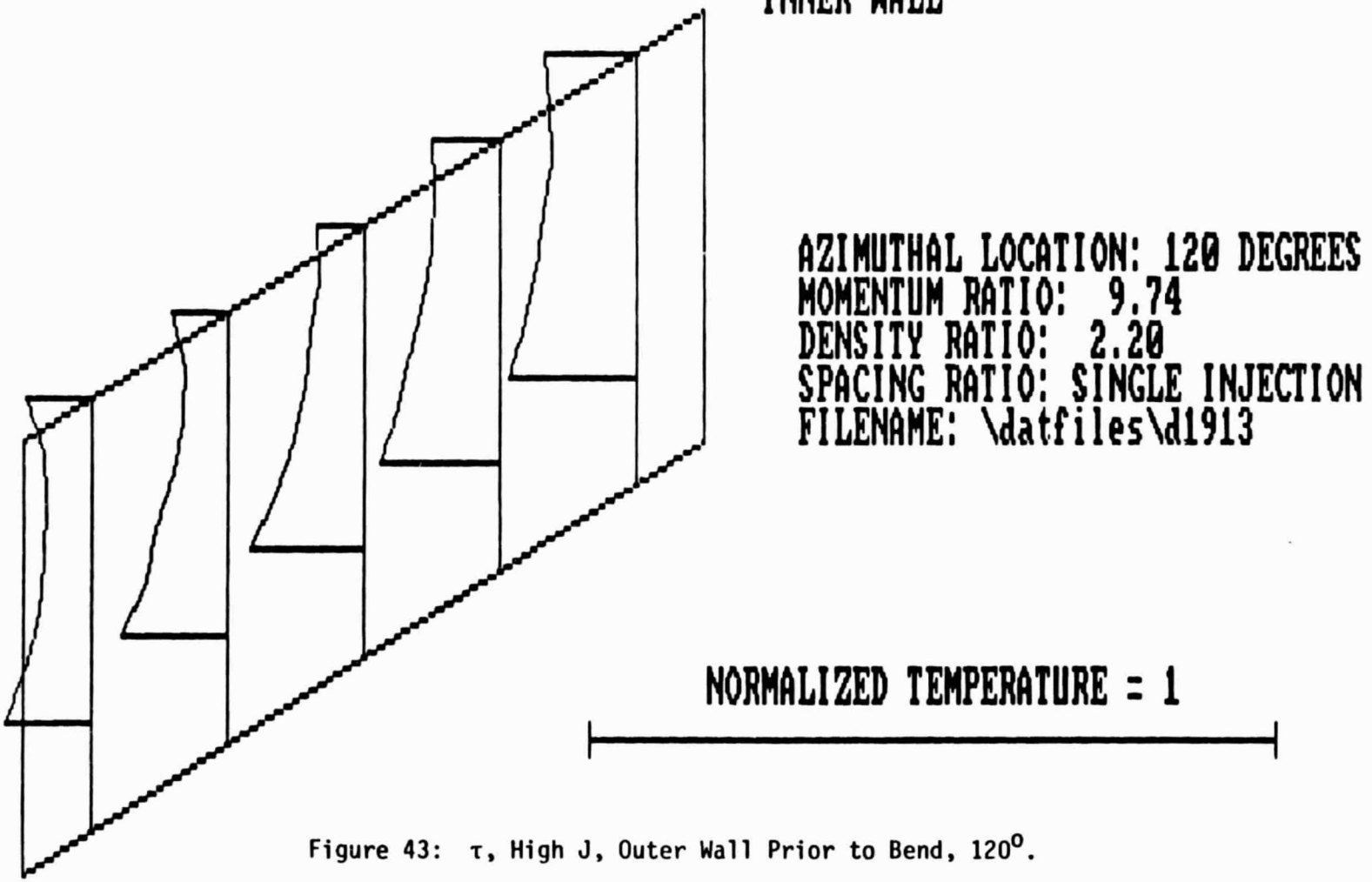

Figure 43: τ, High J, Outer Wall Prior to Bend, 120^{o}.

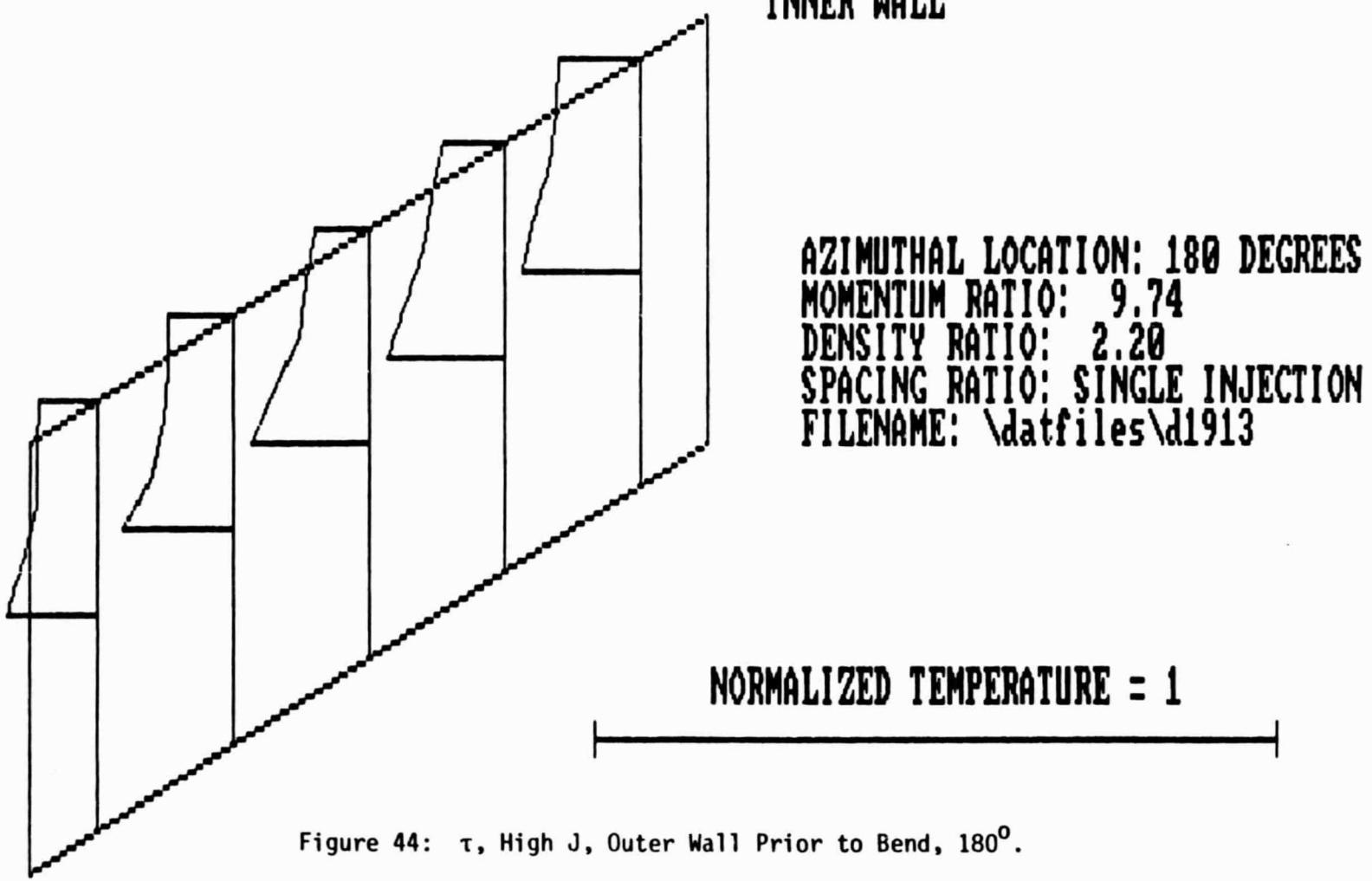

Figure 44: τ, High J, Outer Wall Prior to Bend, 180^{o}.

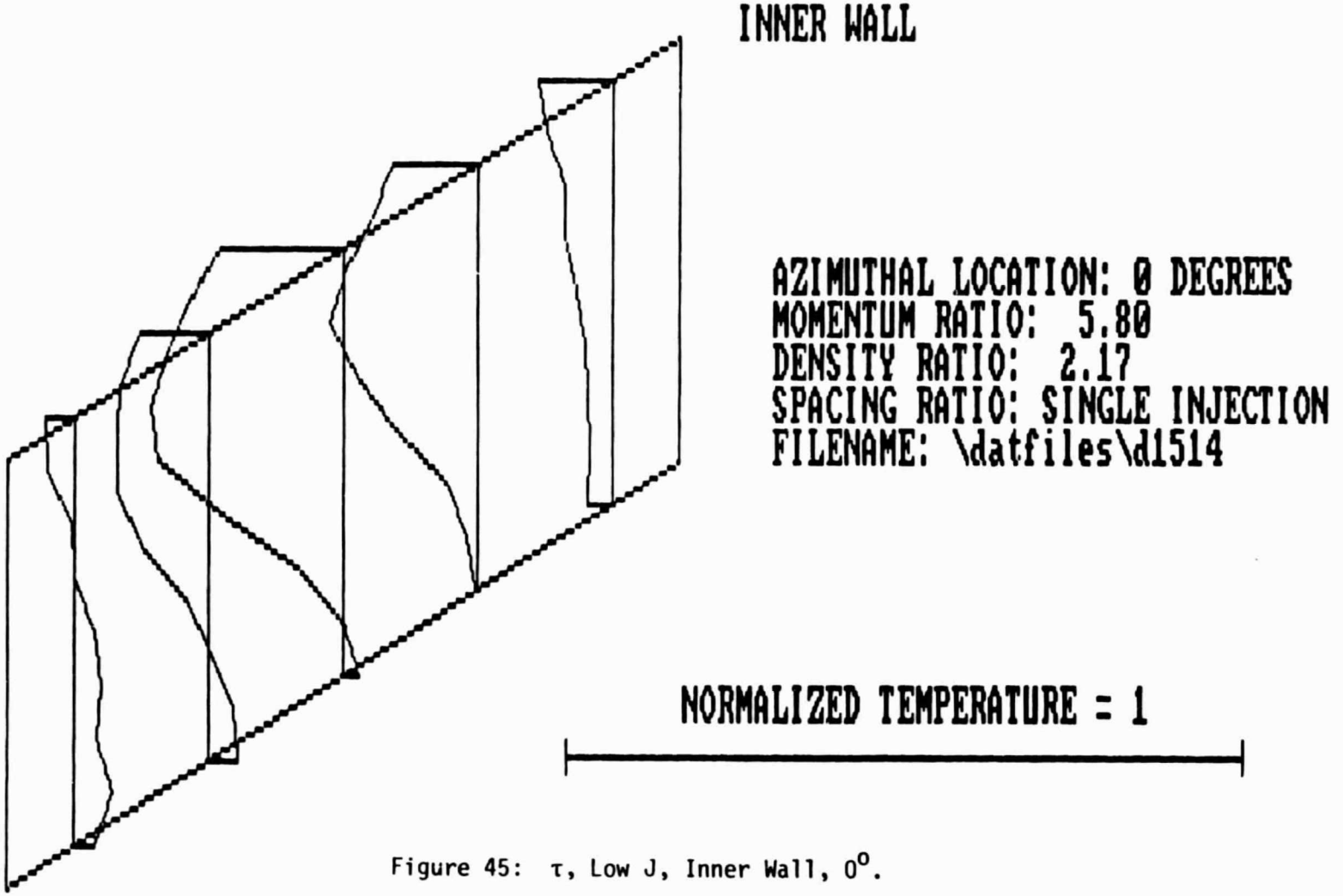

Figure 45: τ, Low J, Inner Wall, 0^{o}.

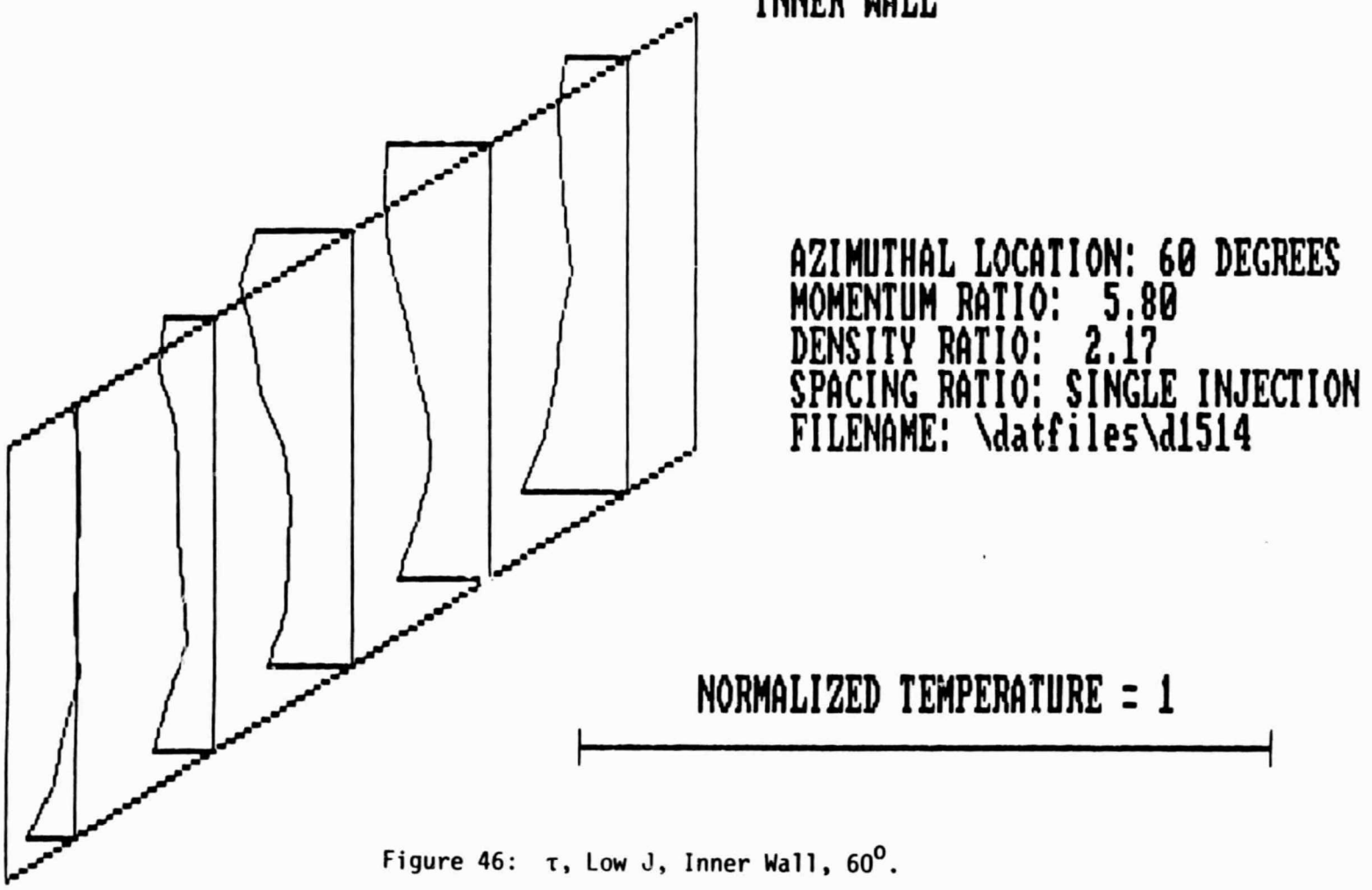

Figure 46: τ, Low J, Inner Wall, 60^{o}.

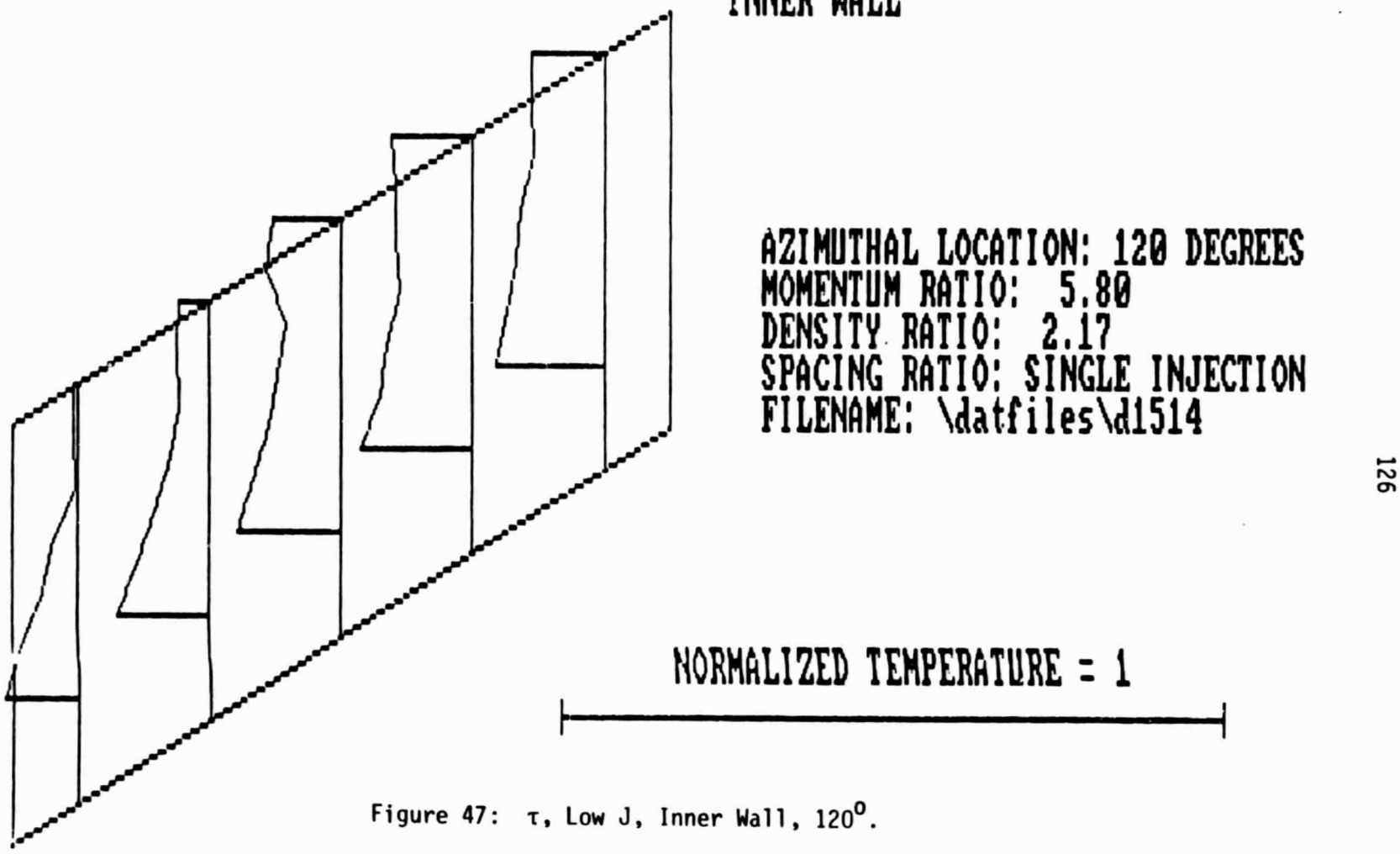

Figure 47: τ, Low J, Inner Wall, 120^{o}.

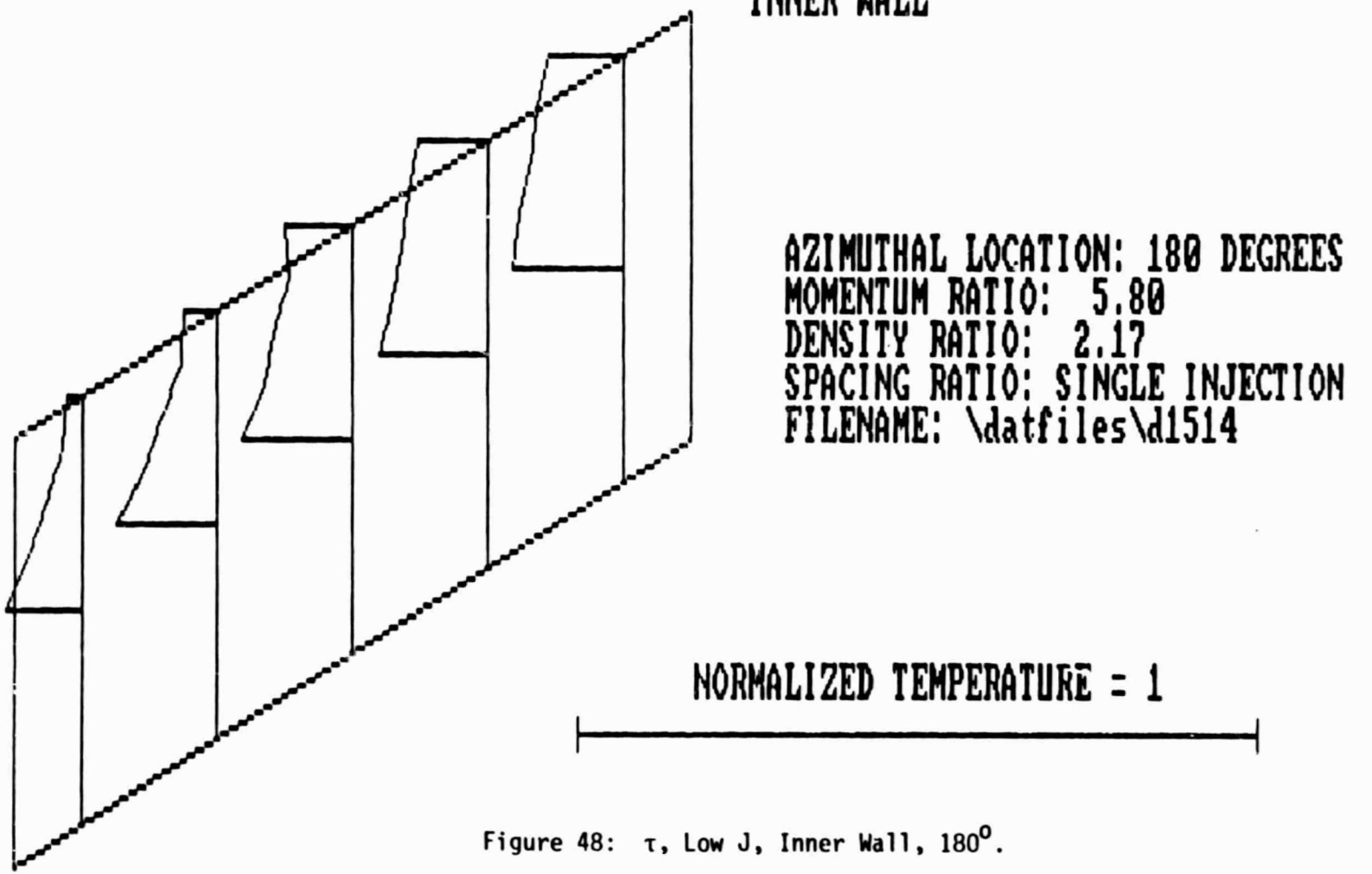

Figure 48: τ, Low J, Inner Wall, 180^{o}.

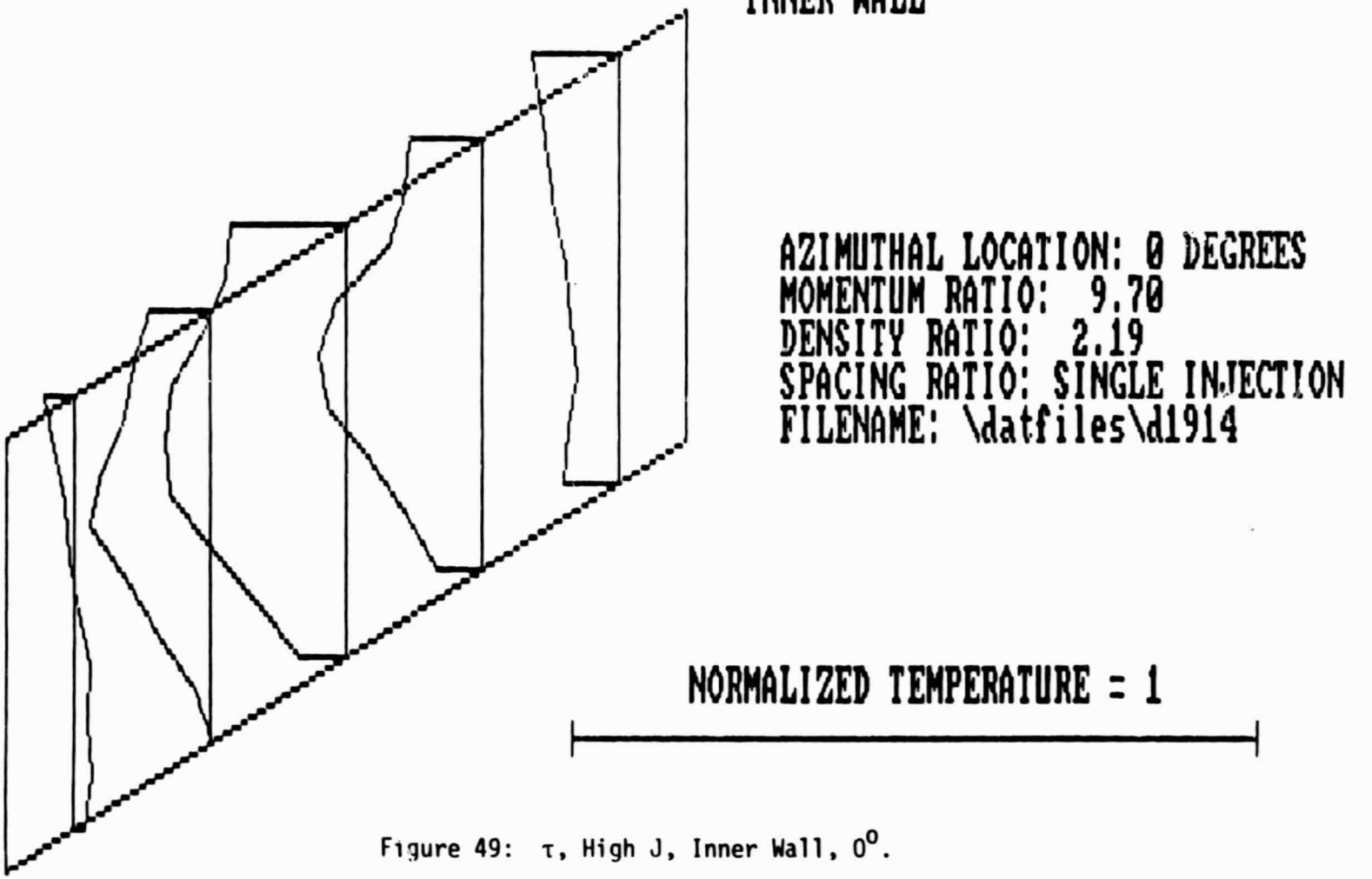

Figure 49: τ, High J, Inner Wall, 0^{o}.

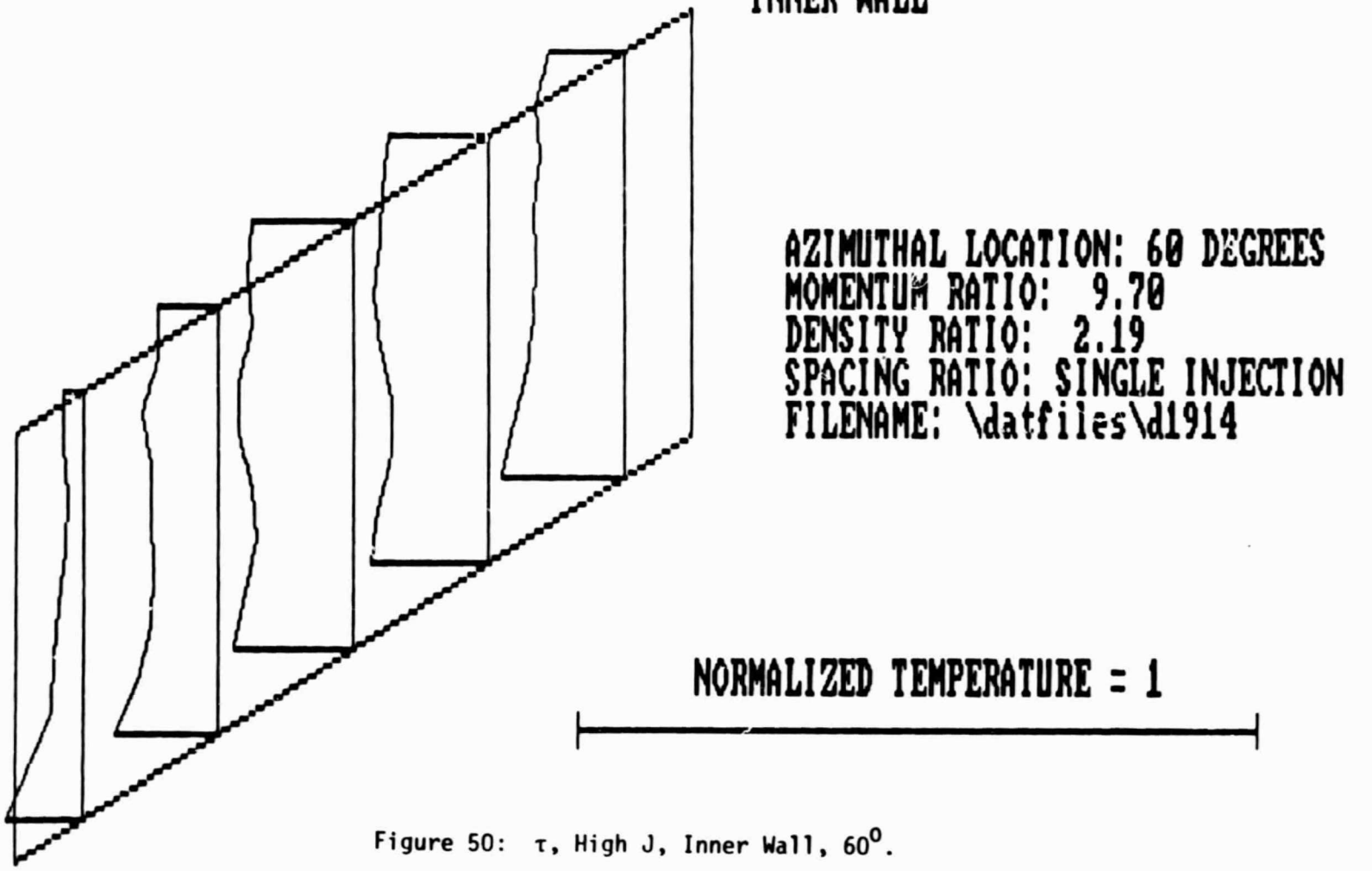

Figure 50: τ, High J, Inner Wall, 60^{o}.

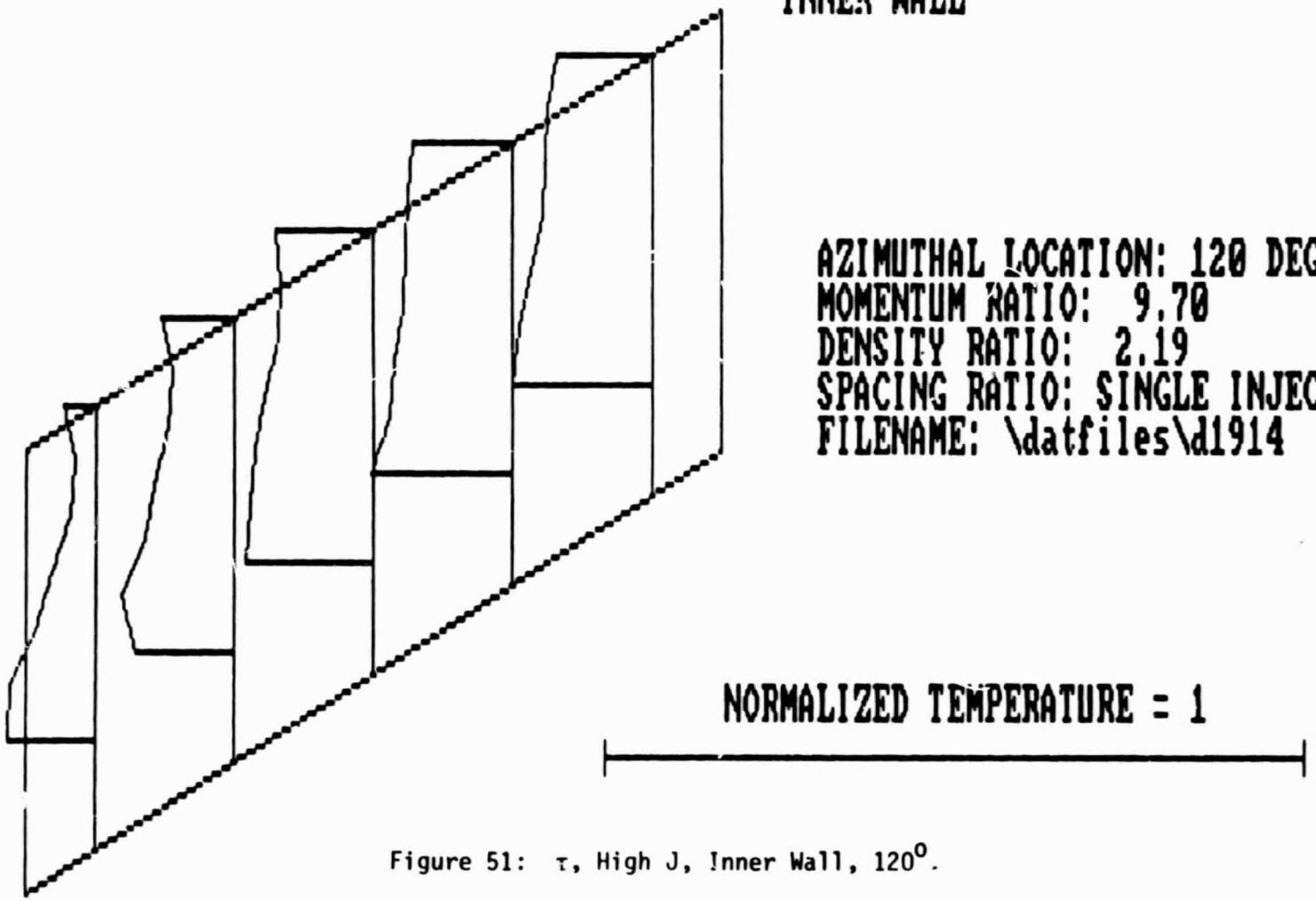

Figure 51: τ, High J, Inner Wall, 120^{o}.

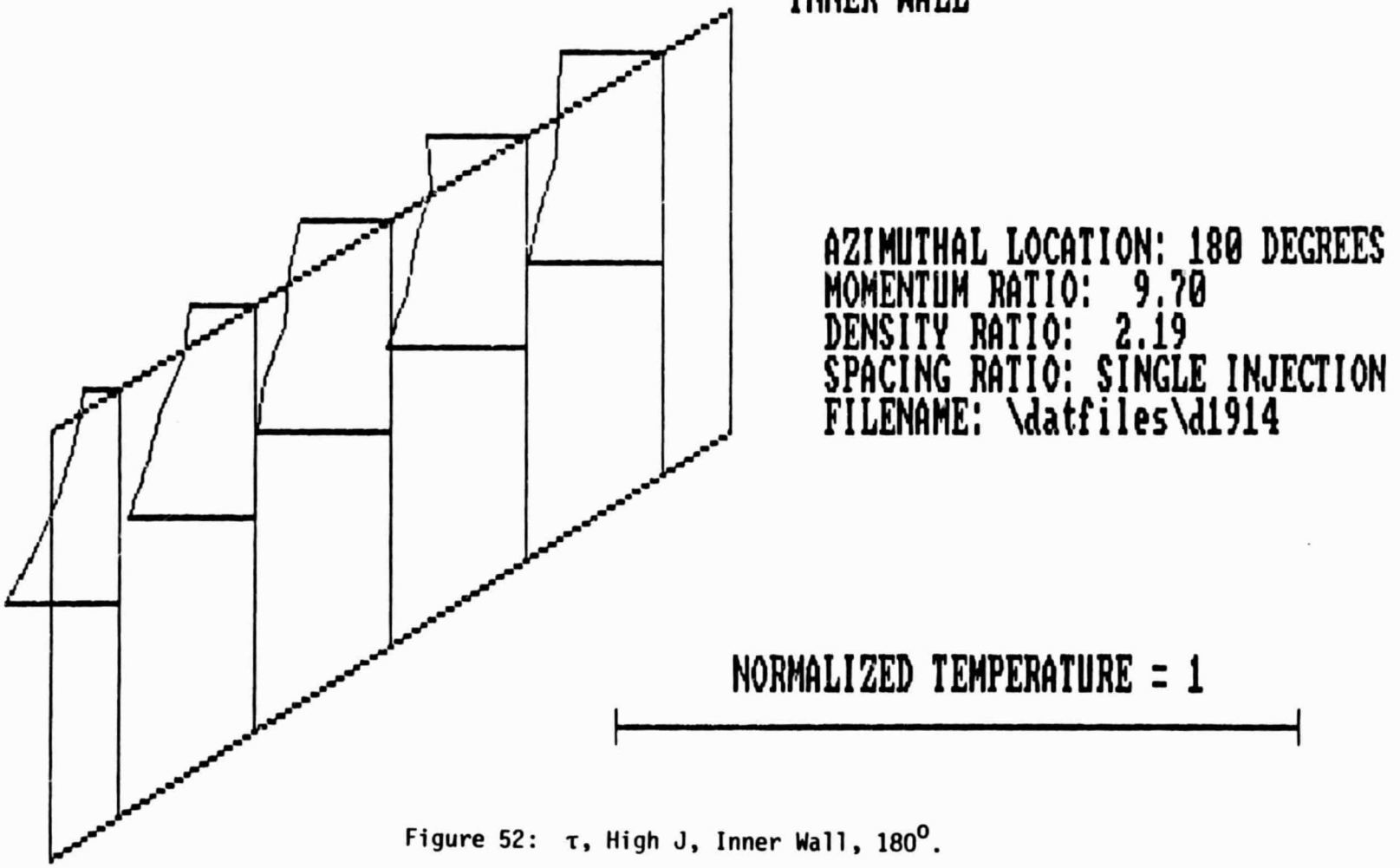

Figure 52: τ, High J, Inner Wall, 180^{o}.

MOMENTUM RATIO: 5.80
DENSITY RATIO: 2.20
SPACING RATIO: SINGLE INJECTION

AZIMUTHAL STATION: 0 DEGREES
RADIAL STATION: 65 UNITS
FILENAME: \datfiles\d1513

NORM. TEMP. = 0.5

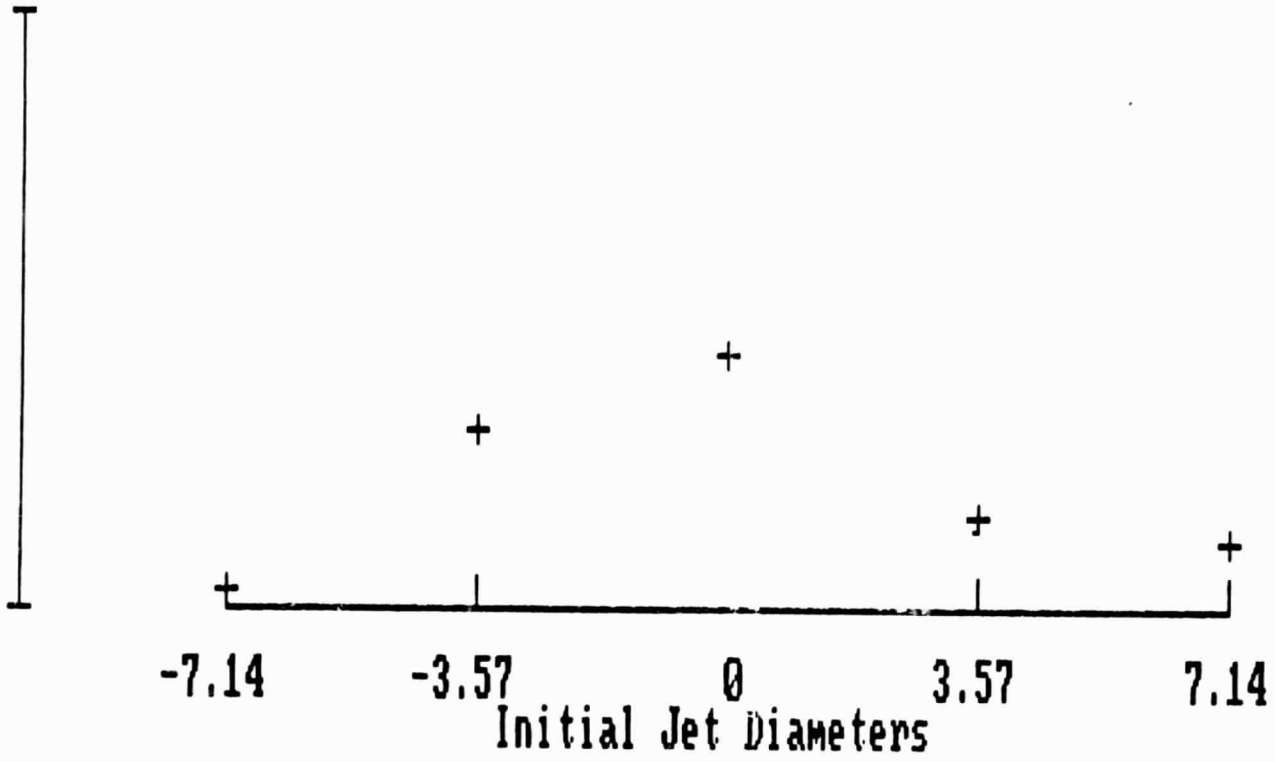

Figure 53: τ, Low J, Outer Wall Prior to Bend, 0^{o}, lateral spreading.

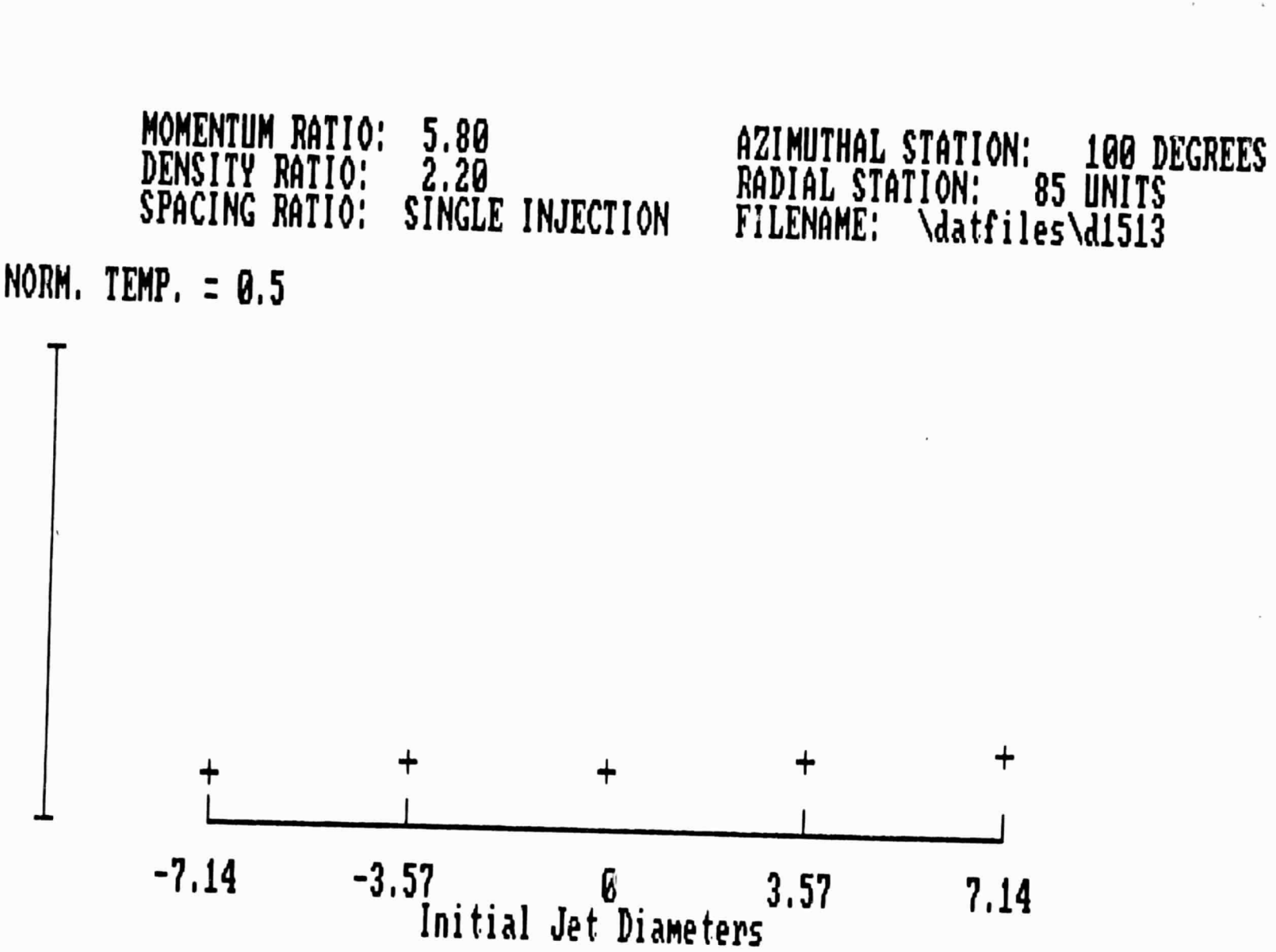

Figure 54: τ, Low J, Outer Wall Prior to Bend, 100^{o}, lateral spreading.

MOMENTUM RATIO: 9.70
DENSITY RATIO: 2.19
SPACING RATIO: SINGLE INJECTION

AZIMUTHAL STATION: 0 DEGREES
RADIAL STATION: 55 UNITS
FILENAME: \datfiles\d1914

NORM. TEMP. = 0.5

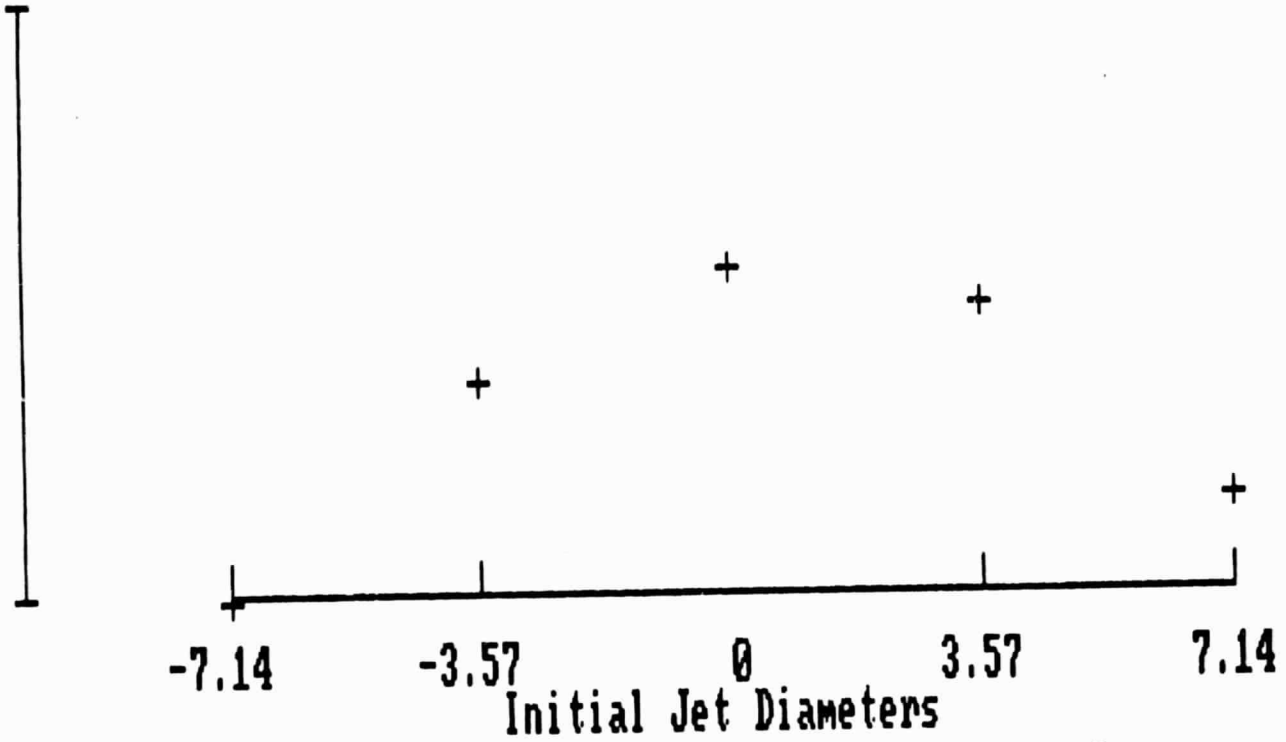

Figure 55: τ, High J, Inner Wall, 0^{o}, lateral spreading.

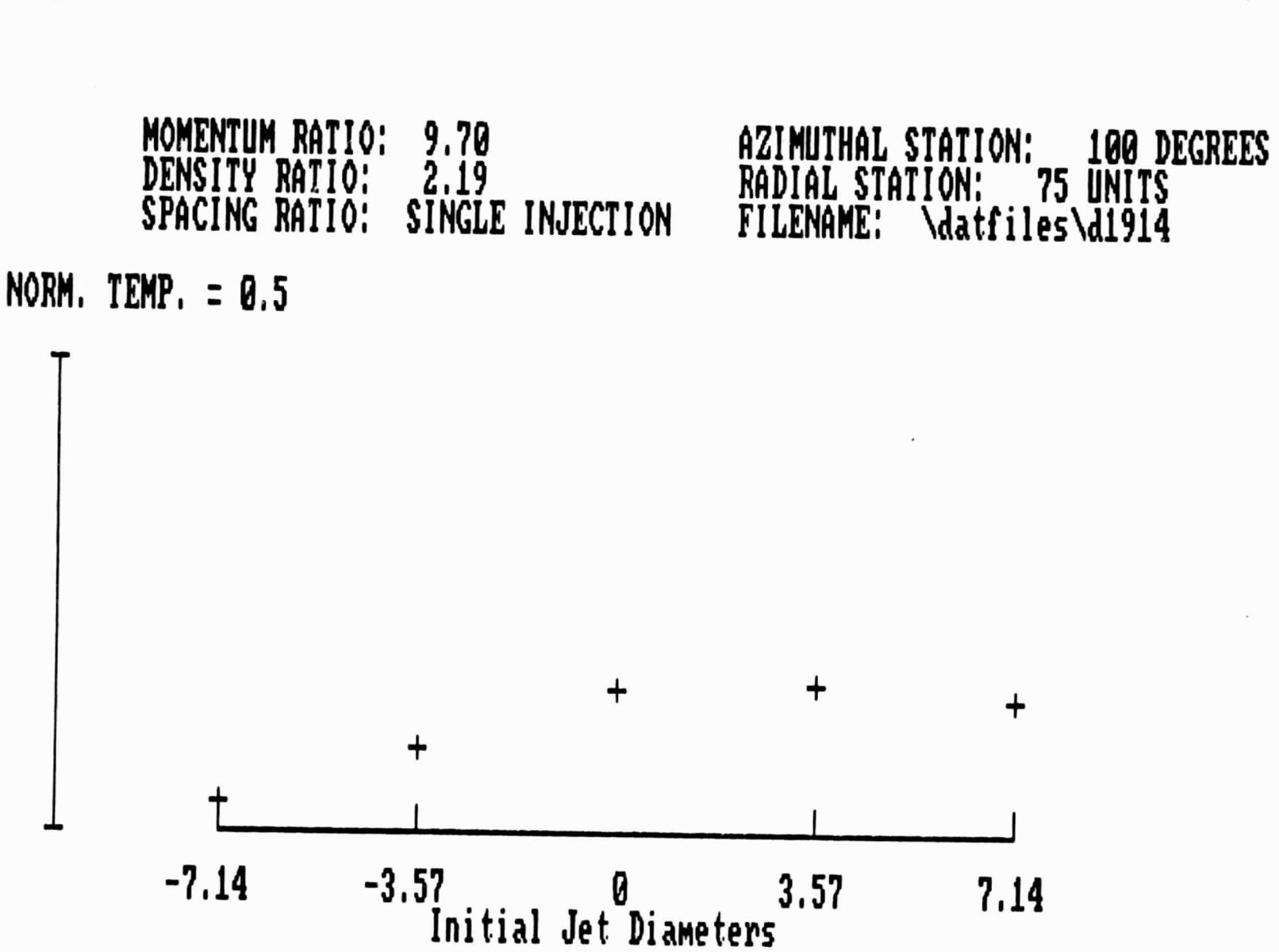

Figure 56: τ, High J, Inner Wall, 100^{o}, lateral spreading.

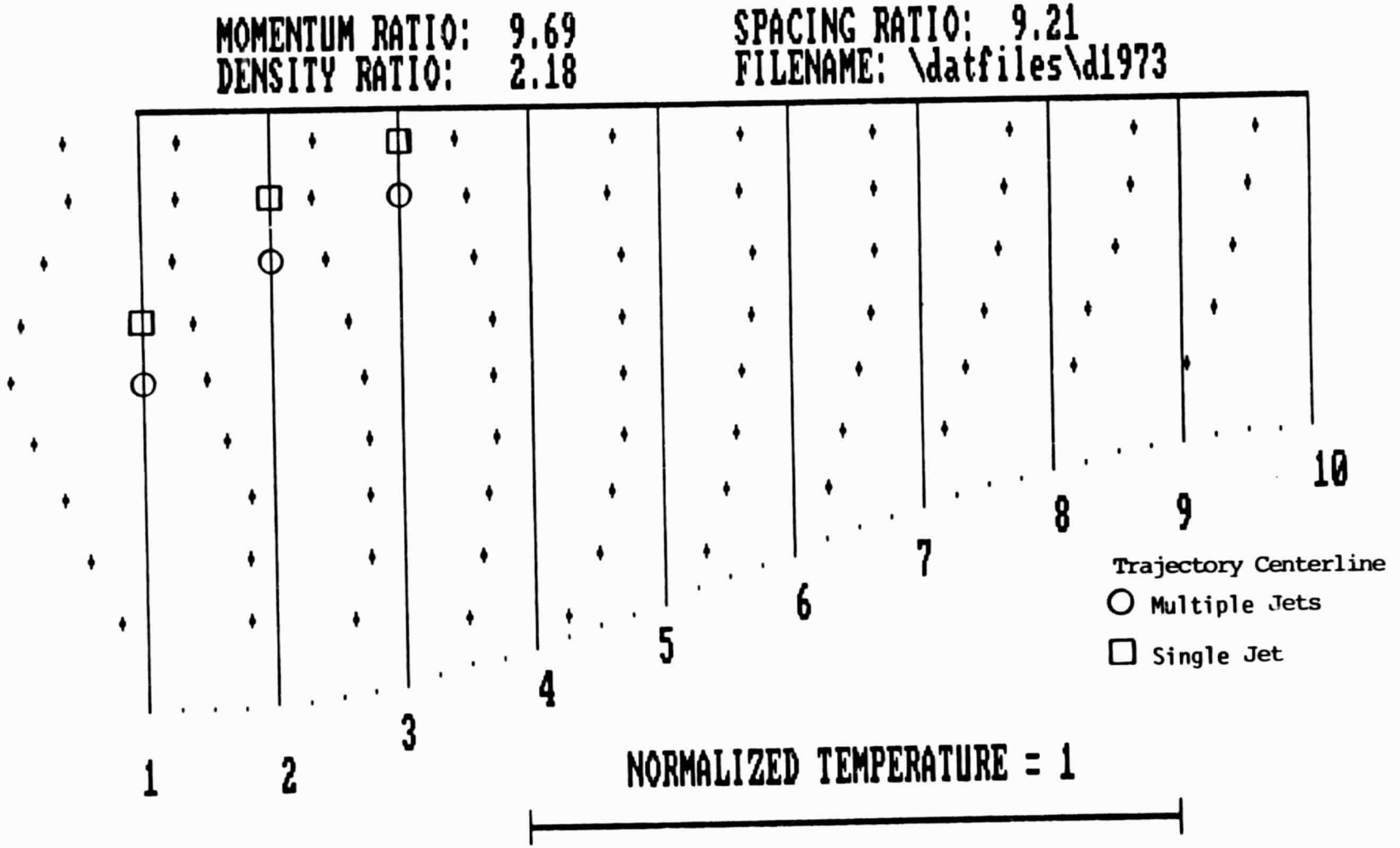

Figure 57: τ, High J, Outer Wall Prior to Bend, 7 jets.

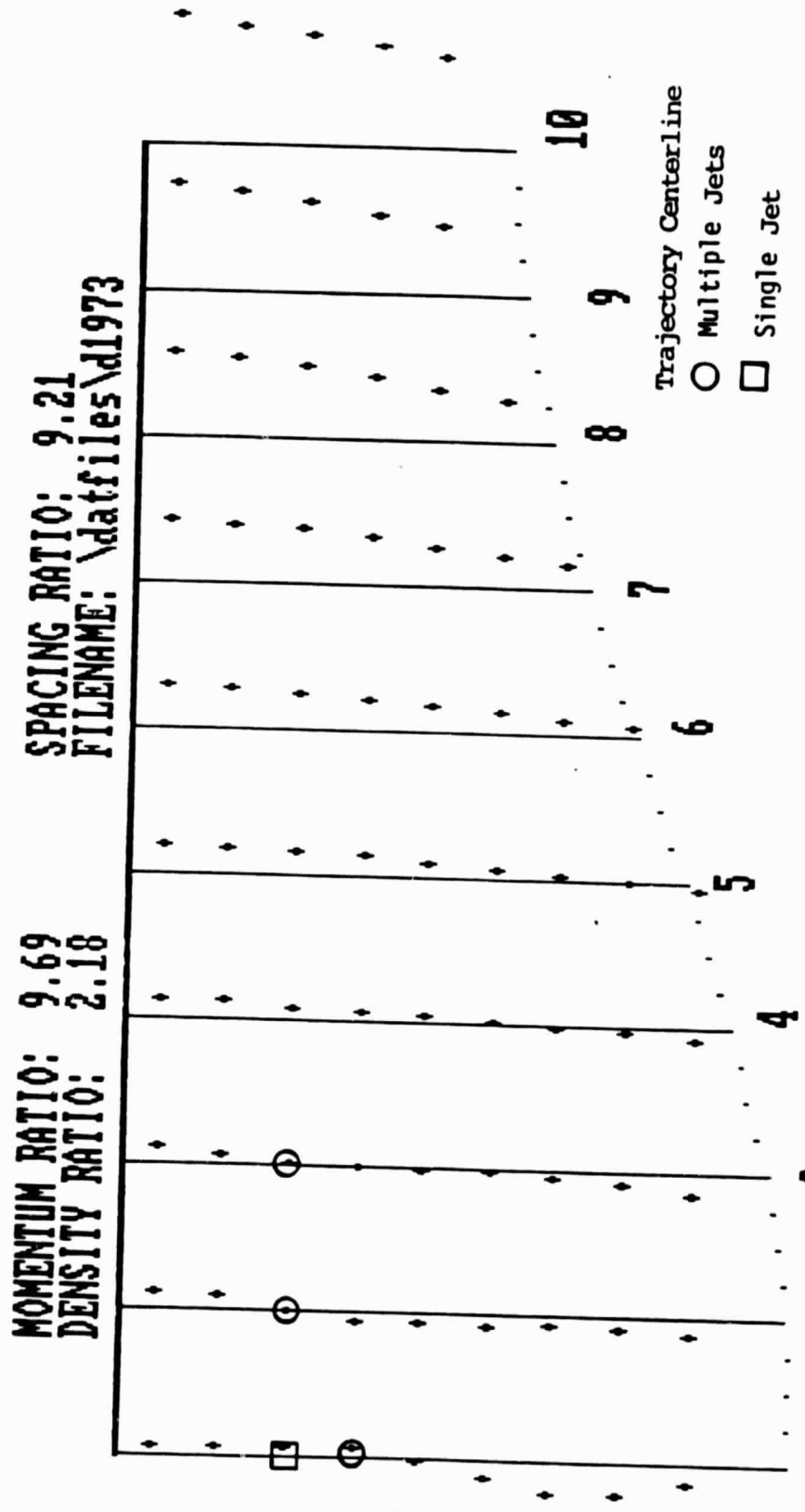

Figure 58: Y, High J, Outer Wall Prior to Bend, 7 jets.

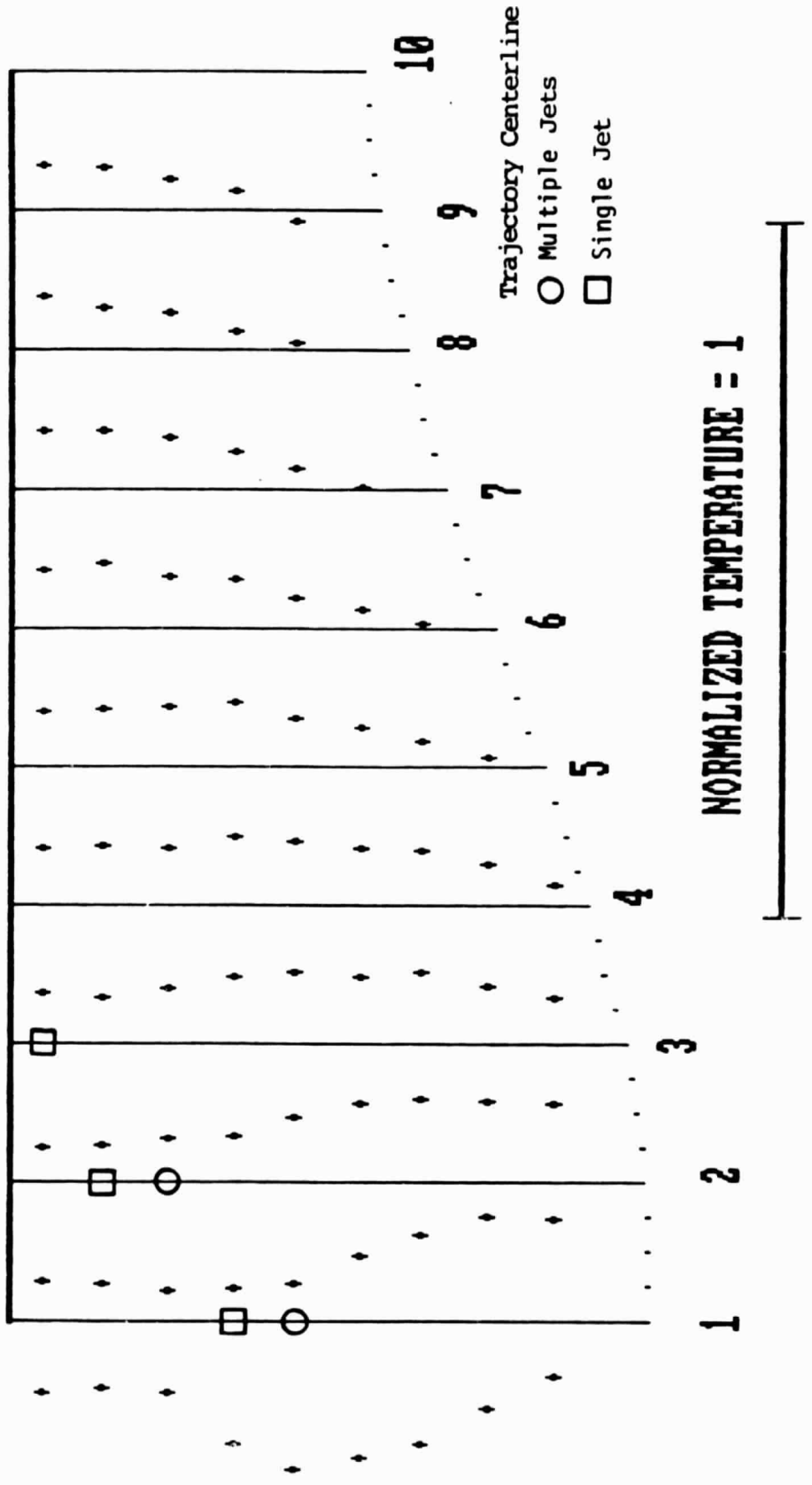

Figure 59: τ, High J, Outer Wall Prior to Bend, 11 jets.

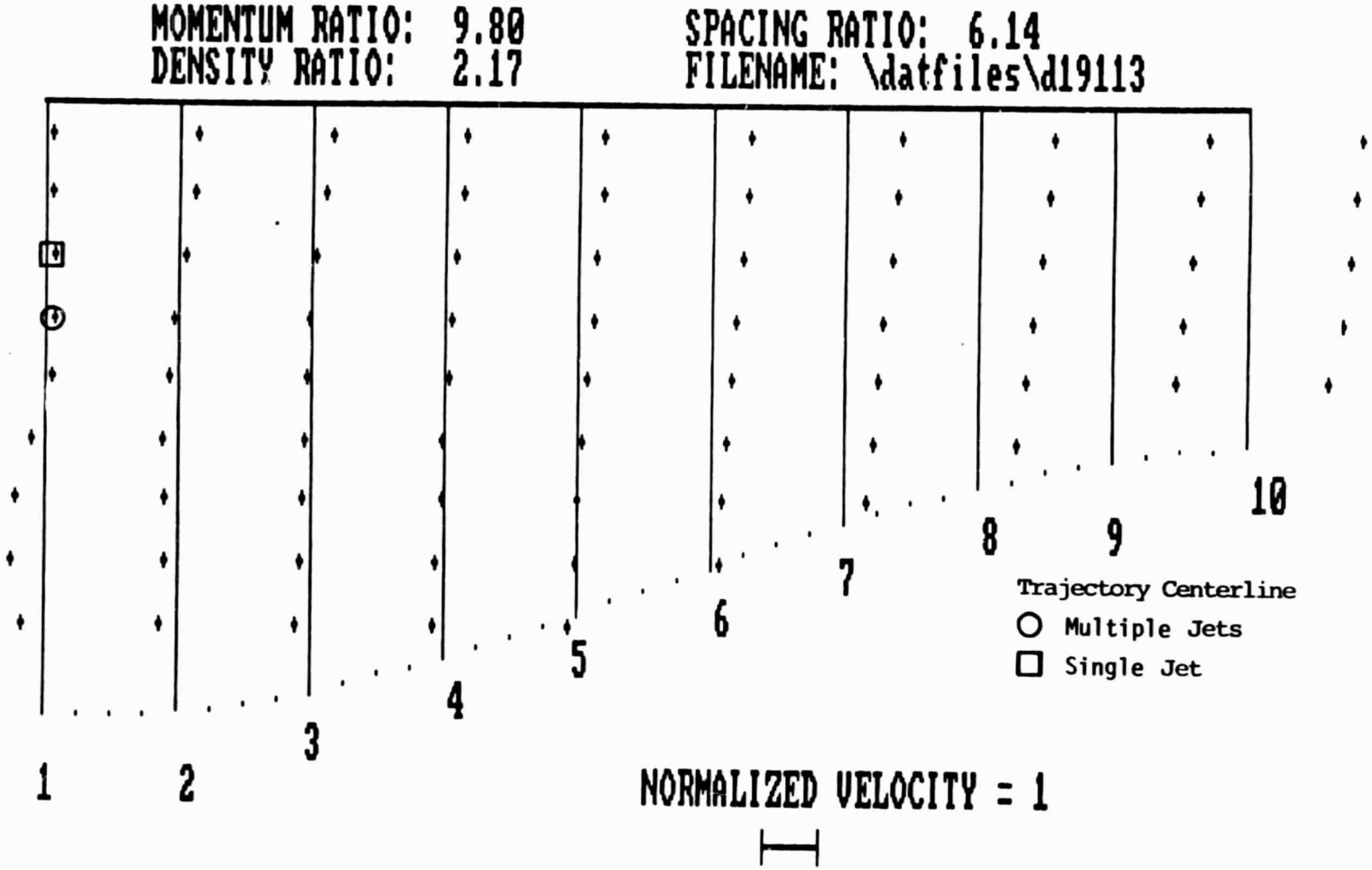

Figure 60: γ, High J, Outer Wall Prior to Bend, 11 jets.

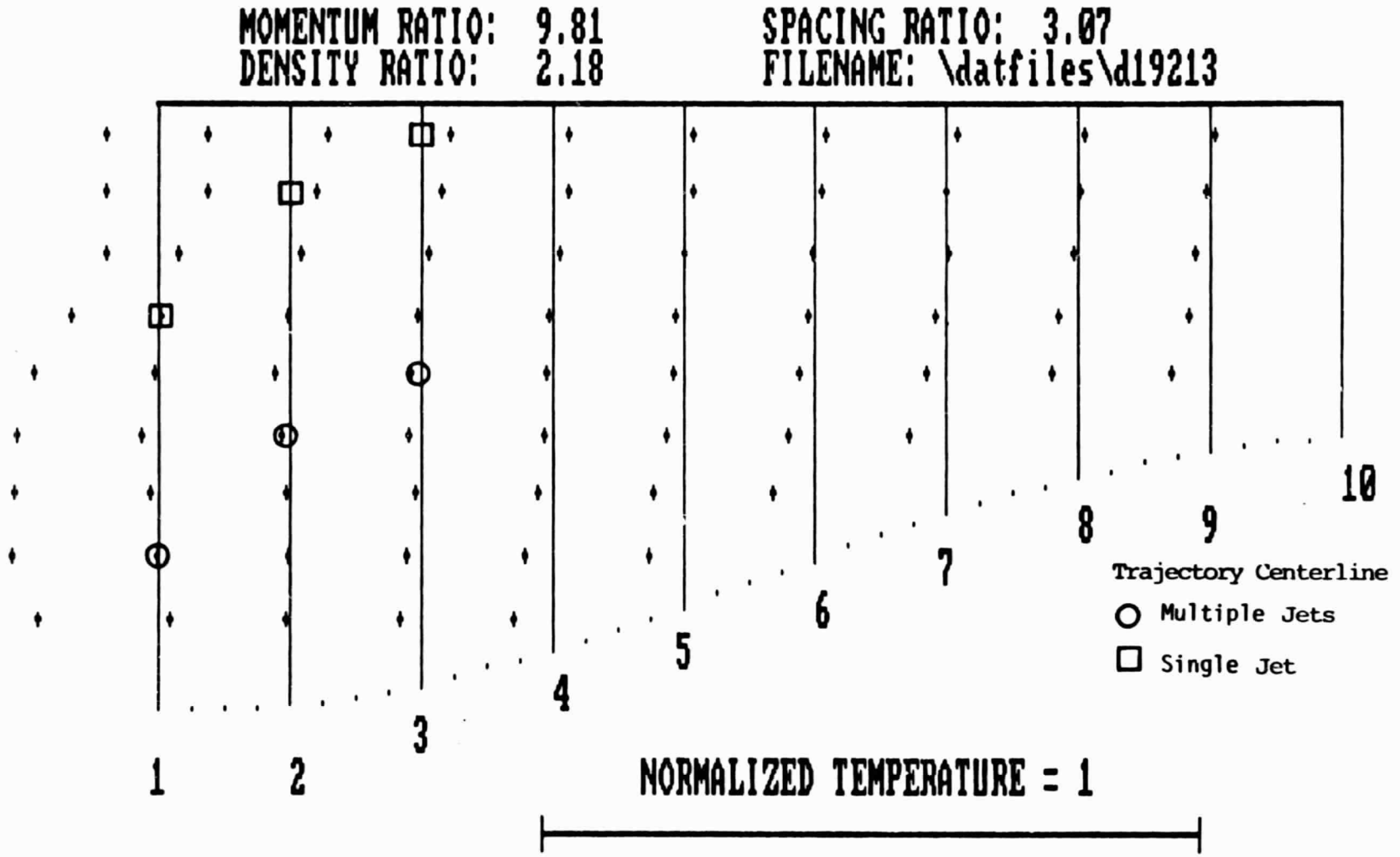

Figure 61: τ, High J, Outer Wall Prior to Bend, 21 jets.

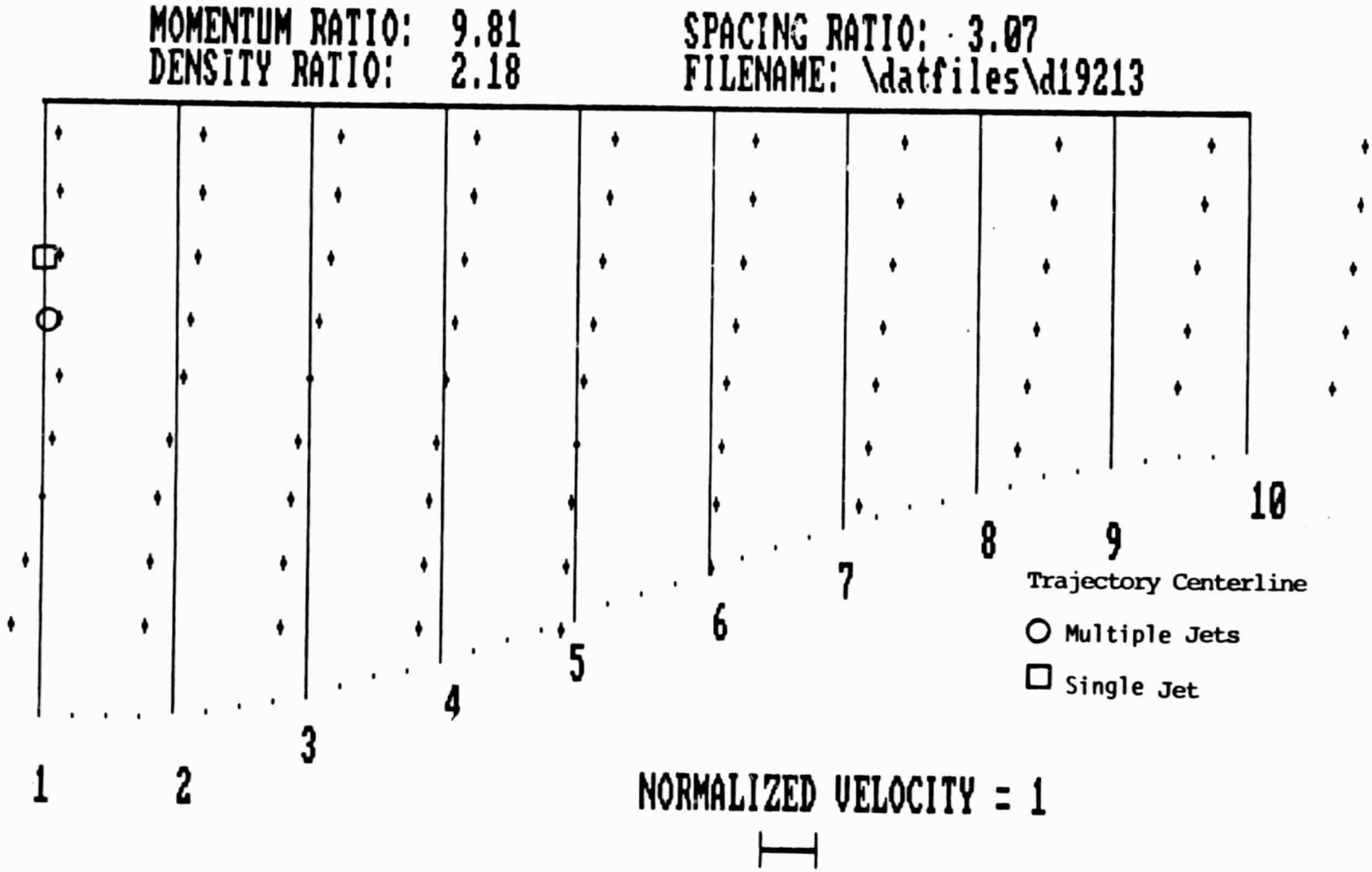

Figure 62: γ, High J, Outer Wall Prior to Bend, 21 jets.

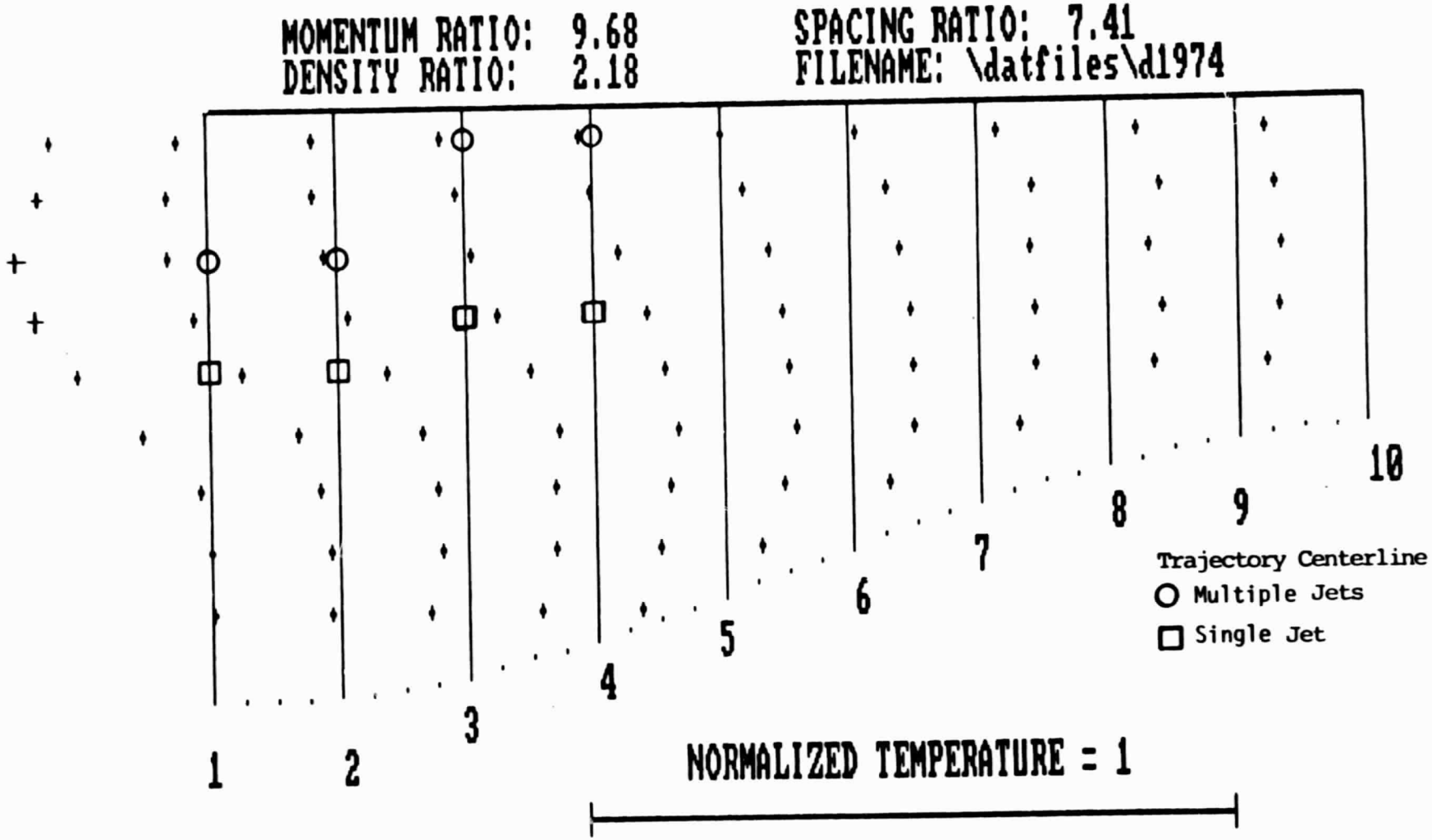

Figure 63: τ, High J, Inner Wall, 7 jets.

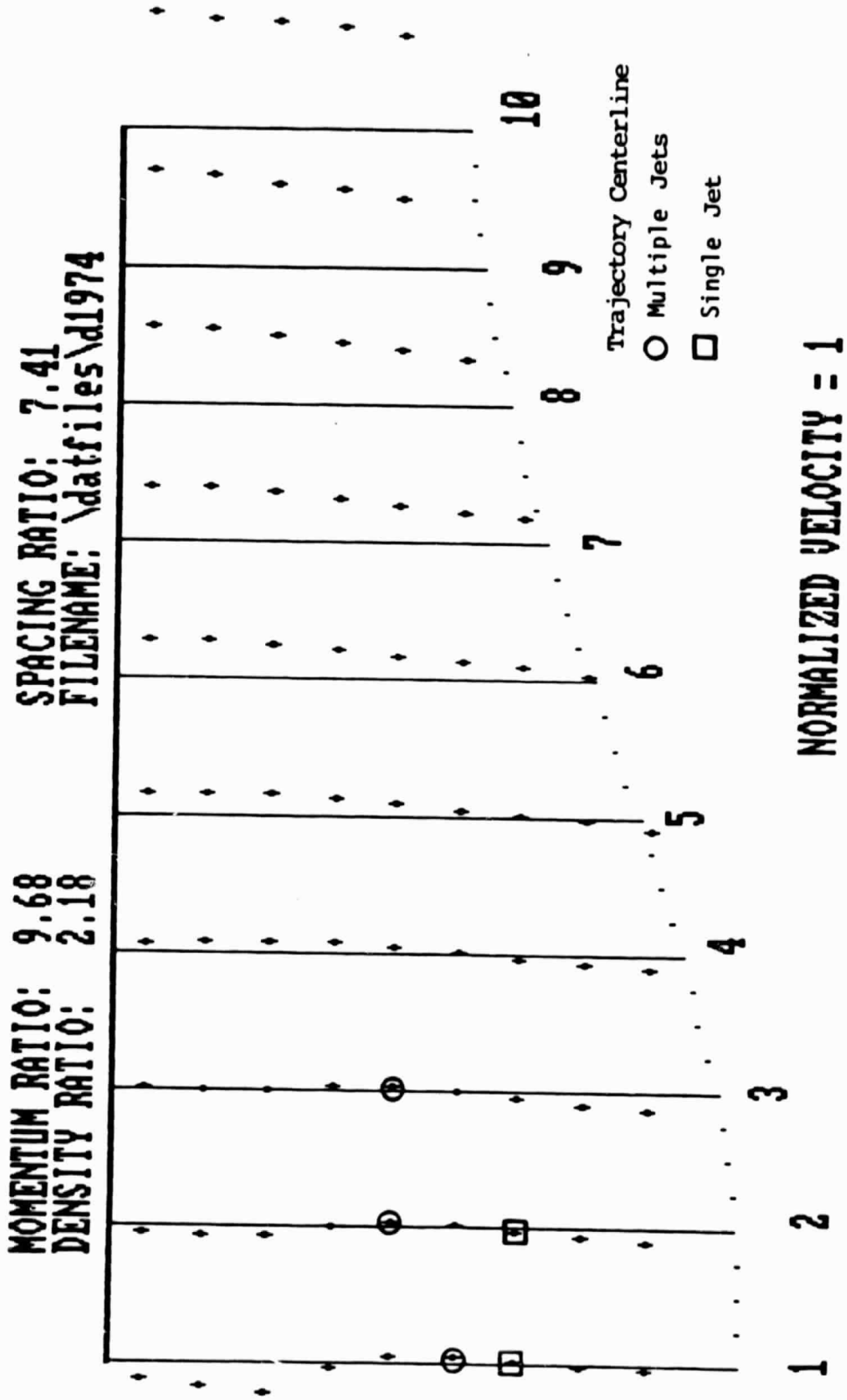

Figure 64: Y, High J, Inner Wall, 7 jets.

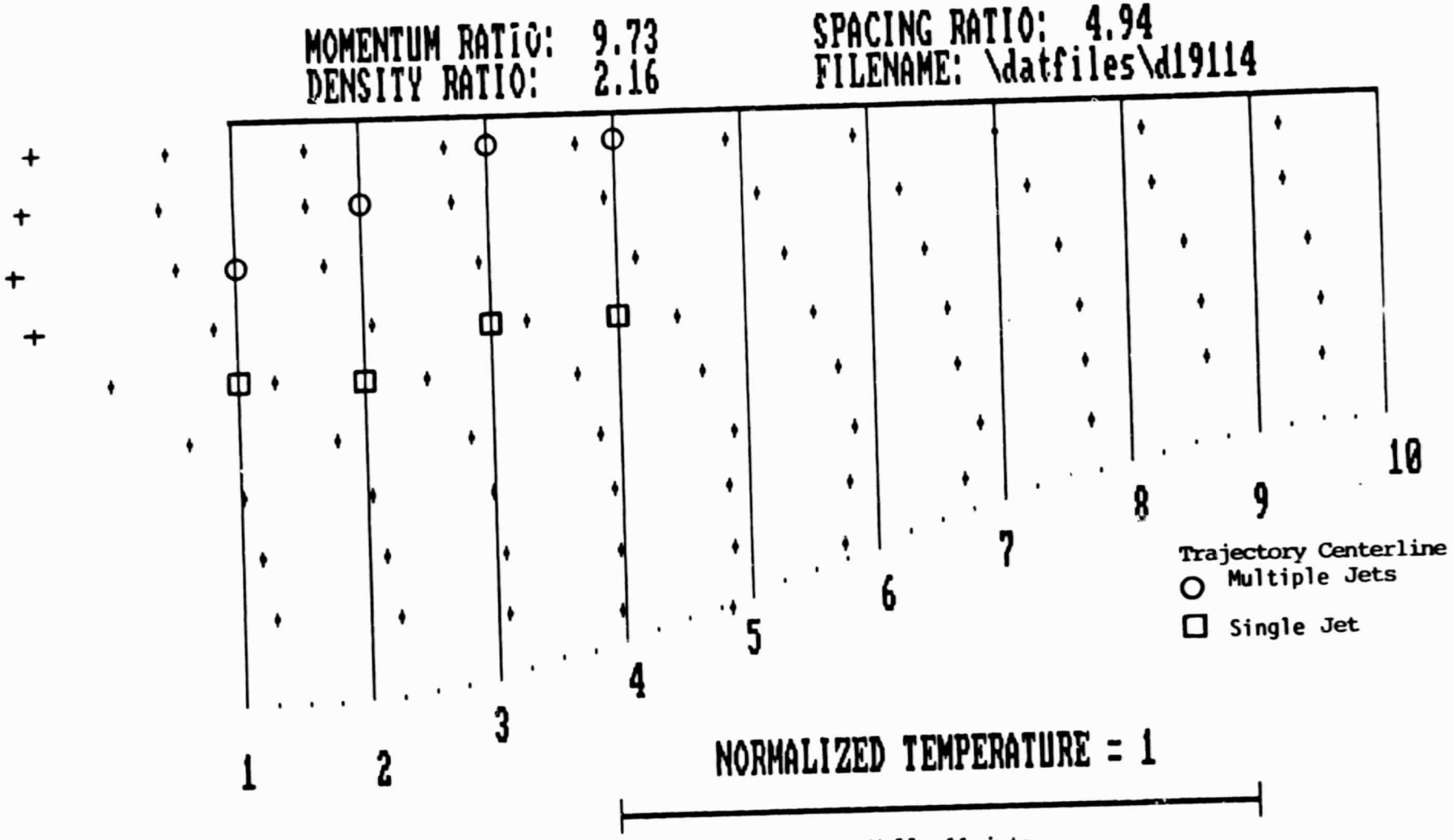

Figure 65: τ, High J, Inner Wall, 11 jets.

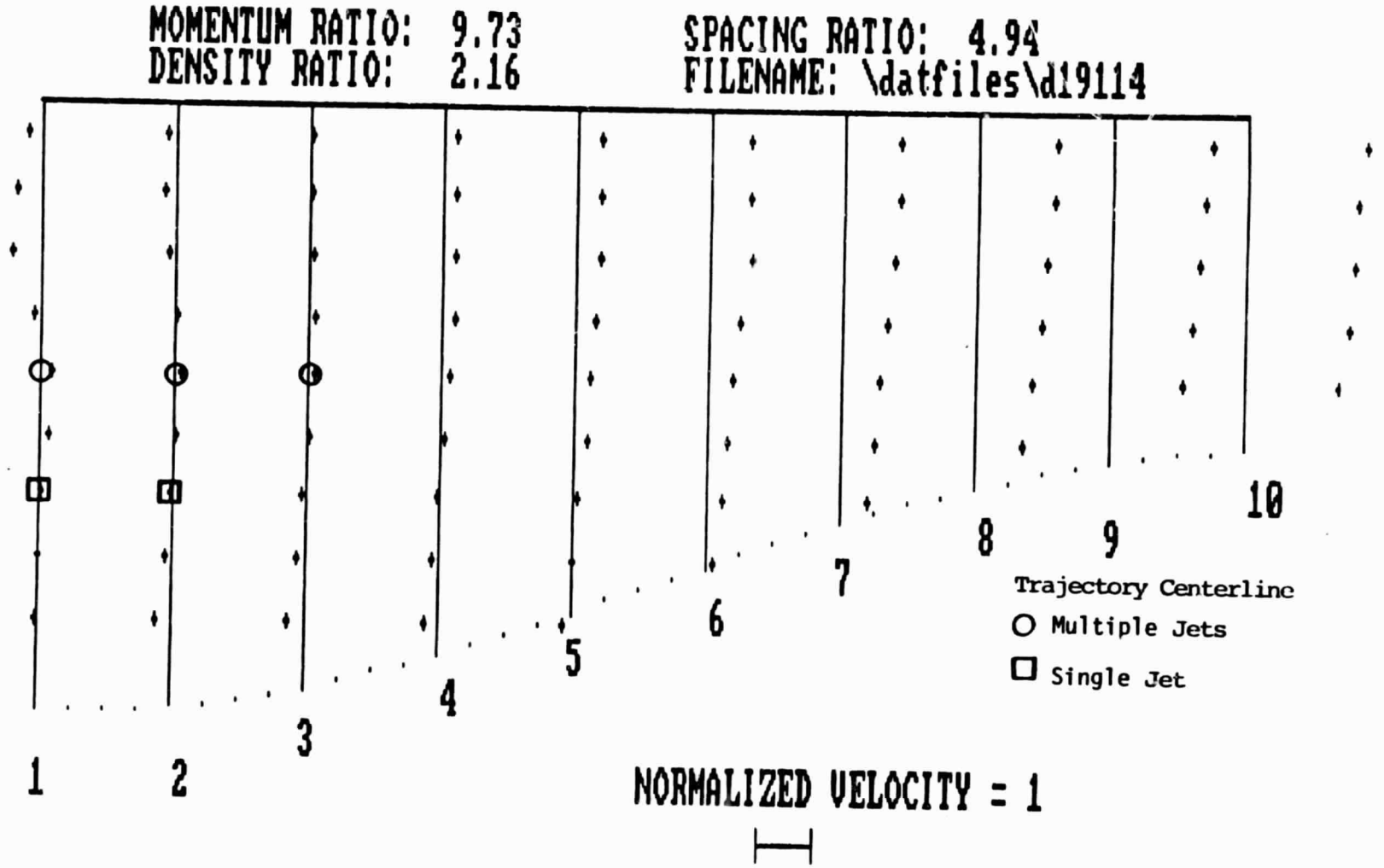

Figure 66: γ, High J, Inner Wall, 11 jets.

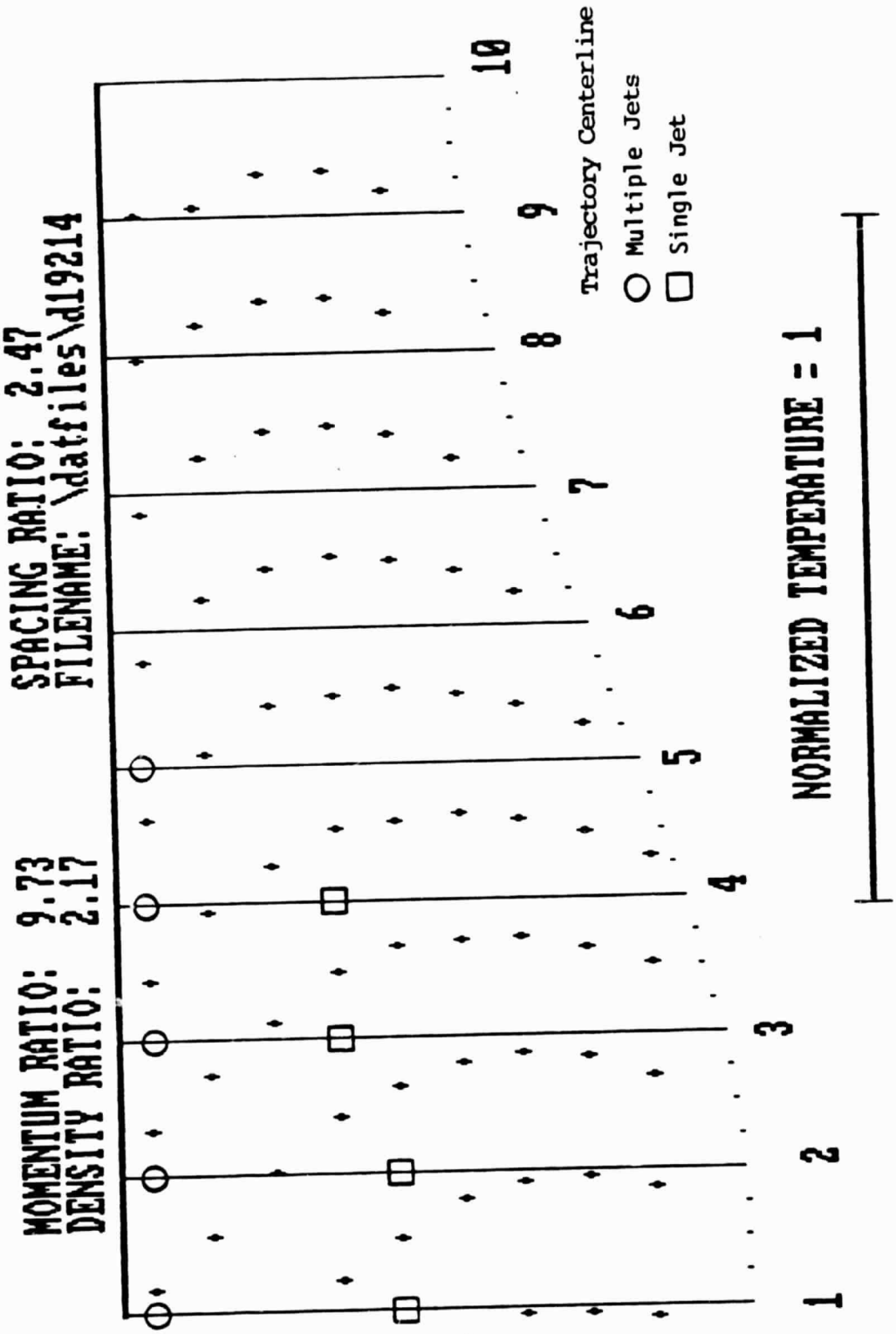

Figure 67: τ, High J, Inner Wall, 21 jets.

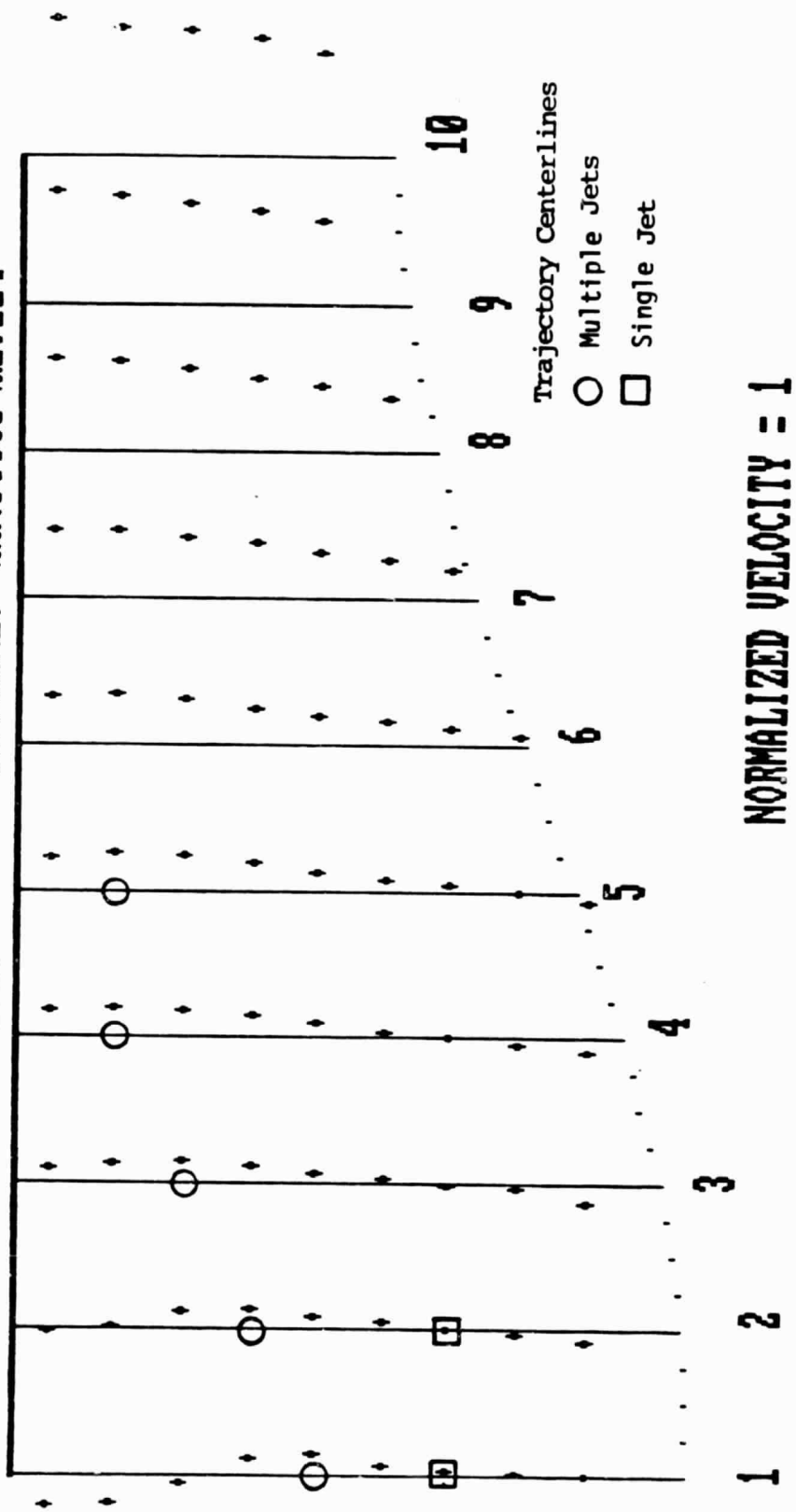

Figure 68: γ, High J, Inner Wall, 21 jets.

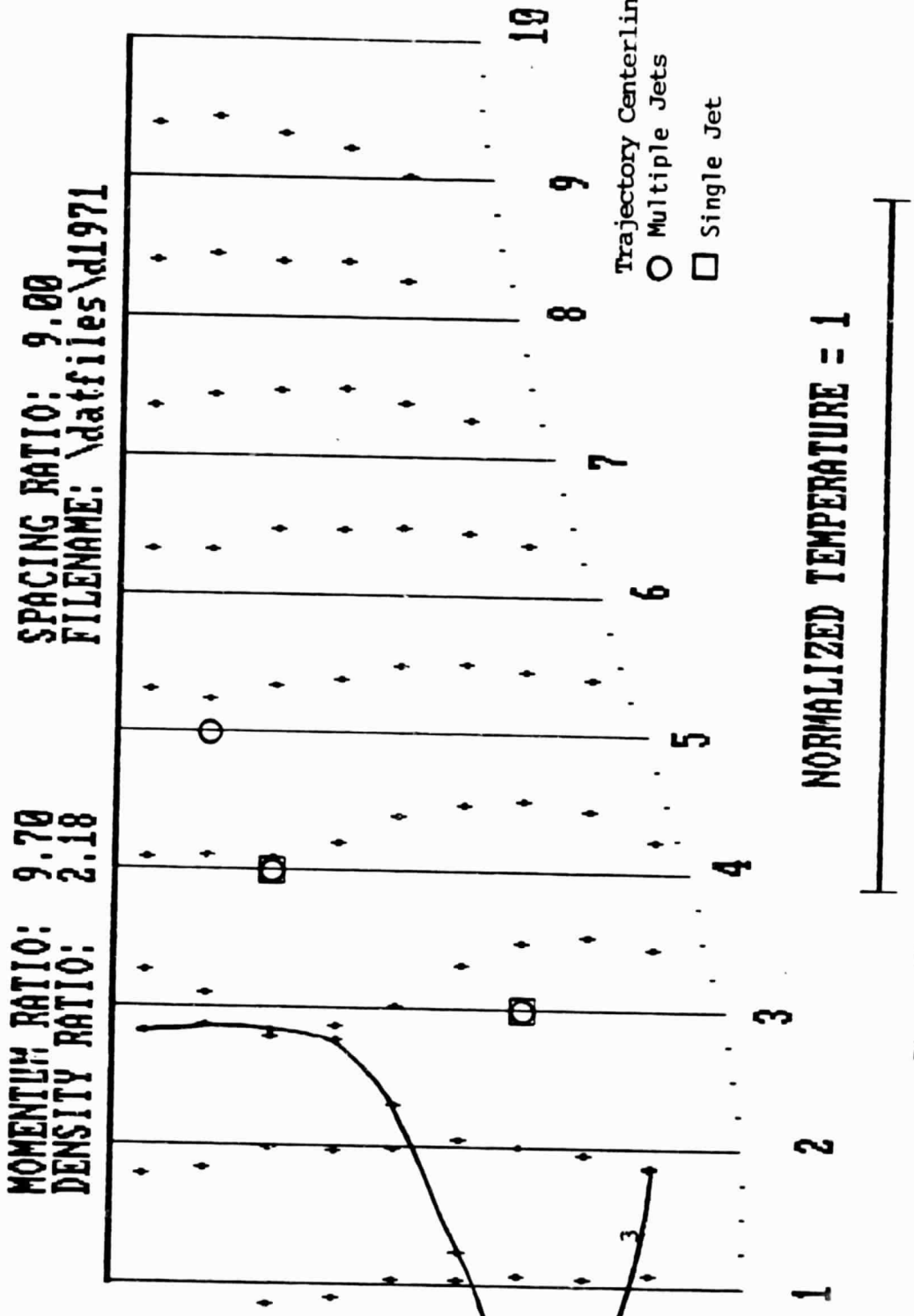

Figure 69: τ, High J, Outer Wall Into Bend, 7 jets.

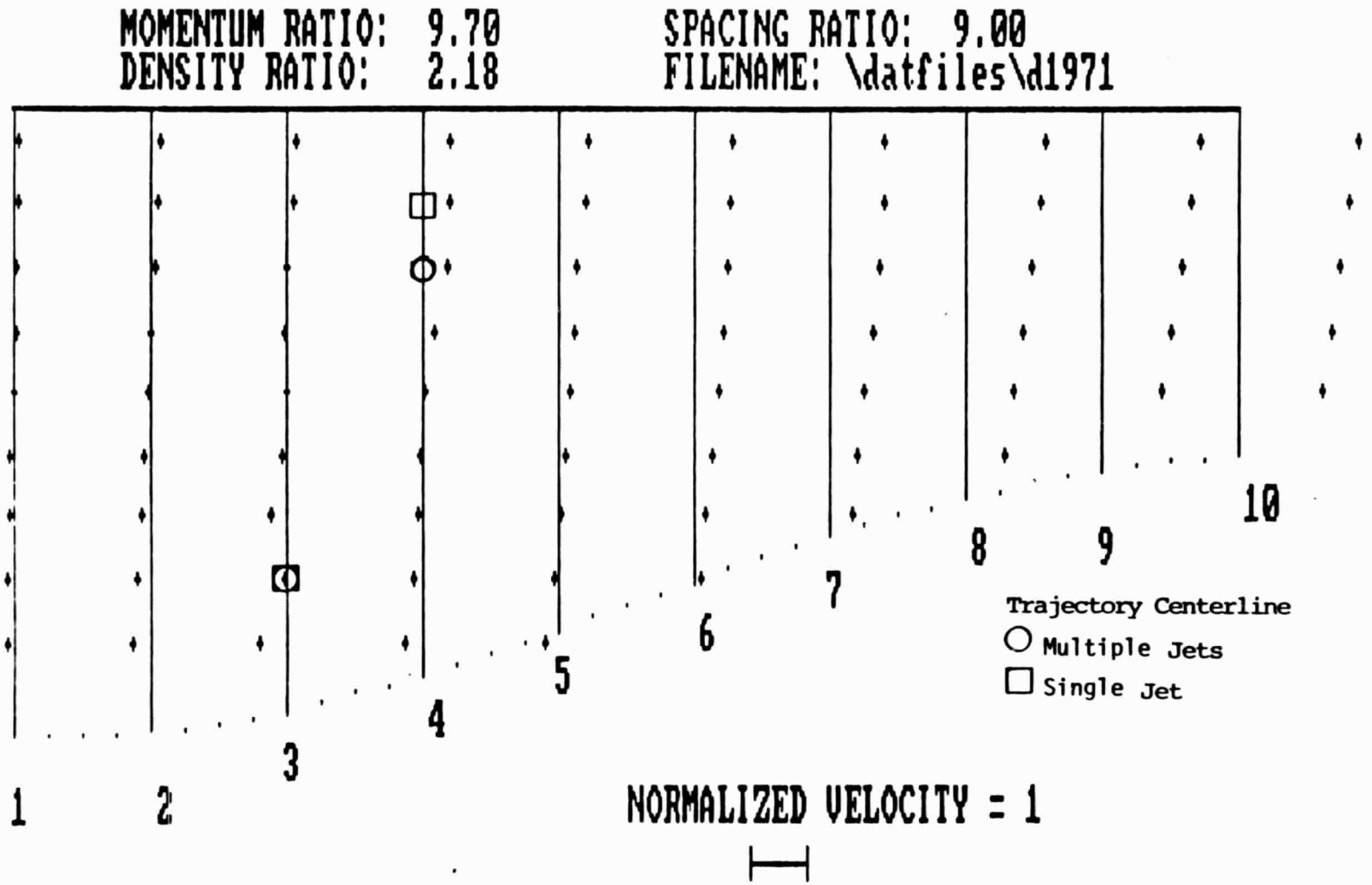

Figure 70: γ, High J, Outer Wall Into Bend, 7 jets.

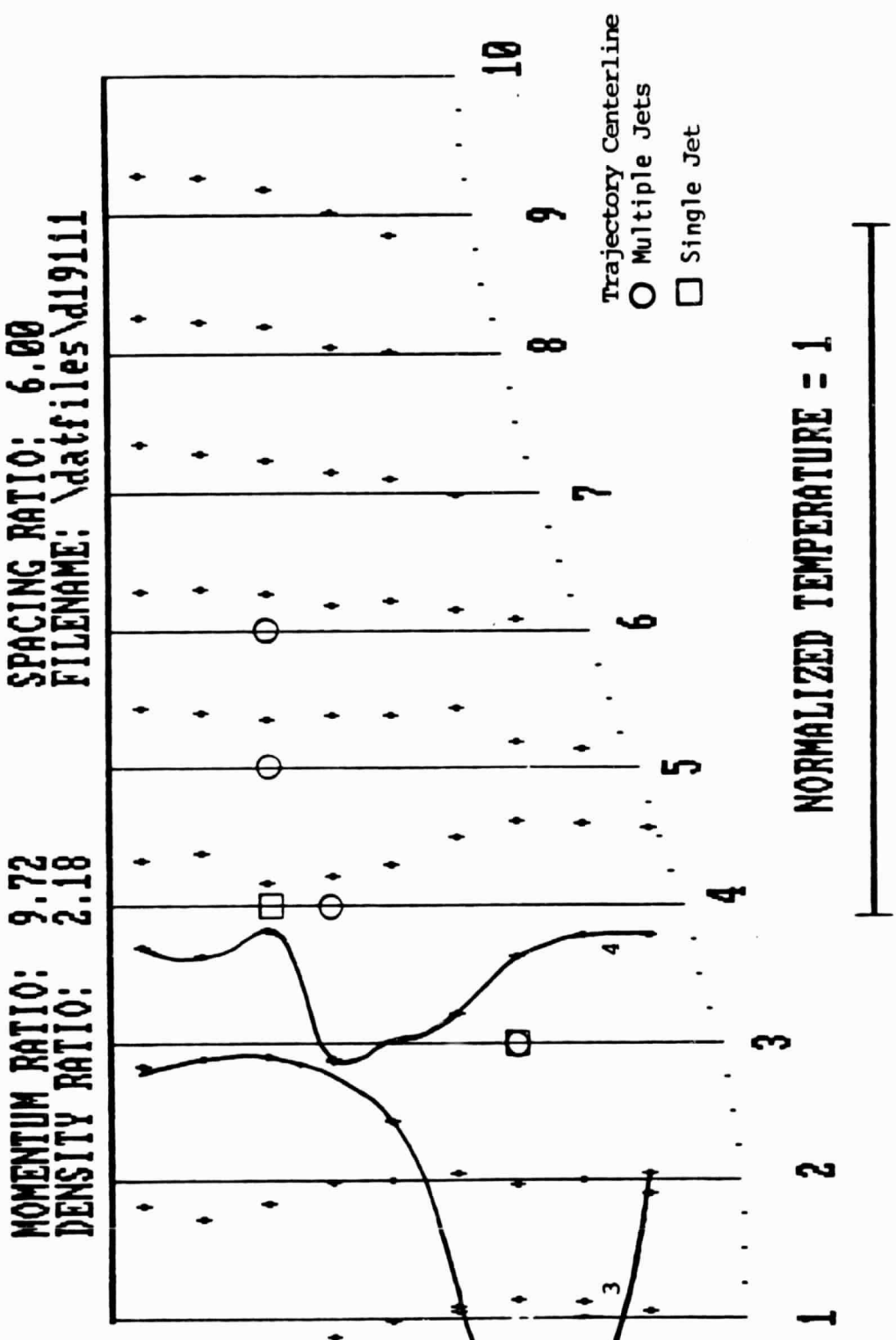

Figure 71: τ, High J, Outer Wall Into Bend, 11 jets.

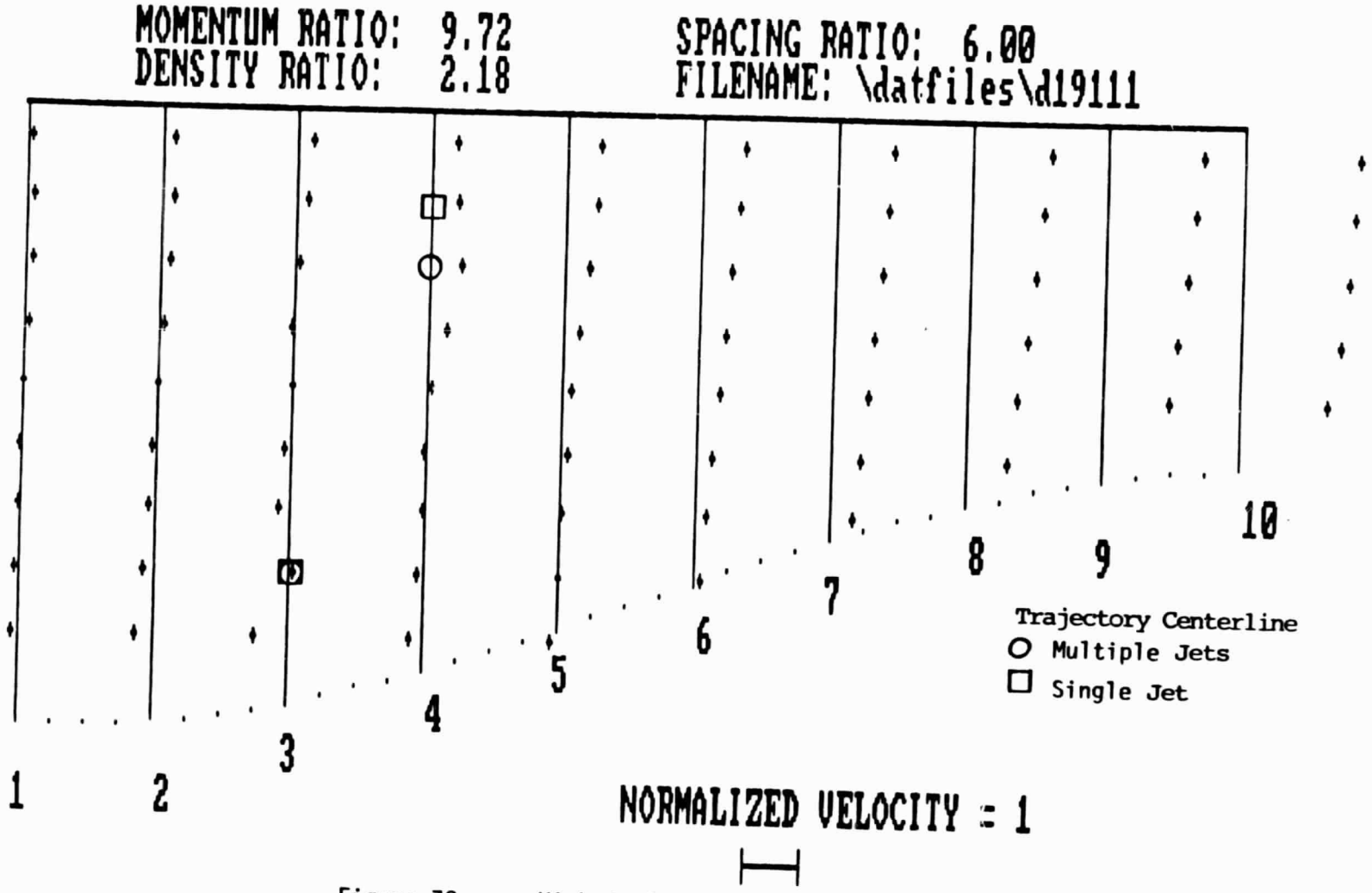

Figure 72: γ, High J, Outer Wall Into Bend, 11 Jets.

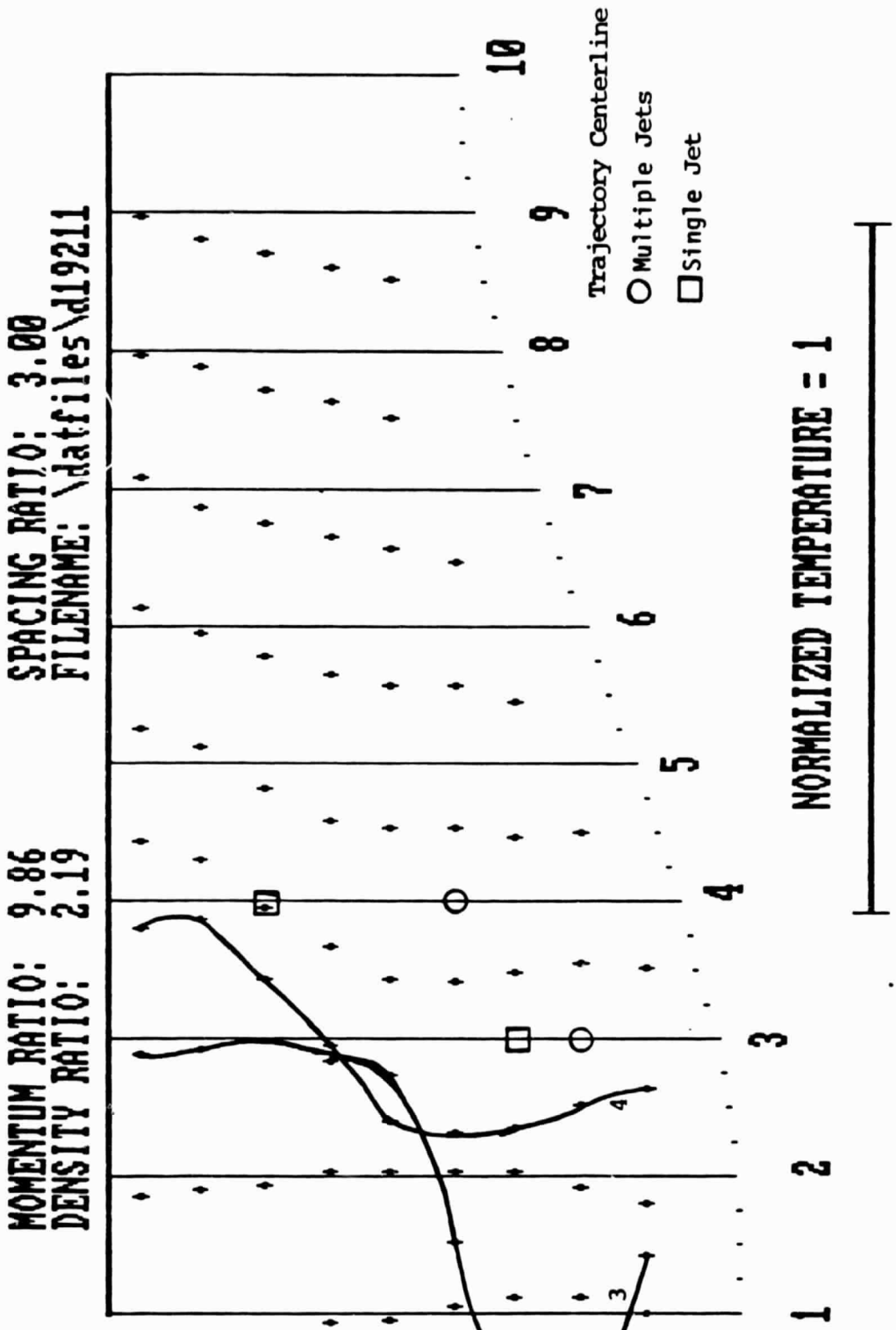

Figure 73: τ, High J, Outer Wall Into Bend, 21 Jets.

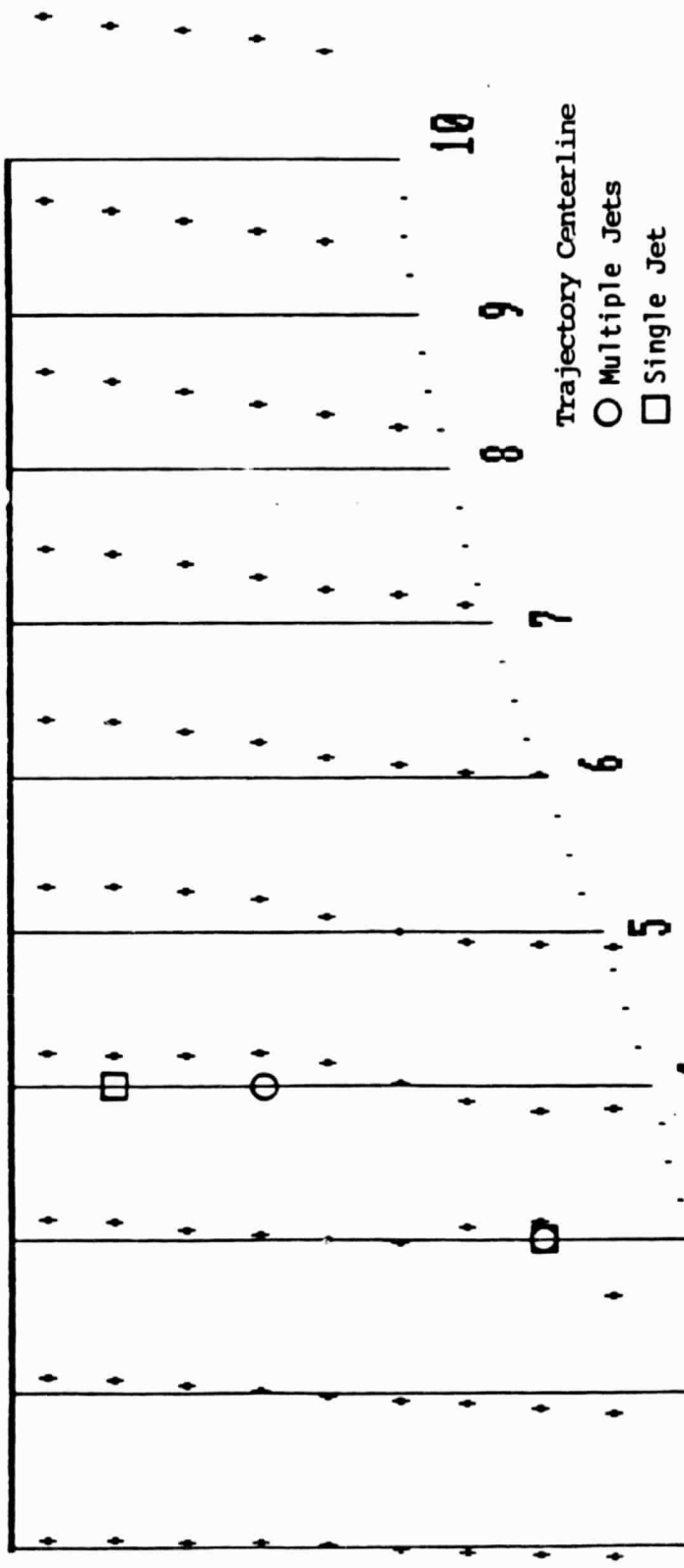

Figure 74: Y, High J, Outer Wall Into Bend, 21 Jets.

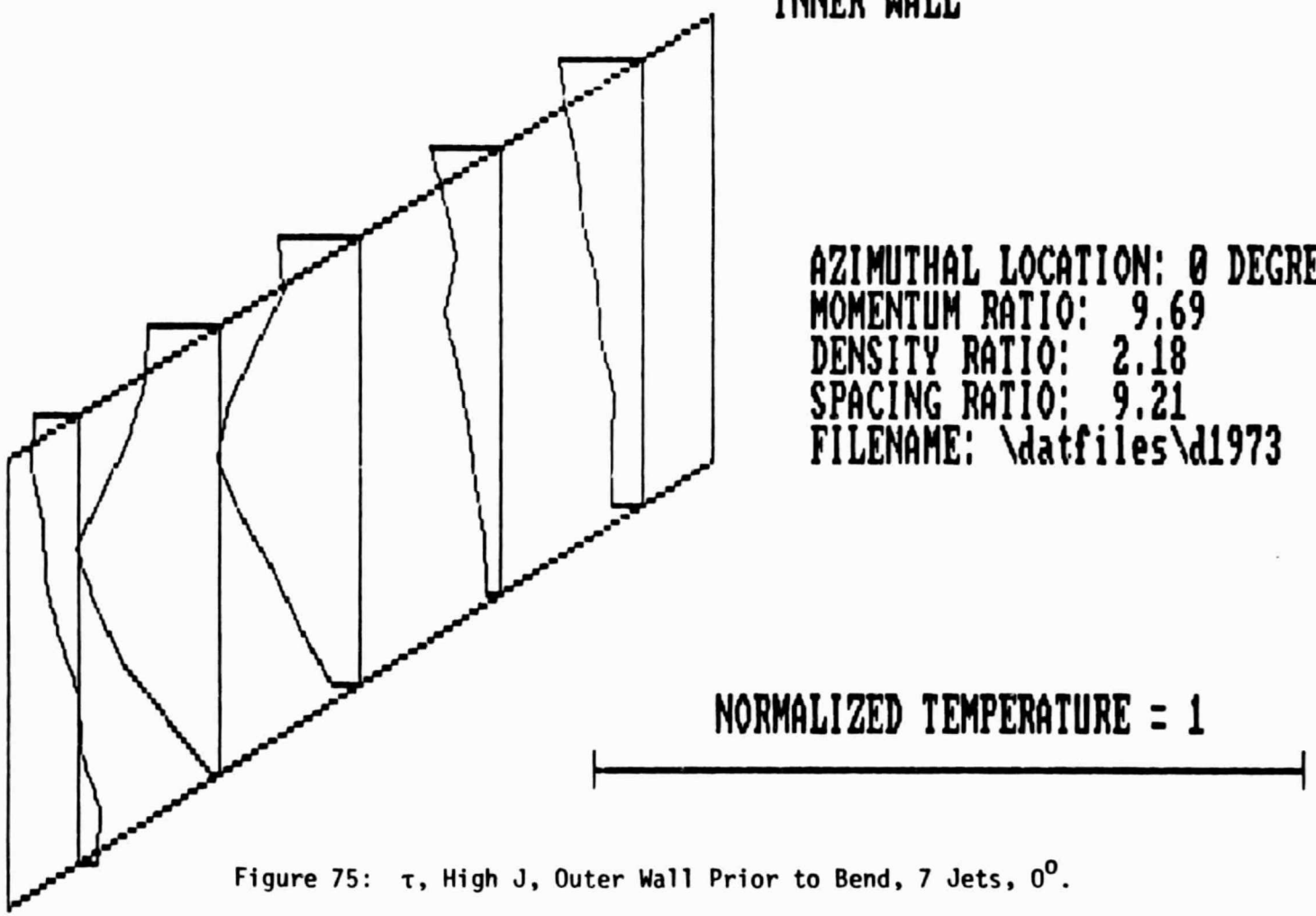

Figure 75: τ, High J, Outer Wall Prior to Bend, 7 Jets, 0^{o}.

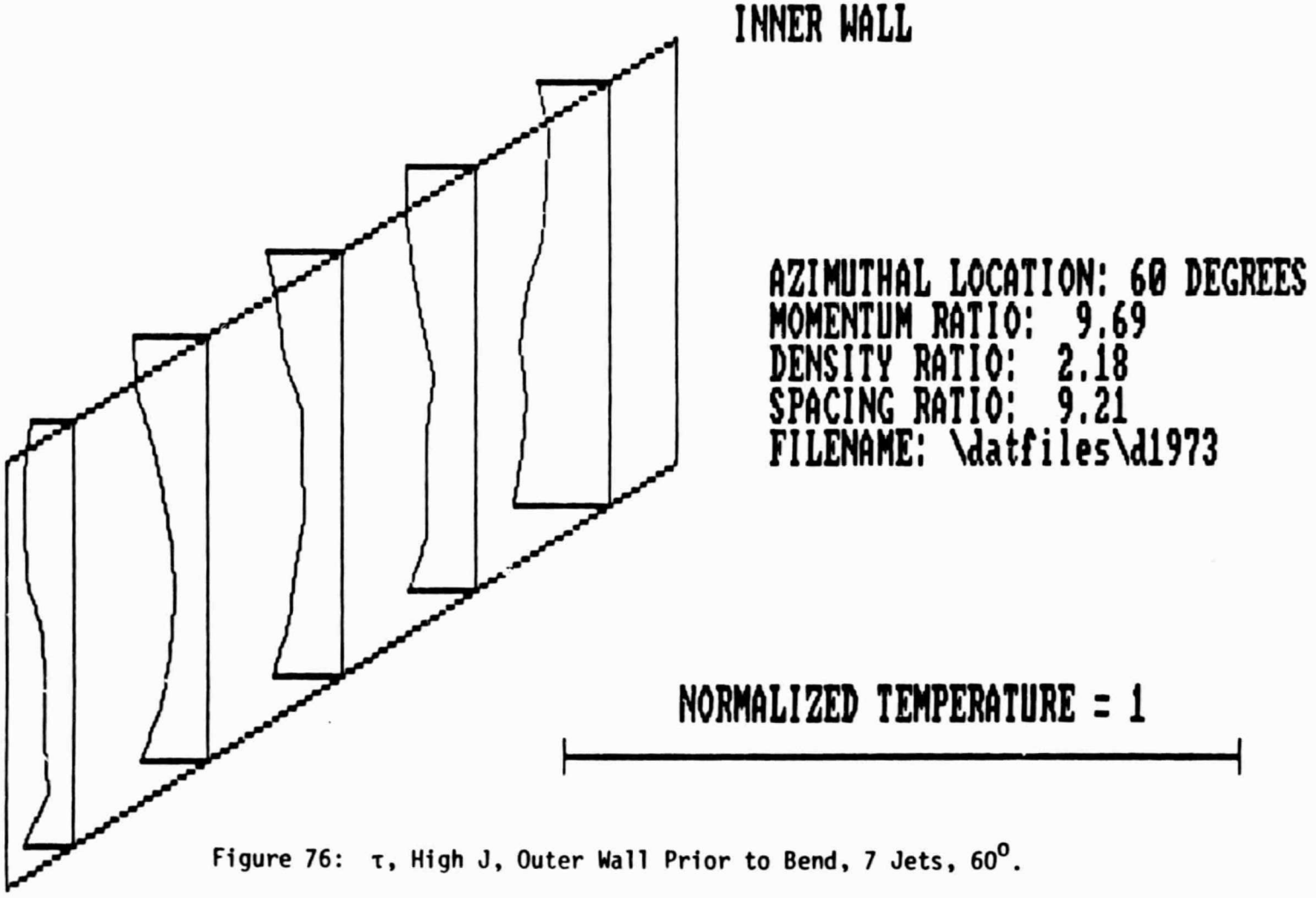

Figure 76: τ, High J, Outer Wall Prior to Bend, 7 Jets, 60^{o}.

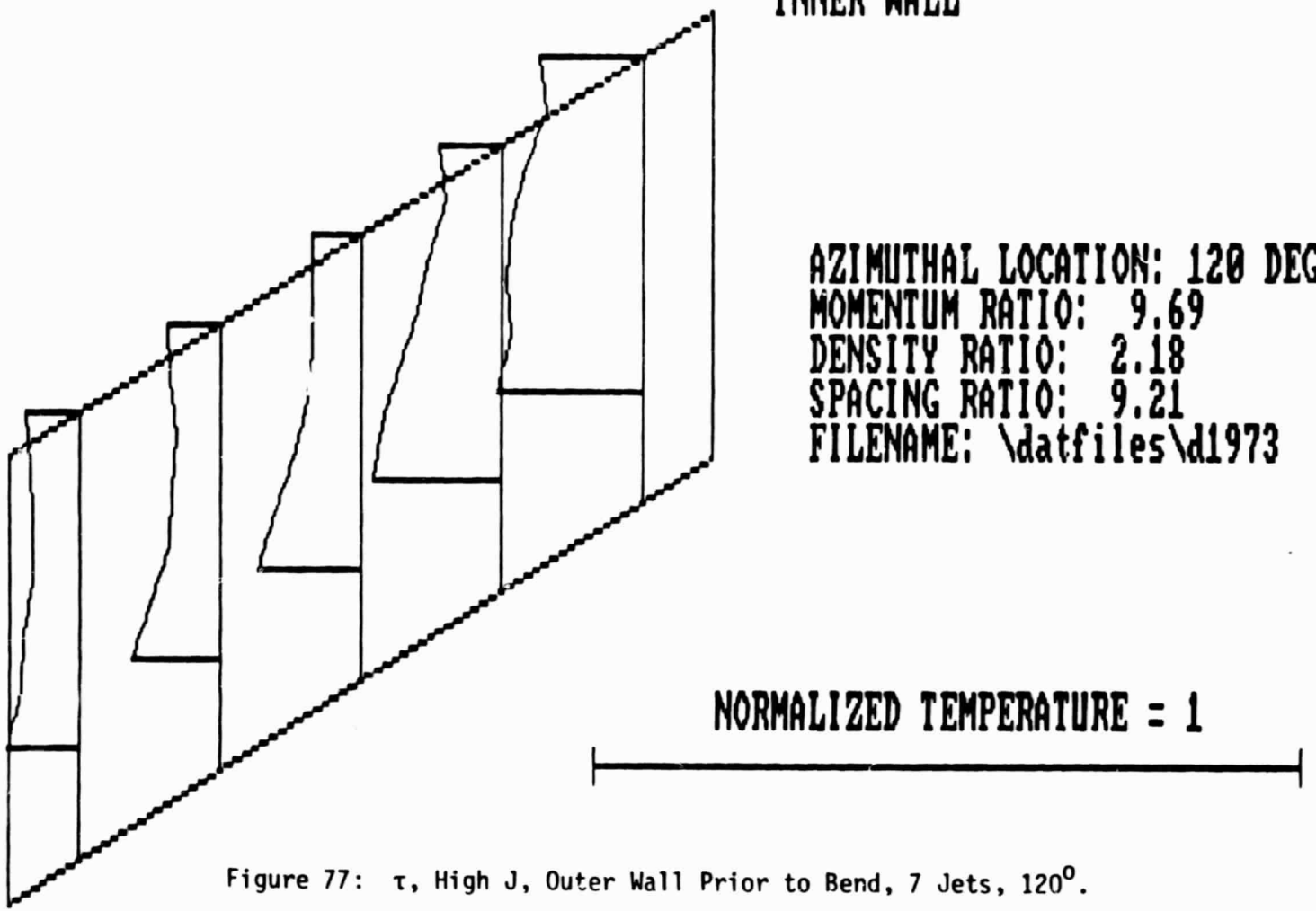

Figure 77: τ, High J, Outer Wall Prior to Bend, 7 Jets, 120^{o}.

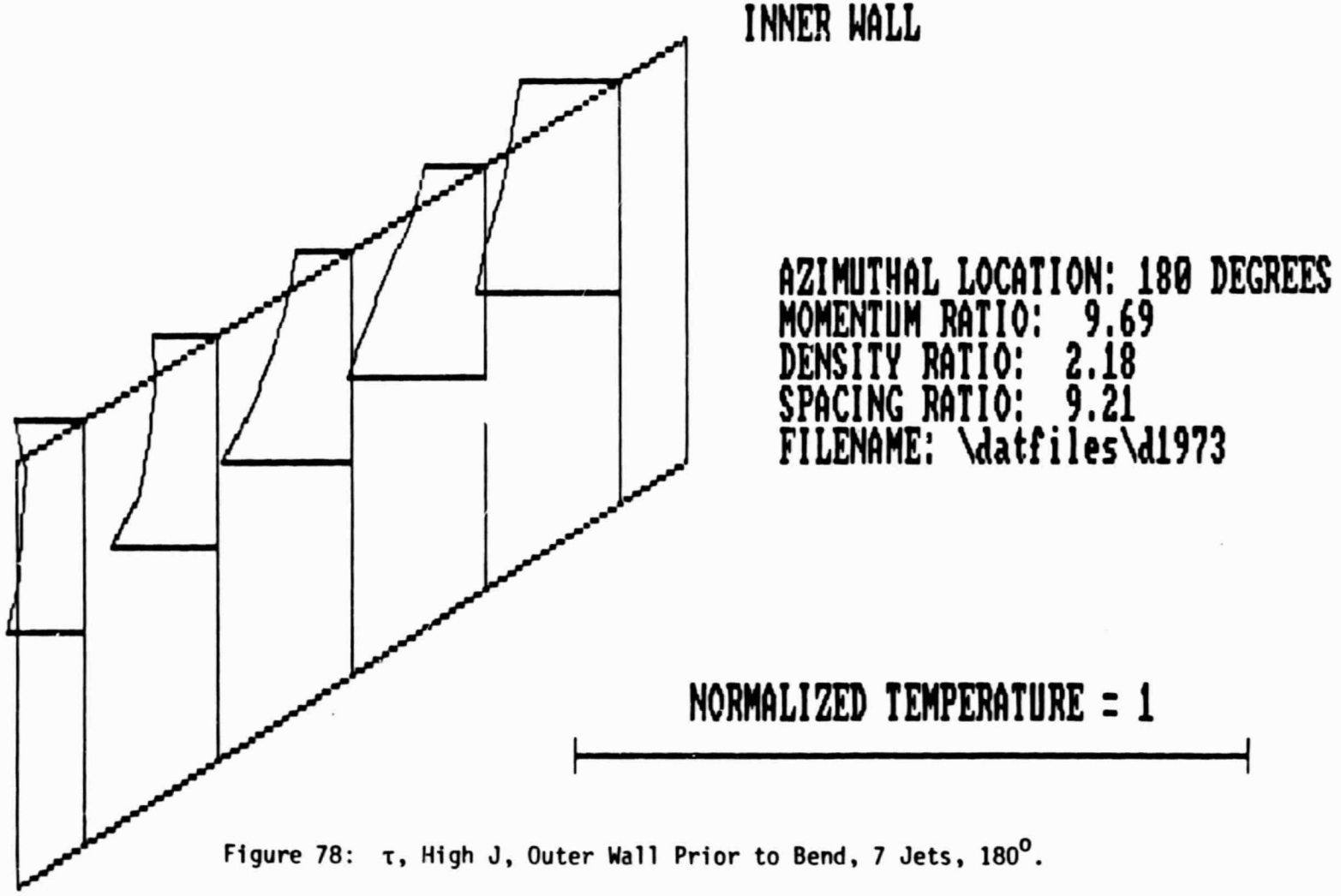

Figure 78: τ, High J, Outer Wall Prior to Bend, 7 Jets, 180^{o}.

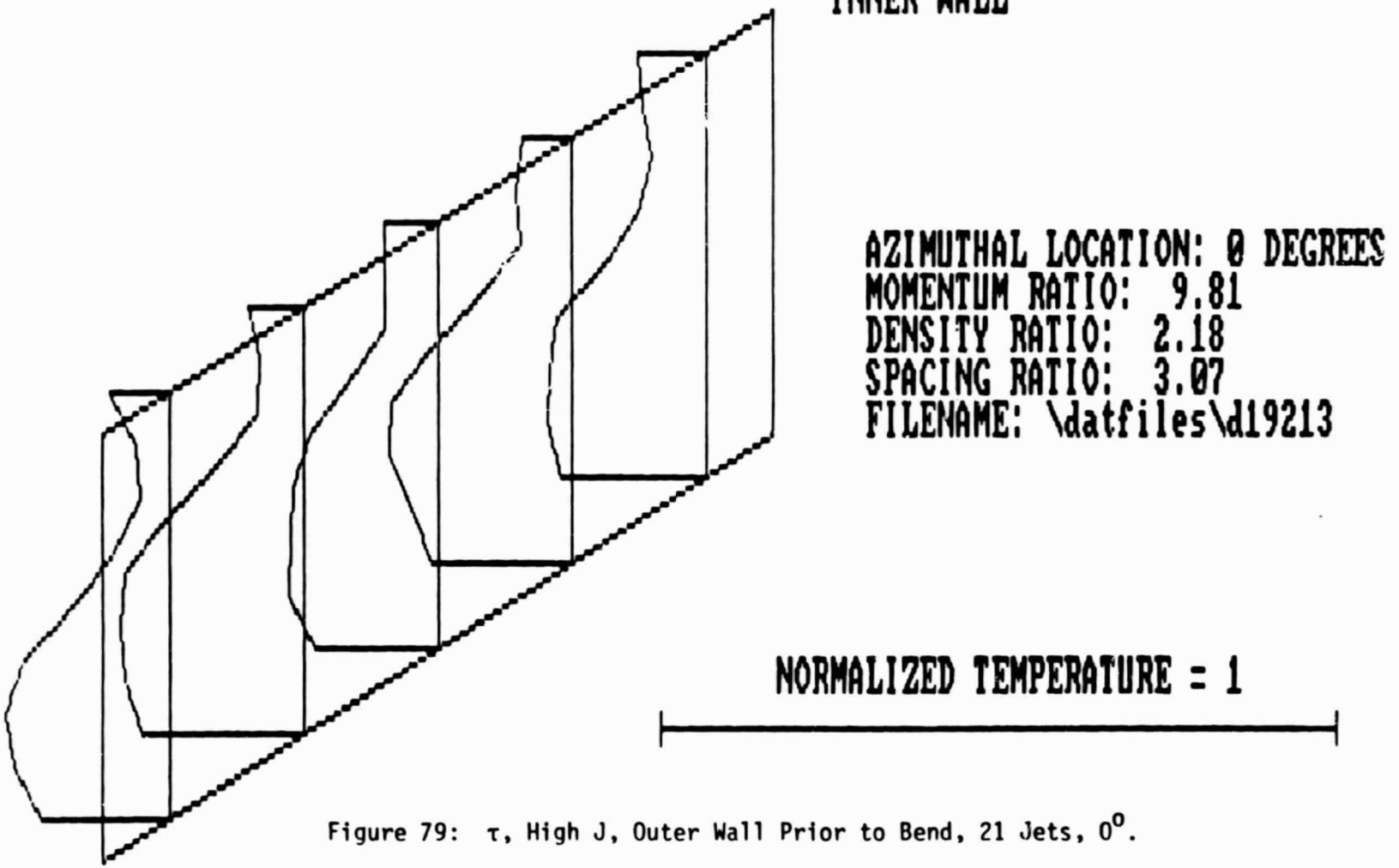

Figure 79: τ, High J, Outer Wall Prior to Bend, 21 Jets, 0^{o}.

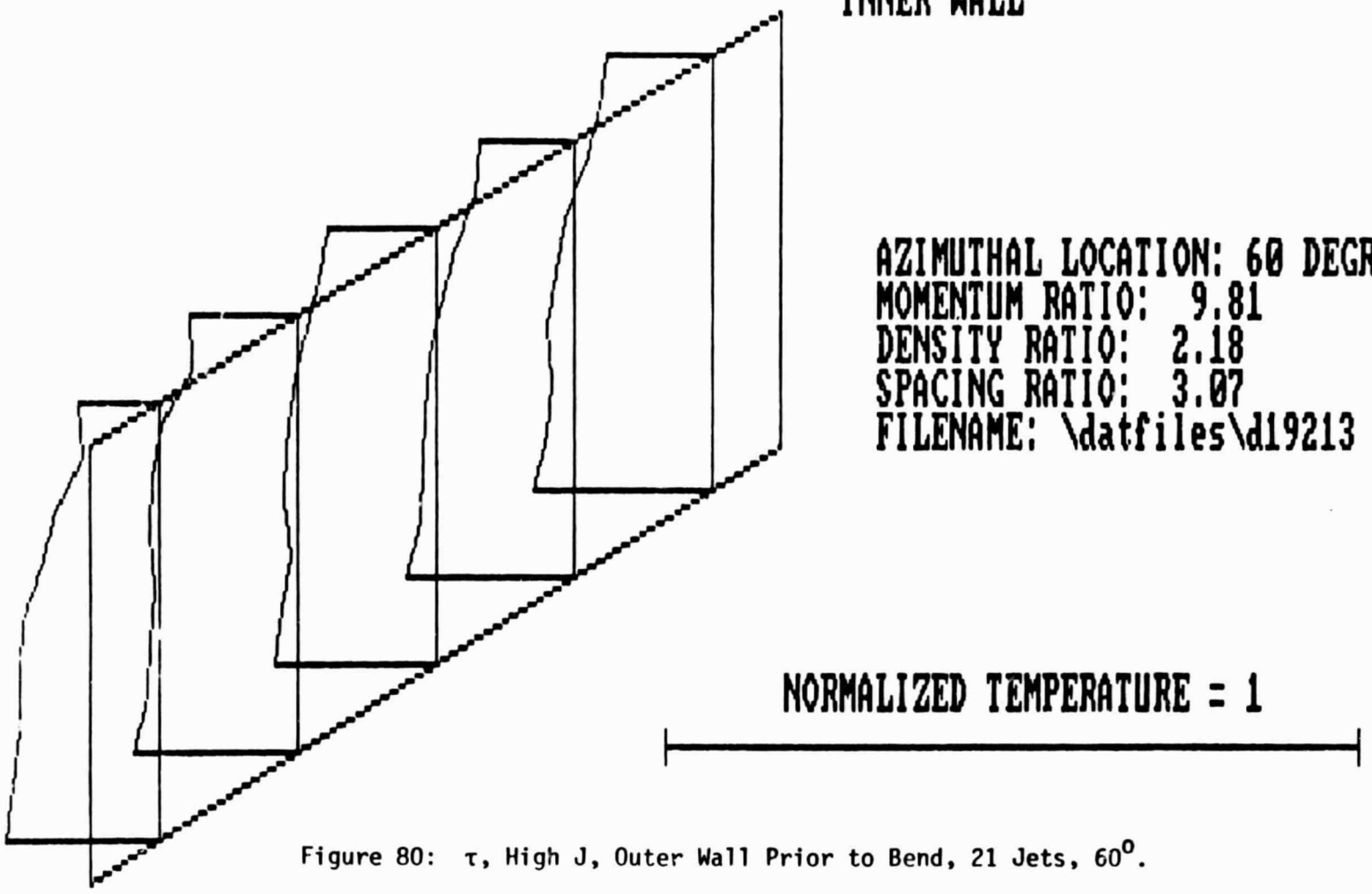

Figure 80: τ, High J, Outer Wall Prior to Bend, 21 Jets, 60^{o}.

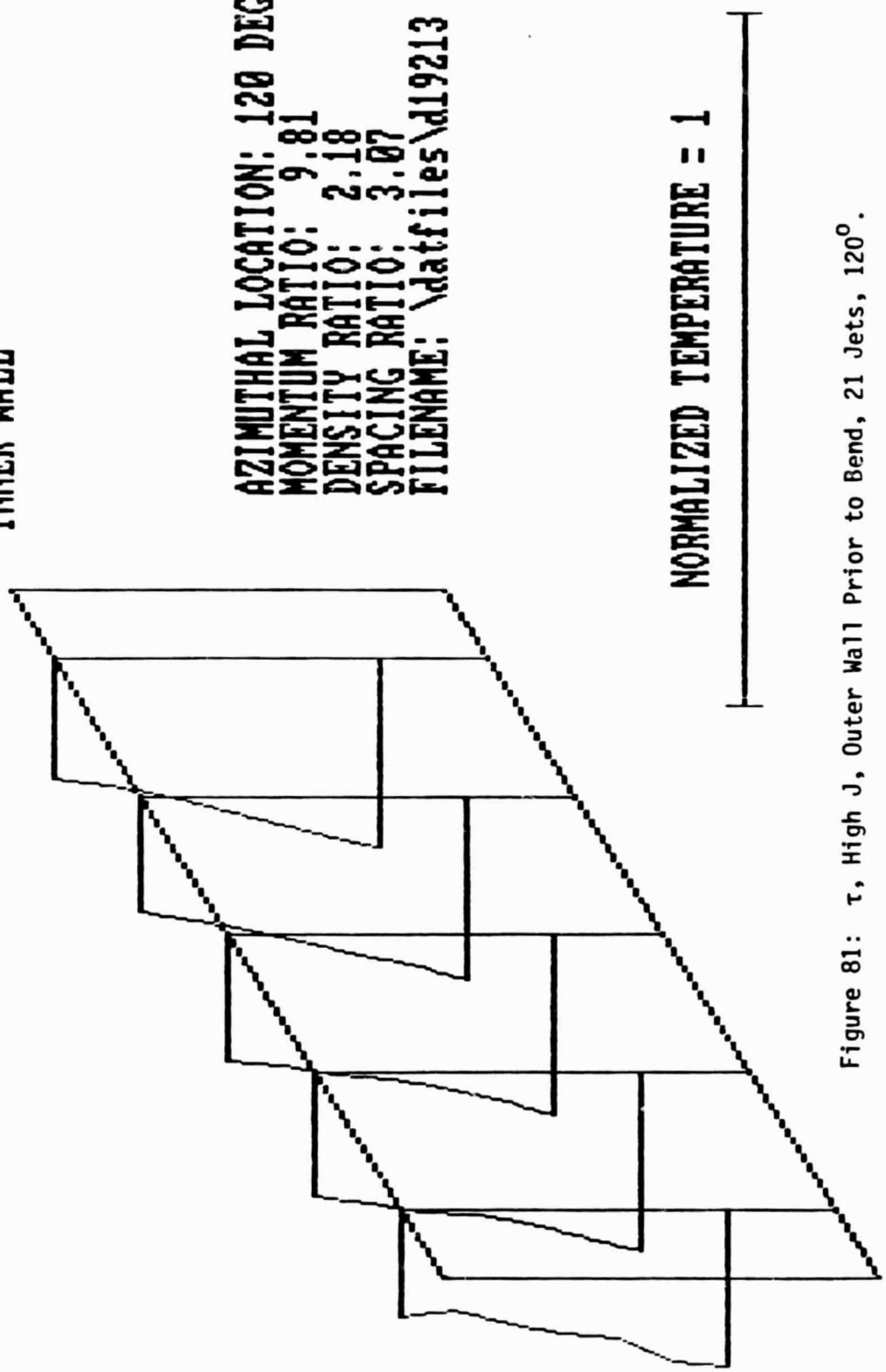

Figure 81: τ, High J, Outer Wall Prior to Bend, 21 Jets, 120^{o}.

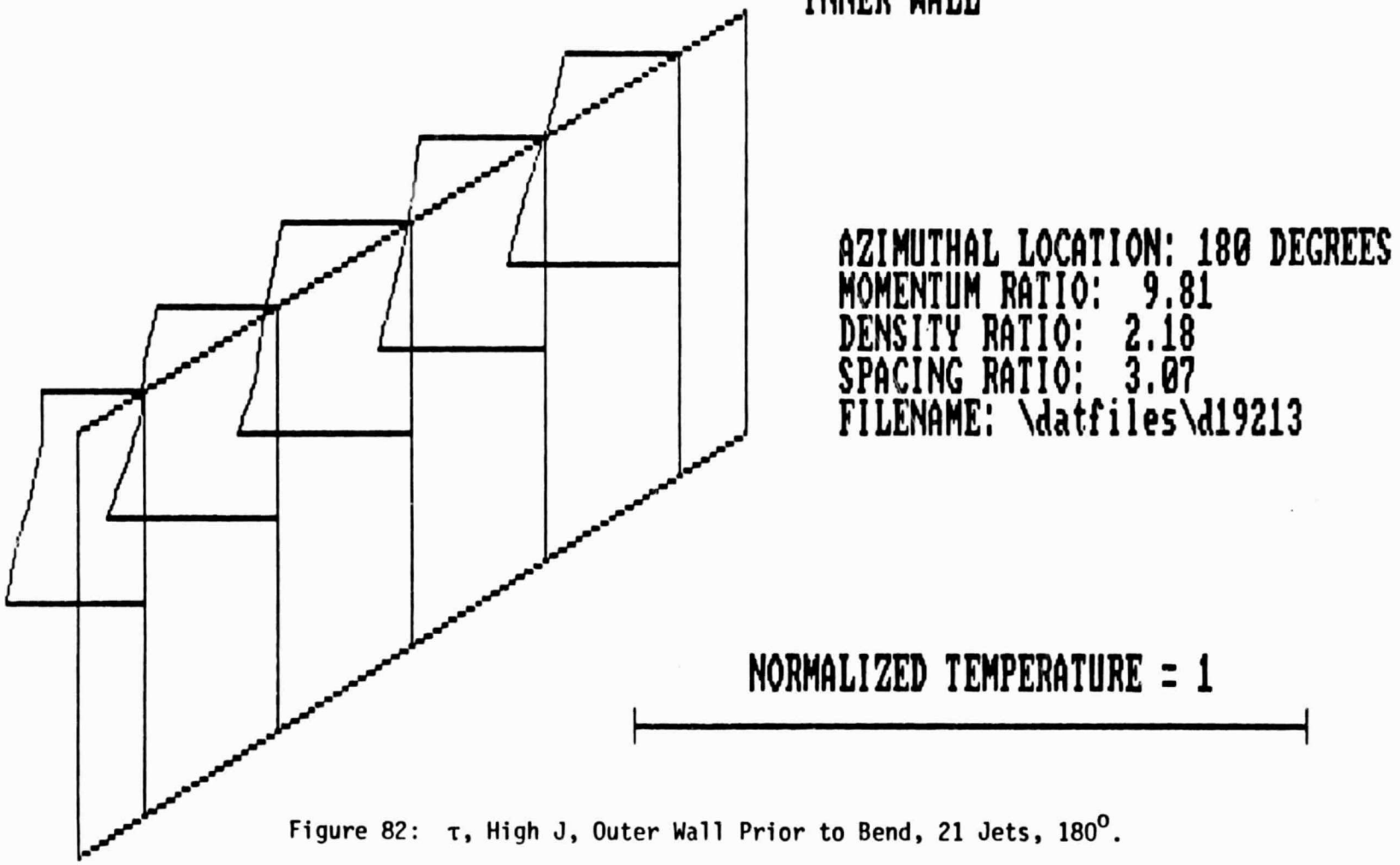

Figure 82: τ, High J, Outer Wall Prior to Bend, 21 Jets, 180^{o}.

APPENDIX 1

PARAMETER CALCULATIONS

1. Velocity is calculated from the Bernoulli equation

$$V = \left[\frac{2\Delta P}{\rho}\right]^{1/2}$$

where ΔP = pitot-static pressure difference ρ = density of oncoming flow.

2. Momentum ratio calculated as

$$J = \frac{\rho_{jet} V^2_{jet}}{\rho V^2}$$

where ρ, V are cross flow conditions.

$$\therefore V_{jet} = \frac{\dot{m}_{jet}}{Area_{jet}}$$

$$\therefore J = \frac{\left[\frac{P}{RT}\right]_{jet} \left[\frac{\dot{m}}{Area}\right]^2_{jet}}{2\Delta P}$$

3. Density ratio is calculated as:

$$Dr = \frac{\rho_{jet}}{\rho}$$

$$Dr = \frac{\left[\frac{P}{RT}\right]_{jet}}{\left[\frac{P}{RT}\right]}$$

Other parameter calculations are straightforward, and need no additional explanation.

APPENDIX 2

SPECIFICATION SHEETS

Properties and Characteristics

MACH NUMBER RANGE

The lower usable limit for Pitot-Static Probes depends on the sensitivity of the readout device used with the probe. A differential pressure of 1" of water, for example is about the minimum that can be measured with 1% accuracy with ordinary slant gauges, so the lower limit is approximately at a Mach Number of 0.08 or a velocity of 70 ft/sec for air at standard atmospheric conditions. There is no minimum Mach Number for the tube itself. The upper limit is at about Mach 0.95 for the total pressure reading and 0.70 for the static as shown in Figure 1. The static reading is accurate to 0.5% to a Mach Number of 0.50 and to 1.5% up to Mach 0.70. At this point the calibration becomes erratic due to the formation of local shock waves on and around the tip of the probe and the reading can vary as much as 10% with slight changes in flow conditions or proximity to solid boundaries. Above Mach 1.0 both the total and static readings vary considerably from true stream values but they can be corrected theoretically.

YAW AND PITCH ANGLE RANGE

If the fluid stream is not parallel to the probe head, errors occur in both total and static readings. These are the most important errors in this type of instrument because they cannot be corrected without taking independent readings with another type of probe.

Figure 2 shows the errors in total and static pressure, velocity, and weight flow at various yaw and pitch angles.

Note that yaw and pitch angle affect the readings exactly the same. The errors in total and static pressure increase quite rapidly for angles of attack higher than 5°, but they tend to compensate each other so the probe yields velocity and weight flow readings accurate to 2% up to angles of attack of 30°. This is the chief advantage of the Prandtl design over other types.

BOUNDARY EFFECTS

The static pressure indication is sensitive to distance from solid boundaries. Figure 3 shows how this error increases the indicated velocity pressure at a Mach Number of 0.25. The probe and boundary form a Venturi passage which accelerates the flow and decreases the static pressure on one side. The curve shows that static readings should not be taken closer than 5 tube diameters from a boundary for 1% accuracy and 10 tube diameters is safer.

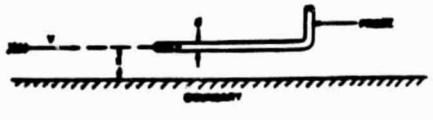

REYNOLDS NUMBER RANGE

Pitot-Static probes are not directly affected by Reynolds Number except at very low velocities. Therefore, in liquids where Mach Number effects are absent, their calibration is substantially constant at all velocities.

The minimum Reynolds Number for the total pressure measurement is about 30 where the characteristic length is the diameter of the impact hole. Below this value the indicated impact pressure becomes higher than the stream impact pressure due to viscosity effects. This error is only noticeable in air under standard atmospheric conditions for velocities under 12 ft/sec with impact holes 0.010" diameter or less.

TURBULENCE ERRORS

Pitot-Static tubes appear to be insensitive to isotropic turbulence which is the most common type. Under some conditions of high intensity, large scale turbulence which make the angle of attack at a probe vary over a wide range, the probe would presumably have an error corresponding to the average yaw or pitch angle caused by the turbulence.

TIME CONSTANT

The speed of reading depends on the length and diameter of the pressure passages inside the probe, the size of the pressure tubes to the manometer, and the displacement volume of the manometer. The time constant is very short for any of the standard tubes down to 1/8" diameter; it increases rapidly for smaller diameters, however. For this reason 1/16" O.D. is the smallest recommended size for ordinary use - this will take 15 to 60 seconds to reach equilibrium pressure with ordinary manometer hook-ups. These tubes have been made as small as 1/32" O.D., but their time constant is as long as 15 minutes and they choke up very easily with fine dirt in the air stream. If very small tubes are required, it is preferable to use separate total and static tubes rather than the combined total-static type. Where reinforcing stems are specified on small sizes, the inner tubes are enlarged at the same point to ensure minimum time constant.

Installation Information

Probes are installed in the fluid stream with the impact hole facing upstream, the head parallel to the flow direction and the stem perpendicular. Types PA and PB (Fig.4) are well suited to mounting on thin-walled ducts where the probe is to be inserted from the outside. Types PC and PD (Fig. 5) are designed with removable pressure take-offs for installation from within the duct, in thick-walled ducts where it is not practical to make an insertion hole of diameter equal to the length of the probe tip. Figure 6 shows limiting lengths and diameters for installation.

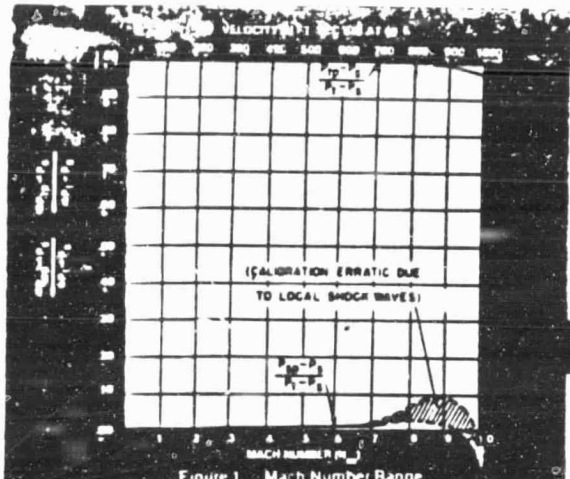

Figure 1 — Mach Number Range

P_t Total pressure (impact pressure, stagnation pressure)
P_s Static Pressure (ambient pressure, stream pressure)
P_{tp} Indicated total pressure
P_{sp} Indicated static pressure

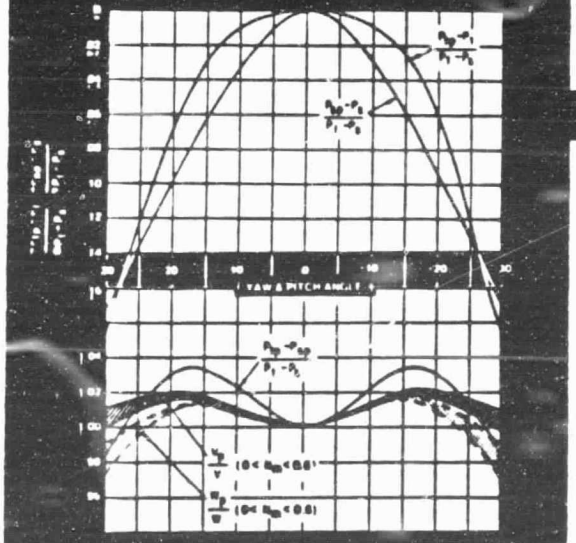

Figure 2 — Yaw and Pitch Angle Errors

V_p Indicated [illegible] as determined by P_{tp} and P_{sp}
W Weight [illegible]
W_p Indicated [illegible] as determined by P_{tp} and P_{sp}

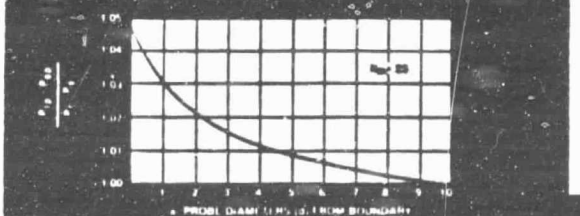

Figure 3 — Boundary Effects

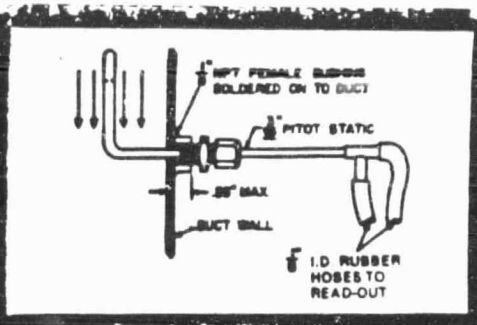

Figure 4 — Thin Wall Installation

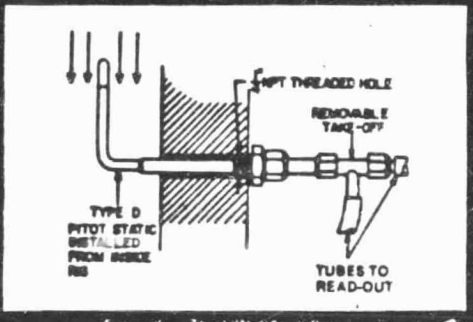

Figure 5 — Thick Wall Installation

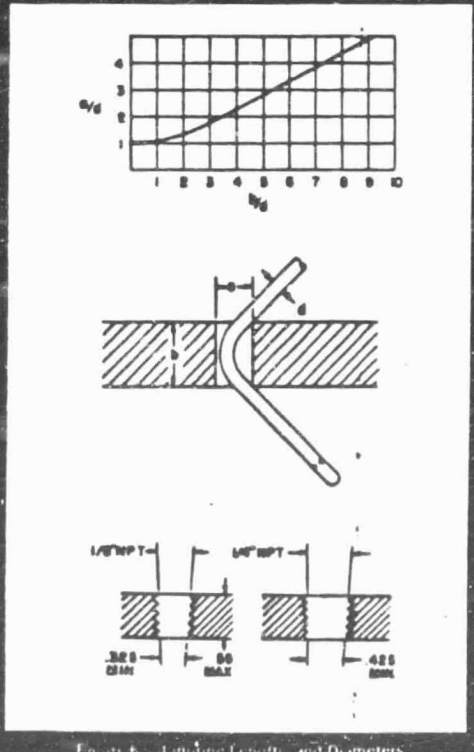

Figure 6 — Limiting Lengths and Diameters

ORIGINAL PAGE IS OF POOR QUALITY

[illegible] MOUNT [illegible]

The AAK line of PC Board mount series Budget priced (B) and Standard (S) include voltages from 3.6 Vdc to 30 Vdc. Critical components in each model are aged, matched, pretested and graded to insure long serviceability. All units are given a minimum burn-in of 2 hours under full load and short circuit conditions. This is why a full 2 year for B series and a full 5 year warranty for S and C series is given and made transferable. OEM contracts are available and custom input/output terminations and voltages will be made upon request.

PC BOARD MOUNTING BUDGET-PRICED (B) SERIES									
5		500	.2	.25	1	3A	BM5.5	[illegible]	[illegible]
5		1000	.2	.25	1	3B	BM51	[illegible]	[illegible]
	±	100	.1	.1	1	3A	BD15.1	[illegible]	[illegible]
±15	±	200	.1	.1	1	3B	BD15.2	[illegible]	[illegible]
	±	300	.1	.1	1	3C	BD15.3	[illegible]	[illegible]
PC BOARD MOUNTING STANDARD (S) SERIES									
		500	.05	.05	.5	3A	SM3.5	[illegible]	[illegible]
3.6		1000	.05	.1	.5	3B	SM31	[illegible]	[illegible]
		2000	.05	.2	.5	3C	SM32	70	[illegible]
		500	.05	.05	.5	3A	SM5.5	[illegible]	[illegible]
5		1000	.05	.1	.5	3B	SM51	[illegible]	[illegible]
		2000	.05	.2	.5	3C	SM52	70	[illegible]
		500	.05	.05	.5	3A	SM6.5	[illegible]	[illegible]
6		1000	.05	.1	.5	3B	SM61	[illegible]	[illegible]
		1500	.05	.2	.5	3C	SM62	75	[illegible]
		200	.01	.05	.5	3A	SM10.2	[illegible]	[illegible]
10		400	.01	.05	.5	3B	SM10.4	[illegible]	[illegible]
		600	.01	.05	.5	3C	SM10.6	70	[illegible]
		200	.01	.05	.5	3A	SM12.2	[illegible]	[illegible]
12		400	.01	.05	.5	3B	SM12.4	[illegible]	[illegible]
		600	.01	.05	.5	3C	SM12.6	70	[illegible]
		200	.01	.05	.5	3A	SM15.2	[illegible]	[illegible]
15		400	.01	.05	.5	3B	SM15.4	[illegible]	[illegible]
		600	.01	.05	.5	3C	SM15.6	70	[illegible]
		100	.01	.05	.5	3A	SM18.1	[illegible]	[illegible]
18		200	.01	.05	.5	3B	SM18.2	[illegible]	[illegible]
		300	.01	.05	.5	3C	SM18.3	74	[illegible]
		100	.01	.05	.5	3A	SM20.1	[illegible]	[illegible]
20		200	.01	.05	.5	3B	SM20.2	[illegible]	[illegible]
		300	.01	.05	.5	3C	SM20.3	70	[illegible]
		100	.01	.05	.5	3A	SM24.1	[illegible]	[illegible]
24		200	.01	.05	.5	3B	SM24.2	[illegible]	[illegible]
		300	.01	.05	.5	3C	SM24.3	70	[illegible]
		100	.01	.05	.5	3A	SM30.1	[illegible]	[illegible]
30		200	.01	.05	.5	3B	SM30.2	[illegible]	[illegible]
		300	.01	.05	.5	3C	SM30.3	70	[illegible]
	±	30	.05	.05	.5	3A	SD12.03	[illegible]	[illegible]
	±	60	.01	.05	.5	3A	SD12.06	[illegible]	[illegible]
±12	±	100	.01	.05	.5	3A	SD12.1	[illegible]	[illegible]
	±	200	.01	.05	.5	3B	SD12.2	[illegible]	[illegible]
	±	300	.01	.05	.5	3C	SD12.3	72	[illegible]
	±	30	.05	.05	.5	3A	SD15.03	[illegible]	[illegible]
	±	60	.01	.05	.5	3A	SD15.06	[illegible]	[illegible]
±15	±	100	.01	.05	.5	3A	SD15.1	[illegible]	[illegible]
	±	200	.01	.05	.5	3B	SD15.2	[illegible]	[illegible]
	±	300	.01	.05	.5	3C	SD15.3	72	[illegible]
	±	400	.01	.05	.5	3D	SD15.4	[illegible]	[illegible]
	±	500	.01	.05	.5	3D	SD15.5	[illegible]	[illegible]

Five Pins, 0.040 (1.0) Dia x 0.20 (5.1) Lg Min
Two Mounting Inserts No. 4-40 x 0.10 (2.5) Pp Min

All Dimensions are in Inches and (mm)

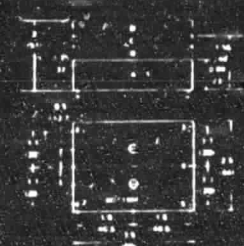

Dual Outputs
2.0 and 2.2 AC Pin Spacing
PIN 1 AC in
2 AC in
3 -Vdc out
4 Common out
5 +Vdc out

Single Outputs

2.0 AC Pin Spacing	2.2 AC Pin Spacing
PIN 1 AC in	PIN 1 AC in
2 AC in	2 AC in
3 -Vdc out	3 No Connection
4 No Connection	4 -Vdc out
5 +Vdc out	5 +Vdc out

CASE 3

GENERAL SPECIFICATIONS

Input Voltage: 105 to 125 vac, 50-400Hz
Output Voltage Accuracy: [illegible] fixed
Operating Temp.: -25 °C to 71 °C
Temp. Coefficient: 0.015 % per °C
Storage Temp.: -25 °C to 85 °C
Input Isolation: 50 Megohms
Current Limiting: Either output to common or other output

POWER SUPPLY OPTIONS

K Option [illegible] 230 VAC input add Suffix K to Model No. and $5.00 to price. 12/15 Option: For [illegible] adjust of ±12V to ±15V dual tracking of any S series unit add suffix 12/15 to Model No. and $4.00 to price. 3V Option: Screwdriver adjustment potentiometer varies output ±3 volts from prescribed output voltage. Add suffix 3V to Model No. and $5.00 to price.

AAK CORPORATION
P O BOX 7 METHUEN MASS 01844 TEL (617) 373-3769

SETRA SYSTEMS, INC.
HIGH OUTPUT PRESSURE TRANSDUCERS

HIGH ACCURACY

Model 239

LOW RANGE PRESSURE TRANSDUCER

Differential Pressures: 0-±0.01 psid to 0-100 psid
(Reference pressure: dry non-corrosive gases)

Absolute Pressures: 0 - 1 psia, 0 - 5 psia

Represented By

Features

- Instant warm-up
- High output: 5 volts or ±2.5 volts
- 0.03% Repeatability
- 0.1% Hysteresis
- 0.1% Non-linearity
- 0.01%/°F Thermal effects
- 0.02% Output noise
- Fast response, less than 1 millisecond
- Withstand high overpressure
- Many options, including remote control

Description

The Model 239 is a complete pressure transducer system for accurate measurement of low pressures. The unique Setra electronic circuitry is combined with a rugged capacitance-type sensor in this transducer. The high output usually requires no further signal conditioning.

The pressure media may be compatible liquid or gas. The reference pressure media must be clean dry air or non-condensable gas. (The reference chamber for absolute pressure units is weld-sealed at high vacuum.)

The high level output signal, excellent stability, combined with fast dynamic response make this transducer well suited for many industrial, laboratory, and aerospace applications requiring the highest accuracy. This unit differs from Model 239E, in that the Model 239 is carefully compensated to minimize both zero and sensitivity shifts due to environmental temperature variations.

Full Scale Ranges

Low Differential Pressure (psid)	
Unidirectional	Bidirectional
0 to 0.02	0 to ±0.01
0 to 0.2	0 to ±0.1
0 to 1	0 to ±0.5
0 to 5	0 to ±2.5
0 to 10	0 to ±5
Higher Differential Pressure (psid)	
Unidirectional	Bidirectional
0 to 20	0 to ±10
0 to 100	0 to ±50
Absolute pressure (psia)	
0 to 1	
0 to 5	

Differential Pressure: Pressure measured relative to a reference pressure. Referred to as pounds per square inch (differential) or psid.

Absolute Pressure: Pressure measured relative to high vacuum. Referred to as pounds per square inch (absolute) or psia.

Applications

- For highest accuracy, obtaining very high linearity, low hysteresis, fast dynamic response, very small temperature effects, insensitivity to motion and vibration, and high stability.
- For high accuracy applications where low power consumption, instant warm-up, and small size are needed.
- For accurate low absolute pressure (vacuum-welded reference chamber), and for low differential pressure measurements when the reference pressure is clean dry air or gas.
- Standard units for most applications connect directly into most A/D converters. Can be attenuated to match low level indicators, scanners, and loggers.
- Many options listed on back page for special instrumentation needs, including remote control.
- Replacing low output strain gage type transducers and associated signal conditioning, getting higher accuracy at much lower cost.

Construction

Setra's patented† variable capacitance sensors approach the ultimate in design simplicity. A stainless steel diaphragm and an insulated electrode form a variable capacitance. As the pressure increases, the capacitance changes. This capacitance is detected and converted to a linear d.c. electric signal by Setra's unique electronic circuit.

Low Pressure and Absolute Pressure

Low range pressure sensors have a thin stretched stainless steel diaphragm positioned close to the electrode. Positive pressure moves the diaphragm toward the electrode, increasing the capacitance. High positive overpressure pushes the diaphragm against the electrode, thereby providing high positive overpressure protection.

Higher Pressure

Higher pressure range sensors have an insulated electrode fastened to the center of the diaphragm, forming a variable capacitance. As the pressure increases, the capacitance will decrease.

†US Patent 3,889,575

Setra systems INC

45 Nagog Park, Acton, Massachusetts 01720 / Telephone: (617) 263-1400

HIGH ACCURACY

Model 239 Specifications

Pressure Ranges	
Unidirectional differential	0 to 0.02, 0.2, 1, 5, 10, 20, 100 psid
Bidirectional differential	0 to ±0.01, 0.1, 0.5, 2.5, 5, 10, 50 psid
Absolute pressure	0 to 1, 5 psia
Positive pressure media	Gases or liquids compatible with stainless steel, hard anodized 6061 aluminum, Buna N "O" ring. (Stainless steel in place of aluminum on special order)
Reference pressure media	
Differential pressure	Clean dry air or other gas. (Non-corrosive, non-condensable)
Absolute pressure	Vacuum sealed, no reference pressure needed
Pressure fittings	1/8" - 27 NPT, internal
Excitation Power	Nominal 24 VDC, 8 milliamperes (0.25 watts), 22 to 30 VDC. Reversed excitation protected. Internal regulation minimizes effect of excitation variation, with <±0.02% FS output change. Will operate on 28 VDC aircraft power per MIL-STD-704A and not be damaged by emergency power conditions.
Zero pressure output	Internally adjustable to 0mv. Factory set within ±20mv
Output impedance	<10 ohms
Non-linearity	<±0.1% full range output (best straight line method)
Thermal effects	Operable 0°F to 175°F
Zero shift (30°F to 150°F)	<±1%FR/100°F (<±2% for 0.02 and ±0.01 psid)
Sensitivity shift (30°F to 150°F)	<±1%FR/100°F (<±2% for 0.02 and ±0.01 psid)
Volume increase due to F.R. pressure	1 x 10⁻³ cu. in.
Natural frequency	2000 Hz nominal
Output noise	<200 microvolts RMS (In band 0 Hz to 10K Hz)
Warm-up shift (typical)	<±1% total, <±0.2% residual shift after 5 minutes
Electrical Connection	2 foot multiconductor cable
Weight	8 ounces
Maximum Working Pressure	**Pressure Range of Transducer** / **Operable Line Pressure** 0.01 and 0-0.02 psid / Near Ambient ±0.1, 0-0.2 psid and higher / Vacuum to 250 psig

Proof Pressure, Acceleration Response, Hysteresis, Full Range Output

Pressure Ranges	Proof Pressure [1] Positive	Proof Pressure [1] Negative	Acceleration Response psi/g	Hysteresis %FR	Elec. Output [4] Volts DC
Low Pressure					
0 to ±0.01, 0.1, 0.5, 2.5, 5 psid	30xFR [2]	5xFR [3]	<0.0002	<0.1% [4]	0 to ±2.5
0 to 0.02, 0.2, 1, 5, 10 psid	30xFR [2]	5xFR [3]	<0.0002	<0.1% [4]	0 to 5
Higher Pressure					
0 to ±10, 50 psid	2xFR	2xFR	<0.05	<0.1%	0 to ±2.5
0 to 20, 100 psid	2xFR	2xFR	<0.05	<0.1%	0 to 5
Absolute Pressure					
0 to 1, 5 psia	30xFR		<0.0002	<0.1%	0 to 5

Notes
(1) Proof Pressure. The maximum pressure that may be applied without changing performance beyond specification (<0.5% F.S. zero shift).
(2) For ±0.1, 0-0.2 psid and higher ranges, up to 1000xFR proof positive pressure on special order (maximum 5000 psig).
(3) For ±0.1, 0-0.2 psid and higher ranges, 30xFR negative pressure overload protection available on special order.
(4) May be slightly higher (up to 0.2%) for ranges 0 to 10 psid, 0 to ±5 psid.
(5) Calibrated into 50K ohm load, operable into loads of 5000 ohms or greater. Internally adjustable ±2%.

Electronic Circuit Information

Four-terminal equivalent circuit, either negative excitation or negative output should be connected to case. Unit calibrated at the factory with negative excitation connected to case.

Options

- Remote calibration signal. Specify percent full scale or adjustable.
- Remote zero pressure adjustment.
- Remote sensitivity adjustment.
- ±24 VDC or ±15 VDC ground referenced excitation. (Allows ground referenced output.)
- 15 VDC, 12 VDC, 10 VDC excitation. (lower output voltage)
- Non-standard output level (maximum 0-10V).
- Compensated temperature range -65°F to +250°F. (Typical temperature effects 2x standard.)
- Intrinsic safety design. (Class 1, Div. 1, Groups C and D)

Ordering Information

Order as Model 239 pressure transducer.
Specify pressure range, noting differential pressure, or absolute pressure, desired electrical output, and desired options.

Outline Drawing

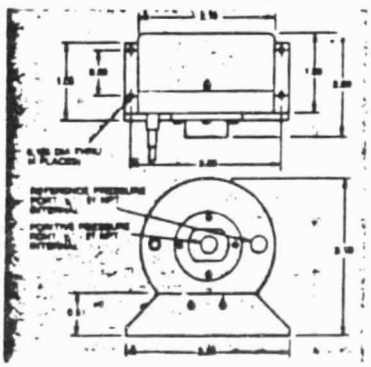

All dimensions are in inches

Specifications subject to change without notice

Setra systems INC.
45 Nagog Park, Acton, Massachusetts 01720 / Telephone: (617) 263-1400

APPENDIX 3

OPERATING PROCEDURES

1. START UP & SHUT DOWN

START-UP AND SHUT-DOWN INSTRUCTIONS
for the
REVERSE FLOW COMBUSTOR
Revised July, 1982

START-UP

1. Verify the operation of the hanging electrical outlets.
2. Plug power supply, ignition system, and temperature indicator into the outlets.
3. Move blower main electrical switch to the "on" position.
4. Check to see that the "primary cooling air" valve is closed.
5. Open "dilution jet air" valve to 1 cm differential to prevent the flow of hot air into the blower.
6. Check to see that the main and small natural gas valves are closed.
7. Set automatic gas shut-off system to "off" position.
8. Set 3-way natural gas valve to "upstream to main valve" position (pointer to the left).

9. Set temperature indicator to monitor central probe of the rake.

10. Supply power to the pressure transducers for delta pressure acquisition.

11. Start blower by depressing the "on" button located on the remote control unit.

12. Supply combustion air at 0.018 kg/sec (40 mm $H_2 0$).

13. Check to see that the exhaust system is open and the ejectors are operational.

14. Set the automatic gas shut-off system to the "manual" mode of operation.

15. Open the small natural gas valve (allowing flow to the central burner only) and supply gas to the ignitor at 20 CFH (as indicated on the small flow meter).

16. Activate the ignition system by depressing the right switch and then the left switch.

17. Listen for the sound of igniting natural gas; verify the ignition by monitoring the central probe temperature.

18. Increase the flow rate through the small natural gas valve to 25 CFH.

19. Open large natural gas valve, supplying gas to all burners at 0.001 kg/sec (18 mm $H_2 0$).

20. Listen for the sound of ignition at the remaining burners.

21. Immediately supply primary cooling air at a rate of at least 0.065 *kg/sec* (55 *mm* $H_2 0$).

22. Switch the 3-way natural gas valve to the "gas manifold" position (pointer to the right).

23. Close small natural gas valve.

24. Take out ignition system plug from the hanging electrical outlet.

25. The combustor is now in the "operational" mode. Keep flow rates within the "operational zone" while adjusting them to produce different temperatures.

    Do not exceed exhaust temperature of 1292°F (700°C).

    Do not exceed bend wall temperatures of 932°F (500°C).

    Do not force the scanning mechanism. If it becomes immovable due to thermal warpage, allow it to cool, thereby relieving the stress.

    Do not over-tighten dilution jet plugs. Close only slightly more than hand tight.

26. Set automatic gas shut-off system to the "automatic" position.

SHUT-DOWN

1. *Close natural gas main valve.*

2. *Allow blower to continue running until the wall temperature has dropped to 140°F (60°C).*

3. *Shut down the blower by depressing the "off" button on the remote control unit. Close all air valves.*

4. *Move automatic gas shut-off system to "off" position.*

5. *Move blower main electrical switch of "off" position.*

B. OPERATING PROCEDURE

If using a multiple probe, call program sectry 2.bas.

Before beginning, if pressure transducers are to be used, call trantes.bas. Upon running it will ask for a channel number. Channel numbers zero through four correspond to transducers one through five. The act of typing a channel number and returning causes 25 pressure measurements to be taken, and the average to be calculated. The last number in the column is the average. Write it down and save it for each transducer.

Load your choice of program for multiple or single probes. It will first ask what the zero values for the transducers are. It will then ask for a jet raw location. Number one is the location furthest into the turn, number two is the second run in the turn, number three is prior to the turn outer wall, and number four is prior to the turn inner wall.

The next question asked is how many operating dilution jets exist. Answer with the appropriate number. Following this, answer how many non-working jets exist between each set of two operating jets. The next question asks which azimuthal increment is desired. Answer with 1 for 10 degrees, 2 for 20 degrees, etc. The following two questions ask you to name an introductory file name and a data file name Do so.

Following that, manometers must be read for the various flow rates. The program will then ask you to enter values and pressures. The units are usually mm water differential and are mentioned in each question. Required entries are: combustor pres-

sure, combustor air flow rate, natural gas flow rate, dilution jet flow rate, and barometric pressure.

Following pressure input, one must key in cooling jet temperature, cross flow temperature, and six wall temperatures (numbers five through ten) in degrees F.

The computer will give you back all of the input parameters in SI units, and ask you for your first temperature. Locate the probe where it asks (should be radial position 95, and zero azimuthal degrees), press button 11 on the Doric trendicator and press F5 on the keyboard. On the Doric, keying F5 on the computer after each. After 15, the pressures are all automatically acquisitioned, their values printed along with the calculated local velocities. The computer will then tell you where to locate the probe. Do so. Repeat the above procedure.

To plot out data radially, choose laspimpt.bas for temperature and laspimpv.bas for velocity. The program will ask for introductory and data file names. Supply them and the plot will be made.

C. Thermocouple Locations

THERMOCOUPLES

1. Right Burner
2. Middle Burner
3. Left Burner
4. Straight Inner Wall

5. Inner Wall at Middle Bend
6. Outer Wall At Exit
7. Outer Wall at Middle Bend
8. Straight Outer Wall
9. Side Wall at Middle Bend
10. Side Wall at Exit
11. Rake
12. Rake
13. Rake
14. Rake
15. Rake
16. Jet Injection Port
17. Exhaust Port
18. Single Probe

APPENDIX 4

COMBUSTOR SOFTWARE

1. SECTRY2.BAS--Data Acquisition

```
10 DIM TFS(25)
50 DIM ZERO(5)
60 INPUT "zero(0)"; ZERO(0)
70 INPUT "zero(1)"; ZERO(1)
80 INPUT "zero(2)"; ZERO(2)
90 INPUT "zero(3)"; ZERO(3)
100 INPUT "zero(4)"; ZERO(4)
120 DIM T(4,9,16)
130 DIM P(4,9,16)
140 DIM V(4,9,16)
150 T(0,1,0) = 100:T(1,1,0)=100:T(2,1,0)=100:T(3,1,0)=100:T(4,1,0)=100
151 T(1,9,0) = 100
152 T(2,9,0) = 100
153 T(3,9,0) = 100
154 T(4,9,0) = 100
160 P(0,1,0)=1234.5:P(1,1,0)=1234.5:P(2,1,0)=1234.5:P(3,1,0)=1234.5:P(4,1,0)=12
4.5
170 V(0,1,0)=11.11:V(1,1,0)=11.11:V(2,1,0)=11.11:V(3,1,0)=11.11:V(4,1,0)=11.11
380 X = 0
450 INPUT "If applicable, what is the jet row location(1 to 4)";JL
455 INPUT "Number of operating dilution jets"; NDJ
460 INPUT "Number of jets between operating jets(use -1 for single jet and no
ts  )";ND
470 IF JL  =  1 THEN SR1 = 3: ELSE IF JL  =  2 THEN SR1 = 3.05 ELSE
  IF JL  =  3 THEN SR1 = 3.07 ELSE IF JL  =  4 THEN SR1 = 2.47
475 REM Row one starts at highest outer wall location with rows two and three
      progressively at lower positions on the outside wall. Row four includes
      dilution jets on the inner wall.
480 INPUT "What azimuthal increment do you wish: 1, 1.5, 2, 3, or 6"; AI
481 IF AI  THEN PRINT "ILLEGAL INCREMENT": GOTO 480
482 PRINT  "Recall that 1 = 10 deg., 1.5 = 15 deg., etc."
485 REM Recall that zero degrees azimuthal position refers to probe position
      fully in combustor.  Also, radial position 95 refers to probe position
      at its fully extended position at the outer wall.
490 INPUT "What file name and number for intro. information"; FIS
495 INPUT "What file name and number for data"; FDS
497 OPEN FIS FOR OUTPUT AS #1
498 OPEN FDS FOR OUTPUT AS #2
500 INPUT "Combustor Pressure (gage) in mm of water-PR"; PR
520 INPUT "Combustion Air Flow Rate in mm water differential-mcr"; MCR
530 INPUT "Cooling Air Flow Rate in mm water differential-MIR"; MIR
540 INPUT "Natural Gas Flow Rate in mm water differential-MGR"; MGF
555 IF NJ  -1 THEN INPUT "Multiple dilution jet flow rate in mm water differ
tial-msjr"; MSJR
560 IF NJ = -1 THEN INPUT "Single Jet Flow Rate in S.C.F.M.-msjr"; MSJR
570 INPUT "Barometric Pressure in inches of Hg-BPR"; BPR
572 INPUT "Cooling Jet Temperature in degrees Farenheit-TJR"; TJR
574 INPUT "Cross Flow Temperature in degrees Farenheit-TR"; TR
580 INPUT "Wall Temperature in degrees Farenheit-T5"; T5R
590 INPUT "Wall Temperature in degrees Farenheit-T6"; T6R
600 INPUT "Wall Temperature in degrees Farenheit-T7"; T7R
610 INPUT "Wall Temperature in degrees Farenheit-T8"; T8R
620 INPUT "Wall Temperature in degrees Farenheit-T9"; T9R
630 INPUT "Wall Temperature in degrees Farenheit-T10"; T10R
700 PRINT "PARAMETER VALUES GIVEN BELOW IN DESIRED UNITS ARE DESIGNATED BY MOD-
      IFIED VARIABLE NAMES AS FOLLOWS:  PR BECOMES P, TR BECOMES T, ETC."
710 MC = .003*(SQR(MCR)): PRINT "mc = " MC " kg/sec"
720 MI = .0094*(SQR(MIR)): PRINT "mi = " MI " kg/sec"
730 MG = .0003*(SQR(MGR)): PRINT "mg = " MG " kg/sec"
732 IF NJ  -1 THEN MSJ = (.001208)*(SQR(MSJR))/NDJ: PRINT "ms  = " MSJ "kg s
```

```
720 IF NJ = -1 THEN MSJ= MSJR*5.23007E-04: PRINT "msj = " MSJ " kg/sec"
730 REM Lines 710 to 730 are orifice meter calibration equations.  These and
      other equations in this section convert to desired units.
740 M = MS + MJ + MC: PRINT "m = " M " kg/sec"
750 BF = 2220*BFR: PRINT "bp = " BF " pascals"
760 P = BF + 9.76699*PR: PRINT "p = " P " pascals"
770 T = 272.15 + (5/9)*(TR - 32): PRINT "t = " T " degrees kelvin"
780 TJ = 272.15 + (5/9)*(TJR - 32): PRINT "tj = " TJ " degrees kelvin"
790 T5 = 272.15 + (5/9)*(T5R - 32): PRINT "t5 = " T5 " degrees kelvin"
800 T6 = 272.15 + (5/9)*(T6R - 32): PRINT "t6 = " T6 " degrees kelvin"
810 T7 = 272.15 + (5/9)*(T7R - 32): PRINT "t7 = " T7 " degrees kelvin"
820 T8 = 272.15 + (5/9)*(T8R - 32): PRINT "t8 = " T8 " degrees kelvin"
830 T9 = 272.15 + (5/9)*(T9R - 32): PRINT "t9 = " T9 " degrees kelvin"
840 T10= 272.15 + (5/9)*(T10R - 32): PRINT "t10= " T10 " degrees kelvin"
850 RO = P/(287*T): PRINT "ro = " RO " kg/cubic meter"
860 ROJ= P/(287*TJ): PRINT "roj = " ROJ " kg/cubic meter"
870 V  = M /(RO*.0259): PRINT "v = " V " meter/sec"
880 VJ = MSJ/(ROJ*3.974E-05): PRINT "vj = " VJ " meter/sec"
890 PRINT "The number of jets used for injection is "NOJ
900 DR = ROJ/RO: PRINT "Density ratio = ";
910 PRINT USING "#.##"; DR
920 J = (ROJ*VJ*VJ)/(RO*V*V): PRINT "Momentum ratio = ";
930 PRINT USING "##.##"; J
940 SR = SP1*(NJ+1): PRINT "Spacing ratio = ";
950 PRINT USING "##.##"; SR
960 PRINT "Azimuthal increment, AI = " AI
970 PRINT "Intro information file is named " FI$
980 PRINT "Data file is named " FD$
990 INPUT "CHECK CALCULATED VALUES. IF ADJUSTMENTS ARE REQUIRED, MAKE THEM
      GIVING TIME FOR CHANGES TO TAKE PLACE.  WERE ADJUSTMENTS NEEDED";F$
1000 IF F$ = "yes" THEN 500
1010 WRITE #1,AI,FI$,FD$,JL,NJ,FR,TR,MCR,MJR,MGR,TJR,MSJR,BFR,T5R,T6R,T7R,T8R,
     T9R,T10R,MC,MJ,MG,M,P,T,TJ,T5,T6,T7,T8,T9,T10,RO,ROJ,V,MSJ,VJ,DR,J,SR,BP,
2
1040 PRINT
1050 PRINT
1060 PRINT
1070 PRINT
1080 PRINT"point     rad      angle   t11        t12        t13        t14
  t15"
1090 PRINT"                           p11        p12        p13        p14
  p15"
1100 PRINT"                           v11        v12        v13        v14
  v15"
1110 PRINT
1120 PRINT
1130 FOR A2 = 0 TO 8 STEP AI
1140 REM recall that 9 refers to radial position 95, 5 to 55, etc.
1150     FOR RA = 9 TO 1 STEP (-1)
1160     GOSUB 6000
1170     NEXT RA
1180 NEXT A2
1190 FOR A2 = A2 TO 10 STEP AI
1200     FOR RA = 9 TO 2 STEP (-1)
1210     GOSUB 6000
1220     NEXT RA
1230 NEXT A2
1240 FOR A2 = A2 TO 12 STEP AI
1250     FOR RA = 9 TO 3 STEP (-1)
1260     GOSUB 6000
1270     NEXT RA
1280 NEXT A2
1290 FOR A2 = A2 TO 14 STEP AI
1300     FOR RA = 9 TO 4 STEP (-1)
1310     GOSUB 6000
1320     NEXT RA
```

```
NEXT AI
FOR AI = AI TO 16 STEP AI
    FOR RA = 9 TO 5 STEP (-1)
    GOSUB 6000
    NEXT RA
NEXT AI
END
ANG = 10*AI
RAD = (RA + .5)*10
PNT = PNT + 1
PRINT USING "###.        ";PNT;
PRINT USING "##.      ";RAD;
PRINT USING "###.       ";ANG;
GOSUB 7010
REM At this location one must include the command to have the computer
    remind the operator which temperature probe is being converted.
REM here is where routine for gathering individual temperature data will o.
GOSUB 8010
REM here is where the algorithm for calculating velocity will go
FOR VEL = 0 TO 4 STEP 1
V(VEL,RA,AI) = ((2e6*(.916*(ABS(P(VEL,RA,AI))))/(P(VEL,RA,AI)*287*T(VEL,RA,AI))) .5
NEXT VEL
PRINT USING "###.        ";PNT;
PRINT USING "##.      ";RAD;
PRINT USING "###.       ";ANG;
PRINT USING "###.         ";T(0,RA,AI),T(1,RA,AI),T(2,RA,AI),T(3,RA,AI),T(
,RA,AI);
PRINT USING "                                  #.####      ";P(0,RA,A
    PRINT USING "#.####      ";P(1,RA,AI),P(2,RA,AI),P(3,RA,AI),P(4,RA,AI);
    PRINT USING "                                  ##.##       ";V(0,RA,AI);
    PRINT USING "##.##       ";V(1,RA,AI),V(2,RA,AI),V(3,RA,AI),V(4,RA,AI);
    PRINT
    PRINT
    LPRINT USING "##.  PNT,RAD,ANG,T(0,RA,AI),T(1,RA,AI),T(2,RA,AI),T(3,RA,AI),
          T(4,RA,AI),P(1,RA,AI),P(2,RA,AI),P(3,RA,AI),P(4,RA,AI),
          V(0,RA,AI),V(1,RA,AI),V(2,RA,AI),V(3,RA,AI),V(4,RA,AI)
    RETURN
REM Temperature subroutine starts here.
REM subroutine to perform temperature acquisition from channe. 5
ADDRESS = 16.5
OUT ADDRESS +4, 101
REM Line 71 gives a gain of 8 with value of 101
OUT ADDRESS +5, 5
REM Line 40 designates channel 5 (temperature)
FOR I = 0 TO 4 STEP 1
PRINT "t" I+1 "="
BEEP
STOP
FOR MI = 1 TO 25 STEP 1
OUT ADDRESS +4, 0
REM Line 60 starts the conversion process
R = INP(ADDRESS +4)
REM Line 80 assigns status byte value to r.  Below, if a bad conversion is
    encountered, it will attempt to convert again.
IF R < 128 THEN 7160
R = R AND 192
IF R = 128 THEN 7210 ELSE 7190
PRINT "BAD CONVERSION": STOP
GOTO 7090
REM Read data from board in line 7140 and 7150.
LOW = INP(ADDRESS + 5)
HIGH = INP(ADDRESS + 6)
REM Below, we are converting to decimal numbers.
VALUET = 256*HIGH + LOW
IF VALUET > 32767 THEN VALUET = VALUET - 65536
VOLTAGET = VALUET/204.8
```

```
7280 TPSD(MI) = VOLTAGE*(1000)/8
7290 Y = Y + TPSD(MI)
7300 NEXT MI
7305 BEEP
7310 PRINT "t"I+11 "=" X/(MI-1)
7315 REM Line 7375 has a conversion in it for Faren. to Kelvin.
7320 T(I,RA,AZ) =   X/(MI - 1)
7330 FOR MIA = 1 TO 25 STEP 1
7340 FSD = FSD +((TPSD(MIA) - T(I,RA,AZ)) ^2)/(25 - 1)
7350 NEXT MIA
7360 SD(I) = FSD ^.5
7370 PRINT "Channel "11+1 " std. dev. is " SD(I)
7375 T(I,RA,AZ) = (5/9)*((1/(MI-1) + 459.69))
7380 X = 0
7390 FSD = 0
7400 NEXT I
7410 RETURN
8000 REM Subroutine to perform A/D conversion of channels 0 through 4 in the
       proper sequence.  The board must be in the I/O mapped mode.  These
       conversions are for pressure.
8020 ADDRESS = 1808
8030 OUT ADDRESS + 4, 130
8040 REM Line 8070 calls gain=4 since input is 0 to 5 volts (max. 32 m/s)
8050 FOR CH = 0 TO 4 STEP 1
8060 OUT ADDRESS + 5, CH
8065 REM Line 8050 designates channel number.
8070 FOR PI = 1 TO 25 STEP 1
8080 OUT ADDRESS + 6, 0
8075 REM Line 8070 starts conversion procedure.
8085 C = INP(ADDRESS + 4)
8090 REM Line 8060 assigns from board the condition of status byte concerning
       conversion.  Below, if an unacceptable conversion occurs, then the
       program will attempt the conversion again.
8095 IF C <> 128 THEN 8100
8100 C = C AND 192
8110 IF C = 128 THEN 8120 ELSE 8130
8120 PRINT "BAD CONVERSION": STOP
8125 GOTO 8080
8130 REM Read data from board below in lines 8140 and 8150.
8140 LOW = INP(ADDRESS + 5)
8150 HIGH = INP(ADDRESS + 6)
8160 REM Below, we convert to decimal values.
8170 VALUEP = 256*HIGH + LOW
8180 IF VALUEP > 32767 THEN VALUEP = VALUEP - 65536
8190 VOLTAGEP = VALUEP/204.8
8192 REM Calibration is 0.1 psi per 2.5 volts of output.
8195 CALIBRATION = .1/2.5
8200 P(CH,RA,AZ) = VOLTAGEP*CALIBRATION/4 - ZERO(CH)
8202 Y = Y + P(CH,RA,AZ)
8204 NEXT PI
8206 P(CH,RA,AZ) = Y/(PI-1)
8209 Y = 0
8210 NEXT CH
8220 RETURN
0
```

2. INFOUT2.BAS--Displays data in tables.

```
10 REM this program is for accessing data files and printing out needed infor-
   mation.
20 INPUT "What is the file name and number for intro. information"; FI$
30 INPUT "What is the file name and number for data"; FD$
40 OPEN FI$ FOR INPUT AS #1
50 OPEN FD$ FOR INPUT AS #2
60 PRINT "ALL INFORMATION NOT ADUIRED BY THE COMPUTER INCLUDING THE INTRO-
        DUCTORY DATA IS AS FOLLOWS:"
70 INPUT #1,A1,FI$,FD$,JL, NJ,PR,TR,MCR,MIR,MGR,TJR,MSJR,BPR,T5R,T6R,T7R,T8R,
        T9R,T10R,MC,MI,MG,M,P,T,TJ,T5,T6,T7,T8,T9,T10,RO,ROJ,V,MSJ,VJ,DR,J,SR,
        BF,NOJ
100 DIM T(4,9,16)
110 DIM P(4,9,16)
120 DIM V(4,9,16)
200 STOP
205 CLS
292 PRINT "The name of the intro. information file is "FI$
294 PRINT "The name of the data file is "FD$
295 PRINT "The chosen azimuthal increment is " A1
296 PRINT "The row in which operational dilution jets appear is "  JL
297 PRINT "The number of dilution jets in operation is "NOJ
298 PRINT "The number of jets between operation dilution jets is " NJ
300 PRINT "The combustor gage pressure in mm of water is " PR
310 PRINT "The combustor cross-flow temperature is " TR
320 PRINT "Combustion air flow rate in mm of water differential is " MCR
330 PRINT "Cooling air flow rate in mm of water differential is " MIR
340 PRINT "Natural gas flow rate in mm of water differential is " MGR
350 PRINT "Cooling jet temperature in degrees Farenheit is " TJR
360 PRINT "Single jet flow rate in S.C.F.M. is " MSJR
370 PRINT "Barometric pressure in inches of Hg is " BPR
380 PRINT "Wall temperature T5R in degrees Farenheit is " T5R
390 PRINT "Wall temperature T6R in degrees Farenheit is " T6R
400 PRINT "Wall temperature T7R in degrees Farenheit is " T7R
410 PRINT "Wall temperature T8R in degrees Farenheit is " T8R
420 PRINT "Wall temperature T9R in degrees Farenheit is " T9R
430 PRINT "Wall temperature T10R in degrees Farenheit is " T10R
440 PRINT "**********************************************************************"
450 PRINT "**********************************************************************"
460 PRINT "**********************************************************************"
480 PRINT "THE FOLLOWING VALUES ARE CALCULATED FROM GIVENS AND INFORMATION SHOWN
        ABOVE."
490 PRINT "COMBUSTION AIR FLOW RATE:                    mc = "MC" kg/sec"
500 PRINT "COOLING AIR FLOW RATE:                       mi = "MI" kg/sec"
510 PRINT "NATURAL GAS FLOW RATE:                       mg = "MG" kg/sec"
520 PRINT "TOTAL MASS FLOW RATE:                        m  = "M" kg/sec"
530 PRINT "ABSOLUTE COMBUSTOR PRESSURE:                 p  = "P" pascals"
540 PRINT "CROSS FLOW TEMPERATURE:                      t  = "T" degrees kelvin"
550 PRINT "DILUTION JET TEMPERATURE:                    tj = "TJ"degrees kelvin"
560 PRINT "WALL TEMPERATURE T5:                         t5 = "T5"degrees kelvin"
570 PRINT "WALL TEMPERATURE T6:                         t6 = "T6"degrees kelvin"
580 PRINT "WALL TEMPERATURE T7:                         t7 = "T7"degrees kelvin"
590 PRINT "WALL TEMPERATURE T8:                         t8 = "T8"degrees kelvin"
600 PRINT "WALL TEMPERATURE T9:                         t9 = "T9"degrees kelvin"
610 PRINT "WALL TEMPERATURE T10:                        t10= "T10"degrees kelvin"
620 PRINT "CROSS FLOW DENSITY:                          ro = "RO"kg/cubic meter"
630 PRINT "DILUTION JET DENSITY:                        roj= "ROJ"kg/cubic meter"
640 PRINT "CROSS FLOW VELOCITY:                         v  = "V"meter/sec"
650 PRINT "DILUTION JET MASS FLOW RATE(each jet):       msj= "MSJ"kg/sec"
660 PRINT "DILUTION JET VELOCITY:                       vj = "VJ"meter/sec"
670 PRINT "DENSITY RATIO:                               dr = "DR
680 PRINT "MOMENTUM RATIO:                              j  = "J
690 PRINT "SPACING RATIO:                               sr = "SR
```

```
700 PRINT ""
704 PRINT "THE UNITS BELOW ARE KELVIN, PSI AND METERS/SECOND."
705 PRINT ""
707 PRINT ""
709 PRINT ""
710 PRINT ""
711 PRINT ""
720 PRINT"point      rad       angle   t11         t12         t13         t14
 t15"
730 PRINT"                             p11         p12         p13         p14
 p15"
740 PRINT"                             v11         v12         v13         v14
 v15"
745 PRINT
750 PRINT
800 FOR A2 = 0 TO 8 STEP A1
810     FOR RA = 9 TO 1 STEP (-1)
820     GOSUB 2000
830     NEXT RA
840 NEXT A2
850 FOR A2 = A2 TO 10 STEP A1
860     FOR RA = 9 TO 2 STEP (-1)
870     GOSUB 2000
880     NEXT RA
890 NEXT A2
900 FOR A2 = A2 TO 12 STEP A1
910     FOR RA = 9 TO 3 STEP (-1)
920     GOSUB 2000
930     NEXT RA
940 NEXT A2
950 FOR A2 = A2 TO 14 STEP A1
960     FOR RA = 9 TO 4 STEP (-1)
970     GOSUB 2000
980     NEXT RA
990 NEXT A2
1000 FOR A2 = A2 TO 16 STEP A1
1010     FOR RA = 9 TO 5 STEP (-1)
1020     GOSUB 2000
1030     NEXT RA
1040 NEXT A2
1950 END
2000 INPUT #1,PNT,RAD,ANG,T(0,RA,A2),T(1,RA,A2),T(2,RA,A2),T(3,RA,A2),
          T(4,RA,A2),P(0,RA,A2),P(1,RA,A2),P(2,RA,A2),P(3,RA,A2),P(4,RA,A2),
          V(0,RA,A2),V(1,RA,A2),V(2,RA,A2),V(3,RA,A2),V(4,RA,A2)
2010 PRINT USING "###.          "; PNT;
2020 PRINT USING "##.       "; RAD;
2030 PRINT USING "###.        "; ANG;
2040 PRINT USING "###.          "; T(0,RA,A2),T(1,RA,A2),T(2,RA,A2),T(3,RA,A2),T(4
,RA,A2);
2050 PRINT USING "                              #.####      "; P(0,RA,A2);
2060 PRINT USING "#.####      "; P(1,RA,A2),P(2,RA,A2),P(3,RA,A2),P(4,RA,A2);
2070 PRINT USING "                               ##.##       "; V(0,RA,A2);
2080 PRINT USING "##.##       "; V(1,RA,A2),V(2,RA,A2),V(3,RA,A2),V(4,RA,A2);
2090 PRINT
2100 PRINT
2110 RETURN
0
```

3. LASPLMPT.BAS--Plots set of radial temperature profiles.

```
100 CLS
110 KEY OFF
115 DIM PNT(9,18)
120 DIM RAD(9,18)
125 DIM ANG(9,18)
130 DIM T(4,9,18)
135 DIM P(4,9,18)
140 DIM V(4,9,18)
310 INPUT "What is the introductory information filename"; FI$
410 INPUT "What is the data filename"; FD$
510 OPEN FI$ FOR INPUT AS #1
610 OPEN FD$ FOR INPUT AS #2
710 INPUT #1,AI,FI$,FD$,JL,NJ,FR,TR,MCR,MIR,MGR,TJR,MSJR,BFR,T5R,T6R,T7R,T8R,T9R
,   T10R,MC,MI,MG,M,F,T,TJ,T5,T6,T7,T8,T9,T10,RD,RDJ,V,MSJ,VJ,DR,J,SF,BF,NDJ
715 AID = AI*10
810 INPUT "What type of plot is this"; PLTYP$
815 FOR A2 = 0 TO 8 STEP (AID/10)
820     FOR RA = 9 TO 1 STEP (-1)
825     GOSUB 5000
830     NEXT RA
835 NEXT A2
840 FOR A2 = A2 TO 10 STEP (AID/10)
845     FOR RA = 9 TO 2 STEP (-1)
850     GOSUB 5000
855     NEXT RA
860 NEXT A2
865 FOR A2 = A2 TO 12 STEP (AID/10)
870     FOR RA = 9 TO 3 STEP (-1)
875     GOSUB 5000
880     NEXT RA
885 NEXT A2
890 FOR A2 = A2 TO 14 STEP (AID/10)
895     FOR RA = 9 TO 4 STEP (-1)
900     GOSUB 5000
905     NEXT RA
910 NEXT A2
915 FOR A2 = A2 TO 18 STEP (AID/10)
920     FOR RA = 9 TO 5 STEP (-1)
925     GOSUB 5000
930     NEXT RA
935 NEXT A2
940 CLS
1010 SCREEN 2
1110 LOCATE 1, 30: PRINT "FILENAME: " FD$
1210 LOCATE 2, 30: PRINT "MOMENTUM RATIO: ";  PRINT USING "##.##";J
1310 LOCATE 3, 30: PRINT "DENSITY RATIO: "; PRINT USING "##.##";DF
1325 IF NDJ = 0 THEN GOTO 1425
1330 IF NDJ = 1 THEN GOTO 1450
1410 LOCATE 4, 30: PRINT "SPACING RATIO: ";PRINT USING "##.##";SF
1411 GOTO 1510
1425 LOCATE 4, 30: PRINT "SPACING RATIO: ";PRINT "NO INJECTION";
1426 GOTO 1510
1450 LOCATE 4, 30: PRINT "SPACING RATIO: ";PRINT "SINGLE INJECTION";
1451 GOTO 1510
1510 LOCATE 5, 30: PRINT PLTYP$
1610 PSET(75,50)
1710 DRAW "R529 U540"
```

```
181  FOR AZ = 0 TO 1 STEP (AID/10)
1815      AZLOC = AZLOC + 1
191       FOR RA = 9 TO 1 STEP (-1)
2         GOSUB 6810
2         NEXT RA
221   NEXT AZ
23    A155 = a15 - (AID*2*3.1415926548/3e0)
2451  FOR AZ = AZ TO 5 STEP (AID/10)
2455      AZLOC = AZLOC + 1
2     GOSUB 6810
2         FOR RA = 9 TO 1 STEP (-1)
2         GOSUB 12405
2         NEXT RA
3     NEXT AZ
3     FOR AZ = AZ TO 10 STEP (AID/10)
3     AZLOC = AZLOC + 1
3     GOSUB 6810
341       FOR RA = 9 TO 2 STEP (-1)
345       GOSUB 12405
3475      NEXT RA
35    NEXT AZ
3505  FOR AZ = AZ TO 12 STEP (AID/10)
3525      AZLOC = AZLOC + 1
35        GOSUB 6810
355       FOR RA = 9 TO 3 STEP (-1)
3575      GOSUB 12405
3e1       NEXT RA
3e5   NEXT AZ
3e    FOR AZ = AZ TO 14 STEP (AID/10)
3e55      AZLOC = AZLOC + 1
3e        GOSUB 6810
3         FOR RA = 9 TO 4 STEP (-1)
3         GOSUB 12405
3         NEXT RA
3     NEXT AZ
3775  FOR AZ = AZ TO 16 STEP (AID/10)
378       AZLOC = AZLOC + 1
379       GOSUB 6810
3e        FOR RA = 9 TO 5 STEP (-1)
3e25      GOSUB 12405
3e5       NEXT RA
3875  NEXT AZ
4     LOCATE 1,1,0
4     PSET(25,190): DRAW"uD de  uD R300 uD de uD L300": LOCATE 22,38: PRINT"NOR
MALIZED TEMPERATURE = 1"
4     LOCATE 1,1,0
4     END
5000  LOCA = LOCA +1
5005  IF EOF(2) THEN GOTO 887
5010  INPUT #2, PNT(RA,AZ),RAD(RA,AZ),ANG(RA,AZ),T(0,RA,AZ),T(1,RA,AZ),T(2,RA,AZ)
,T(3,RA,AZ),T(4,RA,AZ),F(0,RA,AZ),F(1,RA,AZ),P(2,RA,AZ),P(3,RA,AZ),F(4,RA,AZ),V(
0,RA,AZ),V(1,RA,AZ),V(2,RA,AZ),V(3,RA,AZ),V(4,RA,AZ)
5020  RETURN
681   FOR THETA = 0 TO .174e    STEP ((1/3e0)*2*3.1415926548/*5
e91   XCOOR = (THETA*3*57.29577951) + 75
7     PSET(XCOOR,16e)
711   FOR A15 = 0 TO .174e STEP (AID*2*3.1415926548/3e0)
7     XT = XCOOR - 2
7     YT = (16e/8) + 2
7     IF ABS(THETA - A15) <.001 THEN DRAW "u116 d116": LOCATE YT, XT: PRINT AZLOC:
YV=((11e/100)*(100-RAD(RA,AZ))+50):XV=(-(300*(T(2,RA,AZ)-T)/(TJ-T)))+XCOOR:PSET(
XV,YV):PSET(XV,YV-1):PSET(XV,YV+1):PSET(XV+1,YV):PSET(XV-1,YV)
7     NEXT A15
7e    REM 16e represents starting ycoord at 50 plus the primar, zone width of 5
      times its weighting factor of 2
      NEXT THETA
```

ORIGINAL PAGE IS
OF POOR QUALITY

```
7710 THETA = .2617994
7720 RETURN
8910 FOR THETA = THETA    TO 3.1415926540 STEP (5*2*3.1415926540/360)
9010 DELTA = (13*(1 - SIN(THETA))/B1)
9110 ALPHA = ATN(DELTA/((1 - DELTA^2)^.5))
9210 B = ((((13*COS(THETA)*COS(THETA) + B1*COS(ALPHA)*COS(THETA))^2 [illegible] (13*COS(THE
TA)*SIN(THETA) + B1*COS(ALPHA)*SIN(THETA) [illegible] )/(TAN(THETA)*TAN(THETA) + 1))^.5
9310 A = B*TAN(THETA)
9410 X = ((A - 13*COS(THETA))^2 [illegible] (B + 13*SIN(THETA))^2 - 625)/26
95[illegible] [illegible] = (X - 13)^2)^.5
96[illegible] [illegible] (X^2 + [illegible])^.5
9710 XCOOR = (THETA*57.29577951) + 75
9810 YCOOR = (L - 36)*2 + 50
[illegible] YC = YCOOR - 50
10010 PSET(XCOOR,YCOOR)
10110 FOR AIS = AISS TO 3.142 STEP (AID*2*3.1415926540/360)
10210 XT = XCOOR/8
10310 YT = (YCOOR/8) +2
10410 IF ABS(THETA - AIS) [illegible] .001 THEN DRAW "u=yc; d=yc;": LOCATE YT,XT: PRINT AZLU
C:THETA = THETA + .08726646260:GOTO 10620
10510 NEXT AIS
10610 NEXT THETA
10620 RETURN
12405 YV=((116 100)*(100-RAD(RA,AZ))+50):XV=(-(300*(T(2,RA,AZ)-T)/(TJ-T))+XCOOR
:PSET(XV,YV):PSET(XV,YV-1):PSET(XV,YV+1):PSET(XV+1,YV):PSET(XV-1,YV)
12410 RETURN
```

4. LASPLMPV.BAS--Plots set of radial velocity profiles.

```
100 CLS
110 KEY OFF
115 DIM PA(9,18)
120 DIM RA(9,18)
125 DIM ANG(9,18)
130 DIM T(4,9,18)
135 DIM P(4,9,18)
140 DIM V(4,9,18)
310 INPUT "What is the introductory information filename"; FI$
410 INPUT "What is the data filename"; FD$
510 OPEN FI$ FOR INPUT AS #1
610 OPEN FD$ FOR INPUT AS #2
710 INPUT #1,A1,FI$,FD$,J,,NJ,PA,TA,MCA,MJA,MGA,TJA,MSJA,BFA,TSA,T6A,T7A,T8A,T9
.   T10A,MC,MJ,MG,M,P,T,TJ,TS,T6,T7,T8,T9,T10,RG,RGJ,V,MSJ,VJ,DR,J,SR,BF,NGJ
715 A1D = A1*10
810 INPUT "What type of plot is this"; PLTYP$
815 FOR A1 = 0 TO 8 STEP (A1D/10)
820     FOR RA = 9 TO 1 STEP (-1)
825     GOSUB 5000
830     NEXT RA
835 NEXT A1
840 FOR A1 = A1 TO 10 STEP (A1D/10)
845     FOR RA = 9 TO 1 STEP (-1)
850     GOSUB 5000
855     NEXT RA
860 NEXT A1
865 FOR A1 = A1 TO 12 STEP (A1D/10)
870     FOR RA = 9 TO 1 STEP (-1)
875     GOSUB 5000
880     NEXT RA
885 NEXT A1
890 FOR A1 = A1 TO 14 STEP (A1D/10)
895     FOR RA = 9 TO 4 STEP (-1)
896     GOSUB 5000
898     NEXT RA
902 NEXT A1
905 FOR A1 = A1 TO 16 STEP (A1D/10)
907     FOR RA = 9 TO 5 STEP (-1)
909     GOSUB 5000
911     NEXT RA
913 NEXT A1
910 CLS
1010 SCREEN 2
1110 LOCATE 1, 30: PRINT "FILENAME: " FD$
1210 LOCATE 2, 30: PRINT "MOMENTUM RATIO: ";  PRINT USING "##.##";J
1310 LOCATE 3, 30: PRINT "DENSITY RATIO: "; PRINT USING "##.##";DR
1335 IF NGJ = 0 THEN GOTO 1425
1350 IF NGJ = 1 THEN GOTO 1450
1410 LOCATE 4, 30: PRINT "SPACING RATIO: ";PRINT USING "##.##";SR
1411 GOTO 1510
1425 LOCATE 4, 30: PRINT "SPACING RATIO: "; PRINT "NO INJECTION";
1426 GOTO 1510
1450 LOCATE 4, 30: PRINT "SPACING RATIO: "; PRINT "SINGLE INJECTION";
1451 GOTO 1510
1510 LOCATE 5, 30: PRINT PLTYP$
1610 PSET(25,50)
```

```
1810 FOR AZ = 0 TO 1 STEP (AID/10)
1815     AZLOC = AZLOC + 1
1910     FOR RA = 9 TO 1 STEP (-1)
2010     GOSUB 6810
2020     NEXT RA
2110 NEXT AZ
2210 AISS = AIS - (AID*2*3.1415926548/360)
2310 FOR AZ = AZ TO 8 STEP (AID/10)
2315     AZLOC = AZLOC + 1
2320 GOSUB 8910
2410     FOR RA = 9 TO 1 STEP (-1)
2510     GOSUB 12405
2610     NEXT RA
2710 NEXT AZ
2750 FOR AZ = AZ TO 10 STEP (AID/10)
2755     AZLOC = AZLOC + 1
2810     GOSUB 8910
2910     FOR RA = 9 TO 2 STEP (-1)
3010     GOSUB 12405
3075     NEXT RA
3110 NEXT AZ
3150 FOR AZ = AZ TO 12 STEP (AID/10)
3155     AZLOC = AZLOC + 1
3210     GOSUB 8910
3255     FOR RA = 9 TO 3 STEP (-1)
3310     GOSUB 12405
3410     NEXT RA
3425 NEXT AZ
3450 FOR AZ = AZ TO 14 STEP (AID/10)
3455     AZLOC = AZLOC + 1
3510     GOSUB 8910
3575     FOR RA = 9 TO 4 STEP (-1)
3710     GOSUB 12405
3725     NEXT RA
3750 NEXT AZ
3775 FOR AZ = AZ TO 16 STEP (AID/10)
3780     AZLOC = AZLOC + 1
3790     GOSUB 8910
3810     FOR RA = 9 TO 5 STEP (-1)
3825     GOSUB 12405
3850     NEXT RA
3875 NEXT AZ
4710 LOCATE 1,1,0
4715  PSET(350,190): DRAW"u3 e6  u3 R25 u3 d6 u3 L25": LOCATE 20,38: PRINT"NORMA
LIZED VELOCITY = 1"
4714 LOCATE 1,1,0
4720 END
5000 LOCA = LOCA +1
5005 IF EOF(2) THEN GOTO 887
5010 INPUT #2, PNT(RA,AZ),RAD(RA,AZ),ANG(RA,AZ),T(0,RA,AZ),T(1,RA,AZ),T(2,RA,AZ
,T(3,RA,AZ),T(4,RA,AZ),P(0,RA,AZ),P(1,RA,AZ),P(2,RA,AZ),P(3,RA,AZ),P(4,RA,AZ),V(
0,RA,AZ),V(1,RA,AZ),V(2,RA,AZ),V(3,RA,AZ),V(4,RA,AZ)
5020 RETURN
6810 FOR THETA = 0 TO .1746     STEP ((1/360)*2*3.1415926548)*5
6910 XCOOR = (THETA*3*57.295779518) + 25
7010 PSET(XCOOR,166)
7110 FOR AIS = 0 TO .1746 STEP (AID*2*3.1415926548/360)
7210 XT = XCOOR*8
7310 YT = (166/8) + 2
7410 IF ABS(THETA - AIS)<.001 THEN DRAW "u116 d116": LOCATE YT, XT: PRINT AZLOC:
YV=((116/100)*(100-RAD(RA,AZ)))+50:XV=((((V(2,RA,AZ)/V)-1)*25)+XCOOR):PSET(XV,YV
):PSET(XV,YV-1):PSET(XV,YV+1):PSET(XV+1,YV):PSET(XV-1,YV)
7510 NEXT AIS
7610 REM 166 represents starting ycoord at 50 plus the primary zone width of 58
       times its weighting factor of 2
```

```
7715 THETA = .2617994
7720 RETURN
8910 FOR THETA = THETA    TO 3.1415926548 STEP (5*2*3.1415926548/360)
7010 DELTA = (12*(1 - SIN(THETA))/81)
9110 ALPHA = ATN(DELTA/((1 - DELTA 2)^.5))
9210 B = (((12*COS(THETA)*COS(THETA) + 81*COS(ALPHA)*COS(THETA)) 2 + (12*COS(THE
TA)*SIN(THETA) + 81*COS(ALPHA)*SIN(THETA))^2)/(TAN(THETA)*TAN(THETA + 1)) .5
9310 A = B*TAN(THETA)
9410 X = ((A - 12*COS(THETA))^2 + (B + 12*SIN(THETA))^2 - 6262)/26
9510 Y = (65e1 - (A - 12)^2)^.5
9610 L = (X 2 + Y^2) .5
9710 XCOOR = (THETA*57.2957795) + 25
9810 YCOOR = (L - 3e)*2 + 50
9910 YC = YCOOR - 50
10010 PSET(XCOOR,YCOOR)
10110 FOR AIS = AIS8 TO 3.142 STEP (A1D*2*3.1415926548/3e0)
10210 XT = XCOOR/8
10310 YT = (YCOOR/8) +2
10410 IF ABS(THETA - AIS) .001 THEN DRAW "u=yc: d=yc:": LOCATE YT,XT: PRINT A2L2
C:THETA = THETA + .0872664e2e0:GOTO 10e20
10510 NEXT AIS
10610 NEXT THETA
10620 RETURN
12405 YV=(((116/100)*(10^-RAD(RA,A2)))*50):XV=(((V(2,RA,A2)/V)-1)*25)+XCOOR:PSE
(XV,YV):PSET(XV,YV+1):PSET(XV,YV-1):PSET(XV+1,YV):PSET(XV-1,YV)
12415 RETURN
```

5. LATPLTES.BAS--Plots all rake temperatures laterally for a given azimuthal and radial position.

```
10 CLS
20 SCREEN 2
30 DIM PNT(9,18)
40 DIM RAD(9,18)
50 DIM ANG(9,18)
60 DIM T(4,9,18)
70 DIM P(4,9,18)
80 DIM V(4,9,18)
90 INPUT "STATE INTRODUCTORY FILENAME IN QUOTES"; FI$
100 INPUT "STATE DATA FILENAME IN QUOTES"; FD$
110 OPEN FI$ FOR INPUT AS #1
120 OPEN FD$ FOR INPUT AS #2
130 INPUT #1,A1,FI$,FD$,JL,NJ,PR,TR,MCR,MWR,MGR,TJR,MSJR,BPR,T5R,T6R,T7R,T8R,T9R
,T10R,ME,MW,MG,M,P,T,TJ,T5,T6,T7,T8,T9,T10,RD,RDJ,V,MSJ,VJ,DR,J,SR,BP,NDJ
140 INPUT "WHAT TYPE OF PLOT (lateral velocity or temperature)";PLTYP$
145 INPUT"WHAT RADIAL POSITION IS DESIRED(9,8,....1)"; RAP
147 INPUT"WHAT AZIMUTHAL POSITION IS DESIRED(16,16....2,0)"; AZP
148 CLS
149 KEY OFF
150 FOR A2 = 0 TO 6 STEP A1
160     FOR RA = 9 TO 1 STEP (-1)
170     GOSUB 5000
180     NEXT RA
190 NEXT A2
200 FOR A2 = A2 TO 10 STEP A1
210     FOR RA = 9 TO 2 STEP (-1)
220     GOSUB 5000
230     NEXT RA
240 NEXT A2
250 FOR A2 = A2 TO 12 STEP A1
260     FOR RA = 9 TO 3 STEP (-1)
270     GOSUB 5000
280     NEXT RA
290 NEXT A2
300 FOR A2 = A2 TO 14 STEP A1
310     FOR RA = 9 TO 4 STEP (-1)
320     GOSUB 5000
330     NEXT RA
340 NEXT A2
350 FOR A2 = A2 TO 18 STEP A1
360     FOR RA = 9 TO 5 STEP (-1)
370     GOSUB 5000
380     NEXT RA
390 NEXT A2
400 LOCATE 7,45:PRINT"FILENAME:  "FD$
410 LOCATE 5, 9:PRINT"MOMENTUM RATIO: ";:PRINT USING "##.##"; J
420 LOCATE 6, 9:PRINT"DENSITY RATIO:  ";:PRINT USING "##.##";DR
430 LOCATE 7, 9:PRINT"SPACING RATIO:  ";:PRINT "SINGLE INJECTION";
442 LOCATE 5,45:PRINT "AZIMUTHAL STATION:  "; :PRINT (AZP*10);:PRINT "DEGREES";
444 LOCATE 6,45:PRINT "RADIAL STATION:  ";:PRINT ((RAP +.5)*10);:PRINT "UNITS";
450 PSET(296,176):DRAW "r192 l384 r192"
451 PSET (25,176): DRAW"u96 r4 l8 r4 d96 r4 l8 r4":PSET(296,176)
452 DRAW "l192 u5 d5 r96 u5 d5 r192 u5 d5 r96 u5 d5 l384"
460 LOCATE 24,11: PRINT -7.14;
470 LOCATE 24,23: PRINT -3.57;
480 LOCATE 24,37: PRINT 0;
490 LOCATE 24,47: PRINT 3.57;
500 LOCATE 24,59: PRINT 7.14;
510 LOCATE 25,27: PRINT "Initial Jet Diameters";
555 LOCATE 9,1: PRINT"NORM. TEMP. = 0.5"
560 PSET(296,176)
562 LOCATE 1,1
570 END
```

```
5000 INPUT #2,PNT(RA,AZ),RAD(RA,AZ),ANG(RA,AZ),T(0,RA,AZ),T(1,RA,AZ),T(2,RA,AZ),
T(3,RA,AZ),T(4,RA,AZ),P(0,RA,AZ),P(1,RA,AZ),P(2,RA,AZ),P(3,RA,AZ),P(4,RA,AZ),V(0
,RA,AZ),V(1,RA,AZ),V(2,RA,AZ),V(3,RA,AZ),V(4,RA,AZ)
5010 IF RA=RAF AND AZ=AZF THEN GOSUB 6000
5020 RETURN
6000 XCOOR=104: YCOOR=(176-(192*(T(0,RA,AZ)-T)/(TJ-T))): PSET(XCOOR,YCOOR):DRAW
"u2 d4 u2 r4 18 r4"
6010 XCOOR=200: YCOOR=(176-(192*(T(1,RA,AZ)-T)/(TJ-T))): PSET(XCOOR,YCOOR):DRAW
 u2 d4 u2 r4 18 r4"
6020 XCOOR=296: YCOOR=(176-(192*(T(2,RA,AZ)-T)/(TJ-T))): PSET(XCOOR,YCOOR):DRAW
 u2 d4 u2 r4 18 r4"
6030 XCOOR=392: YCOOR=(176-(192*(T(3,RA,AZ)-T)/(TJ-T))): PSET(XCOOR,YCOOR):DRAW
 u2 d4 u2 r4 18 r4"
6040 XCOOR=488: YCOOR=(176-(192*(T(4,RA,AZ)-T)/(TJ-T))): PSET(XCOOR,YCOOR):DRAW
 u2 d4 u2 r4 18 r4"
6050 RETURN
```

6. 3DLAT.BAS--Plots laterally all rake temperatures for all radial positions at a given azimuthal location.

```
100 CLS
200 INPUT "What azimuthal location"; AZI
300 DIM X(9)
400 DIM R(9)
110 KEY OFF
115 DIM PNT(9,18)
120 DIM RAD(9,18)
125 DIM ANG 9,18)
130 DIM T(4,9,18)
135 DIM P(4,9,18)
140 DIM V(4,9,18)
510 INPUT "What is the introductory information filename"; FI$
410 INPUT "What is the data filename"; FD$
510 OPEN FI$ FOR INPUT AS #1
610 OPEN FD$ FOR INPUT AS #2
710 INPUT #1,A1,FI$,FD$,JE,NJ,PR,TR,MCR,MHR,MGR,TJR,MSJR,PPR,TSR,T6R,T7R,TBR,T9R
,   T10R,MC,MH,MG,M,P,T,TJ,TS,T6,T7,TB,T9,T10,RD,RDJ,V,MEJ,VJ,DR,J,SR,BF,NDJ
715 AID = A1*10
610 INPUT "What type of plot is this"; PLTYP$
815 FOR A2 = 0 TO 8 STEP (AID/10)
820     FOR RA = 9 TO 1 STEP (-1)
825     GOSUB 5000
830     NEXT RA
835 NEXT A2
840 FOR A2 = A2 TO 10 STEP (AID/10)
845     FOR RA = 9 TO 2 STEP (-1)
850     GOSUB 5000
855     NEXT RA
858 NEXT A2
860 FOR A2 = A2 TO 12 STEP (AID/10)
865     FOR RA = 9 TO 3 STEP (-1)
870     GOSUB 5000
875     NEXT RA
880 NEXT A2
885 FOR A2 = A2 TO 14 STEP (AID/10)
890     FOR RA = 9 TO 4 STEP (-1)
895     GOSUB 5000
900     NEXT RA
902 NEXT A2
905 FOR A2 = A2 TO 16 STEP (AID/10)
907     FOR RA = 9 TO 5 STEP (-1)
909     GOSUB 5000
911     NEXT RA
913 NEXT A2
910 CLS
1010 SCREEN 2
1015 LINE (50,190)-(50,110)
1020 LINE (50,110)-(350,30)
1025 LINE (350,30)-(350,110)
1030 LINE (350,110)-(50,190)
1100 LOCATE 4,48: PRINT "INNER WALL"
1110 LOCATE 14,50: PRINT "FILENAME: " FD$
1125 AZIT = AZI*10
1150 LOCATE 10,50: PRINT "AZIMUTHAL LOCATION:" AZIT"DEGREES"
1210 LOCATE 11,50: PRINT "MOMENTUM RATIO: ";  PRINT USING "##.##";J
1310 LOCATE 12,50: PRINT "DENSITY RATIO: ";: PRINT USING "##.##";DR
1315 LOCATE 20,45: PRINT "NORMALIZED TEMPERATURE = 1"
1320 PSET(300,165): DRAW "U3 D6 U3 R300 U3 D6"
1325 IF NDJ = 0 THEN GOTO 1425
1350 IF NDJ = 1 THEN GOTO 1450
1410 LOCATE 13,50: PRINT "SPACING RATIO: ";:PRINT USING "##.##";SR
```

```
1425 LOCATE 13,50: PRINT "SPACING RATIO: ";:PRINT "NO INJECTION";
1426 GOTO 1510
1450 LOCATE 13,50: PRINT "SPACING RATIO: ";:PRINT "SINGLE INJECTION";
1451 GOTO 1510
1510 REM now continue with data plotting
1610 PSET(80,102)
1615 Y(9)=102
1620 LIM = 1
1625 X0 = 60
1626 IF AZI = 10 THEN LIM = 2
1627 IF AZI = 12 THEN LIM = 3
1628 IF AZI = 14 THEN LIM = 4
1629 IF AZI = 16 THEN LIM = 5
1630 IF AZI = 18 THEN LIM = 5
1635 FOR LAT = 0 TO 4 STEP 1
1640      FOR RA = 9 TO LIM STEP -1
1645      VALUE =-300*((T(LAT,RA,AZI) -T)/(TJ - T))
1650      IF RA = 9 THEN GOTO 1655
1652      GOTO 1660
1655      X(RA)=X0 + VALUE: PSET(X(RA),Y(RA)): DRAW"l=value;"
1657      GOTO 1667
1660      X(RA) = X0 + VALUE
1670      PSET((X(RA)), (Y(RA)))
1675      LINE ((X(RA + 1)),(Y(RA + 1)))-((X(RA)), (Y(RA)))
1680      IF RA = LIM THEN DRAW "L = VALUE;"
1687      Y(RA - 1) = Y(RA) + 10
1690      NEXT RA
1697 PSET(X0, Y(9)):DRAW "d80 u80"
1698 Y(9) = Y(9) -16
1700 X0 = X0 + 60
1701 IF LAT = 4 THEN GOTO 1705
1702 PSET(X0, Y(9)):DRAW "d80 u80"
1703 PSET (X(RA +1), Y(RA+1))
1705 NEXT LAT
4714 LOCATE 1,1,0
4715 END
5000 LOC# = LOC# +1
5005 IF EOF(1) THEN GOTO 667
5010 INPUT #1, FNT(RA,AZ),RAD(RA,AZ),ANG(RA,AZ),T(0,RA,AZ),T(1,RA,AZ),T(2,RA,AZ
,T(3,RA,AZ),T(4,RA,AZ),P(0,RA,AZ),P(1,RA,AZ),P(2,RA,AZ),P(3,RA,AZ),P(4,RA,AZ),V(
0,RA,AZ),V(1,RA,AZ),V(2,RA,AZ),V(3,RA,AZ),V(4,RA,AZ)
5020 RETURN
```

APPENDIX 5

ERROR ANALYSIS

This error analysis is based on the approximation that error can be estimated using the first term of the Taylor Expansion.

Sources of error in this experiment are from:

thermocouple

conduction

pitot-static tube

flow fluctuations

Doric temperature indicator

Setra Systems transducer

Tecmar A/D board.

1. Temperature Error:

$$\frac{\delta(T)}{T} = \frac{\left[\frac{std.\ dev.}{\sqrt{25}}\right]}{600} + Conduction\ error + Thermocouple\ error$$

$$\frac{\delta(T)}{T} = 100\left[\frac{1.2}{600}\right] + 0.18 + 0.75 = 1.13\%$$

Fluctuation must include Doric flow fluctuations and A/D board.

2. Pressure Error:

$$\frac{\delta(\Delta P)}{\Delta P} = \frac{\left[\frac{\text{std. dev.}}{\sqrt{25}}\right]}{0.004} + \text{pitot-static error}$$

$$\frac{\delta(\Delta P)}{\Delta P} = 100\left[\frac{8\times10^{6}}{0.004}\right] + 4 = 4.2\%$$

Fluctuations seen in standard deviation must include Setra transducer, flow fluctuations, and A/D board.

3. Error in Velocity

Since velocity has multiple components, each having some error associated with it, the Taylor formula will therefore be used:

$$V_{\ell} = \left[\frac{2\Delta P}{\rho_{\ell}}\right]^{1/2}$$

where V_{ℓ}, ρ_{ℓ} are "local" quantities.

$$\rho_{\ell} = \frac{P}{RT_{\ell}} = \frac{P_{atm} + P_{comb}}{R\ T_{\ell}}$$

where P_{atm} = atmospheric pressure

P_{comb} = combustor pressure (gage)

$$\therefore V_{\ell} = \left[\frac{2\Delta P}{\left[\frac{P_{atm}+P_{comb}}{R\ T_{\ell}}\right]}\right]^{1/2}$$

Using the Taylor expansion formula, and taking the absolute value of each term:

$$\frac{\delta V}{V} = \frac{1}{V}\left[\frac{\partial V}{\partial(\Delta P)}\,\delta(\Delta P)\right] + \frac{1}{V}\left[\frac{\partial V}{\partial T_\ell}\,\delta T_\ell\right]$$

$$+ \frac{1}{V}\left[\frac{\partial V}{\partial P_{atm}}\,\delta(P_{atm})\right] + \frac{1}{V}\left[\frac{\partial V}{\partial P_{comb}}\,\delta(P_{comb})\right]$$

After carrying out the differentiation in the first term, and multiplying by 1/V and $\delta(\Delta P)$, one gets:

$$\frac{1}{V}\left[\frac{\partial V}{\partial(\Delta P)}\right] = \frac{\frac{1}{2}\left[\frac{2RT_\ell}{P_{atm} + P_{comb}}\right]\delta(\Delta P)}{\left[\frac{2\Delta PRT_\ell}{P_{atm} + P_{comb}}\right]}$$

$$= \frac{\frac{1}{2}\,\delta(\Delta P)}{\Delta P}$$

Similarly, term two becomes:

$$\frac{1}{V}\left[\frac{\partial V}{\partial T_\ell}\,\delta T_\ell\right] = \frac{\frac{1}{2}\,\delta T_\ell}{T_\ell}$$

Similarly, term three becomes:

$$\frac{1}{V}\left[\frac{\partial V}{\partial P_{atm}}\,\delta(P_{atm})\right] = \frac{\frac{1}{2}\,\delta(P_{atm})}{P_{atm} + P_{comb}}$$

Similarly, term four becomes:

$$\frac{1}{V}\left[\frac{\partial V}{\partial P_{comb}}\,\delta(P_{comb})\right] = \frac{\frac{1}{2}\,\delta(P_{comb})}{P_{atm} + P_{comb}}$$

Therefore, uncertainty in velocity is

$$\frac{\delta V}{V} = \frac{1}{2}\left[\frac{\delta(\Delta P)}{\Delta P} + \frac{\delta(T_\ell)}{T_\ell} + \frac{\delta(P_{atm}) + \delta(P_{comb})}{P_{atm} + P_{comb}}\right]$$

$\frac{\delta(\Delta P)}{\Delta P} = 4.2\%$ from above

$\frac{\delta(T_\ell)}{T_\ell} = 1.13\%$ from above

Combustor and atmospheric errors are estimated by how well manometers can be read. The barometer is ± 0.01 inches Hg. The combustor pressure manometer is ± 0.05 cm water. This gives

$$\frac{\delta(P_{atm}) + \delta(P_{comb})}{P_{atm} + P_{comb}} = \frac{0.01 + 0.0014 \text{ inches Hg}}{29 + 0.06 \text{ inches Hg}} = 0.04\%$$

Therefore

$$\frac{\delta V}{V} = \frac{1}{2}\left[4.2 + 1.13 + 0.04\right]$$

$$\frac{\delta V}{V} = 2.7\%$$

4. Error in Momentum Ratio

$$J = \frac{\rho_1 V_1^2}{\rho V^2} \quad \text{where } \rho, V \text{ are cross flow conditions}$$

$$J = \frac{\left[\frac{P_1}{RT_1}\right] V_1^2}{\left[\frac{P}{RT}\right] V^2}$$

where

$$V_1 = \left[\frac{\dot{m}_1}{\rho_1 A_1}\right]$$

$$V = \left[\frac{\dot{m}}{\rho A}\right]$$

therefore,

$$J = \frac{(\dot{m}_1)^2 P A^2 T_1}{(\dot{m})^2 P_1 A_1^2 T}$$

Use this expression for J, and write the error equations as follows:

$$\frac{\delta(J)}{J} = \frac{1}{J}\left[\frac{\partial J}{\partial \dot{m}_1}\delta(\dot{m}_1)\right] + \frac{1}{J}\left[\frac{\partial J}{\partial \dot{m}}\delta(\dot{m})\right]$$

$$+ \frac{1}{J}\left[\frac{\partial J}{\partial P}\,\delta(P)\right] + \frac{1}{J}\left[\frac{\partial J}{\partial P_l}\,\delta(P_l)\right]$$

$$+ \frac{1}{J}\left[\frac{\partial J}{\partial T_l}\,\delta(T_l)\right] + \frac{1}{J}\left[\frac{\partial J}{\partial T}\,\delta(T)\right]$$

Just as in the velocity error calculations:

$$\frac{1}{J}\left[\frac{\partial J}{\partial \dot{m}_l}\,\delta(\dot{m}_l)\right] = \frac{2\delta(\dot{m}_l)}{\dot{m}_l}$$

$$\frac{1}{J}\left[\frac{\partial J}{\partial \dot{m}}\,\delta(\dot{m})\right] = \frac{2\delta(\dot{m})}{\dot{m}}$$

$$\frac{1}{J}\left[\frac{\partial J}{\partial P}\,\delta(P)\right] = \frac{\delta(P)}{P}$$

$$\frac{1}{J}\left[\frac{\partial J}{\partial P_l}\,\delta(P_l)\right] = \frac{\delta(P_l)}{P_l}$$

$$\frac{1}{J}\left[\frac{\partial J}{\partial T_l}\,\delta(T_l)\right] = \frac{\delta(T_l)}{T_l}$$

$$\frac{1}{J}\left[\frac{\partial J}{\partial T}\,\delta(T)\right] = \frac{\delta(T)}{T}$$

Estimated uncertainties:

$$\dot{m}_l = \frac{0.05CFM}{1.5CMF} = 0.033$$

$$P = \frac{0.5mm}{11mm} + \frac{1mm}{80mm} + \frac{1mm}{40mm} = 0.08295$$

$$P = \frac{0.01 \text{ inches Hg}}{29 \text{ inches Hg}} + \frac{1mm}{23mm} = 0.0438$$

$$T_I = \frac{1}{544} + 0.0075 + 0.00025 = 0.0096$$

(DORIC) (T-C) (TECMAR)

$$T = \frac{1}{1180} + 0.0075 + 0.00025 + 0.0018 = 0.01040$$

(DORIC) (T-C) (TECMAR) (CONDUCTION)

Add all of the above according to the Taylor formula. but using the sum of the squares for a less conservative estimate to get

$$\frac{\delta J}{J} = \pm 18\%$$

5. Error in Density Ratio

$$\rho_I = \frac{P_I}{RT_I}$$

$$\rho = \frac{P}{RT}$$

$$Dr = \frac{\left[\frac{P_I}{RT_I}\right]}{\left[\frac{P}{RT}\right]} = \frac{P_I T}{PT_I}$$

$$\frac{\delta(Dr)}{Dr} = \frac{1}{Dr}\left[\frac{\partial Dr}{\partial P_I}\,\delta(P_i)\right] + \frac{1}{Dr}\left[\frac{\partial Dr}{\partial P}\,\delta(P)\right]$$

$$+ \frac{1}{Dr}\left[\frac{\partial Dr}{\partial T_l}\,\delta(T_l)\right] + \frac{1}{Dr}\left[\frac{\partial Dr}{\partial T}\,\delta(T)\right]$$

$$\frac{\delta(Dr)}{Dr} = \frac{\delta P_l}{P_l} + \frac{\delta P}{P} + \frac{\delta T_l}{T_l} + \frac{\delta T}{T}$$

Using values from the momentum calculation

$$\frac{\delta(Dr)}{Dr} = \pm\ 6.4\%$$

6. Error in Tau

$$\tau = \frac{T_1 - T_3}{T_2 - T_3}$$

where

$$T_1 = T_L$$

$$T_2 = T_l$$

$$T_3 = T$$

$$\frac{\partial \tau}{\tau} = \frac{1}{\tau}\left[\frac{\partial \tau}{\partial T_1}\,\delta(T_1)\right] + \frac{1}{\tau}\left[\frac{\partial \tau}{\partial T_2}\,\delta(T_2)\right] + \frac{1}{\tau}\left[\frac{\partial \tau}{\partial T_3}\,\delta(T_3)\right]$$

Carrying out the differentiation:

$$\frac{\partial \tau}{\tau} = \frac{\delta(T_1)}{T_1 - T_3} + \frac{\delta(T_2)}{T_2 - T_3} + \delta(T_3)\left[\frac{1}{T_1 - T_3} + \frac{1}{T_2 - T_3}\right]$$

For conservative values, take

$$| T_1 - T_3 | = 150\ K$$

$$| T_2 - T_3 | = 350\ K$$

$$T_1 = 500\ K$$

$$T_2 = 300\ K$$

$$T_3 = 650\ K$$

Recall

$$\frac{\delta(T_1)}{T_1} = \pm\ 1.13\%$$

$$\frac{\delta(T_2)}{T_2} = \pm\ 0.96\%$$

$$\frac{\delta(T_3)}{T_3} = \pm\ 1.04\%$$

This gives absolute errors as:

$$T_1 = \pm\ 5.65\ K$$

$$T_2 = \pm\ 2.9\ K$$

$$T_3 = \pm\ 6.75\ K$$

As a less conservative estimate, the square root of the sum of the squares of the terms in the Taylor expansion gives:

$$\frac{\delta(\tau)}{\tau} = \pm 6.5\%$$

(± 3 data point widths)

7. Error in Gamma

$$\gamma = \frac{V_\ell}{V} - 1$$

$$\frac{\delta\gamma}{\gamma} = \frac{1}{\gamma}\left[\frac{\partial\gamma}{\partial V_\ell}\,\delta(V_\ell)\right] + \frac{1}{\gamma}\left[\frac{\partial\gamma}{\partial V}\,\delta(V)\right]$$

$$\frac{\partial\gamma}{\gamma} = \frac{\delta(V_\ell)}{V_\ell - V} + \frac{\delta(V)}{V_\ell - V}$$

Recall

$$\frac{\delta V}{V} = 2.7\%$$

Representative values of V. V_ℓ are 8.15 m/s

Using a less conservative estimate of the square root of the sum of the squares to get

$$\frac{\delta\gamma}{\gamma} = \pm 6.6\%$$

(± 1/4 data point width)

REFERENCES

1. Abramovich, G.N., The Theory of Turbulent Jets. MIT Press, Cambridge, Mass., 1963.

2. Albertson, M.L., Dai, Y.B., Jensen, R.A., and Rouse, H., "Diffusion of Submerged Jets." Trans. ASCE, pp. 639-697, 1950.

3. ASME Research Committee, Fluid Meters, Their Theory and Application. ASME 5th edition, 1959.

4. Batchelor, G.K., An Introduction to Fluid Dynamics. Cambridge University Press, Cambridge, Mass., 1967.

5. Baumeister, T., editor-in-chief, Marks' Standard Handbook for Mechanical Engineers, 8th edition, McGraw-Hill Book Co.

6 Campbell, J.R. and Schetz, J.A., "Analysis of the Injection of a Heated Turbulent Jet into a Cross Flow." NASA TR R-413, 1973.

7. Chien, J.C., and Schetz, J.A., "Numerical Solution to the Three Dimensional Navier-Stokes Equations with Applications to Channel Flows and a Buoyant Jet in a Cross Flow." ASME paper no. 75-APM-21, 1975.

8. Cox, G.B., "Multiple Jet Correlations for Gas Turbine Engine Combustor Design." Journal of Engineering For Power, April, 1976.

9. Dixon, W.J., Introduction to Statistical Analysis. McGraw-Hill Book Co., 1969.

10. Fan, L.N., "Turbulent Buoyant Jets into Stratified or Flowing Ambient Fluids." Col. Inst. of Tech., Civil Eng. Ph.D., 1967.

11. Hoel, P.G., Introduction to Mathematical Statistics. John Wiley and Sons, 1954.

12. Holdeman, J.D., and Walker, R.E., "An Empirical Model for the Mixing of a Pair of Dilution Jets with a Confined Cross Flow." AIAA paper no. 76-48, January, 1976.

13. Hoult, D.D., Fay, J.A., and Forney, L.J., "A Theory of Plume Rise Compared with Field Observations," Journal of Air Pollution Control Association, Vol. 19, No. 8, pp 585-590, 1969.

14. Kamotani, Y. and Greber, I., "Experiments on a Turbulent Jet in a Cross Flow," AIAA Journal, Vol. 10, No. 11, 1972.

15. Kamotani, Y. and Greber, I., "Experiments on Confined Turbulent Jets in a Cross Flow," NASA CR-2392, 1974.

16. Keffer, J.F. and Baines, W.D., "The Round Turbulent Jet in a Cross Wind," Journal of Fluid Mechanics, 15, pp. 481-496, 1963.

17. Keffer, J.F., "The Physical Nature of a Subronic Jet in a Cross Stream," NASA SP-218, pp 19-36, 1969.

18. Lipshitz, A., "Dilution Jets in Accelerated Cross Flows," Ph.D. Dissertation, Case Western Reserve University, May, 1981.

19. Lipshitz A., Greber I., "Turbulent Jet Patterns in Accelerating Cross Flows," AIAA paper 81-0348, 1981.

20. Lipshitz, A., Greber, I., Riddlebaugh, S.M., "Dilution Jet Behavior in the Turn Section of a Reverse Flow Combustor," NASA Technical Memorandum No. 82776, 1982.

21. Morgan, H.E., Turbojet Fundamentals, McGraw-Hill Book Co., New York, 1958.

22. Norgren, C.T. and Humenik, F.M., "Dilution Jet Mixing Study for Gas-Turbine Combustors," NASA TN D-4695, 1968.

23. Platten, J.L. and Keffer, J.F., "Entrainment in Deflected Axisymmetric Jets at Various Angles to the Stream," Univ. of Toronto, Mech. Eng. TP-6808, 1968.

24. Pratte, B.D. and Baines, W.D., "Profiles of Round Turbulent Jets in a Cross Flow," ASCE J. Hyd. Div. 93, HY6, pp 53-64, 1967, corrections, 94, HY3, pp. 815-816, 1968.

25. Ricou, F.FP. and Spalding, D.B., "Measurements of Entrainment by Axisymmetrical Turbulent Jets," Journal of Fluid Mechanics, 11, pp. 21-32, 1961.

26. Rouse, H., Yih, C.S. and Humphreys, H.W., "Gravitational Convection from a Boundary Source," Tellus, 4, pp. 201-210, 1952.

27. Schetz, J.A., "Injection Mixing in Turbulent Flow," Progress in Astronautics and Aeronautics, Vol. 68, AIAA, New York, 1980.

28. Sucec, J. and Bowley, W.W., "Prediction of the Trajectory of a Turbulent Jet Injected into a Cross Flowing Stream," ASME paper no. 76-FE-8, 1976.

29. Weinstein, A.S., Osterle, J.F. and Forstall, W., "Momentum Diffusion From a Slot Jet into a Moving Secondary," Journal of Applied Mechanics, 23, 3, pp. 437-3443, 1956.

30. White, F.M., Fluid Mechanics, McGraw-Hill Book Co., New York, 1979.

31. Zoyev, V.S. and Skubachevskii, L.S., Combustion Chambers for Jet Propulsion Engines, Trans. by W. E. Jones and B. P. Mullins, The MacMillan Co., New York, 1964.